Synthesis of supramolecular architectures using P_n-ligands as building blocks

Dissertation zur Erlangung des
Doktorgrades der Naturwissenschaften (Dr. rer. nat.)
der Naturwissenschaftlichen Fakultät IV – Chemie und Pharmazie
der Universität Regensburg

vorgelegt von

Shining Deng

aus Nanjing, China

Regensburg 2007

Diese Arbeit wurde angeleitet von Prof. Dr. Manfred Scheer.
Promotionsgesuch eingereicht am: 28.März.2007
Tag der mündlichen Prüfung: 23.April.2007
Vorsitzender: Prof. Dr. Rainer Winter
Prüfungsausschuss: Prof. Dr. Manfred Scheer (1. Gutachter)
Prof. Dr. Henri Brunner (2. Gutachter)
Prof. Dr. Burkhard König

Die vorliegende Arbeit wurde in der Zeit von Dezember 2002 bis März 2004 am Institut für Anorganische Chemie der Universität Karlsruhe (TH) und von April 2004 bis März 2007 am Institut für Anorganische Chemie der Universität Regensburg unter Anleitung von Herrn Prof. Dr. Manfred Scheer angefertigt.

Dedicated to my family

路漫漫其修远兮, 吾将上下而求索

"The journey ahead is indistinct and long; I see no ending, yet high and low I'll search with my will unbending"

Qu Yuan, chinese poet, 340-278 B.C.

Contents

1.	**Introduction**	1
2.	**Research Objectives**	9
3.	**Results and Discussion**	10
3.1.	Synthesis and Studies on the Properties of Phosphaferrocenes	10
3.1.1.	Synthesis and studies on the properties of [Cp'''Fe(η^5-P_4C^tBu)] and [Cp'''Fe(η^5-$P_3C_2{}^tBu_2$)]	10
3.1.2.	Synthesis and Studies on the Properties of [Cp'''Fe(η^5-P_3C_2PhH)]	14
3.1.3.	Synthesis and studies on the properties of [Cp'''Fe(η^5-P_5)]	17
3.2	Studies on the chemical properties and coordination behaviour of the polyphosphaferrocene	18
3.2.1.	Triphosphaferrocene [Cp'''Fe(η^5-$P_3C_2{}^tBu_2$)] as a ligand	18
3.2.1.1.	Reaction of [Cp'''Fe(η^5-$P_3C_2{}^tBu_2$)] with CuCl	19
3.2.1.1.1.	[Cp'''Fe(η^5-$P_3C_2{}^tBu_2$)] with CuCl in a stoichiometric ratio of 1:1	19
3.2.1.1.2.	[Cp'''Fe(η^5-$P_3{}^tBu_2C_2$)] with CuCl in a stoichiometry ratio of 1:2	21
3.2.1.2.	Reaction of [Cp'''Fe(η^5-$P_3C_2{}^tBu_2$)] with CuBr and CuI	25
3.2.1.2.1.	[Cp'''Fe(η^5-$P_3C_2{}^tBu_2$)] with CuBr in a stoichiometric ratio of 1:1	25
3.2.1.2.2.	[Cp'''Fe(η^5-$P_3{}^tBu_2C_2$)] with CuBr and CuI in a stoichiometric ratio of 1:2	29
3.2.2.	The Triphosphaferrocene [CpFe(η^5-$P_3C_2{}^tBu_2$)] as a Ligand	34
3.2.2.1.	Reaction of [CpFe(η^5-$P_3C_2{}^tBu_2$)] with CuCl	34
3.2.2.2.	Reaktion of [CpFe(η^5-$P_3{}^tBu_2C_2$)] with CuBr	36
3.2.2.3.	Reaktion of [CpFe(η^5-$P_3{}^tBu_2C_2$)] with CuI	37
3.2.2.4.	Reaktion of [CpFe(η^5-$P_3{}^tBu_2C_2$)] with $Ag[Al\{OC(CF_3)_3\}_4]$	41
3.2.3.	The triphosphaferrocene [Cp'''Fe(η^5-P_3C_2PhH)] as a ligand	43
3.2.3.1.	Reaktion of [Cp'''Fe(η^5-P_3C_2PhH)] with copper halide	43
3.2.3.2.	Reaktion of [Cp'''Fe(η^5-P_3C_2PhH)] with $[(PtCl_2PEt_3)_2]$	46
3.2.3.3.	Reaktion of [Cp'''Fe(η^5-P_3C_2PhH)] with $[W(CO)_5THF]$	49
3.2.4.	The tetraphosphaferrocene [Cp'''Fe(η^5-P_4C^tBu)] as a ligand	54
3.2.4.1.	Reaction of [Cp'''Fe(η^5-P_4C^tBu)] with CuCl	54
3.2.4.1.1.	[Cp'''Fe(η^5-P_4C^tBu)] with CuCl in a stoichiometric ratio of 1:1	54

3.2.4.1.2. [Cp'''Fe(η^5-P_4C^tBu)] with CuCl in a stoichiometric ratio of 1:2 57
3.2.4.2. Reaktion of [Cp'''Fe(η^5- P_4C^tBu)] with CuBr and with CuI 60
3.2.4.2.1. Reaction of [Cp'''Fe(η^5-P_4C^tBu)] with CuBr in a ratio of 1:1 60
3.2.4.2.2. [Cp'''Fe(η^5- P_4C^tBu)] with CuBr and CuI in a ratio of 1:2 63
3.2.4.3. Reaktion of [Cp'''Fe(η^5- P_4C^tBu)] with $Ag[Al\{OC(CF_3)_3\}_4]$ 66
3.2.4.4. Reaktion of [Cp'''Fe(η^5- P_4C^tBu)] with $AuCl[SC_4H_8]$ 70
3.2.5. [Cp'''Fe(η^5-P_5)] as a Ligand in Coordination Chemistry 75
3.2.5.1. Reaction of [Cp'''Fe(η^5-P_5)] with CuCl 75
3.2.5.2. Reaction of [Cp'''Fe(η^5-P_5)] with CuBr 80
3.2.5.2.1. Reaction of [Cp'''Fe(η^5-P_5)] with CuBr in a ratio of 1:2 80
3.2.5.2.2. Reaction of [Cp'''Fe(η^5-P_5)] with CuBr in a ratio of 1:1 83
3.2.5.3. Reaction of [Cp'''Fe(η^5-P_5)] with CuI 85
3.2.5.4. Reaction of [Cp'''Fe(η^5-P_5)] with silver salt 88
3.2.5.4.1. Reaction of [Cp'''Fe(η^5-P_5)] with $Ag[Al\{OC(CF_3)_3\}_4]$ 88
3.2.5.4.2. Reaction of [Cp'''Fe(η^5-P_5)] with $AgSO_3CF_3$ 92

4. Experimental 93

4.1 General remarks 93
4.1.1. Methods 93
4.1.2. Spectroscopy and analysis 93
4.2. Preparation of starting material 94
4.2.1. Synthesis of [Cp'''Fe(η^5-P_4C^tBu)] and [Cp'''Fe(η^5-$P_3C_2{}^tBu_2$)] 94
4.2.2. Synthesis of [Cp'''Fe(η^5-P_3C_2PhH)] 95
4.2.3. Synthesis of [Cp'''Fe(η^5-P_5)] 96
4.3. Synthesis of the complexes based on [Cp'''Fe(η^5-$P_3C_2{}^tBu_2$)] 97
4.3.1. Synthesis of $[\{Cp'''Fe(\eta^5{:}\eta^1{:}\eta^1\text{-}P_3C_2{}^tBu_2)\}(\mu\text{-}CuCl)]_2$ (10) 97
4.3.2. Synthesis of $[\{(Cp'''Fe)_2(\eta^4{:}\eta^1{:}\eta^1\text{-}P_4)\}\{\mu\text{-}CuCl\}_2(MeCN)]_\infty$ (11) 97
4.3.3. Synthesis of $[\{Cp'''Fe(\eta^4{:}\eta^1{:}\eta^1\text{-}P_2C_2{}^tBu_2)\}\{\mu\text{-}CuBr(MeCN)\}]_2$ (13) 98
4.3.4. Synthesis of $[\{(Cp'''Fe)_2(\eta^4{:}\eta^4\text{-}P_4)\}(\mu\text{-}CuBr)_2(MeCN)]_\infty$ (14) 98
4.3.5. Synthesis of $[\{(Cp'''Fe)_2(\eta^4{:}\eta^4\text{-}P_4)\}(\mu\text{-}CuI)_2(MeCN)]_\infty$ (15) 99
4.4. Synthesis of the complexes based on [CpFe(η^5-$P_3C_2{}^tBu_2$)] 99
4.4.1. Synthesis of $[\{CpFe(\eta^5{:}\eta^1{:}\eta^1\text{-}P_3C_2{}^tBu_2)\}(\mu\text{-}CuCl)(MeCN)]_2$ (16) 99

4.4.2. Synthesis of [{CpFe(η^5:η^1:η^1-$P_3C_2{}^tBu_2$)}(μ-CuBr)(MeCN)]$_2$ (17) 100

4.4.3. Synthesis of [{CpFe(η^5:η^1:η^1-$P_3{}^tBu_2C_2$)}$_3$(CuI)$_7$MeCN] (18) 101

4.4.4. Synthesis of [{CpFe(η^5:η^1:η^1-$P_3{}^tBu_2C_2$)}(μ-AgMeCN)]$_2$ (19) 101

4.5. Synthesis of the complexes based on [Cp'''Fe(η^5-P_3C_2PhH)] 102

4.5.1. Synthesis of [{Cp'''Fe(η^5:η^1:η^1-P_3C_2PhH)}$_4$(μ-CuBr)$_4$]$_\infty$ (20) 102

4.5.2. Synthesis of [Cp'''Fe(μ,η^5:η^1-P_3C_2PhH)$PtCl_2PEt_3$] (21) 102

4.5.3. Synthesis of [{Cp'''Fe(μ,η^5:η^1:η^1-P_3C_2PhH)}{W(CO)$_5$}$_2$] (22) 103

4.5.4. Synthesis of [{Cp'''Fe(μ,η^5:η^1:η^1-P_3C_2PhH)}{W(CO)$_5$}$_3$] (23) 103

4.6 Synthesis of the complexes based on [Cp'''Fe(η^5-$P_4C{}^tBu$)] 104

4.6.1. Synthesis of [{Cp'''Fe(η^4-$P_3C{}^tBuP(O){}^tBu$)}$_4${(μ-Cu_2Cl)(MeCN)$_2$}$_2$ {(μ-CuCl)$_2$ (MeCN)}$_2$] (24) 104

4.6.2. Synthesis of [{Cp'''Fe(η^5:η^1:η^1:η^1-$P_4C{}^tBu$)}$_2$(μ-CuCl)$_2$]$_\infty$ (25) 104

4.6.3. Synthesis of [{Cp'''Fe(η^5-$P_4C{}^tBu$)}$_2$($P_8C_4{}^tBu_4$)$_2$(Cu_3Br_3)$_2$(MeCN)$_2$] (26) 105

4.6.4. Synthesis of [{Cp'''Fe(η^5:η^1:η^1:η^1-$P_4C{}^tBu$)}$_2$(μ-CuBr)$_2$]$_\infty$ (27) 105

4.6.5. Syntheses of [{Cp'''Fe(η^5:η^1:η^1:η^1-$P_4C{}^tBu$)}$_2$(μ-CuI)$_2$]$_\infty$ (28) 106

4.6.6. Syntheses of [Ag_2{Cp'''Fe(η^5:η^1:η^1-$P_4C{}^tBu$)}$_2${Cp'''Fe(η^5:η^1-$P_4C{}^tBu$)}$_2$] [Al{$OC(CF_3)_3$}$_4$]$_2$ (29) 106

4.6.7. Syntheses of [CpFe(η^5:η^1-$P_4{}^tBuC$) AuCl(SC_4H_8)] (30) 107

4.7. Synthesis of the complexes based on [Cp'''Fe(η^5-P_5)] 108

4.7.1. Synthesis of [{Cp'''Fe(η^5:η^1:η^1:η^1-P_5)}(μ-CuCl)(MeCN)]$_\infty$ (31) 108

4.7.2 Synthesis of [{Cp'''Fe(η^5:η^1:η^1:η^1-P_5)}(μ-CuBr)]$_\infty$ (32) 108

4.7.3. Synthesis of [{Cp'''Fe(η^5:η^1:η^1-P_5)}$_4$(μ-CuBr)$_3$]$_\infty$ (33) 109

4.7.4. Synthesis of [{Cp'''Fe(η^5:η^1:η^1-P_5)}$_4$(μ-CuI)$_4$]$_\infty$ (34) 109

4.7.5. Synthesis of [Ag{Cp'''Fe(η^5 η^2:η^1-P_5)}$_2$]$_n$[Al{$OC(CF_3)_3$}$_4$]$_n$ (35) 110

4.7.6. Reaction of [Cp'''Fe(η^5-P_5)] with $AgSO_3CF_3$ 110

5. Conclusions 111

5.1 Triphosphaferrocene [Cp'''Fe(η^5-$P_3C_2{}^tBu_2$)] as a ligand 111

5.2 The Triphosphaferrocene [CpFe(η^5-$P_3C_2{}^tBu_2$)] as a Ligand 113

5.3 The Triphosphaferrocene [Cp'''Fe(η^5-P_3C_2PhH)] as a Ligand 114

5.4 Tetraphosphaferrocene [Cp'''Fe(η^5-$P_4C{}^tBu$)] as a ligand 116

5.5 Pentaphosphaferrocene [Cp'''Fe(η^5-P_5)] as a ligand 118

6. Notes and References 121

7. Appendix 124

7.1. Directory of abbreviations 124

7.2. Directory of compounds 125

7.3. Crystallographic Data for the Reported Structures 127

8. Acknowledgments 150

1. Introduction

Since the first synthesis of $[Ti(\eta^5\text{-}P_5)_2]^{2-}$ by Ellis and coworkers[1], the search for characterizable decaphosphaferrocene complexes has been a challenge in the field of phosphorus-containing complexes.[2] In addition, the lower phosphorus-containing complexes with $[(RC)_nP_{5-n}]^-$ ligands (n = 1–3) are of particular interest since η^5-phospholyl complexes show activity in various homogeneous catalysis applications.[3,4,5] Among the series of ferrocene complexes with $[(RC)_nP_{5-n}]^-$ ligands (n = 0–5) the syntheses of **A**[6] and **E**[7] have been benchmarks in the development of polyphospholyl complex chemistry.[8]

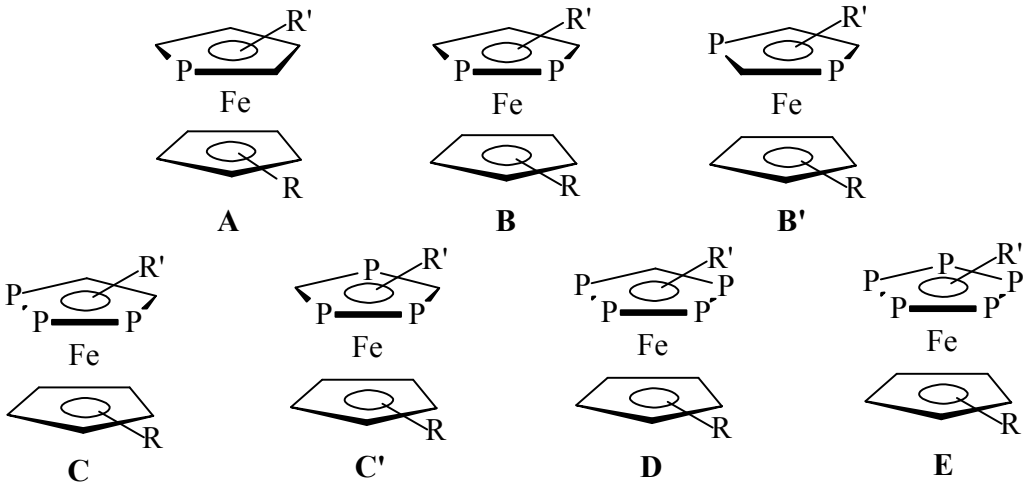

Other ferrocenes of type **B**[9] as well as **B'** and **C'**[10,11,12,13] were synthesized later using phosphaalkyne as starting material, the missing 1,2,3-triphosphaferrocene **C** was only recently synthesized by Scherer and coworkers by treating the tetraphosphabicyclobutadiene complex $[\{Cp'''(CO)_2Fe\}_2(\mu,\eta^1\text{:}\eta^1\text{-}P_4)]$ with diphenylacetylene.[14]

An electrochemical investigation of the polyphosphaferrocenes shows[15,16] that the replacement of CR fragments by phosphorus atoms in the phospholyl ring enhances the electron richness and thus increases the electron density at the iron center. This modification made the phosphaferrocenes more difficult to oxidize.

Unlike the simple metallocene analogues, the complexes of phosphaferrocene have ligating potential to transition metal centers with the ring phosphorus lone-pair electrons not only in π-ligation but also in η^1-or η^2-metal ligation.

The η^1-ligating behaviour of the triphosphaferrocene [CpFe(η^5-$P_3C_2{}^tBu_2$)] (**C´1**) towards several transition metal ligand (ML_n) centres (M = Cr, Mo, W, L = CO, *n* = 5; M = Fe, L = CO, *n* = 4) has been explored.[10,11,17,18] In all cases one of the two adjacent phosphorus atoms of the P_3C_2-ring is bonded to the metal center in the η^1-type with its lone pair electrons (Figure 1.1).

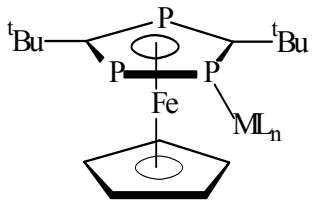

Figure 1.1. η^1-ligated complex involving one lone pair of electrons of the phosphorus atom.

Both lone pairs of electrons on the adjacent phosphorus ring atoms of [Cp*Fe(η^5-$P_3C_2{}^tBu_2$)] (**C´2**) can participate in the ligation to transition metals as shown in the tetrametallic dinickel(0) tetracarbonyl complex [{Cp*Fe(η^5-$P_3C_2{}^tBu_2$)}$_2$Ni$_2$(CO)$_4$] (**F**) in Figure 1.2[17].

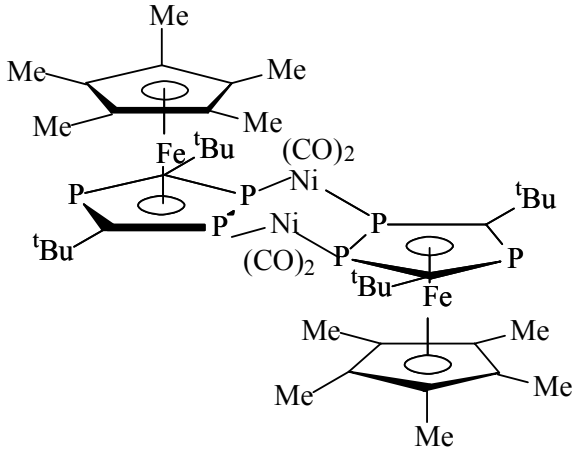

F

Figure 1.2. Complex **F** involving the lone pair electrons of the adjacent phosphorus atoms.

Another example is the η^2-ring-edge ligation of pentaphosphaferrocene to iridium(I) in compound **G** and the analogous Rh(I) complex **H** involving the pentaarsaferrocene.[19]

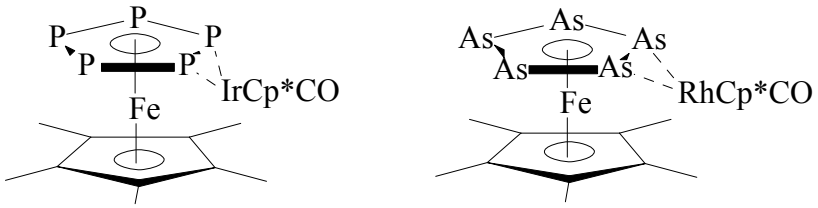

G **H**

Figure 1.3. Examples of η^2-ring-edge ligated complexes **G** and **H.**

The unusual bonding in these compounds was found to involve an η^2-ligation mode either through the P–P or As–As multiple bonds and an obvious elongation of P–P and As–As bond length in comparison to the uncoordinated compounds were resulted.

Very recently several square planar Pt(II) complexes such as $[PtCl_2(PEt_3)\{CpFe(\eta^5\text{-}P_3C_2{}^tBu_2\}]$ have been prepared by Nixon and coworkers. These complexes are non-fluxional in solution and they unexpectedly always exclusively give the cis- isomers[20] rather than the expected less sterically demanding trans isomers (Figure 1.4). Under some conditions both of the two adjacent phosphorus atoms in **C´2** can coordinate transition metal centers simultaneously such as the bis Pt(II) adduct *cis*, *cis*-$[\{PtCl_2(PMe_3)\}\mu\text{-}\{CpFe(\eta^5\text{-}P_3C_2{}^tBu_2)\}\{PtCl_2(PMe_3)\}]$ **I2,** which were obtained by Nixon and coworkers from further ligation of the other adjacent phosphorus atoms of the $\eta^5\text{-}P_3C_2{}^tBu_2$ ring in **I1**.

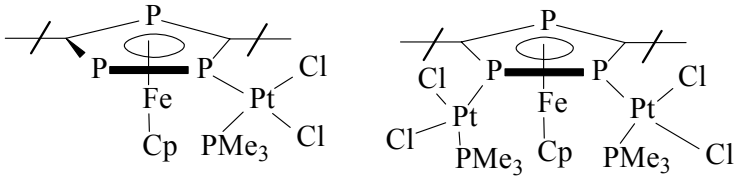

I1 **I2**

Figure 1.4. Two square planar Pt(II) complexes with cis conformations.

Except for the above-mentioned triphosphaferrocene, two other compounds containing "naked" P_n-ligands have been studied for their reactivity, properties, and coordination behaviour. The μ-P_2 complex $[\{CpMo(CO)_2\}_2(\mu,\eta^2\text{-}P_2)]$ (**J**) and the *cyclo*-P_5 complex

[Cp*Fe(η^5-P_5)] (**K**) (Figure 1.5) were prepared by the thermolysis of P_4 with the low-valent complexes $[CpMo(CO)_2]_2$ and $[Cp^*Fe(CO)_2]_2$, respectively.[21,22,23]

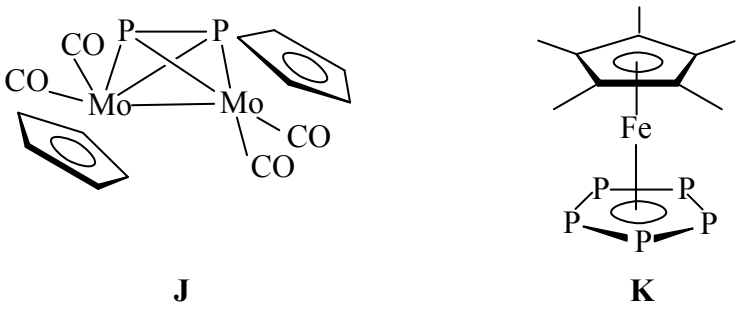

J **K**

Figure 1.5. Two examples of complexes with a "naked" P_n-ligand.

In our group the use of the P_2-ligand complex **J** in the coordination chemistry towards a cationic complex of Ag(I) and Cu(I) to form molecular dicationic complexes as well as the formation of 1D chain polymers was investigated.[24]

The reaction of $Ag(CF_3SO_3)$ and **J** in CH_3CN results in the quantitative formation of $[Ag_2\{Cp_2Mo_2(CO)_4(\mu,\eta^2{:}\eta^2\text{-}P_2)\}_2\{Cp_2Mo_2(CO)_4(\mu,\eta^2{:}\eta^1{:}\eta^1\text{-}P_2)\}_2][CF_3SO_3]_2$ (**L**), in which two tetrahedral Mo_2P_2 ligands bridge the two Ag(I) centers with an end-on mode whereas the other two Mo_2P_2 ligands coordinate these two silver centers with a side-on mode (Figure 1.6).

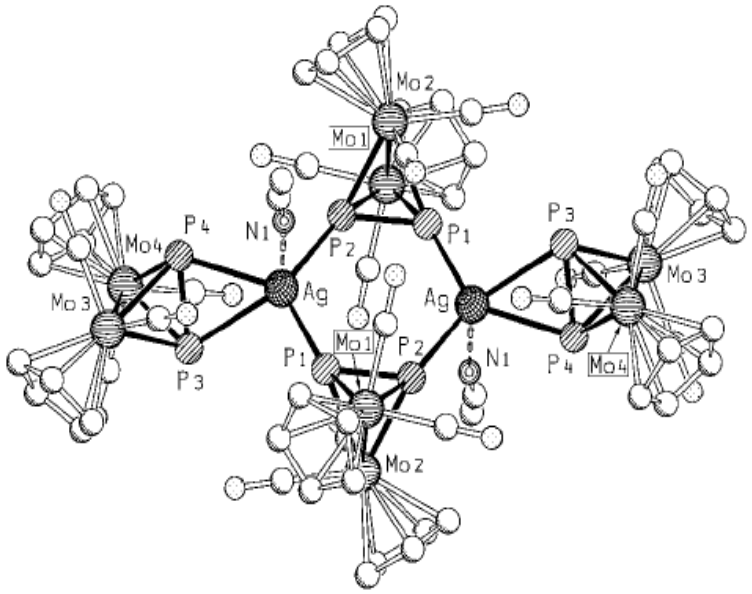

Figure 1.6. Molecular structure of the dianion from **L** (hydrogen atoms are omitted for clarity). [24]

The reaction of CuBr with **J** yields a linear 1D chain of $[Cu(\mu\text{-}Br)\{Cp_2Mo_2(CO)_4(\mu,\eta^2{:}\eta^1{:}\eta^1\text{-}P_2)\}]_\infty$ (**M**) consisting of planar six-membered Cu_2P_4 and four-membered Cu_2Br_2 rings, alternately arranged in an orthogonal manner (Figure 1.7).[24]

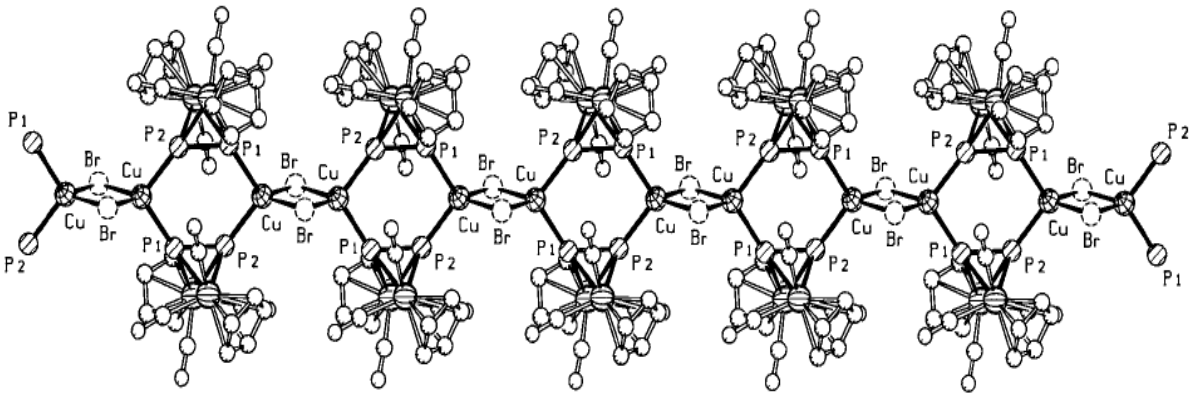

Figure 1.7. Section of the 1D polymer chain structure of **M** (hydrogen atoms are omitted for clarity). [24]

In the last decade O.J. Scherer and coworkers have intensively researched the reactivity of $[Cp^*Fe(\eta^5\text{-}P_5)]$ towards organometallic fragments. Besides its capacity to form cationic triple-decker complexes[25] or undergo P_5-transfer reactions,[26] there are reactions known in which the cyclo-P_5 ring remains intact, or is cleaved to form polymer chain. Other fragments such as P_4/P_1, P_3/P_2, and P_2 have been reported.[27, 28,29,30] In the case where the cyclo-P_5 ring remains intact, a significant lengthening of the P–P bonds was resulted in the $\eta^5{:}\eta^1$, $\eta^5{:}\eta^2$, and $\eta^5{:}\eta^2{:}\eta^2{:}\eta^1$ coordination modes to organometallic fragments.[19,31,32,33]

In our group the reactivity of $[Cp^*Fe(\eta^5\text{-}P_5)]$ with Cu(I) halides[34] has been investigated and it was found that with CuCl the 1D polymer $[CuCl\{Cp^*Fe(\eta^5{:}\eta^1{:}\eta^1\text{-}P_5)\}]_\infty$ (**N**) (Figure 1.8) is obtained. With CuBr and CuI, however, the corrugated 2D polymers $[CuX\{Cp^*Fe(\eta^5{:}\eta^1{:}\eta^1{:}\eta^1\text{-}P_5)\}]_\infty$ (X = Br (**O**), I (**P**)) (Figure 1.9), respectively, are obtained.

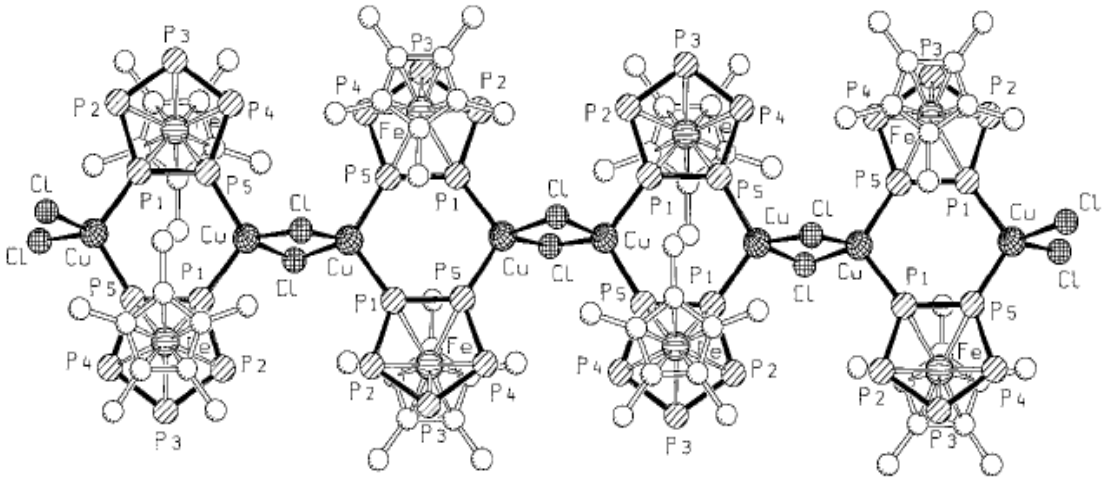

Figure 1.8. Section of the 1D chain structure of complex **N** (H atoms are omitted for clarity). [34]

In the crystal lattice of both **O** and **P**, the tetrahedrally distorted Cu(I) units coordinate to one halogen atom and three phosphorus atoms, each coming from three different [Cp*Fe(η^5-P_5)] fragments (Figure 1.9). Thus, a 1,3,4 substitution pattern at the cyclo-P_5 ring through an η^5:η^1:η^1:η^1 coordination mode is created because of the additional third coordination to the Cu(I)X moiety at the cyclo-P_5 rings in [CuX{Cp*Fe(η^5:η^1:η^1:η^1-P_5)}]$_\infty$ (X = Br (**O**), I (**P**)). When compared to structure **N**, novel 2D coordination polymers were formed with layers separated by Cp*Fe moieties.

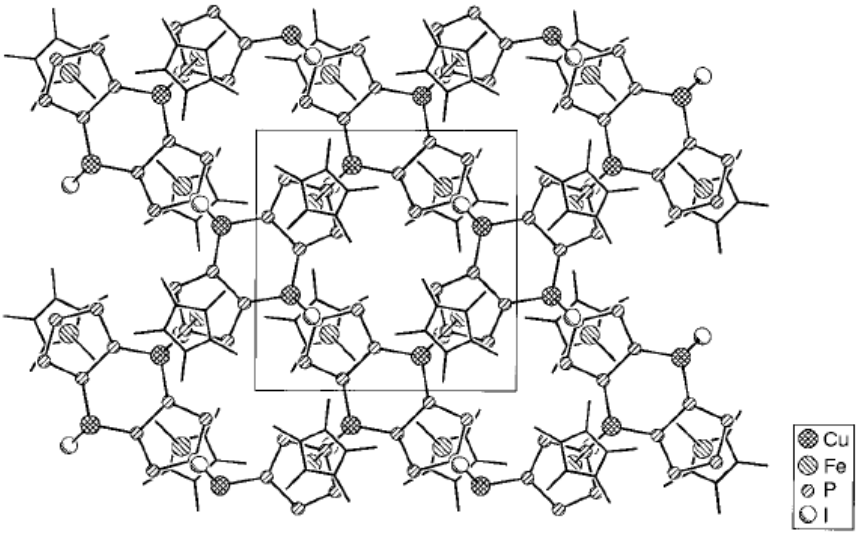

Figure 1.9. View of the layered 2D complex **P** orthogonal to the crystallographic a,b plane (H atoms are omitted for clarity). [34]

The Cu_2P_4 rings **O** and **P** are in a boat-like conformation, unlike the planar Cu_2P_4 rings in the 1D polymer of **N**. In comparison with the starting complex [Cp*Fe(η^5-P_5)] the P–P bond lengths of the complex $[CuX\{Cp^*Fe(\eta^5:\eta^1:\eta^1:\eta^1\text{-}P_5)\}]_\infty$ (X = Br, I) do not change. The tendency for the reaction of [Cp*Fe(η^5-P_5)] with CuCl on the one hand and CuBr/CuI on the other to yield products with different structures is difficult to explain. The CuCl product **O** contains linear chains that are separated from each other by π stacking between Cp* and cyclo-P_5 moieties of different chains, $[CuX\{Cp^*Fe(\eta^5:\eta^1:\eta^1:\eta^1\text{-}P_5)\}]_\infty$ (X = Br, I) to form 2D networks through additional metal coordination to the cyclo-P_5 rings rather than π stacking. [34]

When pentaphosphaferrocene was treated with CuCl, a spherical fullerene-like molecule containing 90 noncarbon core atoms complex $[\{Cp^*Fe\text{-}(\eta^5:\eta^1:\eta^1:\eta^1:\eta^1\text{-}P_5)\}_{12}\{CuCl\}_{10}\{Cu_2Cl\}_5\{Cu(CH_3CN)_2\}_5]$ (**Q**) was yielded.[35] When the stoichiometry of the starting materials and the concentration conditions change, it is possible to obtain exclusively soluble spherical molecules of the formula $[\{Cp^xFe(\eta^5:\eta^1:\eta^1:\eta^1:\eta^1\text{-}P_5)\}_{12}\{CuBr\}_{10}\{Cu_2Br_3\}_5\{Cu(CH_3CN)_2\}_5]$ (Cp^x = η^5-C_5Me_5 (**R**), η^5-C_5Me_4Et (**S**)) by reacting [Cp*Fe(η^5-P_5)] (**E**) with CuBr.

In complexes **R** and **S** all phosphorus atoms of the *cyclo*-P_5 ring of [Cp*Fe(η^5-P_5)] coordinate to the copper atoms of CuBr, which are further coordinated by phosphorus atoms of other *cyclo*-P_5 rings, leading to the formation of six-membered P_4Cu_2 rings around the central *cyclo*-P_5 ring (Figure 1.10a). The five- and six-membered ring alternation is similar to that seen in the fullerenes with the difference being due to the distorted tetrahedral coordination sphere of the Cu(I) ions. The six-membered rings are not planar, but folded along the Cu···Cu axis. The pseudo-hemispherically formed $[Cu_{10}Br_{10}\{Cp^xFe(\eta^5\text{-}P_5)\}_6]$ half-shells (Figure 1.10a) are joined by five $[Cu_2Br_3]^-$ and five $[Cu(CH_3CN)_2]^+$ units (Figure 1.10b).

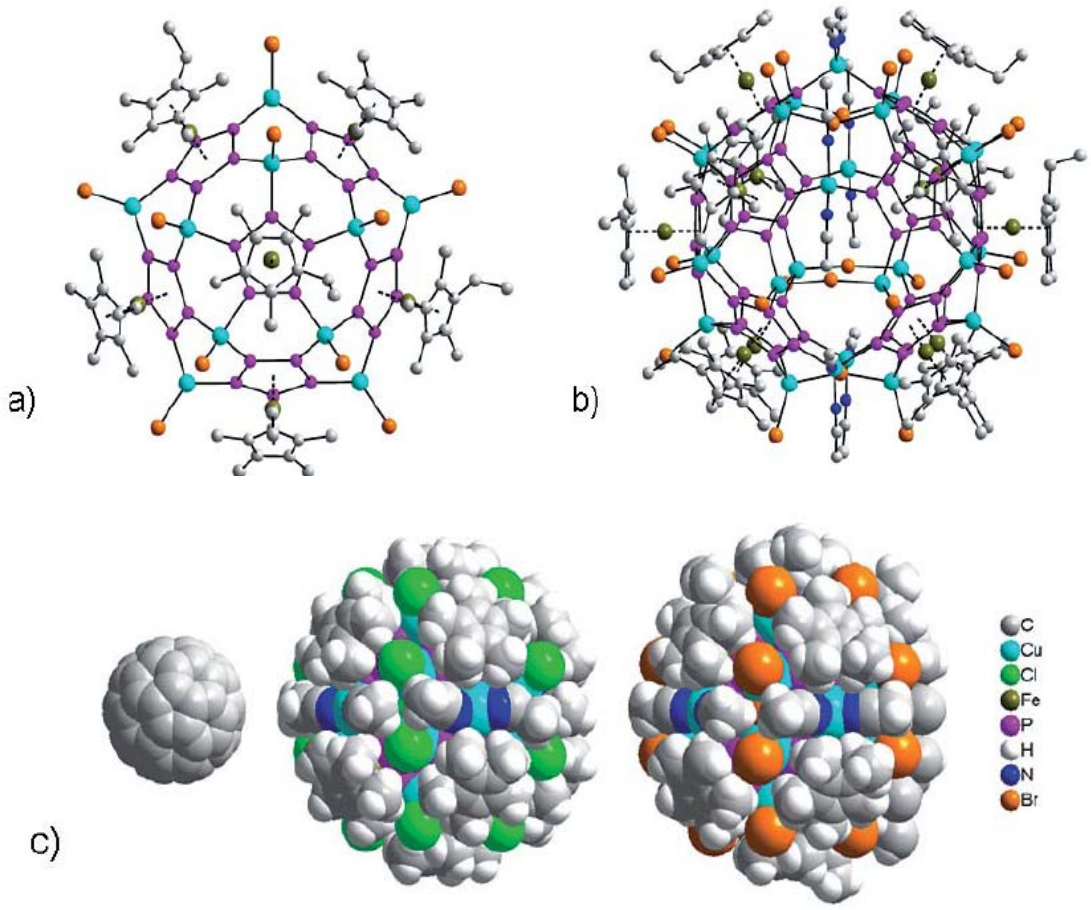

Figure 1.10 (a) View of a half shell of a molecule of **S**; (b) Complete ball-and-stick structure of a molecule of **S**; (c) Size comparison of the spherical molecules of C_{60}, **Q,** and **S** (space-filing model). [35]

In comparison with complex **Q,** the spherical bodies of **R** and **S** are slightly larger. Complex **S**, for example, has an inside 12.9 Å (**R**: 12.2 Å) and an outside 21.4/23.7 Å (**R**: 21.4 Å) diameter that is about three times larger than the C_{60} fullerene (Figure 1.10c).[36] While heterofullerenes are known containing only a few boron, nitrogen,[37] and phosphorus atoms,[38] the complexes **Q, R,** and **S** exhibit a complete heteroatom composition and therefore represent a novel class of fullerene-like molecules.

2. Research objectives

The discussed background presents many researched areas and introduces the unique position of P_n ligands complexes in supramolecular chemistry to form well defined spherical aggregates and networks as well as 1D and 2D polymers. It is substantive to continue investigating the chemistry of the phosphaferrocene as supramolecular building blocks with the modification of the $[(RC)_nP_{5-n}]$-ring (n = 0 – 2) by the replacement of one or more CR fragments by phosphorus atoms in the phospholyl ring and hydrogen atoms by the bulky *tert*-butyl groups in the cyclopentadienyl ring of the phosphaferrocenes. Characterization of the resulting aggregates with the assistance of various techniques including NMR spectroscopy, mass spectrometry, and X-ray crystallography is also appropriate. The objectives of this work were as follows:

- Synthesis and investigation of the properties of P-rich phosphaferrocene derivatives.
- Use of phosphaferrocenes including $[Cp'''Fe(\eta^5\text{-}P_3C_2{}^tBu_2)]$, $[CpFe(\eta^5\text{-}P_3C_2{}^tBu_2)]$, $[Cp'''Fe(\eta^5\text{-}P_3C_2PhH)]$, $[Cp'''Fe(\eta^5\text{-}P_4C{}^tBu)]$ and $[Cp'''Fe(\eta^5\text{-}P_5)]$ as building blocks with different transition metals to form novel supramolecular architectures.
- Study of the properties of the obtained complexes.

3. Results and discussion

The general goal lies in the use of P_n ligand complexes as linking units for the formation of supramolecular aggregates[35] such as 1D and 2D polymers and networks.[34] Thus, apart from the synthesis of 1,2,3-triphosphaferrocene[14] and pentaphosphaferrocene,[7] which were initially prepared by Scherer and coworkers, methods for 1,2,4-tri- and 1,2,3,4-tetraphosphaferrocene complexes by using bicyclo-tetraphosphine complex as starting material were developed.

3.1 Synthesis and studies of the properties of phosphaferrocenes

3.1.1. Synthesis and studies of the properties of [Cp'''Fe(η^5-P_4C^tBu)] and [Cp'''Fe(η^5-$P_3C_2{}^tBu_2$)]

A mixture of [{Cp'''$(CO)_2$Fe}$_2$(μ,η^1:η^1-P_4)] (**1**) and ^{t}BuC≡P in a ratio of 1:3 was stirred in toluene at 110 °C for 36 h. The color of this mixture changed from bright orange to brown during this time and the characteristic carbonyl band of **1** was not present in the IR-spectrum. The target complex was separated from its by-products by chromatographic methods (Equation 3.1).

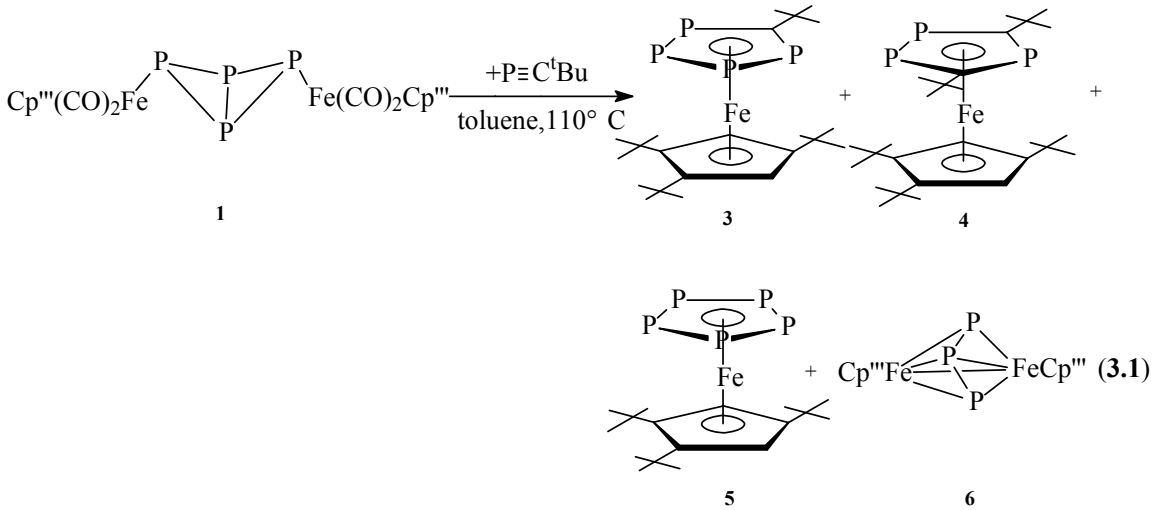

1 **3** **4** **5** **6** (**3.1**)

Cp''' = η^5-$C_5H_2{}^tBu_3$

In each of these thermolysis reactions a very broad signal appears in the $^{31}P\{^{1}H\}$ NMR spectrum of the reaction mixture at δ = 92 ppm ($\omega_{1/2}$ = 300 Hz), which suggests the presence of a polymeric product. The main products isolated are complexes **3** and **4**, whereas the known cyclo-P_5 complex **5**[39] and **6** could only be obtained in small amounts.[40] The yield and ratio of the products can be influenced by the reaction time. When the reaction mixture is stirred for about 24 h, the most abundant product is compound **3** and complexes **5** and **6** are not detected. When the mixture is stirred for 48 h, the yield of compound **4** is larger than that of **3** and the yield of compound **5** increases, too, while compound **6** is absent.

The structure of the main products suggests a P_3/P_1 fragmentation[41,42,43] of the bicyclo-tetraphosphine complex **1**. Similar observations were made for an indanyl-substituted derivative of **1** and 1-methylcyclohexylphosphaalkyne by Scherer and coworkers.[44] The crystals of complexes **3** and **5** are green and those of **4** are brown, whereas complex **6** forms red pink crystals. The compounds are readily soluble in toluene and CH_2Cl_2 and slightly soluble in nonpolar solvents, such as alkanes. They can be stored in a Schlenk tube under nitrogen at low temperature.

The structures, NMR and mass spectra of compounds **3** and **4** have been discussed previously[40] and will not be addressed further.

Complex **6** contains the first triphosphaallyl unit in a binuclear complex. Cyclo-P_3C_2 ligands[45,46] and organoallylic EtE_3 units (E = P, As)[47] were the only known phosphorus or allylic groups to bridge two metal centers until the present work.

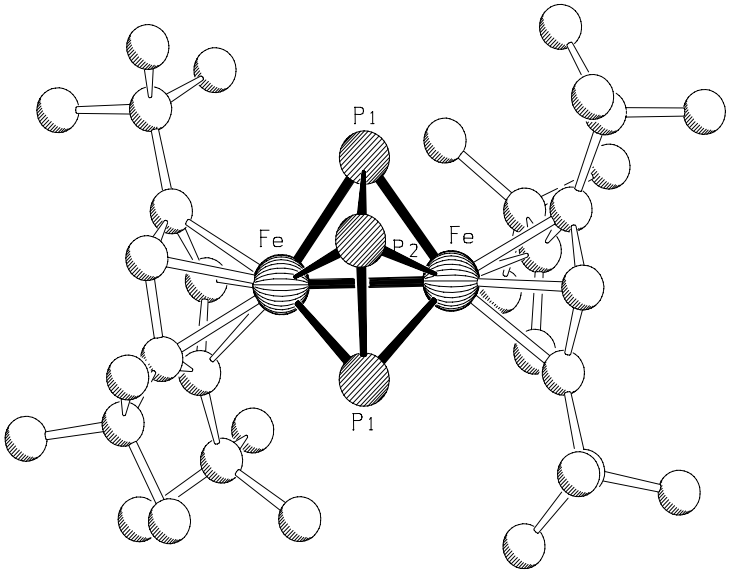

Figure 3.1.1. Molecular structure of **6** in the crystal (Hydrogen atoms are omitted for clarity). Selected bond lengths (Å) and angles (°): Fe–P1 2.2059(12), Fe–P2 2.4463(13), Fe–Fe 2.5893(11), P1–P2 2.1481(14), Fe–C1 2.102(3), Fe–C2 2.158(3), Fe–C3 2.102(4), Fe–C4 2.103(4), Fe–C5 2.104(4), C1–Fe–P1 125.95(11), C1–Fe–P2 108.35(11), P1–Fe–Fe 53.91(4), P1–P2–P1 100.66(8), P1–P2–Fe 56.95(4), Fe–P2–Fe 63.91(4).

In the ^{1}H NMR spectrum of compound **6** there are two singlets. The singlet at δ = 1.30 ppm represents two chemically and magnetically equivalent *tert*-butyl groups and the one at δ = 1.21 ppm arises from the third *tert*-butyl group on the Cp'''-Ring.

The ^{31}P NMR spectrum shows two groups of signals representing an AA'M spin system, which is similar to that of compound **4**. The triplet at δ = -380.9 ppm belongs to the P_M atom and the two P_A and P_A' atoms show their signal in the form of doublet at δ = 677.8 ppm. The $^{2}J(P_A,P_M)$ coupling constant is 390.2 Hz and that of $^{2}J(P_M,P_M')$ is 32.6 Hz.

The molecular structure of **6**[48] (Figure 3.1.1) reveals a cis orientation of the Cp''' groups, whereas the allylic P_3 unit is directed away from the Fe–Fe axis. The P–P bond length of the allylic P_3 moiety is 2.148(1) Å and thus shorter than a single bond and slightly longer than the P–P double bond of the EtP_3 unit in $[\{(tripod)Co\}_2(\mu,\eta^3\text{-}EtP_3)]$ (2.110 Å; tripod = $CH_3C(CH_2PPh_2)_3$).[47] The distance between the Fe atoms (2.589 (1) Å) is in the same range as those of various $[\{Cp'Fe(CO)_2\}_2]$ complexes.[49] Since the electronic structure of **6** was not clear upon initial inspection, density functional theory (DFT) calculations were performed. Theoretical methods have proven to be a useful tool in analyzing the structure

and properties of phosphorus-containing transition-metal complexes.[1,2,50] Calculations were performed on the original complex **6** to analyze the steric influence of the bulky ^{t}Bu groups (compound **6a** has H atoms in place of the ^{t}Bu groups found in **6**). Structure optimizations on **6** and **6a** confirm close-lying low-spin doublet states (Table 3.1.1) with an unpaired electron delocalized over the d orbitals of both Fe atoms. Comparison of the results obtained for **6** and **6a** indicates that the steric repulsion between the ^{t}Bu groups has an important influence on the electronic structure. For **6a,** calculations yielded two almost degenerate $^2A_2$ and $^2B_1$ states with the latter one being slightly less stable. These two states differ by the occupancy of the a_2 and b_1 orbitals, which are composed of d_{xz} and d_{xy} orbitals of the Fe and Fe' atoms (with both Fe atoms located on the y axis).

Table 3.1.1. Comparison of the relative energies of different electronic states ΔE[kJ/mol] and selected structural parameters ([Å], [°]) for the central Fe_2P_3 unit of compounds **6a** and **6** (BP86 calculations).

	6a (C_{2v})[a]		**6** (C_2)[a]		exp
	$^2A_2$	$^2B_1$	^2A	^2B	
ΔE	-3.2	0.0	9.1	0.0	
Fe–Fe′	2.483	2.741	2.640	2.832	2.589
Fe–P1	2.215	2.192	2.219	2.202	2.225
Fe–P′1	2.215	2.192	2.215	2.196	2.206
Fe–P2	2.488	2.361	2.481	2.365	2.446
Fe–C	2.114–2.126	2.093–2.120	2.090–2.166	2.080–2.157	2.102–2.158
P2–P1(1′)	2.189	2.272	2.191	2.263	2.148
P1–P2–P1′	99.89	94.46	97.99	93.40	100.71
Fe–P1–Fe′	68.18	77.40	73.07	80.19	71.51
Fe–P2–Fe′	59.86	70.95	64.28	73.57	63.92

[a] Symmetry point group

The $(b_1)^2(a_2)^1$configuration of the $^2A_2$ state facilitates a weak Fe–Fe′ bond interaction. Promoting one electron from the b_1 to a_2 orbital results in the $^2B_1$ state ($(b_1)^1(a_2)^2$), which weakens the Fe···Fe' interaction and facilitates the $P_3 \rightarrow$Fe π donation. In **6** the stability of the ^2A and ^2B states, which correspond to the $^2A_2$ and $^2B_1$ states of **6a**, respectively, is reversed. The ^2A state is now less stable because of the stronger Fe–Fe' interaction which results in a higher repulsion between bulky Cp'''-ligands.

To rationalize the differences between different states of **6** and **6a** an atoms-in-molecules (AIM)[51] topological analysis of the electronic charge density for both systems (Figure 3.1.2) was performed. The bonding of the ^2B state of **6** is similar to the $^2B_1$ state of **6a**. The

^2A and $^2A_2$ states, however, differ because of the absence of the Fe–Fe' bond in **6**, which is a result of the repulsion between the bulky ^{t}Bu groups.

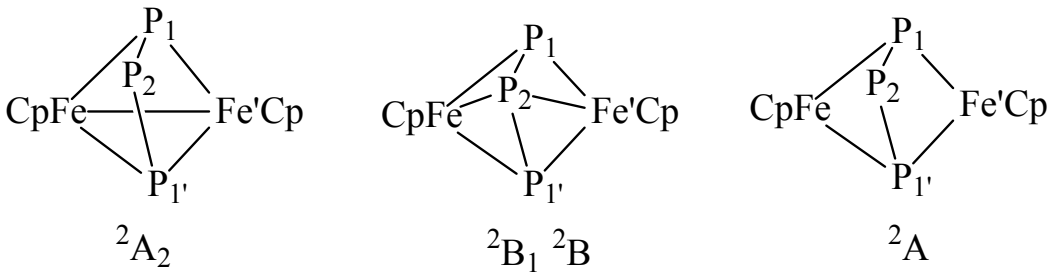

Figure 3.1.2. Bonding schemes of the compounds **6a** ($^2A_2$ and $^2B_1$ states) and **6** (^2A and ^2B states) from the AIM analysis of electronic charge densities (Cp denotes η^5-C_5H_5 in **6a** and η^5-$C_5H_2{}^tBu_3$ in **6**).

The structural parameters calculated for the slightly less stable ^2A state of **6** are in better agreement with experimental data than those calculated for the ^2B state. Thus, the $\mu,\eta^2{:}\eta^2$-coordination of the allylic P_3 ligand is the most probable one. Results obtained for **6** and **6a** show that the weak Fe···Fe' interaction and repulsion between the bulky ^{t}Bu groups are two competing effects. The DFT method may not be accurate enough to properly describe the balance of the two interactions. The energy difference between the two states is certainly within its margin for error. The delocalization of the unpaired electron over both Fe atoms is the reason that signals for an AA'M spin system are observed in the ^{31}P NMR spectrum of **6**, however, the paramagnetism might cause the large chemical shift differences in both signals, which is especially pronounced for the P1 and P1' atoms.

3.1.2. Synthesis and studies on the properties of [Cp'''Fe(η^5-P_3C_2PhH)]

According to the synthetic procedure developed by Scherer and coworkers,[44] the mixture of [{Cp'''$(CO)_2$Fe}$_2$($\mu,\eta^1{:}\eta^1$-P_4)] **1** and PhC≡CH in a ratio of 1:3 was stirred in toluene at 110°C for 36 h. The reaction mixture was separated by column chromatography, which yielded a red (**8**) and a green fraction (**9**) (Equation **3.2**).

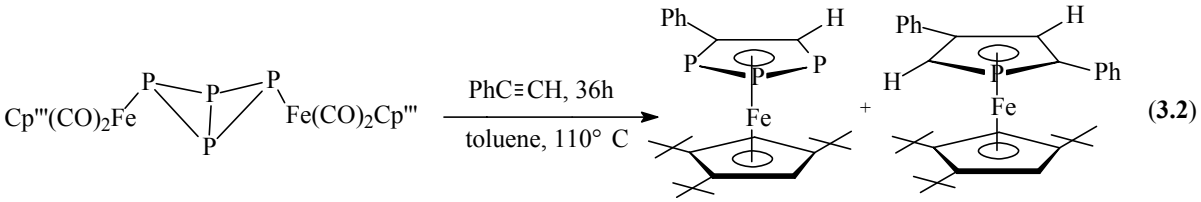

1 **8** **9**

The oily compound [Cp'''Fe(η^5-P_3C_2PhH)] (**8**) dissolves readily in CH_2Cl_2, THF, and in nonpolar solvents such as alkanes. It can be stored under an inert atmosphere at ambient conditions.

The five-membered P_3C_2-ring of the sandwich complex **8** is composed of a P_3 moiety originating from the butterfly complex **1** and PhC≡CH. The phosphorus atoms in this P_3C_2-ring assume the 1, 2 and 3 positions. The related complexes [$Cp^RFe(\eta^5$-$P_3C_2Ph_2)$] (R = Cp''', $^iPr_5C_5$) were prepared and studied by Scherer and coworkers.[14]

In the EI-MS of compound **8** the molecular ion [Cp'''Fe(η^5-P_3C_2PhH)]$^+$ was found. Furthermore, fragments such as [Cp'''Fe(P_2C_2PhH)]$^+$ and [Cp'''Fe($P_2C_2H_2$)]$^+$ were also detected.

The ^{1}H NMR spectrum of **8** displays eight signals. The protons on the three *tert*-butyl groups give rise to the singlets at δ = 1.09, 1.12, and 1.41 ppm and the two protons (H_b and H_c) on the cyclopentadiene ring to two doublet of doublets at δ = 4.00 and 4.19 ppm. The doublet of doublet of doublets at δ = 6.24 ppm is assigned to the proton (H_a) on the P_3C_2-ring. The last two multiplets at δ = 7.07 and 7.80 ppm are attributable to the protons on the phenyl group. From the ^{31}P, ^{1}H coupled NMR spectrum the coupling constant of $J(H_a,P_{A'})$ = 40.08, $J(H_a,P_M)$ = 10.81 and $J(H_a,P_A)$ = 4.52 Hz were obtained (Figure 3.1.3).

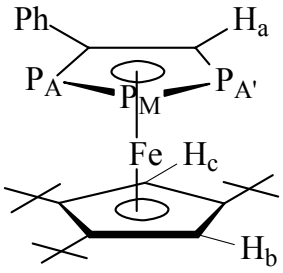

8

Figure 3.1.3. Molecular structure of compound **8**.

In the $^{31}P\{^{1}H\}$ NMR spectrum of **8** three signal groups of doublet of doublets which representing an AA'M spin system were detected. The signal at δ = 51.7 ppm is attributable to the P_A atom with a coupling constant $J(P_A,P_M)$ = 427.4 Hz and $J(P_A,P_{A'})$ = 4.4 Hz, the signals at δ = 48.9 ppm with $J(P_M,P_{A'})$ = 399.6 Hz belong to the $P_{A'}$ and those at δ = 15.2 ppm represent the P_M in the P_3C_2-ring.

Compound **9** is an air sensitive green solid. It dissolves readily in CH_2Cl_2, THF, and nonpolar solvents such as alkanes. It can be stored under an inert atmosphere at ambient conditions.

The EI-MS of compound **9** revealed the molecular ion $[Cp'''Fe(\eta^5\text{-}PC_4Ph_2H_2)]^+$. In addition, peaks corresponding to the cation $[Cp'''Fe(C_4Ph_2H_2)]^+$ with highst relative abundance and to the cation $[(C_5H_3{}^tBu{}^iPr)Fe(PC_4Ph_2H_2)]^+$ were detected.

For compound **9** one can assume three possible isomeric structures (Figure 3.1.4). For the isomer **9c**, a triplet would be expected in the proton-coupled ^{31}P NMR spectrum, whereas isomer **9b** would be expected to display either a triplet or a singlet, depending on whether the *ortho*-protons on the two neighboring phenyl groups couple to the phosphorus atom or not. Finally, isomer **9a** would be expected to display either a doublet, due to coupling with H_a, or a doublet of doublets, due to coupling with H_a and the *ortho*-protons of the phenyl group at the 2-position. The ^{31}P NMR spectrum of complex **9** does, in fact, display a doublet of doublets at δ = -64.1 ppm ($J(P,H_a)$ = 35.6 Hz; $J(P,H)$ = 4.9 Hz) and therefore it can be inferred that complex **9** adopts the structure **9a**.

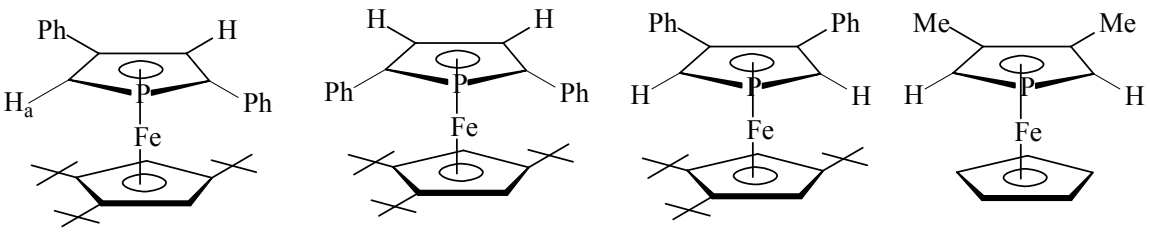

9a **9b** **9c** $[CpFe(\eta^5\text{-}PC_4Me_2H_2)]$

Figure 3.1.4. Possible isomeric structures of compound **9** and the molecular structure of $[CpFe(\eta^5\text{-}PC_4Me_2H_2)]$.

The arrangement of the phenyl groups in the PC_4-ring of **9** (2 and 4 positions) is thus in contrast to that of the methyl groups in the PC_4-ring of the similar phosphaferrocene $[CpFe(\eta^5\text{-}PC_4Me_2H_2)]$ (positions 3 and 4), prepared by Mathey and coworkers.[52,53] The reason for this may be due to the steric demand of the relatively bulky phenyl groups in **9**.

3.1.3. Synthesis and studies on the properties of [Cp'''Fe(η^5-P_5)]

A mixture of [{Cp'''$(CO)_2$Fe}$_2$] and white phosphorus (P_4) in a ratio of 1:1 was refluxed in decalin at 188 °C for 3 h.[39] The color of the reaction mixture changed from bright orange to greyish green during the stirring. Afterwards the reaction mixture was separated by column chromatography and a green fraction of **5** was yielded (Equation 3.3).

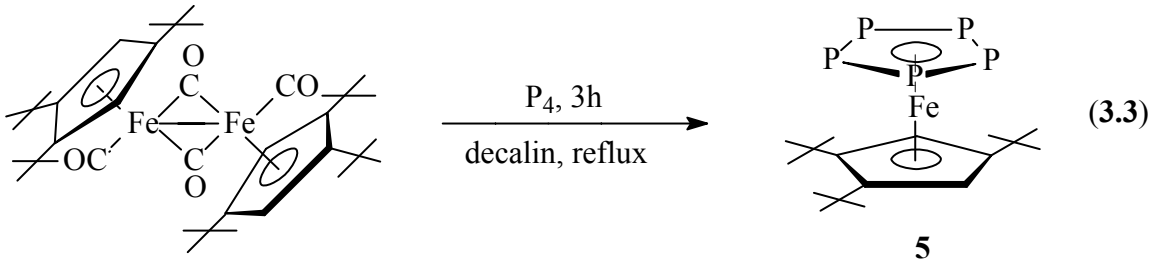

5 (**3.3**)

The green complex [Cp'''Fe(η^5-P_5)] (**5**) dissolves readily in CH_2Cl_2, THF, and is soluble in nonpolar solvents such as alkanes. It can be exposed to air for a short time and stored under an inert atmosphere at ambient conditions.

In the EI-MS of compound **5** the molecular ion [Cp'''Fe(η^5-P_5)]$^+$ was found. Furthermore, fragment attributable to the cation [Cp'''Fe(P_3)]$^+$ was also detected.

The ^{1}H NMR spectrum of compound **5** shows three signal groups: the peak at δ = 3.95 ppm represents two protons on the cyclopentadiene ring while the two singlets at δ = 1.08 and 1.21 ppm correspond to the protons of the *tert*-butyl groups on the cyclopentadiene ring.

As expected a singlet was also observed at δ = 165.4 ppm in the ^{31}P{^{1}H} NMR spectrum.

3.2. Study of the chemical properties and coordination behaviour of polyphosphaferrocenes

3.2.1. Triphosphaferrocene [Cp'''Fe(η^5-$P_3C_2{}^tBu_2$)] as a ligand

Different triphosphaferrocenes [Fe(η^5-$P_2C_3{}^tBu_3$)(η^5-C_5R_5)] (R = H, Me) as ligands to prepare triphosphaferrocene transition metal carbonyl complexes were studied by Nixon and coworkers. It was observed that the first coordinating site involved one of the two adjacent phosphorus atoms in the P_3C_2 ring. Typical examples are [$W(CO)_5${CpFe(η^5-$P_3C_2{}^tBu_2$)}][11] and [$M(CO)_n${Cp*Fe(η^5-$P_3C_2{}^tBu_2$)}] (M = Cr, Mo, or W, n = 5).[10,18]

In the solid-state structure of [{Cp*Fe(η^2,η^5-$P_3C_2{}^tBu_2$)}{Cp*Rh(CO)}], the [Cp*Rh(CO)] fragment is η^2-ligated to the P–P edge of the cyclo-P_3C_2 ring and the P–P bond lengh elongates, by which the P–P bond order decreases because of the back donation from the appropriate d-orbitals of the Rh(I) center to the ring π^* orbitals.[54]

Interestingly, in complexes [{Cp*Fe(η^5-$P_3C_2{}^tBu_2$)}{$M(CO)_5$}] the [$M(CO)_5$] fragment undergoes a rapid 1,2-shift between the two adjacent P atoms of the cyclo-P_3C_2 ring in solution as indicated by their $^{31}P\{^1H\}$ NMR spectra (Figure3.2.1).

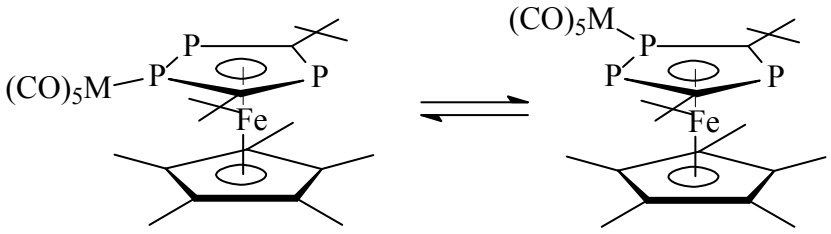

M = Cr, Mo, or W, n = 5

Figure 3.2.1. 1,2-shift between the two adjacent P atoms of the cyclo-P_3C_2 ring in [{Cp*Fe(η^5-$P_3C_2{}^tBu_2$)}{$M(CO)_5$}].

In the present work, the triphosphaferrocenes [Cp'''Fe(η^5-$P_3{}^tBu_2C_2$)], [CpFe(η^5-$P_3{}^tBu_2C_2$)] and [Cp'''Fe(η^5-P_3C_2PhH)] were used to ligate CuX (X = Cl, Br, I) as well as Ag(I) and Au(I) salts. Different substitution pattern of the triphospholyl ring and the cyclopentadiene ring can influence the ligation properties of selected transition metals and the stability of the triphospholyl ring.

3.2.1.1. Reaction of [Cp'''Fe(η^5-$P_3C_2{}^tBu_2$)] with CuCl

3.2.1.1.1. [Cp'''Fe(η^5-$P_3C_2{}^tBu_2$)] with CuCl in a stoichiometric ratio of 1:1

Since the two adjacent phosphorus atoms in the cyclo-P_3C_2 ring of the triphosphaferrocene can ligate to transition metal centers in an end-on or side-on mode, it is reasonable to use Cu(I) salts to form complexes and it is expected, with the coordination feature of Cu(I), that different oligomers and polymers should be formed.

A solution of CuCl in acetonitrile was carefully layered onto a solution of [Cp'''Fe(η^5-$P_3C_2{}^tBu_2$)] (**4**) in CH_2Cl_2 in a 1:1 stoichiometric ratio at room temperature. Thus the air-sensitive dark red crystalline dimeric copper complex [{Cp'''Fe(η^5:η^1:η^1-$P_3C_2{}^tBu_2$)}(μ-CuCl)]$_2$ (**10**) were obtained, in which two phosphaferrocenes bridge two CuCl units (equation 3.4).

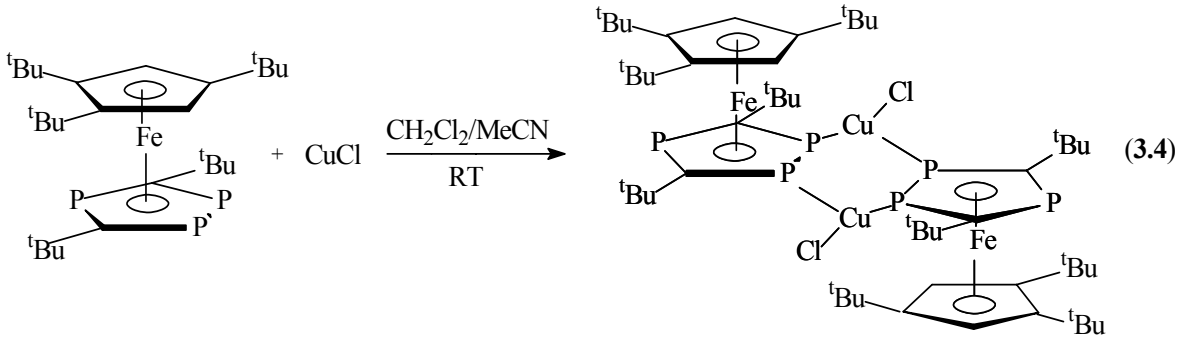

(3.4)

10

The red crystalline compound **10** is only sparingly soluble in polar solvents such as CH_2Cl_2, CH_3CN, and THF; it is insoluble in less polar solvents like toluene and hexane. It is air sensitive and can be stored under an inert atmosphere at ambient conditions.

In the ESI-MS of compound **10** in MeCN the molecular ion is not found, but appropriate fragments such as [{Cp'''Fe($P_3C_2{}^tBu_2$)}$_2$$Cu_2Cl$]$^+$, [{Cp'''Fe($P_3C_2{}^tBu_2$)}$_2$Cu]$^+$ and [{Cp'''Fe($P_3{}^tBu_2C_2$)}CuMeCN]$^+$ were detected. These peaks suggest that the dimeric copper complex exists in solution.

In the ^{1}H NMR spectrum of the reaction mixture there are two singlets at δ = 0.9 and 1.0 ppm, representing the protons of the ^{t}Bu groups on the Cp''' ring. The singlet at δ = 1.1 ppm belongs to the protons of the two ^{t}Bu groups on the P_3C_2-ring; and the singlet at δ = 4.1 ppm represents the two protons on the Cp''' ring. All these peaks are shifted upfield in comparison to the uncoordinated triphosphaferrocene **4** (δ = 1.24, 1.25, 1.36, and 4.6 ppm).

The $^{31}P\{^1H\}$ NMR spectrum of the reaction mixture represents an AM_2 spin system with a triplet peak at 52.8 ppm and a broad signal at 27.6 ppm with a line width at half height ($\omega_{1/2}$) of 90 Hz. The $^2J(P_AP_M)$ coupling constant is 44.2 Hz and is comparable to that of the starting material **4** (43.9 Hz). The comparison with the phosphorus chemical shifts of the free complex **4** ($\delta(P_A)$ = 52.9 ppm and $\delta(P_M)$ = 43.2 ppm) shows an upfield shift from the coordination of the lone pairs of the adjacent phosphorus atoms in the cyclo-P_3C_2 ring to copper atoms that also cause a broad signal while the chemical shift of the P_A-atom remains almost unchanged. The broad signal at $\delta(P_M)$ = 27.6 ppm shows there is no detectable coupling between the phosphorus and the copper centers.

Complex **10** crystallizes in the monoclinic space group $P2_1/n$. The structure was determined by single-crystal X-ray diffraction as illustrated in Figure 3.2.2.

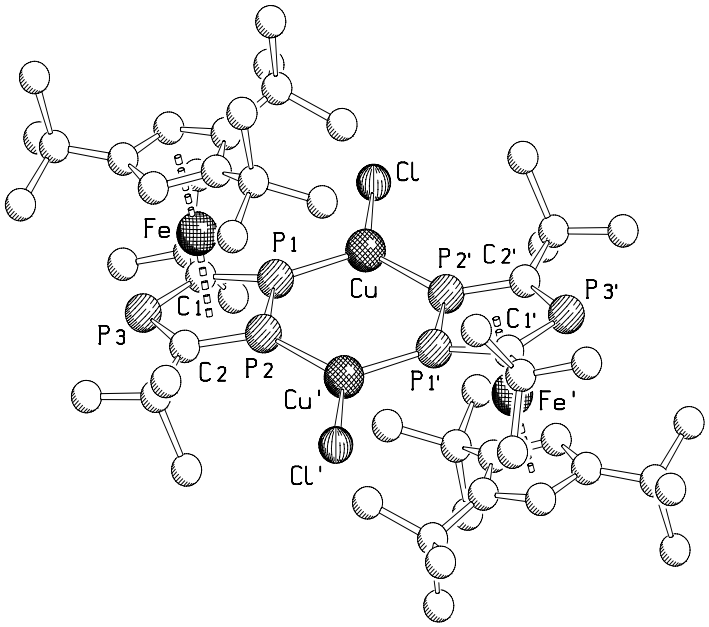

Figure 3.2.2. Molecular structure of $[(CuCl)_2\{Cp'''Fe(\eta^5{:}\eta^1{:}\eta^1\text{-}P_3{}^tBu_2C_2)\}_2]$ (**10**) in the crystal (H atoms are omitted for clarity). Selected bond lengths (Å) and angles (°): P1–P2 2.0717(19), P1–Cu 2.1057(13), P2–Cu 2.2804(13), P1–C1 1.751(4), P2–C2 1.705(4), P3–C1 1.670(5), P3–C2 1.792(5), P1–Fe 2.3346(14), P2–Fe 2.4568(14), P3–Fe 2.3009(13), Cu–Cl 2.1539(19), C1–Fe 2.266(5), C2–Fe 2.249(4), Cu–P1–P2 121.40(6), P_1–P2–Cu 124.14(6), P1–Cu–P2 114.20(6), P2–P1–C1 104.91(18), P1–P2–C2 95.72(18), P1–Fe–P2 51.16(5), P1–P2–Fe 61.37(5), C1–P3–C2 102.0(2), P2–Cu–Cl 126.60(6), P1–Cu–Cl 119.15(6).

Compound **10** consists of two triphosphaferrocene units which bridge two CuCl fragments *via* the two adjacent phosphorus atoms in the $P_3C_2{}^tBu_2$ ring system, thus forming a six-membered ring. The two copper atoms lie above and below the plane defined by the phosphorus atoms P1, P2, P1´ and P2´ (deviation of copper atoms from P1P2P1´P2´ plane = 0.100(1) Å). This arrangement of the two copper centers is different to that of the similar compound $[\{Cp^*Fe(\eta^5{:}\eta^1{:}\eta^1\text{-}P_3{}^tBu_2C_2)\}\{Ni(CO)_2\}]_2$ (**F**, Figure 1.2), in which the six-membered ring consisting of four phosphorus and two nickel atoms exhibits a boat configuration.[17, 54]

The coordination geometry of the copper atoms in **10** is trigonal planar with an average P–Cu–Cl angle of 122.88(6)° and two different P–Cu bond lengths of 2.1057(13) Å and 2.2804(13) Å. The P–P bond length (2.707(19) Å) in **10** is shorter than that in the uncoordinated triphosphaferrocene (2.121(3) Å), indicating that the two adjacent phosphorus atoms participate in η^1-bonding to the Cu atoms through the phosphorus lone pairs. In comparison, the elongation of the P–P bond lengths in $[Cp^*RhCO\{CpFe(\eta^5\text{-}P_3C_2{}^tBu_2)\}]$ arises from the back bonding of the rhodium d orbitals to the ring π^* orbitals.[54]

3.2.1.1.2. $[Cp'''Fe(\eta^5\text{-}P_3C_2{}^tBu_2)]$ with CuCl in a stoichiometry ratio of 1:2

A triphosphaferrocenic oligomer is formed when phosphaferrocene reacts with copper chloride in a 1:1 ratio. It is interesting to see whether a different complex will result when more than one equivalent of copper chloride is used.

Direct mixing of CuCl and **4** in a ratio of 2:1 in a mixture of acetonitrile and CH_2Cl_2 at room temperature forms a brown powder, which could not be satisfactorily characterised, but when two equivalents of CuCl in an acetonitrile solution was layered onto a CH_2Cl_2 solution of **4** at room temperature, the dark brown crystalline $[\{(Cp'''Fe)_2(\mu,\eta^4{:}\eta^1{:}\eta^1\text{-}P_4)\}\{(\mu\text{-}CuCl)_2(MeCN)\}]_n$ (**11**) was formed after four weeks (equation 3.5). The P_3C_2-ring of **4** was fragmented to form a new triple-decker unit $[\{(Cp'''Fe)_2(\eta^4\text{-}P_4)\}]$ during the course of the reaction. This triple-decker unit coordinates readily to copper atoms to give a one-dimensional coordination polymer.

Monomeric triple-decker compounds [{($Cp^RFe)_2(\eta^4$-$P_4)$}] (R = 1,3-$(Me_3Si)_2C_5H_3$ and 1,3,4-$(Me_3Si)_3C_5H_2$) resulting from the reaction of [$Cp^RFeBr(CO)_2$] and NaP_5 were reported by Hey-Hawkins and coworkers.[55]

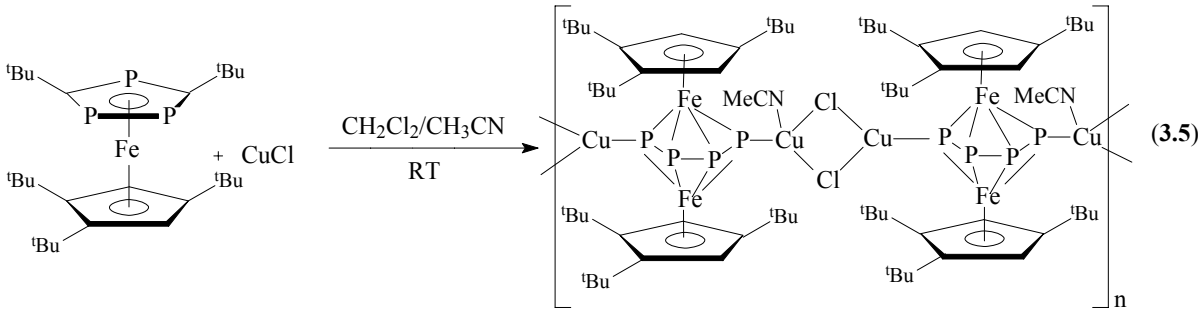

4 **11** **(3.5)**

The polymeric compound **11** dissolves sparingly in DMF, and is insoluble in common solvents such as CH_2Cl_2, THF, and hexane. It is air sensitive and can be stored under an inert atmosphere at ambient conditions.

The most abundant ion found in the ESI-MS spectra of complex **11** in MeCN at room temperature is the $[(Cp'''Fe)_2(\eta^4\text{-}P_4)]^+$ cation. In addition, a peak was detected corresponding to the $[\{(Cp'''Fe)_2(P_4)\}Cu_2]^{2+}$ cation confirming the existence of the metal coordinated triple-decker unit. In EI-MS spectrum the peak attributing to the $[(Cp'''Fe)_2(\eta^4\text{-}P_4)]^+$ cation with 100% relative abundant was also detected. This indicates that the triple-decker $[(Cp'''Fe)_2(\eta^4\text{-}P_4)]$ moiety is very stable.

Due to its poor solubility, complex **11** was difficult to characterise by NMR, but adequate solubility for the mother liquor was observed.

The ^1H NMR spectrum of the mother liquor shows three peaks. The signal at δ = 4.60, reveals the two protons on the Cp'''-ring and the singlets at δ = 1.16 and 1.11 ppm represent the three ^{t}Bu-groups on the Cp'''-ring, respectively.

There are two broad signals in the $^{31}P\{^1H\}$ NMR spectrum of the reaction mixture of **11**. One signal at δ = 66.5 ppm may be attributed to two phosphorus atoms in the middle of the $[\{(Cp'''Fe)_2(\mu,\eta^4\text{:}\eta^1\text{:}\eta^1\text{-}P_4)\}]$ moiety with a line width at half height ($\omega_{1/2}$) of 510 Hz; the other signal at δ = 113.5 ppm ($\omega_{1/2}$= 610 Hz) may be assigned to the two phosphorus atoms at the end of the P_4 skeleton. The latter chemical shift is downfield in comparison with that of the two phosphorus atoms in the middle of the P_4 moiety due to coordination of the copper atoms to the two phosphorus atoms.

Table 3.2.1. $^{31}P\{^{1}H\}$ NMR spectra of **4** and its copper complexes in different solvents. For the reaction of **4** with CuBr and CuI, respectively will be compared in chapter 3.2.1.2.

Mother liquor of the reaction	Solvent	$\delta(P_A)$ (ppm)	$\delta(P_M)$ (ppm)	$J(P_A,P_M)$ (Hz)	„Phosphabut-adiene“ (ppm)	
Starting material **4**	CD_2Cl_2	53.2	41.2	43.9		
	CD_2Cl_2/MeCN: 6:1	53.1	41.0	44.0		
	CD_2Cl_2/MeCN: 3:1	53.0	40.9	44.0		
	CD_2Cl_2/MeCN: 2:1	53.0	40.8	44.0		
	THF-d_8/MeCN: 3:1	54.6	43.1	44.0		
	C_6D_6	52.8	43.0	43.8		
4 + CuCl (1:1)	THF-d_8/MeCN: 3:1	52.8	27.6(br)	44.2		
4 + CuBr (1:1)	CD_2Cl_2/MeCN: 3:1	50.4	28.7(br)	44.7		
	THF-d_8/MeCN: 3:1	51.6	28.4(br)	44.7		
4 + CuCl (1:2)	CD_2Cl_2/MeCN: 3:1	51.9	37.2	43.8	115.6	69.1
	C_6D_6/CH_2Cl_2/MeCN:2:1:1	51.6	37.4	44.5	113.5	66.5
4 + CuBr (1:2)	CD_2Cl_2/MeCN: 3:1	52.8	41.4	43.9	120.6	76.2
4 + CuI (1:2)	C_6D_6/DMF: 1:2	51.8	39.1	44.1	118.4	72.9

The $^{31}P\{^{1}H\}$ NMR spectrum of the mother liquor shows two additional signals, one triplet at δ = 51.6 ppm and one doublet at δ = 37.4 ppm. According to the $^{31}P\{^{1}H\}$ NMR study of triphosphaferrocene and its copper complexes in different solvents (Table 3.2.1), the chemical shift of the triplet signal and coupling constant of these phosphorus spectra are similar to that of the uncoordinated compound **4**. A small difference in chemical shift of the doublet signal in the NMR spectrum in comparison with the starting material indicates that a weak interaction between the Cu(I) species and the two adjacent phosphorus atoms in the cyclo-P_3 ring of the starting material **4** may exist in the solution. The integration ratio of these signals at δ = 66.5, 113.5, 51.6, and 37.4 (4:4:1:2) matches the ratio of polymer **11** and that of the starting material (2:1). There is no ^{31}P NMR spectroscopic evidence of the missing $^{t}Bu_2C_2P$ fragment after the formation of the tetraphosphabutadiene complex in the reaction mixture of **11**.

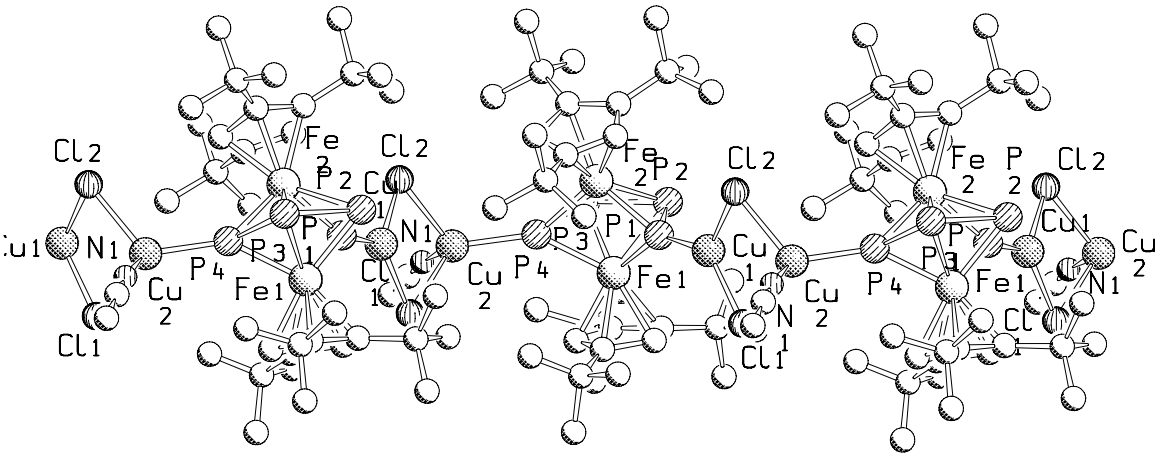

Figure 3.2.3. Section of the 1D polymeric structure of [{$(Cp'''Fe)_2(\mu,\eta^4{:}\eta^4\text{-}P_4)$} {$(CuCl)_2(MeCN)$}] (**11**) (H atoms are omitted for clarity). Selected bond lengths (Å) and angles (°): P1–P2 2.0956(19), P2–P3 2.3728(18), P3–P4 2.1023(17), P1–Cu1 2.1626(14), P4–Cu2 2.2285(12), P1–Fe1 2.2436(13), P2–Fe1 2.3538(13), P3–Fe1 2.3528(13), P4–Fe1 2.2657(12), P1–Fe2 2.2462(13), P2–Fe2 2.3464(14), P3–Fe2 2.3482(11), P4–Fe2 2.2591(12), Cu1–P1–P2 135.69(7), P1–P2–P3 105.44(7), P2–P3–P4 105.99(6), P3–P4–Cu2 128.46(7), Cl1–Cu1–Cl2 102.86(6), P1–Cu1–Cl2 125.17(6), Cl1–Cu1–P1 131.91(6), Cl1–Cu2–P4 121.23(6), Cl1–Cu2–Cl2 93.33(5), Cl2–Cu2–P4 116.65(5).

The solid-state structure of **11** has been established by X-ray crystallography as shown in Figure 3.2.3. Complex **11** contains two phosphorus atoms at the two ends of the "phosphabutadiene" fragment in the triple-decker and are σ-bonded to two copper atoms in the [$(\mu\text{-}CuCl)_2(MeCN)$] unit to afford a one-dimensional polymer structure. The coordination geometry of one copper atom (Cu2) is tetrahedral with a Cu–P bond length of 2.2285(12) Å and an average Cl–Cu–P bond angle of 118.9°. The other copper atom (Cu1) coordinates trigonally to one phosphorus atom and two chlorine atoms with a Cu–P bond length of 2.1626(14) Å and an average Cl–Cu–P bond angle of 128.5°. Three P–P bonds in the P_4 skeleton show inequality: two short bonds (P1–P2 2.0956(19) and P3–P4 2.1023(17)

Å) and one long bond (P2–P3 2.3728(18) Å). A similar example for the inequable P_4 skeleton was also found in [{1,3,4-$(Me_3Si)_2C_5H_3Fe$}$_2$(μ,η^4:η^4-P_4)] (two short: 2.090(2) and 2.093(2) Å, and one long: 2.436(2) Å)[55] (Figure 3.2.4).

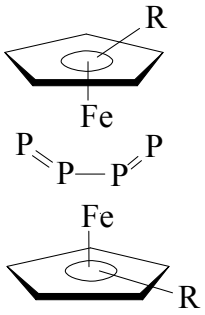

R = -$SiMe_3$

Figure 3.2.4. Different P-P bonds in the complex [{1,3,4-$(Me_3Si)_2C_5H_3Fe$}$_2$(μ,η^4:η^4-P_4)].

3.2.1.2. Reaction of [Cp'''Fe(η^5-$P_3C_2{}^tBu_2$)] with CuBr and CuI

3.2.1.2.1. [Cp'''Fe(η^5-$P_3C_2{}^tBu_2$)] with CuBr in a stoichiometric ratio of 1:1

After layering an acetonitrile solution of CuBr onto a red CH_2Cl_2 solution of [Cp'''Fe(η^5-$P_3C_2{}^tBu_2$)] (**4**) in a ratio of 1:1, the reaction mixture was kept at room temperature. A brown solution was formed.

The $^{31}P\{^1H\}$ NMR spectra of this reaction mixture shows two signals, a triplet at δ = 51.6 ppm and another broad doublet at δ = 28.4 ppm. These signals are similar to those of **10** indicating that there could be a dimeric complex **12** with CuBr present in the reaction mixture (equation 3.6 and Table 3.2.1).

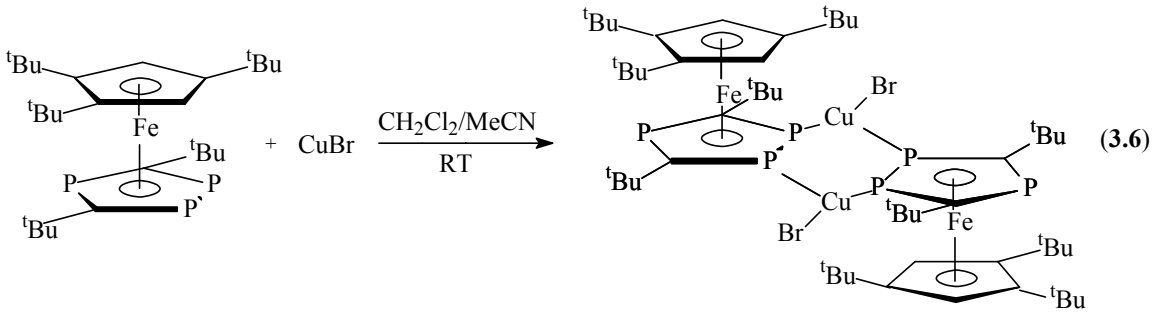

(3.6)

12

These analyses are confirmed by the mass spectra of the reaction mixture. The ESI-MS in MeCN at room temperature shows the corresponding fragments such as $[\{Cp'''Fe(P_3C_2{}^tBu_2)\}_2\{Cu(MeCN)\}_2]^+$, $[\{Cp'''Fe(P_3C_2{}^tBu_2)\}_2Cu]^+$, and $[\{Cp'''Fe(P_3C_2{}^tBu_2)\}Cu]^+$. Ions in the solution like those in the mass spectra of **10** were detected. These data indicate the presence of the dimeric complex with copper bromide.

Since no crystals were obtained from the previously mentioned reaction, another experiment was carried out. A solution of CuBr in CH_3CN was layered onto **4** in CH_2Cl_2 in the ratio of 1:1 and after the two reactants diffused completely, the reaction mixture was concentrated and kept at -28 °C for two weeks. Dark brown plates of complex **13** were obtained (Equation 3.7).

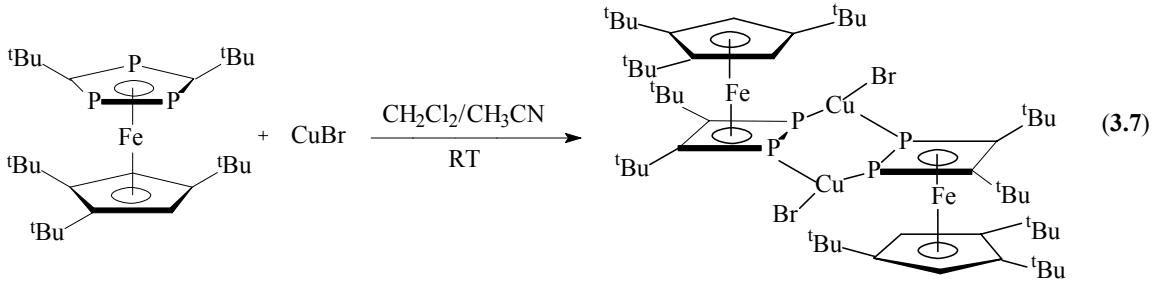

(3.7)

13

The P_3C_2-ring of the starting material **4** in this reaction is fragmented. Only the two adjacent phosphorus atoms of the P_3C_2-ring remain in the synthesized P_2C_2 four-membered ring. Two fragments of $[Cp'''Fe(\eta^4\text{-}P_2C_2{}^tBu_2)]$ are linked by two CuBr units to form a novel dimeric complex $[\{Cp'''Fe(\eta^4{:}\eta^1{:}\eta^1\text{-}P_2C_2{}^tBu_2)\}(\mu\text{-}CuBr)]_2$ (**13**). This experiment shows that

with different reaction conditions, the cyclo-P_3C_2 ring can split to rearrange into a four-membered 1,2-diphosphete ring.

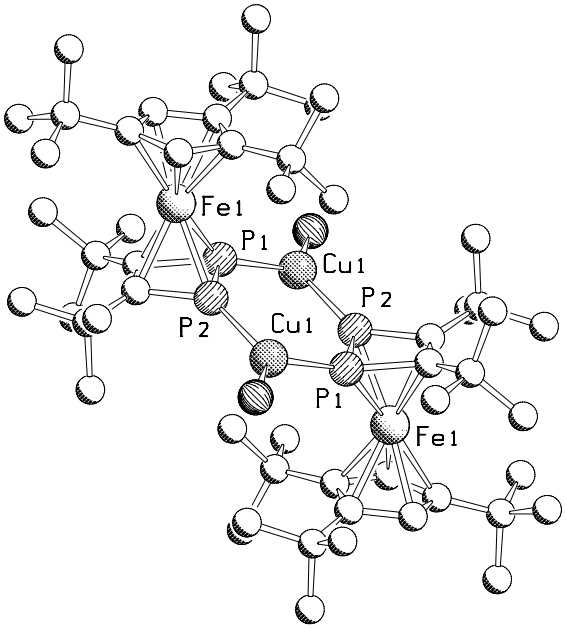

Figure 3.2.5. Molecular structure of $[(CuBr)_2\{Cp'''Fe(\eta^4{:}\eta^1{:}\eta^1\text{-}P_2C_2{}^tBu_2)\}_2]$ (**13**) in the crystal (H atoms are omitted for clarity). Selected bond lengths (Å) and angles (°): P1–P2 2.1480(5), P1–C7 1.8647(5), P2–C6 1.7598(6), P1–Cu1 2.2483(4), P2–Cu1 2.2245(7), Cu1–Br1 2.2863(6), P1–Fe1 2.2588(6), P2–Fe1 2.2809(6), C6–Fe1 2.1445(7), C7–Fe1 2.1666(8), C6–C7 1.4061(4), P1–Cu1–P2 99.803(11), Cu1–P2–P1 133.398(11), Cu1–P1–P2 126.79(2), C6–P2–P1 78.433(15), P2–P1–C7 77.847(12), P2–C6–C7 105.595(14), C6–C7–P1 98.123(22).

Complex **13** crystallizes in the triclinic space group $P\bar{1}$ and the structure is illustrated in Figure 3.2.5. In complex **13**, two copper centers are bridged by two cyclo-P_2C_2 rings, thus forming a six-membered ring with a planar conformation. This P_4Cu_2-ring together with the two P_2C_2-rings adopts a chair conformation. The copper atoms here are in a trigonal planar coordination mode with two phosphorus atoms and one bromine atom (average P–Cu–Br angle of 130.09°). The average P–Cu bond length is 2.2364 Å. The P–P bond length in **13** (2.1480(5) Å) is longer than that of the starting material **4** (2.121(3) Å) because of the greater ring strain of the four-membered ring in comparison to the five-membered ring. This P-P bond length is almost the same as that in the complex [1,2-η-{(3,4-di-*tert*-butyl-η^4-1,2-

diphosphete)-Fe(CO)$_3$}(Cr(CO)$_5$)$_2$] (2.147(2) Å) synthesized by Zenneck and coworkers and the both P–P bond lengths are shorter than that in the complex [(3,4-di-*tert*-butyl-η^4-1,2-diphosphete)(η^8-COT)-Ti] (2.175 Å (av)).[56] The reason for that is the lone pairs of the two phosphorus atoms of the P_2C_2-ring participate in η^1-bonding to the metal atoms. The average P–C bond length of P_2C_2-ring in complex **13** (1.8123 Å (av)) is similar to that in the two diphosphete complexes as shown below (1.816, 1.811 Å (av)).

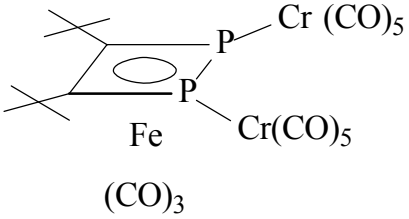

[1,2-η-{(3,4-di-*tert*-butyl-η^4-1,2-diphosphete)-Fe(CO)$_3$}(Cr(CO)$_5$)$_2$]

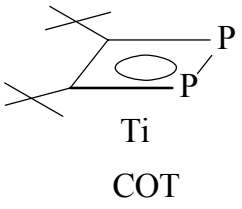

[(3,4-di-*tert*-butyl-η^4-1,2-diphosphete)(η^8-COT)-Ti]

Since there are 17 electrons in the valence orbitals of the [{Cp'''Fe(η^4-$P_2C_2{}^tBu_2$)}] moieties, complex **13** must be paramagnetic. This is confirmed by ESR spectroscopy. In the ESR spectrum a signal at g_1 = 2.026 shows a hyperfine splitting with a = 10 mT, suggesting that there are unpaired electrons delocalized over the whole plane of the two four-membered rings, P_2C_2, and six-membered ring P_4Cu_2. The half field signal for an antiferromagnetic coupling of g_2 = 5.3 indicates the existence of two unpaired electrons in this compound. The g_1 factor for the ferrocenium cation, implies 17 valence electrons for the two iron atoms (Figure 3.2.6).

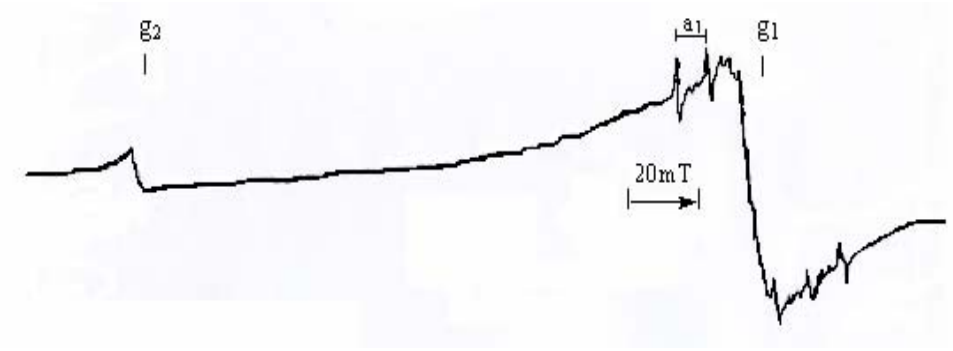

Figure 3.2.6. X-band ESR spectrum of the compound **13**.

3.2.1.2.2. [Cp'''Fe(η^5-$P_3{}^tBu_2C_2$)] with CuBr and CuI in a stoichiometric ratio of 1:2

The cyclo-P_3C_2 ring can be fragmented when [Cp'''Fe(η^5-$P_3{}^tBu_2C_2$)] is treated with two equivalents of CuCl or one equivalent of CuBr. It is assumed that apart from the accessible coordination of the Cu(I) center, the size of the halide also affects the ring fragmentation. In order to gain further insight into the coordination behaviour of triphosphaferrocene with copper halides, similar procedures to those for the synthesis of **11** were carried out. When two equivalents of CuX (X = Br, I), respectively, in acetonitrile were layered onto a CH_2Cl_2 solution of **4**, the air sensitive dark brown crystalline compounds [{(Cp'''Fe)$_2$(μ,η^4:η^1:η^1-P_4)}{(μ-CuX)$_2$(MeCN)}]$_n$ (X = Br (**14**), I (**15**)) were formed. Even with one equivalent of CuI, compound **15** was obtained. As with the complex **11**, the P_3C_2-ring of the starting material **4** was fragmented and rearranged to form a new triple-decker [{(Cp'''Fe)$_2$(η^4-P_4)}] unit during the reaction (reaction equation **3.8**).

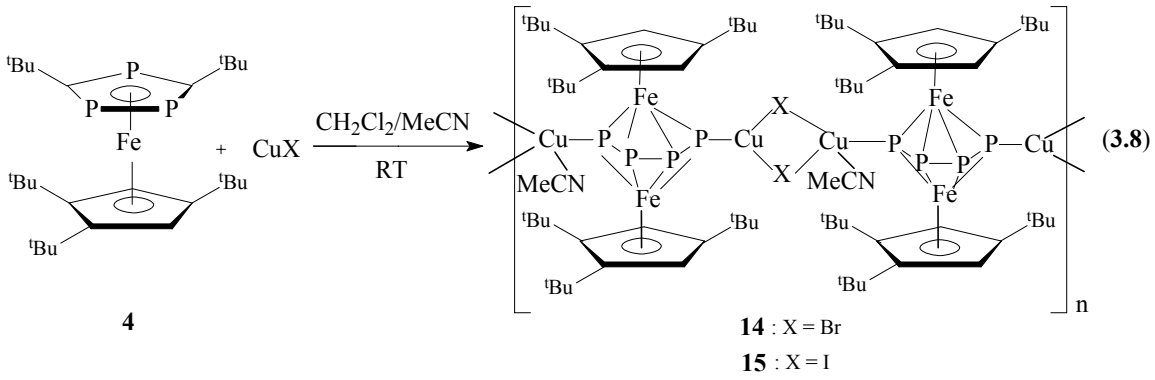

4 **14** : X = Br **15** : X = I **(3.8)**

The polymeric compounds **14** and **15** can be stored under an inert atmosphere. They are sparingly soluble in DMF and do not dissolve in common solvents such as CH_2Cl_2, toluene or THF.

The ESI-MS of **14** at room temperature displays peaks corresponding to the cations of [{(Cp'''Fe)$_2$(P_4)}$_2$Cu]$^+$, [{(Cp'''Fe)$_2$(P_4)}Cu]$^+$ and [(Cp'''Fe)$_2$(P_4)]$^+$. In the ESI-MS spectrum of complex **15**, the signals attributed to the cations of [{(Cp'''Fe)$_2$(P_4)}Cu_2I]$^+$, [{(Cp'''Fe)$_2$(P_4)}Cu_2]$^{2+}$ and [{(Cp'''Fe)$_2$(P_4)}]$^+$ were also detected.

Due to the poor solubility of the polymer in common solvents, the reaction solution of **14** and **15** were taken for NMR measurement. There are two broad signals in the $^{31}P\{^1H\}$ NMR spectrum of the reaction solution of **14**: one signal at δ = 76.2 ppm with a line width at half

height ($\omega_{1/2}$) of 520 Hz and the other signal at δ = 120.6 ppm ($\omega_{1/2}$= 490 Hz), which is assigned to the two phosphorus atoms at the end of the P_4 skeleton.

In the $^{31}P\{^1H\}$ NMR spectrum of the reaction solution of **15**: one signal at δ = 72.9 ppm with a line width at half height ($\omega_{1/2}$) of 1300 Hz and the other signal at δ = 118.4 ppm ($\omega_{1/2}$= 650 Hz), which is assigned to the two phosphorus atoms at the end of the P_4 skeleton (Table 3.2.1).

The NMR spectra of **14** and **15** reveal that there are two different chemically inequivalent phosphorus atoms and this suggests that oligomers should exist in solution, in which two phosphorus atoms at the end of the P_4 skeleton coordinate to the copper atoms.

As in the case of **11**, the $^{31}P\{^1H\}$ NMR spectra of the reaction solution of **14** and **15** show also two additional signals (**14**: 52.8 and 41.4 ppm, **15**: 51.8 and 39.1ppm), which are only marginally different compared to those of the starting material (Table 3.2.1). These signals indicate that there are weak interactions between the Cu(I) species and the unreacted starting materials.

Table 3.2.2. ^{31}P NMR spectra of $[\{(Cp'''Fe)_2(\mu,\eta^4{:}\eta^1{:}\eta^1\text{-}P_4)\}\{(\mu\text{-}CuX)_2(MeCN)\}]_n$ in DMF/C_6D_6 and $[\{(Cp^RFe)_2(\mu,\eta^4\text{-}P_4)\}]$ in C_6D_6.

	Chemical shift (ppm)
$[\{(Cp^RFe)_2(\mu{:}\eta^4\text{-}P_4)\}]$	104.9 (br)
11	78.5 (br)
14	82.3 (br)
15	90.2 (br)

Cp^R = 1,3,4-$(Me_3Si)_3C_5H_2$, X = Cl (**11**), Br (**14**), I (**15**)

Since these triple-decker copper polymers (**11, 14** and **15**) dissolve sparingly in DMF, the NMR spectra of these solutions were recorded. In each NMR spectrum of the three solutions at room temperature, one broadened signal was detected (Table 3.2.2). These signals are comparable to that of $[\{(Cp^RFe)_2(\mu,\eta^4\text{-}P_4)\}]$[55] and indicate that in solution the polymer chain may be depolymerised to $[(Cp'''Fe)_2(\eta^4\text{-}P_4)]$ moieties and a dynamic process was occurred (Figure 3.2.7). Considering the somewhat different chemical shifts in these spectra, there must be a weak interaction between the triple-decker $[(Cp'''Fe)_2(\eta^4\text{-}P_4)]$ unit and copper halides.

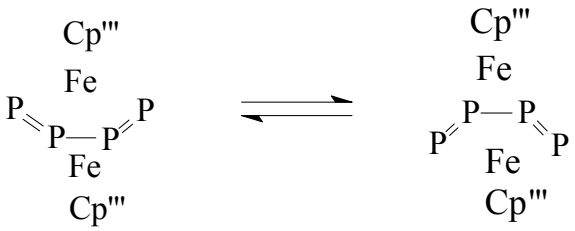

Figure 3.2.7. Proposed dynamic behaviour of the [(Cp'''Fe)$_2$(η^4-P$_4$)] moiety in solution.

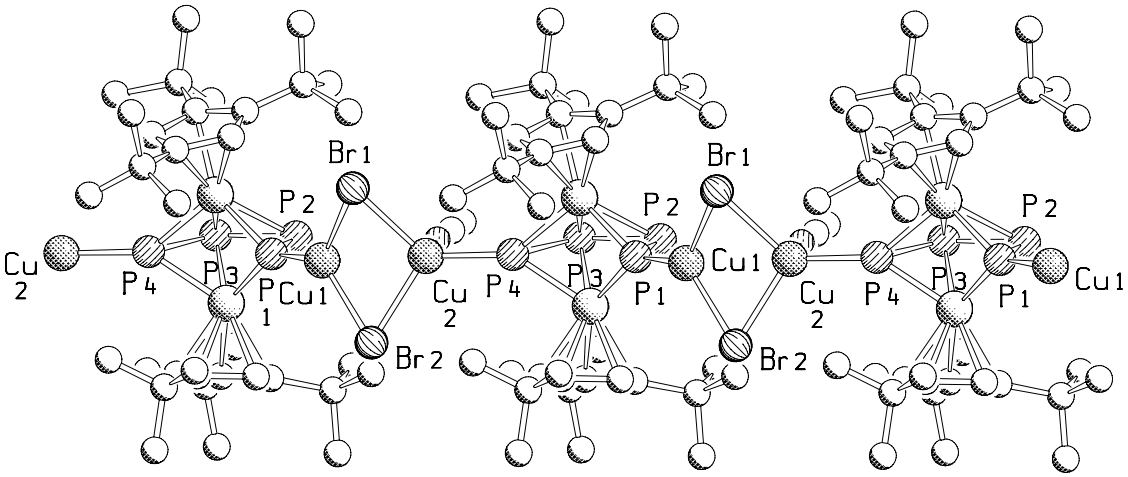

Figure 3.2.8. Section of the structure of [{(CuBr)$_2$MeCN}{(Cp'''Fe)$_2$(μ,η^4:η^4-P$_4$)}] (**14**) in the crystal (H atoms are omitted for clarity). Selected bond lengths (Å) and angles (°): P1–P2 2.093(6), P2–P3 2.303(7), P3–P4 2.121 (6), P4–Cu2 2.160(5), P1–Cu1 2.183(6), P1–Fe1 2.233(6), P2–Fe1 2.348(5), P3–Fe1 2.348(5), P4–Fe1 2.225(5), P1–Fe2 2.236(6), P2–Fe2 2.344(5), P3–Fe2 2.348(6), P4–Fe2 2.250(5), Cu1–Br1 2.389(3), Cu1–Br2 2.403(3), Cu2–Br1 2.437(5), Cu2–Br2 2.449(4), Cu1–P1–P2 129.8(3), P1–P2–P3 106.5(3), P2–P3–P4 106.4(3), P3–P4–Cu2 124.2(3), Br1–Cu1–Br2 104.6(13), Br1–Cu1–P1 129.43(19), Br2–Cu1–P1 125.28(18), Br1–Cu2–Br2 101.79(14), Br1–Cu2–P4 128.1(2), Br2–Cu2–P4 123.1(2).

The solid-state structures of **14** and **15** have been established by X-ray crystallography and the structures are shown in Fig. 3.2.8 and Fig. 3.2.9, respectively. In these complexes two

phosphorus atoms at the end of the "tetraphosphabutadiene" fragment in the triple-decker complex are bound to two copper atoms in the [(μ-CuX)$_2$(MeCN)] unit to form a one-dimensional polymer. Similar to complex **11**, the coordination geometry of one copper atom (Cu2) is tetrahedral with a Cu2–P4 bond length of 2.1596(5) Å for **14** and 2.2458 (18) Å for **15** and X–Cu2–P4 bond angles averaging 125.6°(2) for **14** and 117.64°(6) for **15**. The other copper atom (Cu1) coordinates planar trigonally to one phosphorus atom and two chlorine atoms with Cu1–P1 bond lengths equal to 2.183(6) Å for **14** and 2.1994(16) Å for **15** and X–Cu1–P1 bond angles averaging 127.36° for **14** and 126.3° for **15**. In parallel with the case of complex **11** and [{(Cp^{R}Fe)$_2$(μ:η^4-P$_4$)}], three P–P bonds in the P$_4$ skeleton show inequality, two short bonds (P1–P2 2.093(6) Å and P3–P4 2.121(6) Å in **14**) and (P1–P2 2.103(2) Å and P3–P4 2.105(2) Å in **15**) and one long bond (P2–P3 2.303(7) Å in **14** and 2.3382(19) Å in **15**) (Table 3.2.3). The P–Fe bond length of these tetraphosphabutadiene moieties are also found to be in two groups: short Fe–P$_1$ (**14**: 2.233(6), **15**: 2.2429(17) Å) and Fe–P$_4$ (**14**: 2.225(5), **15**: 2.2480(16) Å) bonds; and long Fe–P$_2$ (**14**: 2.348(5), **15**: 2.3520(15) Å) and Fe–P$_3$ bonds (**14**: 2.348(5), **15**: 2.3531(15) Å).

Table 3.2.3. Comparison of the different P-P bond length in complexes [{(Cp^{R}Fe)$_2$(μ:η^4-P$_4$)}] and **11**, **14** and **15**.

	"short bonds" (Å)		"long bond" (Å)
	P1–P2	P3–P4	P2–P3
[{(Cp^{R}Fe)$_2$(μ:η^4-P$_4$)}]	2.090 (2)	2.093 (2)	2.436 (2)
11	2.0956 (19)	2.1023 (17)	2.3728 (18)
14	2.093 (6)	2.121 (6)	2.303 (7)
15	2.103 (2)	2.105 (2)	2.3382 (19)

Cp^R = 1,3,4-(Me$_3$Si)$_3$C$_5$H$_2$

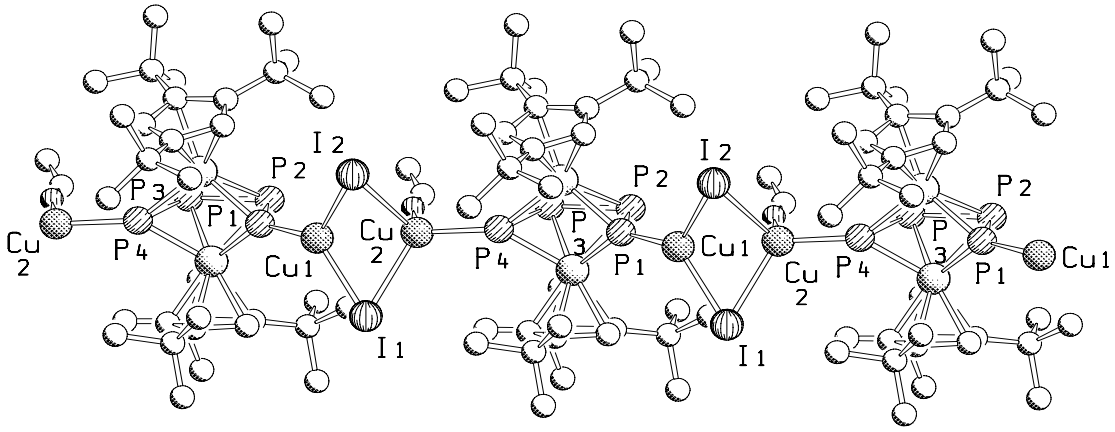

Figure 3.2.9. Section of the structure of [{(CuI)$_2$(MeCN)}{(Cp'''Fe)$_2$(μ,η^4:η^4-P$_4$)}] (**15**) in the crystal (H atoms are omitted for clarity). Selected bond lengths (Å) and angles (°): P1–P2 2.103(2), P2–P3 2.3382(19), P3–P4 2.105(2), P4–Cu2 2.2458(18), P1–Cu1 2.1994(16), P1–Fe1 2.2429(17), P2–Fe1 2.3520(15), P3–Fe1 2.3531(15), P4–Fe1 2.2480(16), P1–Fe2 2.2467(16), P2–Fe2 2.3515(18), P3–Fe2 2.3480(17), P4–Fe2 2.2565(16), Cu1–I1 2.5652(8), Cu1–I2 2.5639(8), Cu2–I1 2.7003(12), Cu2–I2 2.7116(2), Cu1–P1–P2 129.83(8), P1–P2–P3 106.09(9), P2–P3–P4 106.41(9), P3–P4–Cu2 115.19(9), I1–Cu1–I2 107.20(3), I1–Cu1–P1 128.17(5), I2–Cu1–P1124.41(5), I1–Cu2–I2 99.3(4), I1–Cu2–P4 119.46(6), I2–Cu2–P4 115.82(6).

3.2.2. The Triphosphaferrocene [CpFe(η^5-$P_3C_2{}^tBu_2$)] as a Ligand

3.2.2.1. Reaction of [CpFe(η^5-$P_3C_2{}^tBu_2$)] with CuCl

Due to the similarity of the structures of [CpFe(η^5-$P_3C_2{}^tBu_2$)] and [Cp'''Fe(η^5-$P_3C_2{}^tBu_2$)], it was of interest to determine whether the difference in the substitution pattern of the cyclopentadiene rings would affect the reactivities and the coordination properties of the triphosphaferrocene. Thus, one and two equivalents of CuCl were reacted with [CpFe(η^5-$P_3C_2{}^tBu_2$)], respectively. From both reactions the same red crystals of **16** were obtained. The formation is similar to the dimeric copper complex [{Cp'''Fe(η^5:η^1-$P_3C_2{}^tBu_2$)}(μ-CuCl)]$_2$ (**10**), in which two phosphaferrocenes are linked by two CuCl centers (equation 3.9). But in contrast to **10**, complex **16** reveals tetrahedrally coordinated copper atoms.

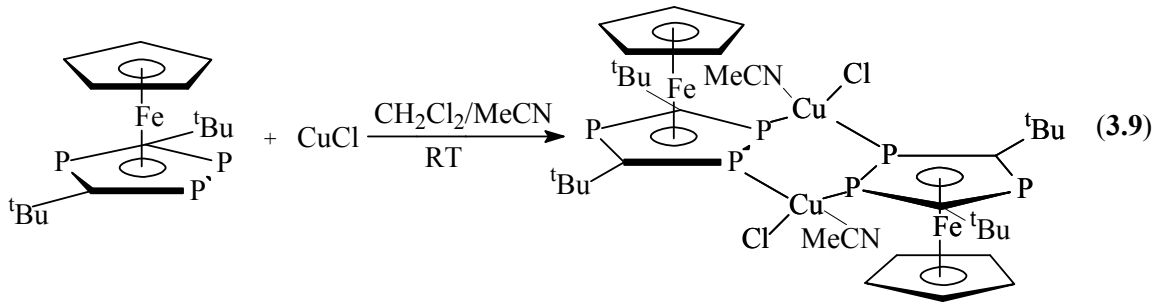

(**3.9**)

16

The red crystalline compound **16** is soluble in MeCN, but it dissolves only sparingly in CH_2Cl_2 and THF. The complex is stable at room temperature and can be stored under an inert atmosphere.

In the positive ESI-MS spectrum of **16** at room temperature, a peak with 100% relative abundance was assigned to the cation of [{CpFe($P_3C_2{}^tBu_2$)}$_2$Cu]$^+$. Another peak was detected corresponded to the [{CpFe($P_3C_2{}^tBu_2$)}$_2$$Cu_2$Cl]$^+$ cation. This indicates the existence of the dimeric complex of **16** in solution.

The ^{1}H NMR spectrum of **16** in CD_2Cl_2 displays two singlets at δ = 1.33 ppm and δ = 4.79 ppm, which represent the protons on the ^{t}Bu group and the Cp ring (signals of the free ligand are at δ = 1.29 ppm and δ = 4.71 ppm).[54]

The ^{31}P{^{1}H} NMR spectrum of **16** in CD_2Cl_2 shows one slightly broadened triplet ($\delta(P_A)$ = 33.1 ppm) and one broad doublet ($\delta(P_M)$ = 15.4 ppm) with coupling constant of $J(P_A,P_M) \approx$

45.7 Hz. Compared with the corresponding chemical shifts of the free ligand [CpFe(η^5-$P_3C_2{}^tBu_2$)] ($\delta(P_A)$ = 40.2 ppm and $\delta(P_M)$ = 39.6 ppm),[17] the doublet peak is broadened and shifted upfield due to the coordination of the two adjacent phosphorus atoms in the P_3C_2-ring with their lone pairs to copper atoms.

Complex **16** crystallizes in the monoclinic space group $P2_1/n$ and, as is the case with the dimeric copper complex **10,** compound **16** consists of two CuCl fragments doubly bridged by two triphosphaferrocene units *via* the two adjacent phosphorus atoms of the $P_3C_2{}^tBu_2$ ring system. In parallel with complex **10**, a six-membered ring is formed which is not strictly planar (deviation of the copper atoms from the P2P3P2´P3´ plane = 0.189(1) Å). The two five-membered P_3C_2 rings and the P2P3P2´P3´ plane are coplanar, and a "stair-like" arrangement of the whole molecule can be determined (Figure 3.2.10).

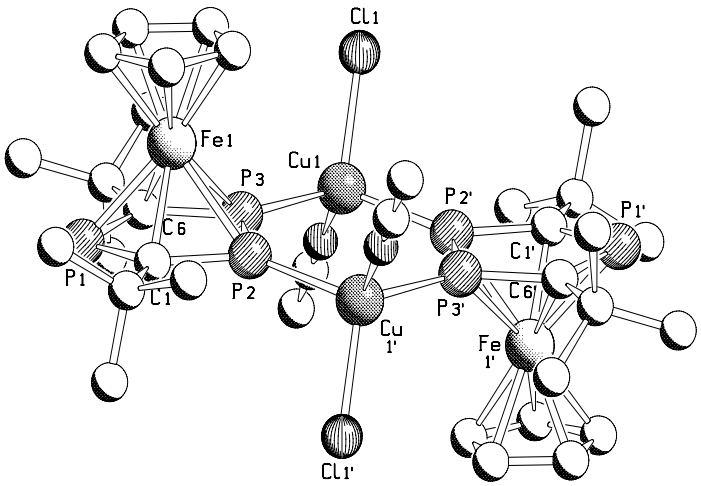

Figure 3.2.10. Molecular structure of [$(CuCl)_2${CpFe(η^5:η^1:η^1-$P_3{}^tBu_2C_2$)}$_2$] (**16**) (H atoms are omitted for clarity). Selected bond lengths (Å) and angles (°): P2–P3 2.1163(2), P2–Cu 2.2891(3), P3–Cu 2.2804(4), P2–C1 1.7742(3), P3–C6 1.7740(3), P1–C1 1.7661(3), P1–C6 1.7841(3), P2–Fe1 2.3405(2), P3–Fe1 2.3351(2), P1–Fe1 2.3026(2), Cu1–Cl1 2.2902(2), C1–Fe1 2.1311(1), C6–Fe1 2.1340(2), Cu–P2–P3 123.569(4), P2–P3–Cu1 124.560(4), P2–Cu1–P3 111.018(4), P3–P2–C1 99.181(5), P2–P3–C6 99.906(5), P2–Fe1–P3 53.826(2), P2–P3–Fe1 63.219(2), C1–P1–C6 99.249(5), P3–Cu1–Cl1 113.491(3), P2–Cu1–Cl1 105.506(3).

The copper atoms are tetrahedrally bonded to two phosphorus atoms of two different cyclo-P_3C_2 rings, one chlorine atom, and one nitrogen atom of an acetonitrile molecule (average P–Cu–Cl angle 109.50(8)°). This is in contrast to complex **10** where the copper atoms coordinate trigonally to two phosphorus atoms and one chlorine atom. The reason may be the steric hindrance of the bulky ^{t}Bu groups attached to the cyclopentadiene ring of complex **10** to allow only the trifold coordination of copper atom. The Cu–P bond lengths (2.2847(19) Å) in **16** are longer than that in the complex **10** (2.1930(15) Å) suggesting that the Cu–P interaction is also influenced by the coordination geometry. Likewise, no variation of the P–P bond lengths was found in **16** (2.116(2) Å) and the free ligand [CpFe(η^5-$P_3C_2{}^tBu_2$)] (2.114(1) Å).

3.2.2.2. Reaction of [CpFe(η^5-$P_3C_2{}^tBu_2$)] with CuBr

With the same layering technique as in the procedure for the preparation of **10**, [CpFe (η^5-$P_3C_2{}^tBu_2$)] and CuBr were reacted in a ratio of 1:1. The reaction solution was kept at room temperature and red crystalline plates were yielded.

This compound dissolves moderately in MeCN and sparingly in CH_2Cl_2. It can be stored under an inert atmosphere at ambient conditions.

The structure of the red crystalline complex was determined by single-crystal X-ray diffraction and shown to consist of a polymer chain in which tetraphosphabutadiene moieties bridge $(CuBr)_2$ units in a similar manner to that observed in complex **11**. However, due to crystal twinning, the structure could only be partly solved.

The ESI-MS spectrum of the mother liquor in MeCN reveals the peaks attributed to the cations of $[\{FeCp(P_3C_2{}^tBu_2)\}_2Cu_2BrMeCN]^+$, $[\{FeCp(P_3C_2{}^tBu_2)\}_2Cu]^+$, and $[\{FeCp(P_3C_2{}^tBu_2)\}Cu_2Br(MeCN)_2]^+$ suggests, that there should be a dimeric copper complex (**17**) similar to **16** (Figure 3.2.11) in the reaction solution.

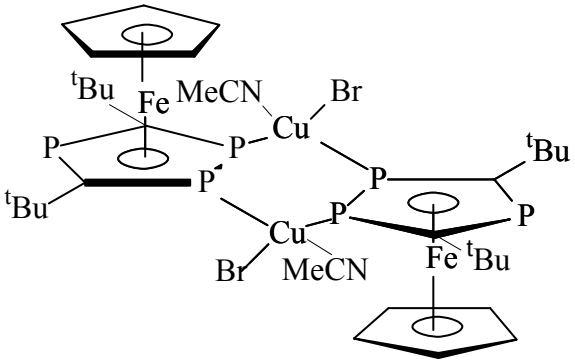

17

Figure 3.2.11. Proposed structure of the dimeric complex **17.**

The $^{31}P\{^{1}H\}$ NMR spectrum of the mother liquor shows one triplet (δ = 33.5 ppm) and one broadened doublet signal (δ = 14.6 ppm). The broadened doublet is shifted 25 ppm upfield compared to the starting material. This NMR spectrum, which is very similar to that of compound **16** and **19** (Table 3.2.4), may confirm the existence of the dimeric copper complex **17** in mother liquor.

Table 3.2.4. $^{31}P\{^{1}H\}$ NMR of [CpFe(η^5-$P_3C_2{}^tBu_2$)] and its dimeric complexes.

Compound	solvent	δ(P_A) (ppm)	δ(P_M) (ppm)	J(P_A,P_M) (Hz)
[CpFe(η^5-$P_3C_2{}^tBu_2$)]	$CDCl_3$	40.2 (t)	39.6 (d)	45.4
16	CD_2Cl_2/MeCN: 3:1	33.1 (t)	15.3 (br)	45.4
17	CD_2Cl_2/MeCN: 3:1	33.5 (t)	14.6 (br)	44.6
18 [a)]	CD_2Cl_2/MeCN: 3:1	34.9 (br)	8.2 (br)	
19 [b)]	THF-d_8/CH_2Cl_2: 3:1	34.3 (t)	12.7 (d)	44.3

[a)] For the synthesis of **18** c.f. chapter 3.2.2.3

[b)] For the synthesis of **19** c.f. chapter 3.2.2.4

Unfornunately, no single crystal suitable to X-ray diffraction of **17** could be obtained.

3.2.2.3. Reaction of [CpFe(η^5-$P_3C_2{}^tBu_2$)] with CuI

Previous studies of the coordination behaviour of [Cp'''Fe(η^5-$P_3C_2{}^tBu_2$)] (**4**) and [CpFe(η^5-$P_3C_2{}^tBu_2$)] (**7**) with copper halides showed that dimeric copper complexes **10**, **13**, **16** and **17** were obtained when the triphosphaferrocene reacts with CuCl or CuBr in a ratio of 1:1, but

only one polymer product was yielded, regardless of whether one or two equivalents of CuI were used to react with **4**. Thus, two equivalents of copper iodide were used when treated with [CpFe(η^5-$P_3C_2{}^tBu_2$)].

An acetonitrile solution of CuI was carefully layered onto a CH_2Cl_2 solution of [CpFe(η^5-$P_3C_2{}^tBu_2$)] in a 2:1 stoichiometry at room temperature. Slow diffusion yielded an air-sensitive red crystalline compound **18** (equation 3.9), which can be stored under an inert atmosphere at ambient conditions. The same product was obtained by treating of [CpFe(η^5-$P_3C_2{}^tBu_2$)] and CuI in a 1:1 stoichiometric ratio.

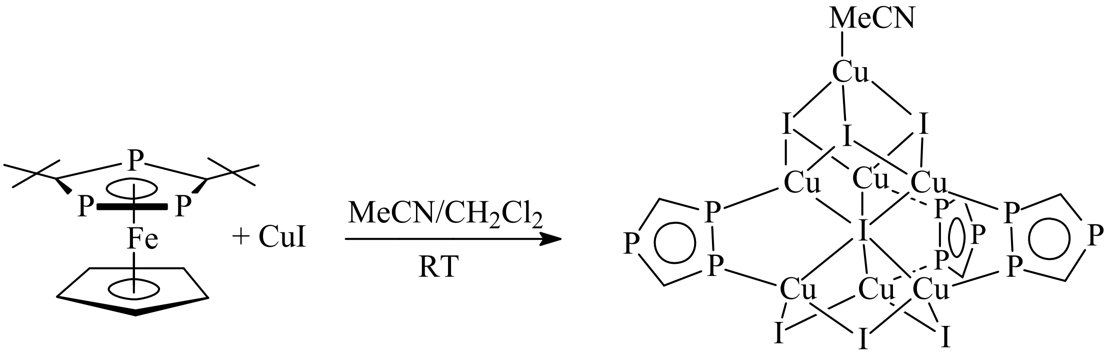

(3.9)

18

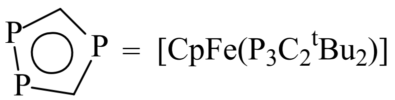

Compound **18** dissolves moderately in CH_2Cl_2, MeCN, sparingly in THF, and not in nonpolar solvents such as alkanes.

In the EI-MS spectrum of **18**, the $[\{CpFe(P_3C_2{}^tBu_2)\}_3Cu_7I_6]^+$, $[\{CpFe(P_3C_2{}^tBu_2)\}_3Cu_5I_6]^+$ and $[\{CpFe(P_3C_2{}^tBu_2)\}_3Cu_4I_5]^+$ cations were detected. These fragments show a successive loss of copper and iodine atoms from the original molecule under the condition of electron impact.

The ^1H NMR spectrum of **18** shows three signals, two multiplets (δ = 0.80 and 1.23 ppm) representing the ^{t}Bu group on the P_3C_2-ring of the molecule. This indicates that the protons on the two ^{t}Bu groups are chemically and magnetically inequivalent. The third signal at δ = 3.56 ppm belongs to the protons on the cyclopentadiene ring.

In the $^{31}P\{^1H\}$ NMR spectrum of **18** there are two broad signals centered at δ = 8.2 and 34.9 ppm, respectively. In comparison with the corresponding chemical shifts of the free complex [CpFe(η^5-$P_3{}^tBu_2C_2$)] ($\delta(P_A)$ = 39.6 ppm and $\delta(P_M)$ = 40.2 ppm), a significant

upfield shift of the signal corresponding to the adjacent phosphorus atoms in the P_3C_2 ring is observed.

The molecular structure of **18** was determined by single-crystal X-ray diffraction as illustrated in Figure 3.2.11. In complex **18** three fragments of [CpFe(η^5-$P_3C_2{}^tBu_2$)] are connected to each other through the two adjacent phosphorus atoms of the P_3C_2 rings and the copper atoms of $(CuI)_7$ unit.

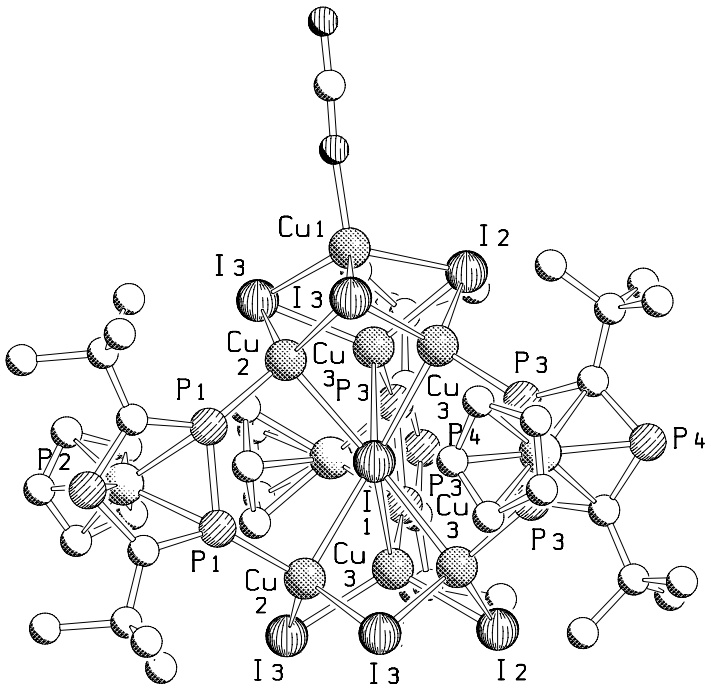

Figure 3.2.12. Molecular structure of **18** in the crystal (H atoms are omitted for clarity). Selected bond lengths (Å) and angles (°): P1–P1 2.1102(6), P3–P3 2.1093(5), P1–C31 1.752(12), P2–C31 1.779(15), P3–C41 1.7499(9), P1–Cu2 2.2337(4), P3–Cu3 2.2425(3), Cu1–I2 2.712(5), Cu1–I3 2.671(3), Cu2–I1 2.897, Cu2–I3 2.5889(11), Cu3–I1 2.9077(15), Cu3–I2 2.5848(14), Cu3–I3 2.5975(14), Cu3–P3–P3 123.42(7), Cu2–P1–P1 122.60(9), Cu2–I1–Cu2 102.48(8), Cu3–I1–Cu3 103.86(6), Cu2–I1–Cu3 144.60(3).

The $(CuI)_7$ unit consists of a cubic shaped $(CuI)_4$ unit and a chair-like six-membered $(CuI)_3$ ring. The three copper atoms of the $(CuI)_3$ unit are bonded to an iodine atom (I1) of the $(CuI)_4$ unit. In this distorted cubic $(CuI)_4$ unit all Cu atoms exhibit the tetrahedral coordination geometry which shows a "cubane"-like tetranuclear cuprous halide cluster (Figure 3.2.13). One of the causes of the distortion is probably the variation of the Cu····Cu

distances (ranging from 2.731(5) to 3.060(3) Å), which is quite common in Cu^I clusters.[57] It indicates that a weak attractive potential between the metal centers, which is, very sensitive to steric effects and the electronic properties of the ligands[58]. The average Cu–I bond length (2.708 Å) in the $(CuI)_4$ unit is slightly longer than those in the complexes $Cu_4I_4(PPh_2Me)_4$ (2.698 Å) and $Cu_4I_4(PPh_3)_4$ (2.691 Å)[59] and longer than that in the similar complex $[\{Cp^*Fe(\eta^5:\eta^1:\eta^1\text{-}P_3C_2{}^tBu_2)\}_4(CuI)_7]$ (2.683 Å) obtained in our group by Andrea Schindler[60]. The average Cu–P bond length (2.238 Å) in the $(CuI)_4$ unit is almost the same as that in $[\{Cp^*Fe(\eta^5:\eta^1:\eta^1\text{-}P_3C_2{}^tBu_2)\}_4(CuI)_7]$ (2.237 Å) but slightly shorter than those in $Cu_4I_4(PPh_2Me)_4$ (2.250 Å) and $Cu_4I_4(PPh_3)_4$ (2.252 Å).

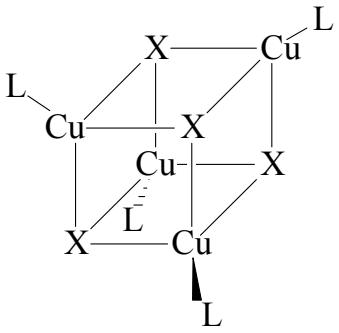

Figure 3.2.13. Tetranuclear cuprous halide cluster $Cu_4(\mu_3\text{-}X_4)L_4$.

The iodine atom (I1) in the core connected to six copper atoms has a relatively longer average distance (2.902 Å) in comparison to the rest of the Cu–I bond lengths (2.631Å) and is shorter than that in $[\{Cp^*Fe(\eta^5:\eta^1:\eta^1\text{-}P_3C_2{}^tBu_2)\}_4(CuI)_7]$ (2.941 Å) (Figure 3.2.12). One copper atom of the $(CuI)_4$ unit and one of the $(CuI)_3$ unit are bridged by the two adjacent phosphorus atoms of the cyclo-P_3C_2 ring on the triphosphaferrocene moiety with the "side on" coordination mode.

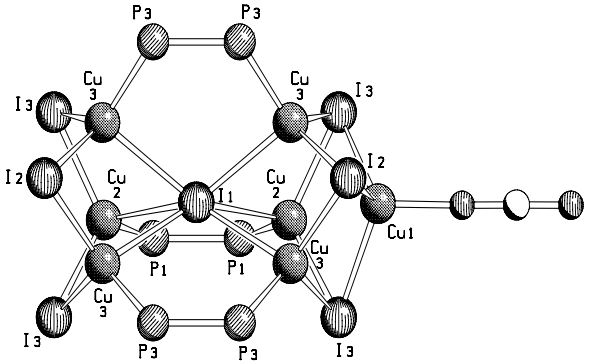

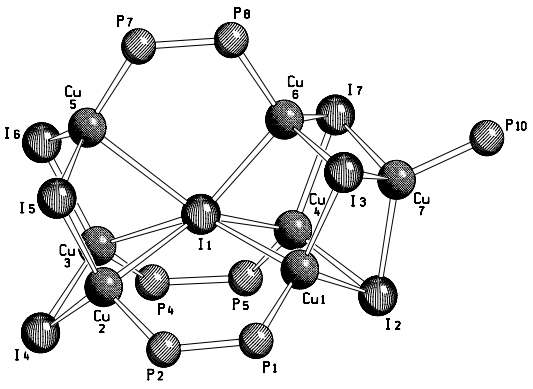

18 $[\{Cp^*Fe(\eta^5:\eta^1:\eta^1\text{-}P_3{}^tBu_2C_2)\}_4(CuI)_7]$

Figure 3.2.14. Cage structure of **18** and [{Cp*Fe(η^5:η^1:η^1-$P_3{}^tBu_2C_2$)}$_4$(CuI)$_7$].

The only difference in the structures between **18** and [{Cp*Fe(η^5:η^1:η^1- $P_3C_2{}^tBu_2$)}$_4$(CuI)$_7$] is the "head" copper atom (Cu1 and Cu7, respectively) of the (CuI)$_7$ unit. In the [{Cp*Fe(η^5:η^1:η^1-$P_3C_2{}^tBu_2$)}$_4$(CuI)$_7$] the copper atom (Cu7) coordinates to a phosphorus atom of a fourth [Cp*Fe(η^5-$P_3C_2{}^tBu_2$)] fragment whereas in **18** the copper atom (Cu1) coordinates to the nitrogen atom of a MeCN molecule (Figure 3.2.14).

3.2.2.4. Reaction of [CpFe(η^5-$P_3C_2{}^tBu_2$)] with Ag[Al{OC(CF_3)$_3$}$_4$]

Previous experiments with different silver salt solutions such as $AgCF_3SO_3$, $AgCF_3CO_2$ and Ag[Al{OC(CF_3)$_3$}$_4$] layered onto the [CpFe(η^5-$P_3C_2{}^tBu_2$)] solution result in precipitation of silver on the schlenk wall after a few days. The reason may come from the instability of silver salts in solution. It is reasonable to stir the reaction mixture in a minimal amount of time. Thus, direct mixing of the reactants was carried out rather than the layering technique. A mixture of [CpFe(η^5-$P_3C_2{}^tBu_2$)] with Ag[Al{OC(CF_3)$_3$}$_4$] in a 1:1 ratio in a solution of CH_2Cl_2 and MeCN was stirred at room temperature for one hour, afterwards the black powder that was produced during the reaction was filtered and the filtrate was kept at about 4 °C until the air- and light-sensitive red orange crystalline compound **19** was formed (equation 3.10).

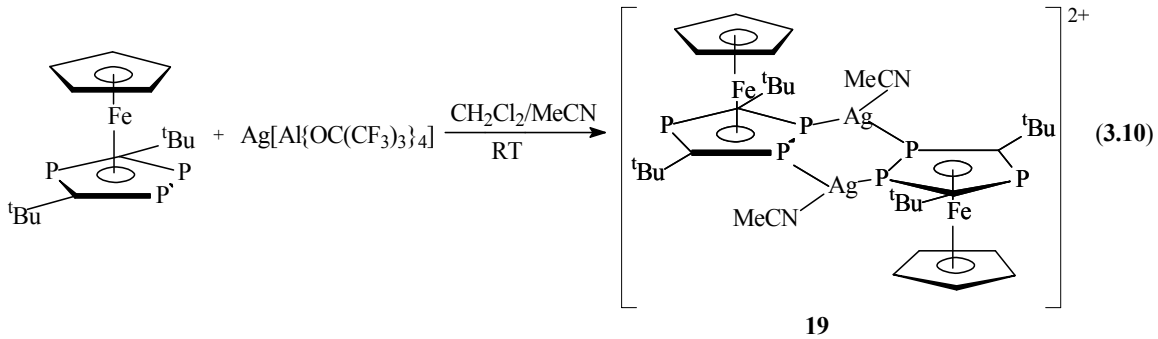

(**3.10**)

19

Compound **19** dissolves in THF, MeCN, and sparingly in CH_2Cl_2; it is not soluble in nonpolar solvents such as alkanes. It can be stored under an inert atmosphere at low temperature.

In the negative ESI-MS spectrum of **19** in MeCN at room temperature a peak with 100% relative abundance corresponding to the $[Al\{OC(CF_3)_3\}_4]^-$ anion was detected. The positive ESI-MS spectrum reveals a peak with the highest relative abundance corresponds to the $[\{CpFe(\eta^5\text{-}P_3C_2{}^tBu_2)\}_2Ag]^+$ cation. In addition, a peak attributed to the $[\{CpFe(\eta^5\text{-}P_3C_2{}^tBu_2)\}AgMeCN]^+$ cation was detected. This indicates that the dimeric silver complex $[\{CpFe(\eta^5\text{-}P_3C_2{}^tBu_2)\}_2Ag_2]^{2+}$ is most likely present in solution.

The ^1H NMR spectrum of **19** shows two signals. One singlet at $\delta = 1.43$ ppm represents the ^tBu group of the P_3C_2 ring. The singlet at $\delta = 3.58$ ppm belongs to the protons on the cyclopetadiene ring.

In the $^{31}P\{^1H\}$ NMR spectrum of **19** there are two signals, one triplet at $\delta = 34.3$ ppm and one broad doublet at $\delta = 12.7$ ppm which represent the two adjacent phosphorus atoms of the P_3C_2 ring. The corresponding chemical shifts of **19** are shifted upfield in comparison to that in the free complex $[CpFe(\eta^5\text{-}P_3{}^tBu_2C_2)]$ ($\delta(P_M) = 39.6$ ppm and $\delta(P_A) = 40.2$ ppm). An upfield shift of the signals is also observed in **16** and **17** (Table 3.2.2.).

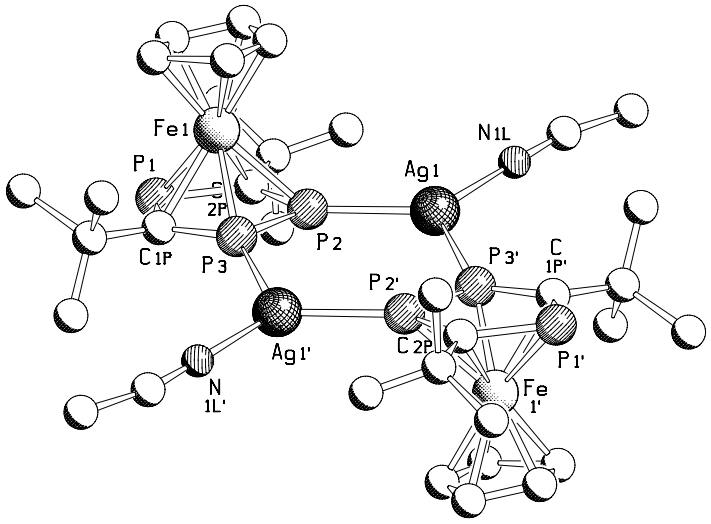

Figure 3.2.15. Structure of the cationic part of complex **19** (H atoms are omitted for clarity). Selected bond lengths (Å) and angles (°): P2–P3 2.0893(3), P2–Ag1 2.4323(3), P3–Ag1 2.4623(4), P1–C1 1.7510(3), P1–C2 1.8225(3), P1–Fe1 2.3092(3), P2–Fe1 2.3301(2), P3–

Fe1 2.2709(3), C1–Fe1 2.1397(2), C2–Fe1 2.1084(2), Ag1–P2–P3 121.332(7), Ag1–P3–P2 119.374(5), P2–Ag1–P3 115.416(4).

Similar to the dimeric copper complexes **10** and **16**, the cationic part of compound **19** consists of two triphosphaferrocene units doubly bridged to two silver centers by the two adjacent phosphorus atoms of the $P_3C_2{}^tBu_2$ ring system forming a six-membered ring (Figure 3.2.15). The two silver atoms lie above and below the plane defined by the phosphorus atoms P2, P3, P´2 and P´3 (deviation of silver atoms from P2P3P´2P´3 plane = 0.424(1) Å) and are triply coordinated to two phosphorus atoms of two different P_3C_2 rings and one nitrogen atom of an acetonitrile molecule, creating a P–Ag–P angle of 115.42(4)°. The two slightly different Ag–P bond lengths are observed (2.4323(3), 2.4623(4) Å) in **19** and both are remarkably longer than the Cu–P bond length (2.2847(19) Å) in the compound **16**. The P–P bond length (2.0893(3) Å) in **19** is shorter than that in **16** (2.116(2) Å) and the free complex [Fe(η^5-$P_3C_2{}^tBu_2$)] (2.114(1) Å)[54].

3.2.3. The triphosphaferrocene [Cp'''Fe(η^5-P_3C_2PhH)] as a ligand

3.2.3.1. Reaction of [Cp'''Fe(η^5-P_3C_2PhH)] with copper halides

While the previous investigation of the reactivity and coordination behaviour of 1,2,4-triphosphaferrocenes shows that only two adjacent phosphorus atoms can coordinate to a copper center keeping the cyclo-P_3C_2 ring intact or fragmented during the reaction, no coordination of the third phosphorus atom occurs because of the probable steric hindrance of the two bulky *tert*-butyl groups. It is expected that 1,2,3-triphosphaferrocene would form oligomers or polymers with 1,2-, 1,3- or 1,2,3-coordination modes. Copper(I) halides were treated with [Cp'''Fe(η^5-P_3C_2PhH)] and red crystals were obtained from a layering reaction involving CuBr/MeCN and [Cp'''Fe(η^5-P_3C_2PhH)]/CH_2Cl_2 (equation 3.11). Treatment of [Cp'''Fe(η^5-P_3C_2PhH)] with CuCl and CuI, respectively, yielded amorphous products which could not be adequately characterised.

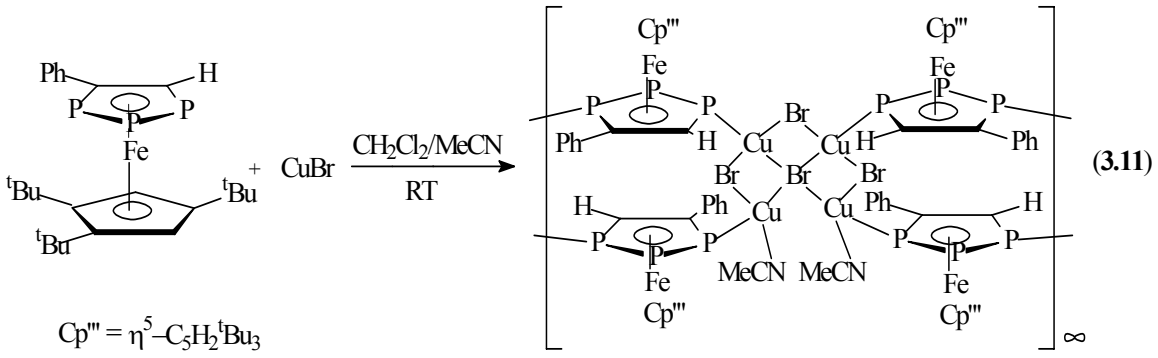

(**3.11**)

20

Complex **20** dissolves sparingly in CH_2Cl_2 and MeCN, and is not soluble in THF and toluene. It can be stored under an inert atmosphere at ambient conditions.

Because of the limited solubility of the complex **20**, the mother liquor of the reaction mixture was used for NMR measurement. Three slightly broadened doublet of doublets (δ = 40.5, 37.7 and 0.2 ppm) representing a AA'M spin system were present in the $^{31}P\{^1H\}$ NMR spectrum. In comparison to the signals of the uncoordinated [Cp'''Fe(η^5-P_3C_2PhH)] compound (δ = 51.7, 48.9 and 15.2 ppm), a 10 – 15 ppm upfield shift is observed. The coupling constants ($J(P_A,P_M)$ = 436.4 and $J(P_M,P_{A'})$ = 419.6 Hz) are somewhat larger than that of starting material [Cp'''Fe(η^5-P_3C_2PhH)] ($J(P_A,P_M)$ = 427.4 and $J(P_M,P_{A'})$ = 399.6 Hz).

In the ESI-MS spectrum of **20** in MeCN, peaks corresponding to the cations $[\{Cp'''Fe(P_3C_2PhH)\}_2Cu_3Br_2]^+$, $[\{Cp'''Fe(P_3C_2PhH)\}_2Cu_2Br]^+$ and $[\{Cp'''Fe(P_3C_2PhH)\}_2Cu]^+$ were detected.

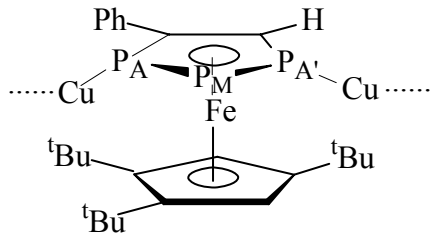

Figure 3.2.16. Possible oligomers in the solution of complex **20**.

The NMR and mass spectra suggest that complex **20** is depolymerised to oligomers in solution (Figure 3.2.16).

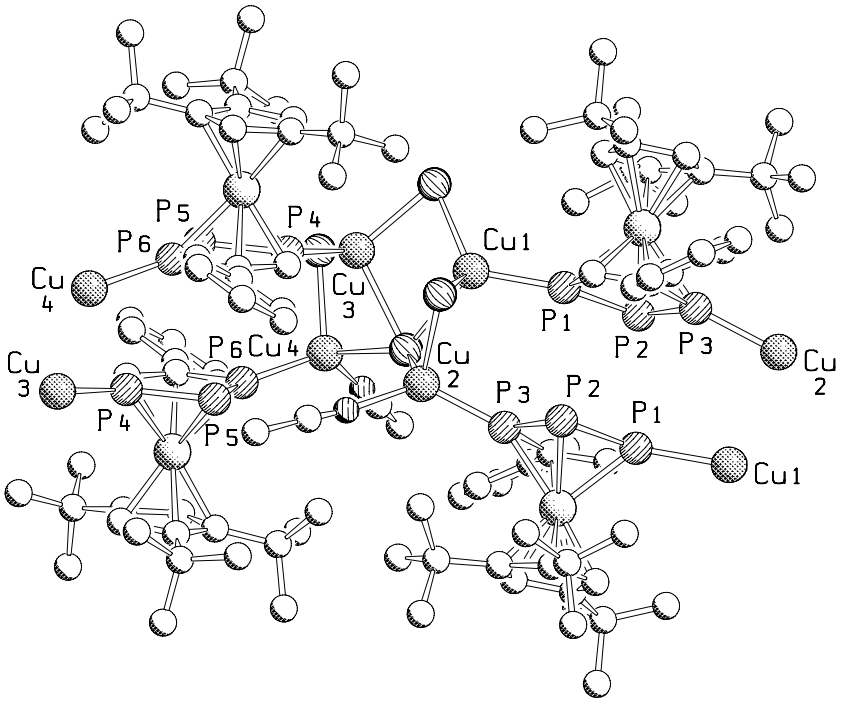

Figure 3.2.17. Section of the 1D polymeric structure of complex **20** (H atoms are omitted for clarity). Selected bond lengths (Å) and angles (°): P1–P2 2.128(2), P2–P3 2.124(2), P1–C18 1.743(5), P3–C37 1.781(5), P1–Cu1 2.2394(17), P3–Cu2 2.2175(16), P4–P5 2.122(2), P5–P6 2.117(2), P4–C36 1.744(6), P6–C44 1.782(5), P6–Cu4 2.2214(17), P4–Cu3 2.2012(17), Cu1–Br1 2.4701(10), Cu1–Br2 2.7372(10), Cu1–Br3 2.4153(10), Cu2–Br1 2.4797(10), Cu2–Br2 2.5245(10), Cu3–Br2 2.6205(9), Cu3–Br3 2.4347(10), Cu3–Br4 2.4761(10), Cu4–Br2 2.6240(10), Cu4–Br4 2.4701(10), P1–Cu1–Br3 121.68(5), P4–Cu3–Br3 119.25(5), P3–Cu2–Br1 102.59(5), P6–Cu4–Br2 114.36(5).

The structure of complex **20** has been established by X-ray crystallography and is shown in Figure 3.2.17. It consists of a polymer chain, in which a $(CuBr)_4$ unit is doubly bridged by the [Cp'''Fe(η^5-P_3C_2PhH)] moieties in a 1,3 coordination mode. Each copper atom of this unit which consists of three annelated four-membered $(CuBr)_2$ rings, coordinated in a distorted tetrahedral fashion to one phosphorus atom from four different [Cp'''Fe(η^5-P_3C_2PhH)] units with an average P–Cu–Br angle of 114.5° and P–Cu bond length of 2.2199 Å (Figure 3.2.18). The P–P bond lengths in the cyclo-P_3C_2 rings (P1–P2 2.128 (2), P2–P3 2.124 (2) Å) of complex **20** are comparable to that in [Cp'''Fe(η^5-$P_3C_2Ph_2$)][14] (P1–P2 2.1287(14), P2–P3 2.1193(15) Å).

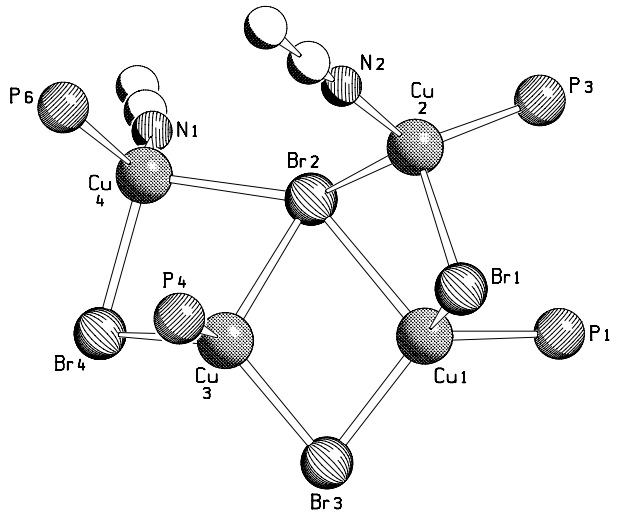

Figure 3.2.18. Cage structure of $(CuBr)_4$ in **20**.

3.2.3.2. Reaction of [Cp'''Fe(η^5-P_3C_2PhH)] with [($PtCl_2PEt_3$)$_2$]

According to the results of Nixon and coworkers, the Pt(II) center of $[\{PtCl_2(PR_3)\}_2]$ coordinates to 1,2,4-triphosphaferrocene to form the sterically unfavourable *cis*-isomers and the complexes are non-fluxional in solution.[20] Similar results were expected from the reaction of 1,2,3-triphosphaferrocene with a half equivalent of $[\{PtCl_2(PEt_3)\}_2]$. Furthermore, one and two equivalents of $[\{PtCl_2(PEt_3)\}_2]$ were also used to react with the triphosphaferrocene.

A mixture of [Cp'''Fe(η^5-P_3C_2PhH)] and $[\{PtCl_2(PEt_3)\}_2]$ in CH_2Cl_2 in a ratio of 2:1 was stirred at room temperature for one hour to form a brown solution. After remove of the solvent under vacuum, a brown powder of **21** was obtained (equation 3.12).

The compound **21** is soluble in CH_2Cl_2 and THF, but not in nonpolar solvents such as alkanes. It can be stored under an inert atmosphere at low temperature.

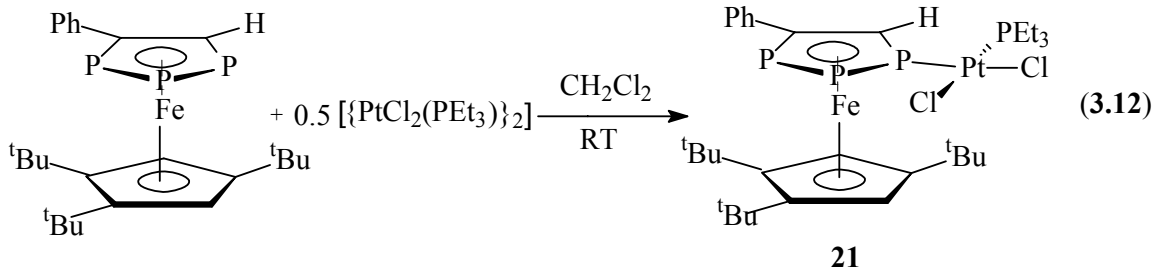

(**3.12**)

21

The $^{31}P\{^{1}H\}$ NMR spectrum of **21** contains four signal groups. The doublet of doublet of doublets signal with ^{195}Pt satellites centered at δ = 77.1 ppm is attributed to P_c, which coordinates to the Pt(II) center with a large coupling constant $J(P_c,Pt)$ = 4017.5 Hz. The coordination of P_c (not P_a) with Pt was confirmed by the P–H coupling constant ($J(P_c,H_a)$ = 28.2, $J(P_a,H_a)$ = 6.5 Hz) in the ^{31}P NMR spectrum. In comparison to the uncoordinated compound [Cp'''Fe(η^5-P_3C_2PhH)] ($\delta(P_c)$ = 48.9 ppm) this signal is shifted about 10 ppm downfield. The reason may be the back bonding from the d-orbitals of the Pt center to the P_c atom. The signals attributed to P_a are centered at δ = 17.4 ppm and have the smallest P-Pt coupling constant ($J(P_a,Pt)$ = 30 Hz), while the signals centered at δ = -68.2 ppm which have the largest P–P coupling constant ($J(P_b,P_c)$ = 517.5 Hz) must belong to the P_b atom. The doublet at δ = 9.9 ppm belongs to the P_d atom with ^{195}Pt satellites centered at δ = 0.1 and 20.2 ppm ($J(P_d,Pt)$ = 3212.9 Hz). The P_d and P_c atoms must be in the cis position, because of its relatively small coupling constant ($J(P_d,P_c)$ = 28.0 Hz), otherwise the coupling between P_c and P_d would be much larger (about 500Hz) (Figure 3.2.19). The sharp signals representing these four phosphorus atoms in the $^{31}P\{^{1}H\}$ NMR spectrum of **21** at room temperature indicate that no dynamic process exists in solution.

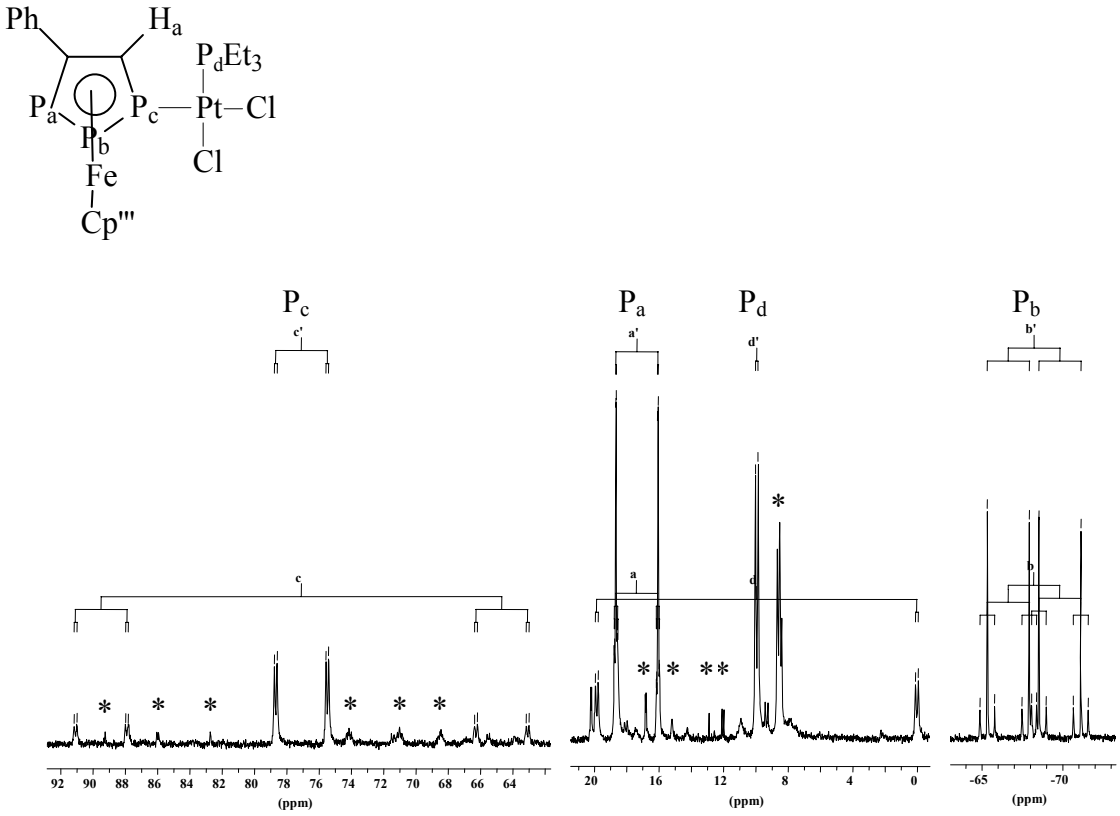

Figure 3.2.19. $^{31}P\{^{1}H\}$ NMR spectrum of complex [{Cp'''Fe(μ,η^5:η^1-P_3C_2PhH)}{$PtCl_2(PEt_3)$}]. Signals with a, b, c, and d represent the P atoms coupled with the isotope ^{195}Pt (peaks marked with an asterisk are due to impurity).

In the mass spectra of the reaction solutions of [Cp'''Fe(η^5-P_3C_2PhH)] with one and two equivalents of [{$PtCl_2(PEt_3)$}$_2$] no signals representing the expected product or its fragments are detected.

The ^{31}P NMR spectra of the reaction solutions of [Cp'''Fe(η^5-P_3C_2PhH)] with one and two equivalents of [{$PtCl_2(PEt_3)$}$_2$] show one singlet at δ = 11.3 ppm with two satellites (δ = -0.5 and 23.1 ppm, *J*(P,Pt) = 3831.3 Hz) attributed to the phosphorus atom of [{$PtCl_2(PEt_3)$}$_2$]. Except for minor impurities, no other peaks appear in the spectrum. The NMR and mass spectral data suggest that the triphosphaferrocene decomposes when more equivalents of [$PtCl_2(PEt_3)$] are present.

A possible explanation for the coordination of only one [$PtCl_2(PEt_3)$] unit to the P_3C_2-ring of compound **8**, as illustrated in equation 3.12, is that the quadratic planar coordination mode of platinum is sterically demanding. It is difficult for a second [$PtCl_2(PEt_3)$] unit to coordinate to the cyclo-P_3C_2 ring of compound **8**, as in the case of the complex [CpFe(η^5-$P_3C_2{}^tBu$)] does,[20] because of the bulky Cp'''-group.

3.2.3.3. Reaction of [Cp'''Fe(η^5-P_3C_2PhH)] with [$W(CO)_5$THF]

Since 1,2,3-triphosphaferrocene has three phosphorus atoms in the phospholyl ring, it is attractive to explore whether all three phosphorus atoms can coordinate to metal centers simultaneously. An alternative approach with tungstenpentacarbonyl units as Lewis acids was used for this purpose.

In a first approach, one and two equivalents, respectively, of [$W(CO)_5$THF] were mixed with [Cp'''Fe(η^5-P_3C_2PhH)] and stirred for one hour. Afterwards, the red-orange solutions were concentrated to about one-third of the original volume and the concentrates were kept at -28 °C. From both concentrates the air sensitive red-orange crystalline compound **22** was obtained (equation 3.13).

Complex **22** dissolves in CH_2Cl_2 and THF, moderately in nonpolar solvents such as alkanes. It can be stored under an inert atmosphere at low temperature.

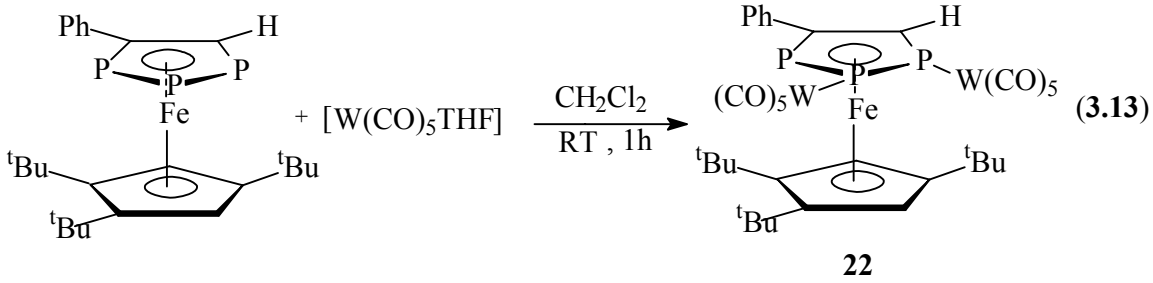

22 (**3.13**)

In the EI-MS spectrum of **22** the fragment with the highest relative abundance is attributable to the [Cp'''Fe(P_3C_2PhH)]$^+$ cation. In addition, the cations [Cp'''Fe(P_3C_2PhH)$W(CO)_5$]$^+$ and [Cp'''Fe(P_3C_2PhH)W]$^+$ are also detected in the mass spectra. These mass spectral data indicate that an adduct compound of [Cp'''Fe(η^5-P_3C_2PhH)] and [$W(CO)_5$] must exist.

The solid-state structures of **22** have been established by X-ray crystallography as shown in Figure 3.2.20. In complex **22,** two phosphorus atoms in the cyclo-P_3C_2 ring coordinate to two tungsten centers with an average P–W bond length of 2.502 Å. The coordination geometry of the two phosphorus atoms is distorted trigonal. Due to the repulsion between the two bulky $W(CO)_5$ units, the two P–W bonds curl upwards slightly from the cyclo-P_3C_2 plane in order to keep the two $W(CO)_5$ units away from each other. In comparison to the P2–P3 bond length

(2.130(3) Å), the P1–P2 bond length is obviously shorter (2.112(3) Å) resulting from the coordination of the lone pairs of the two phosphorus atoms to the tungsten centers.

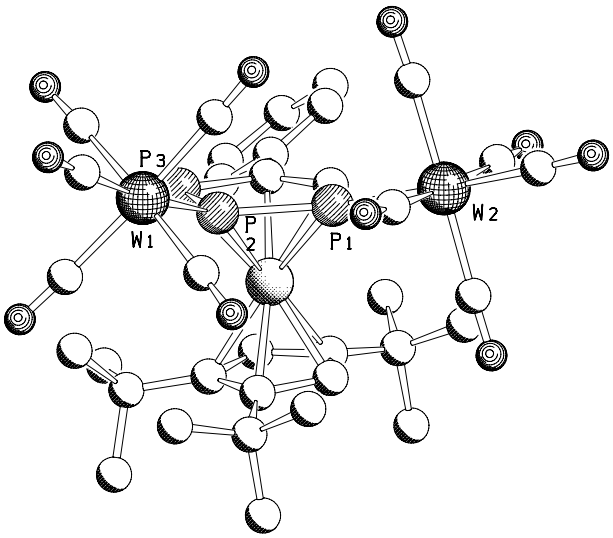

Figure 3.2.20. Molecular structure of **22** in the crystal (Hydrogen atoms are omitted for clarity). Selected bond lengths (Å) and angles (°): P1–P2 2.112(2), P2–P3 2.130(2), P1–C22 1.746(8), P3–C21 1.772(6), P1–W2 2.488(2), P2–W1 2.515(2), Fe–P1 2.332(2), Fe–P2 2.369(2), Fe–P3 2.363(2), P1–P2–P3 100.54(11), P3–P2–W1 124.69(10), P2–P1–W2 137.41(11), W2–P1–C22 122.7(3), P2–P1–C22 97.5(3).

In the $^{31}P\{^{1}H\}$ NMR spectrum of **22** at room temperature, except for a broadened doublet (δ = 38 ppm) attributable to the $P_{A'}$ atom which shifts by 10 ppm upfield relative to that of the starting material ($\delta(P_{A'})$ = 48 ppm), one unexpectedly huge upfield shift of P_M (δ = -81 ppm, in the starting material $\delta(P_M)$ = 15 ppm) was found. The P_A (δ = 49 ppm) signal of the complex is slightly different from that of the starting material (52 ppm). As the temperature is reduced, the signals of the $^{31}P\{^{1}H\}$ NMR spectrum become clearer. At -40 °C the spectrum shows sharp signals. The doublet of doublets at δ = 49 ppm attributing to the P_A and the doublet of doublets at δ = 37.4 ppm representing the $P_{A'}$ show tungsten satellites with coupling constants $J(P_A,W)$ = 250.6 and $J(P_{A'},W)$ = 251.8 Hz, respectively. These spectra indicate that complex **22** exhibits a dynamic process in solution. At room temperature, the two tungsten centers change their positions between the three phosphorus atoms of the P_3C_2-ring very quickly and is manifested by the three broad signals in the $^{31}P\{^{1}H\}$ NMR spectrum. At low temperature, this motion is slower and the two tungsten centers are fixed on the P_A and

$P_{A'}$ of the P_3C_2-ring (Figure. 3.2.21). It is difficult to explain why the two tungsten centers coordinate to the P_M and $P_{A'}$ atoms in the solid state, but to the P_A and $P_{A'}$ in solution at low temperature.

The coupling constant of $J(P_M,P_{A'})$ (466.3 Hz) is slightly larger than that of $J(P_A,P_M)$ (462.3 Hz), but in the starting material exactly the opposite is observed ($J(P_A,P_M)$ = 427.4 and $J(P_M,P_{A'})$ = 399.6 Hz).

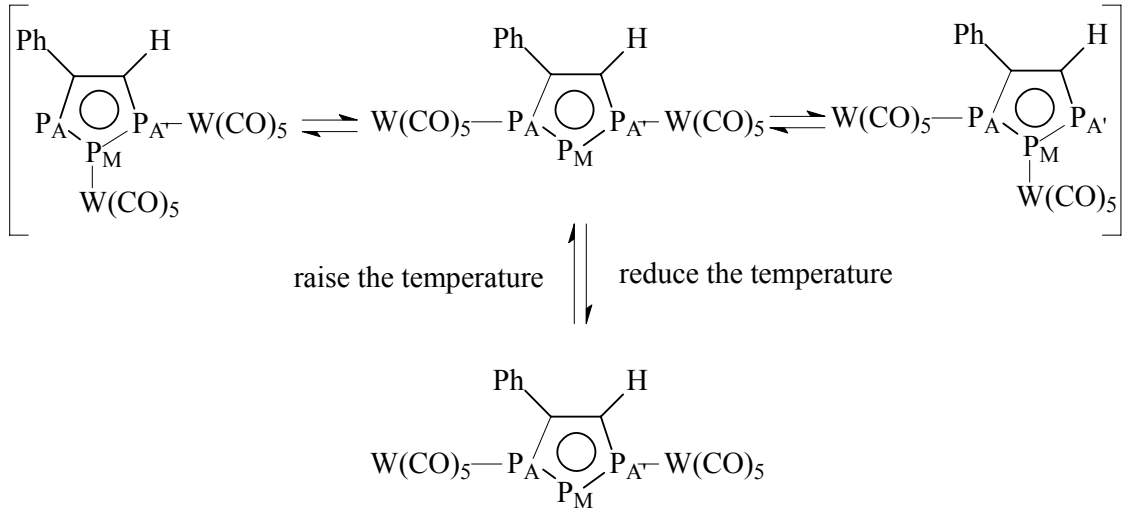

Figure.3.2.21. Proposed dynamic behaviour of **22** in solution.

As discussed previously, treatment of [Cp'''Fe(η^5-P_3C_2PhH)] with one half equivalent of [{$PtCl_2(PEt_3)$}$_2$], one or two equivalents of [$W(CO)_5THF$] and two equivalents of CuBr, respectively, yields products in which the P_3C_2-ring is coordinated to metal centers in a 1-, 1,2-, and 1,3-coordination mode, respectively. When an excess (> three equivalents) of [$W(CO)_5THF$] was stirred with [Cp'''Fe(η^5-P_3C_2PhH)] over night and the reaction solution was kept at -28 °C for one week, orange-red plates of **23** were obtained (equation 3.14).

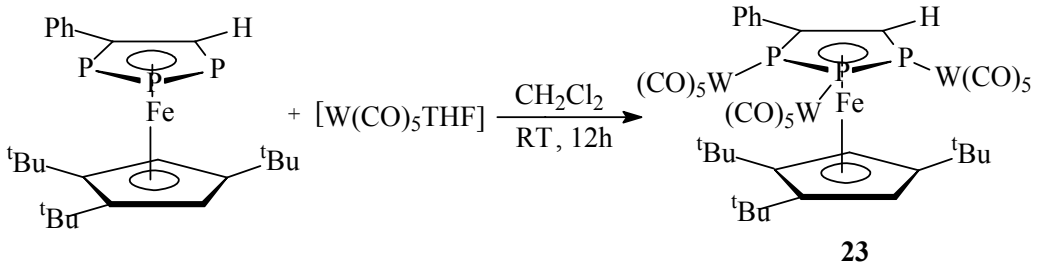

(**3.14**)

23

Complex **23** dissolves readily in CH_2Cl_2 and THF, moderately in nonpolar solvents such as alkanes. It is air sensitive and can be stored under an inert atmosphere at low temperature.

In the EI-MS spectra of **23** no molecular ion was detected, but fragments such as $[Cp'''Fe(\eta^5\text{-}P_3C_2PhH)\{W(CO)_5\}_2]^+$, $[Cp'''Fe(\eta^5\text{-}P_3C_2PhH)W(CO)_5]^+$, and $[Cp'''Fe(\eta^5\text{-}P_3C_2PhH)W]^+$ were found. These data indicate that $[Cp'''Fe(\eta^5\text{-}P_3C_2PhH)\{W(CO)_5\}_3]$ can not exist under the electron impact conditions and suggests it may be not as stable as $[Cp'''Fe(\eta^5\text{-}P_3C_2PhH)\{W(CO)_5\}_2]$ (**22**).

The solid-state structure of **23** has been established by X-ray crystallography as shown in Figure 3.2.22.

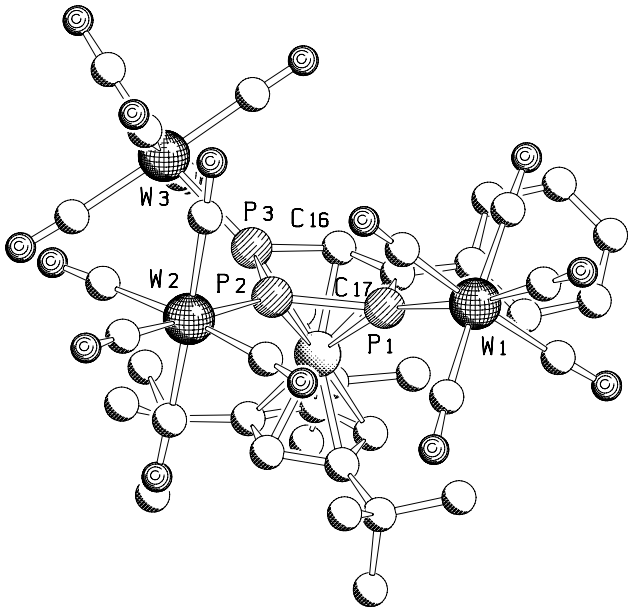

Figure 3.2.22. Molecular structure of **23** in the crystal (Hydrogen atoms are omitted for clarity). Selected bond lengths (Å) and angles (°): P1–P2 2.125(2), P2–P3 2.121(2), P1–C17 1.755(7), P3–C16 1.751(6), P1–W1 2.5154(15), P2–W2 2.5135(17), P3–W3 2.5120(17), Fe–P1 2.3653(17), Fe–P2 2.3808(19), Fe–P3 2.3508(19), P1–P2–P3 99.45(9), P1–P2–W2 130.49(8), W2–P2–P3 129.43(8), W1–P1–P2 128.19(8), W3–P3–P2 133.92(9).

Complex **23** possesses three phosphorus atoms in the phospholyl ring coordinated to three different $[W(CO)_5]$ units. The P2–W2 bond, which is coplanar with the cyclo-P_3C_2 ring, has a bond length similar to the other two P–W bonds (P2–W2 2.5135(17), P1–W1 2.5154(15), P3–W3 2.5120(17) Å). Because of the repulsion of the two ^{t}Bu groups on the cyclopentadienal ring, the P1–W1 and P3–W3 bonds are bent upwards from the cyclo-P_3C_2 plane (Figure 3.2.22 and Figure 3.2.23). The average distance of W–P in **23** (2.514 Å) is longer than that in **22** (2.502 Å), the average P–P bond length (2.123 Å) is slightly longer than that in **22** (2.121

Å) and is almost same as that in complex [Cp'''Fe(η^5-$P_3C_2Ph_2$)] (2.124 Å).[9] The average P–Fe bond length in **23** (2.366 Å) is longer than that in **22** (2.355 Å). All these bond length elongations in **23** compared to **22** may be caused by steric factors.

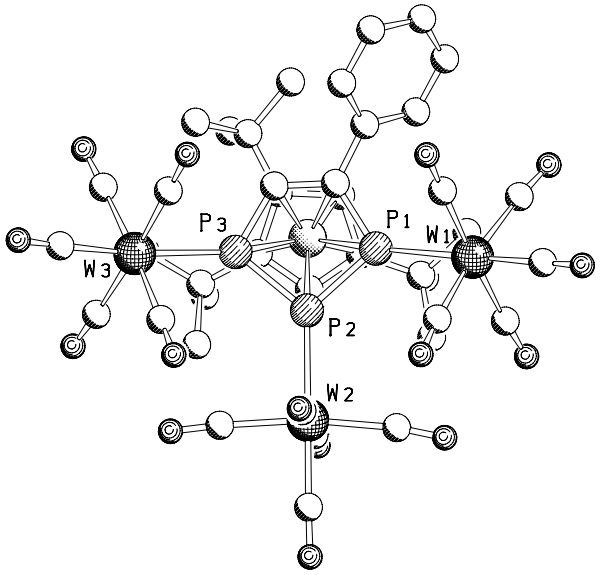

Figure 3.2.23. Top view of the molecule of **23** in the solid-state configuration. Hydrogen atoms are omitted for clarity.

The $^{31}P\{^1H\}$ NMR spectrum of complex **23** shows three slightly broadened doublet of doublets attributed to the P_A (δ = 2.7 ppm), $P_{A'}$ (δ = -3.7 ppm), and P_M (δ = -54.9 ppm) atoms, respectively. All signals shift upfield in comparison to the uncoordinated complex **8**. Compared to the chemical shift of P_M in complex **22**, the upfield shift here is not so enormous (Table 3.2.5). The coupling constant $J(P_M,P_{A'})$ (412.4 Hz) and $J(P_A,P_M)$ (446.7 Hz) are somewhat smaller than that of complex **22** ($J(P_M,P_{A'})$ = 466.3 and $J(P_A,P_M)$ = 462.3 Hz).

Table 3.2.5. Comparison of the ^{31}P NMR spectral data of [Cp'''Fe(η^5-P_3C_2PhH)] and its tungsten complexes **22** and **23**.

	$\delta(P_A)$ (ppm)	$\delta(P_M)$ (ppm)	$\delta(P_{A'})$ (ppm)	$J(P_A,P_M)$ (Hz)	$J(P_M,P_{A'})$ (Hz)
[Cp'''Fe(η^5-P_3C_2PhH)]	51.7	15.2	48.9	427.1	399.6
[Cp'''Fe(η^5-P_3C_2PhH){$W(CO)_5$}$_2$]	49.1	-80.9	38.0	462.3	466.3
[Cp'''Fe(η^5-P_3C_2PhH){$W(CO)_5$}$_3$]	2.7	-54.9	-3.7	446.7	412.4

3.2.4. Tetraphosphaferrocene [Cp'''Fe(η^5-P_4C^tBu)] as a ligand

Until now, the chemical properties and the ligation abilities of the cyclo-P_nC_{5-n} (n =1-5) moieties in the 1,3-di-phosphaferrocenes [Fe(η^5-$P_2C_3{}^tBu_3$)(η^5-C_5R_5)] (R = H[11]; R = Me[10]) and the 1,2,4-tri-phosphaferrocenes [Fe(η^5-$P_3C_2{}^tBu_2$)(η^5-C_5R_5)] (R = H[11]; R = Me[13]) were studied in the Nixon group, while these of [Fe(η^5-P_5)(η^5-C_5R_5)] (R = Me) were studied in our group. These investigations show that the lone pair of electrons on each phosphorus atom in the cyclo-P_nC_{5-n} (n =1-5) ligands gives a ligation propensity that leads to binuclear and tetranuclear adducts, polymer chains, or even fullerene-like nanoballs, in which the cyclo-P_nC_{5-n} ring remains intact or fragmentises. The ligation mode of the cyclo-P_nC_{5-n} ligand toward the transition metal center can be either side-on or end-on. In the 1,2,4-triphosphaferrocene metal complexes, only two neighboring phosphorus atoms of the P_3C_2 ring ligate to the metal center. It is interesting to study how the replacement of one or more CR fragments by a phosphorus atom in the phospholyl ring affects the tetraphospholyl ring and how the ligation properties and steric factors are influenced. The investigations of tetraphosphaferrocene ([Cp'''Fe(η^5-P_4C^tBu)]) as a ligand for copper halides, silver and gold salts were executed in this work and are discussed.

3.2.4.1. Reaction of [Cp'''Fe(η^5-P_4C^tBu)] with CuCl

3.2.4.1.1. [Cp'''Fe(η^5-P_4C^tBu)] with CuCl in a stoichiometric ratio of 1:1

CuCl in CH_3CN was layered onto a solution of [Cp'''Fe(η^5-P_4C^tBu)] in CH_2Cl_2 in a 1:1 ratio and kept at room temperature for two months. The color of the mixture turned gradually from green to dark green with some brown tone; red brown plates of [{Cp'''Fe(η^4-$P_3C^tBuP(O)^tBu$)}$_4${(μ-Cu_2Cl)(MeCN)$_2$}$_2${(μ-CuCl)$_2$(MeCN)}$_2$] (**24**) were obtained. This compound does not dissolve in common solvents such as CH_2Cl_2 and THF and can be stored under an inert atmosphere at ambient conditions.

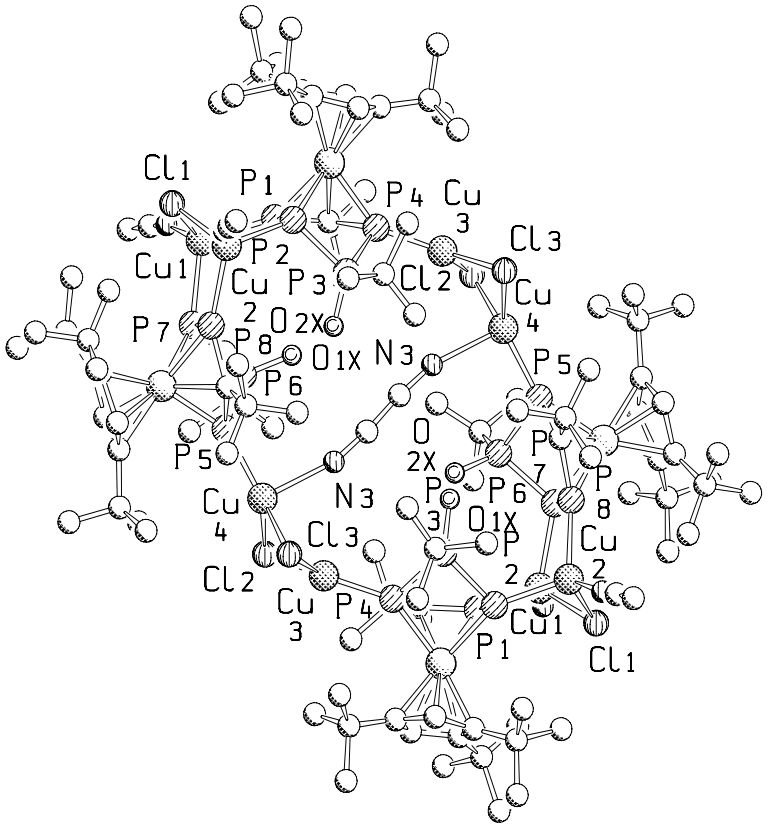

Figure 3.2.24. Molecular structure of **24** in the crystal (Hydrogen atoms are omitted for clarity, the N3CCN3 bridge in the structure represents two disordered CH_3CN molecules). Selected bond lengths (Å) and angles (°): P1–P2 2.1404(4), P2–P3 2.1244(3), P3–P4 2.1596(2), P1–Cu1 2.2474(4), P2–Cu2 2.2784(4), P7–Cu1 2.4139(5), P8–Cu2 2.3677(4), P4–Cu3 2.1256(4), Cu1–Cl1 2.3520(3), Cu2–Cl1 2.2784(4), Cu3–Cl2 2.2764(3), Cu3–Cl3 2.2801(3), P4–P3–P2 88.556(9), Cu2–Cl1–Cu1 89.917(6), P1–Cu1–P7 110.581(10), Cu3–Cl3–Cu4 75.209(7), Cl2–Cu3–Cl3 96.9291(7), Cl2–Cu3–P4 134.081(10), P4–Cu3–Cl3 128.444(10), Cl2–Cu4–Cl3 93.225(6).

The molecular structure of **24** was determined by single-crystal X-ray diffraction as illustrated in Figure 3.2.24. In compound **24** four tetraphosphaferrocene units are connected by two $(CuCl)_2$ fragments via one phosphorus atom and doubly connected by two Cu_2Cl fragments via two phosphorus atoms of the P_4C-ring. This implies that two chloride ions have been lost. The whole molecule is a ring with four tetraphosphaferrocene moieties.
The phosphorus atoms P3 and P6 are each connected to a ^{t}Bu group and an oxygen atom indicating that the cyclo-P_4C ring has been partially oxidized during the long reaction time. Each of the two Cu_2Cl units in the structure of **24**, may be seen as imparting a positive

charge to the molecule. Meanwhile the oxygen atoms O1x and O2x, which form double bonds with P6 and P3, respectively (av bond length: 1.547Å), [61] could be connected through a proton (hydrogen bridge). The P_3C-coordination mode of the P_4C unit in **24** would mean that the ferrocene moieties represent only 17 VE species. However, the diamagnetism of the overall complex suggests that these moieties are best described as 18 VE $[Cp'''Fe(\eta^4\text{-}P_3C^tBuP(O)^tBu)]^-$ species. The molecule is thus neutral (Figure 3.2.25). Unfortunately, no Raman and IR spectra could be recorded to proof the existence of the hydrogen atom. It is difficult to explain the origin of the oxygen atoms, which may come from the solvent or poorly sealed schlenks over the long reaction time. The *tert*-butyl group connected on the phosphorus atom may have come from the decomposed starting material. The coordination geometry of two copper atoms (Cu3) in the complex **24** are trigonal planar whereas the rest copper atoms are tetrahedrally coordinated and two of them (Cu4) are bridged by two disordered MeCN molecules.

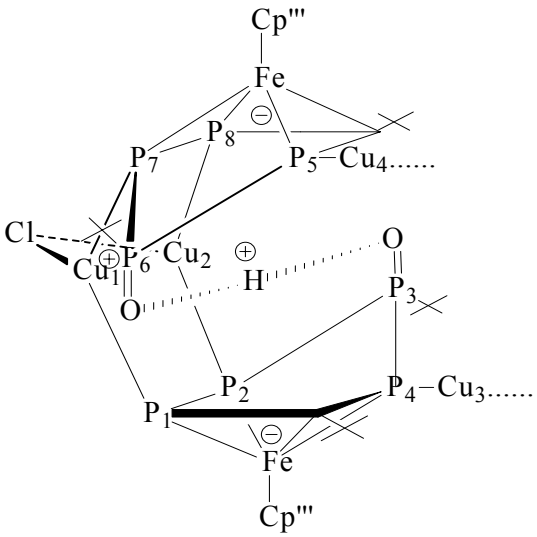

Figure 3.2.25. Proposed charge balance in the half of complex **24**.

The average distance of coordinated phosphorus-iron atoms in complex **24** (2.3183 Å) is shorter than that in the uncoordinated tetraphosphaferrocene (2.3673 Å). There are two groups of P–Cu bonds: a long group that represents bond lengths of the two adjacent phosphorus atoms bound to the copper atoms in the double bridge (P1–Cu1: 2.2474(4) Å, P2–Cu2: 2.2784(4) Å), and a group with short bond lengths represents the phosphorus atoms bound to the copper atoms of the $(CuCl)_2$ bridge (P4–Cu3: 2.1256(4) Å, P5–Cu4: 2.2217 Å). The average bond length of P2–P3 and P3–P4 (2.1503 Å) is longer than that of

the uncoordinated tetraphosphaferrocene (2.1185 Å) because the P_4C-ring of complex **24** is η^4-ligated instead of η^5 to the iron atom and the P3 as well P6 atoms are out of the ring plane.

In the ^{31}P NMR spectrum of the reaction solution of **24,** four broad signals at δ = 15.3, 25.1, 57.0, and 87.9 ppm were detected. This alludes to the fact that the four phosphorus atoms of the P_4C ring in the compound **24** are chemically and magnetically inequivalent. In comparison to the starting material **3** (δ = 80.4, 122.8 ppm) the chemical shifts of the phosphorus atoms are shifted upfield. Since complex **24** shows broad signals, no coupling constant can be resolved.

In the ESI-MS spectrum, peaks corresponding to $[Cp'''Fe(P_4O^tBuC)Cu_2Cl]^+$ and $[Cp'''Fe(P_4O^tBuC)CuCl]^+$ are detected.

3.2.4.1.2. [Cp'''Fe(η^5-P_4C^tBu)] with CuCl in a stoichiometric ratio of 1:2

Since one more phosphorus atom is present in the phospholyl ring of [Cp'''Fe(η^5-P_4C^tBu)] compared to triphosphaferrocene, it is also expected that the cyclo-P_4C ring can coordinate to more metal centers. Indeed, when two equivalents of CuCl in MeCN were carefully layered onto a CH_2Cl_2 solution of [Cp'''Fe(η^5-P_4C^tBu)], brown crystals of the polymeric complex $[\{Cp'''Fe(\eta^5:\eta^1:\eta^1:\eta^1\text{-}P_4C^tBu)\}_2(\mu\text{-}CuCl)_2]_\infty$ (**25**) were formed, in which a [Cp'''Fe(η^5-P_4C^tBu)] moiety is linked via two phosphorus atoms in the phospholyl ring by two Cu centers to another [Cp'''Fe(η^5-P_4C^tBu)] moiety. The third phosphorus atom of this phospholyl ring coordinates to a copper atom of a $(CuCl)_2$ unit, which is bridged again by two [Cp'''Fe(η^5-P_4C^tBu)] moieties (Equation 3.15) to form a second chain.

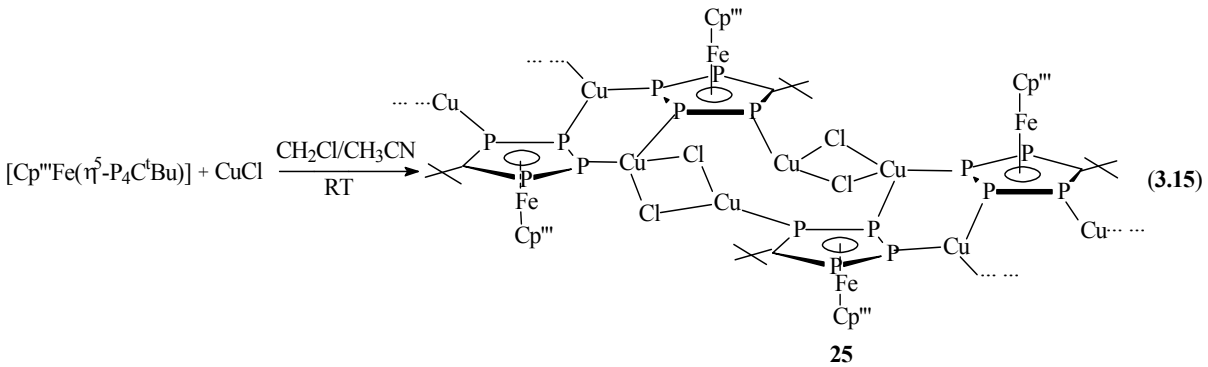

25 **(3.15)**

Complex **25** is sparingly soluble in CH_2Cl_2 and acetonitrile, but insoluble in toluene and hexane; it can be stored in an inert atmosphere at ambient conditions.

The molecular structure of **25** was determined by single-crystal X-ray diffraction and is illustrated in Figure 3.2.26.

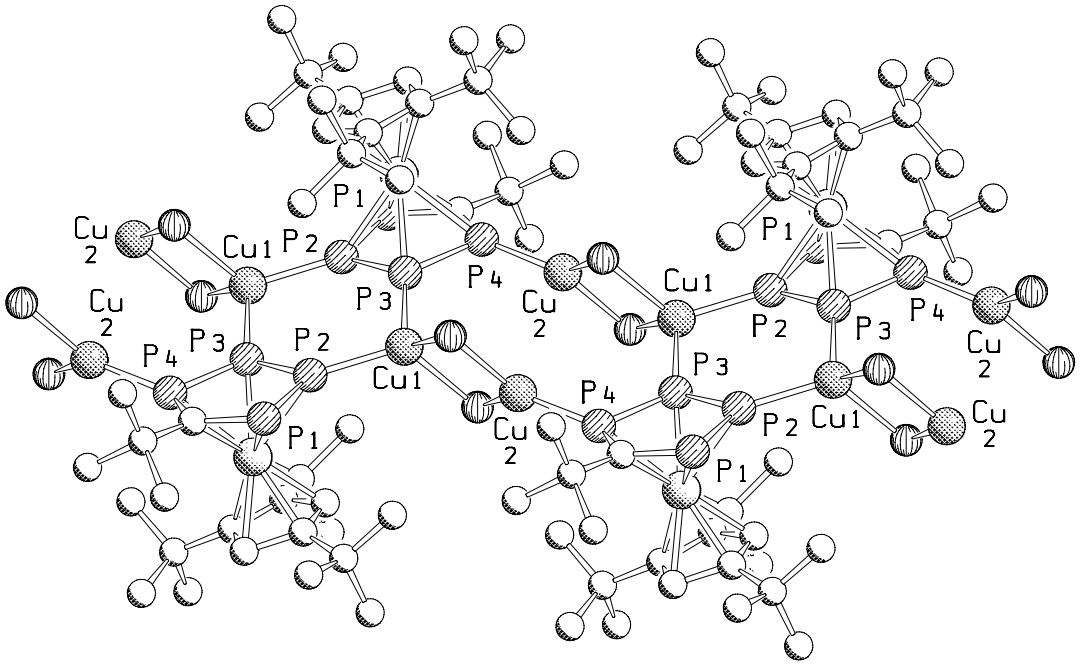

Figure 3.2.26. Section of the 1D polymeric structure of **25** in the crystal (Hydrogen atoms are omitted for clarity). Selected bond lengths (Å) and angles (°): P1–P2 2.1176(5), P2–P3 2.1173(6), P3–P4 2.0826(6), P2–Cu1 2.2350(6), P3–Cu1 2.2879(6), P4–Cu2 2.1490(5), Cu1–Cl1 2.3284(8), Cu1–Cl2 2.3827(8), Cu2–Cl1 2.2566(8), Cu2–Cl2 2.2580(8), Cu1–P2–P3 123.392(23), P2–P3–Cu1 127.016(19), P3–Cu1–P2 105.641(3), P3–P4–Cu2 115.523(26), Cl1–Cu2–Cl2 102.552(8), Cl1–Cu1–Cl2 96.762(8), P4–Cu2–Cl1 127.17(13), Cl1–Cu2–Cl2 102.55(8), P4–Cu2–Cl2 130.27(22).

In the solid state structure of **25**, the tetraphosphaferrocene bridges $(CuCl)_2$ fragments to form a chain, and two chains connect each other via the P–Cu bonds. Two P_4C rings bridge two copper atoms, thus forming a six-membered ring. One of the two copper atoms, Cu(1), coordinates tetrahedrally with two phosphorus atoms and two chlorine atoms while the other copper atom, Cu(2), is in a trigonal planar environment and is surrounded by one phosphorus atom and two chlorine atoms. The distances between the Cu(1) atom and the

two phosphorus atoms are different (Cu(1)–P(2): 2.2350(6) Å, Cu(1)–P(3): 2.2879(6) Å) and are both longer than the Cu(2)–P(4) (2.1490(5) Å) bond lengths. The P–P bond lengths of P(2)–P(3) (2.1173(6) Å) and P(3)–P(4) (2.0826(6) Å) in complex **25** are shorter than those in the uncoordinated tetraphosphaferrocene **3** (2.131(12) Å, 2.106(14) Å). This is an effect of the three phosphorus atoms participating in η^1-bonding with the Cu atoms through the phosphorus lone pairs. The other P(1)–P(2) bond lengths differ only slightly (**25**: 2.1176(5) Å, **3**: 2.119(11) Å).

The positive ESI-MS of **25** in MeCN at room temperature shows a peak with 100% relative abundance corresponding to $[Cp'''Fe(P_4C^tBu)CuMeCN]^+$. In addition, fragments corresponding to $[\{Cp'''Fe(P_4C^tBu)\}_2Cu]^+$ and $[\{Cp'''Fe(P_4C^tBu)\}_2Cu_2Cl]^+$ were also detected. These ESI-MS results suggest that the polymeric structure of **25** is cleaved by MeCN and oligomers are present in solution. This suggestion is confirmed by the ^{31}P NMR spectrum of the reaction solution in a mixture of C_6D_6, CH_2Cl_2, and CH_3CN.

The $^{31}P\{^1H\}$ NMR spectrum of the reaction mixture at room temperature presents broad signals of an AA´MM´ spin system with $\delta(P_A)$ (107.1 ppm) and $\delta(P_M)$ (57.7 ppm). In comparison with the phosphorus chemical shifts of the free complex **3** ($\delta(P_A)$ = 122.8 ppm and $\delta(P_M)$ = 80.4 ppm), an obvious upfield shift occurred probably due to the coordination of the lone pairs of the phosphorus atoms in the P_4C ring to the copper atoms. Since the four phosphorus atoms of each P_4C-ring of polymer **25** are not chemically equivalent, this signal pattern suggests that a dynamic process occurs in solution at room temperature.

Variable temperature spectra were thus recorded in a 3:1 mixture of THF-d_8 and CH_3CN. At room temperature in this mixture, there are signals of an AA´MM´ spin system at 119.2 and 73.6 ppm. By lowering the temperature to 0 °C, a slightly high field shift of the signals at 115.6 and 67.9 ppm is observed. When the temperature is reduced, the signals broaden further and at -30 °C the spectrum is reminiscent of an ADMN spin system. The broad signals, attributable to P_A and $P_{A'}$, are split into two broad signals centered at about 116 and 106 ppm, respectively (Figure 3.2.28). The integration ratio of these three broad signals is 1:1:2. These spectral data indicate that at room temperature, a fast equilibrium between **25a** and **25b** takes place and the oligomer $[\{Cp'''Fe(\eta^5\text{-}P_4C^tBu)\}_2(CuClMeCN)_2]$ **25a** may be dominant, in which two phosphorus atoms (P_M and $P_{M'}$) of the P_4C-ring are coordinated to the copper(I) centers. However, at low temperature this exchage slows down. The monomer $[\{Cp'''Fe(\eta^5\text{-}P_4C^tBu)\}\{CuCl(MeCN)_2\}]$ **25b** takes the dominat side of the equilibrium and is revealed in the ^{31}P NMR spectrum (Figure 3.2.27).

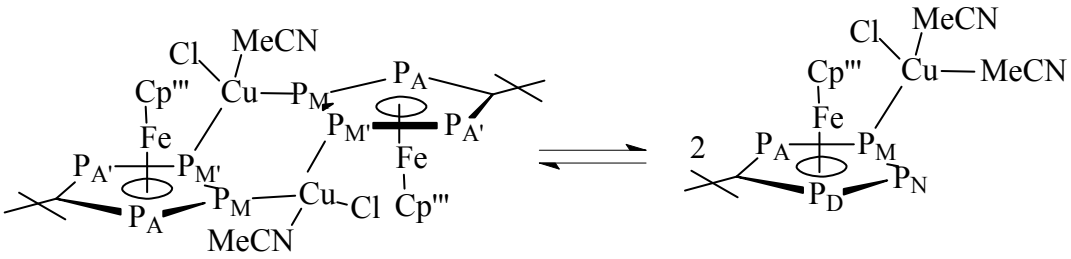

25a **25b**

Figure 3.2.27. Proposed equilibrium of oligomer **25a** and monomer **25b** in solution.

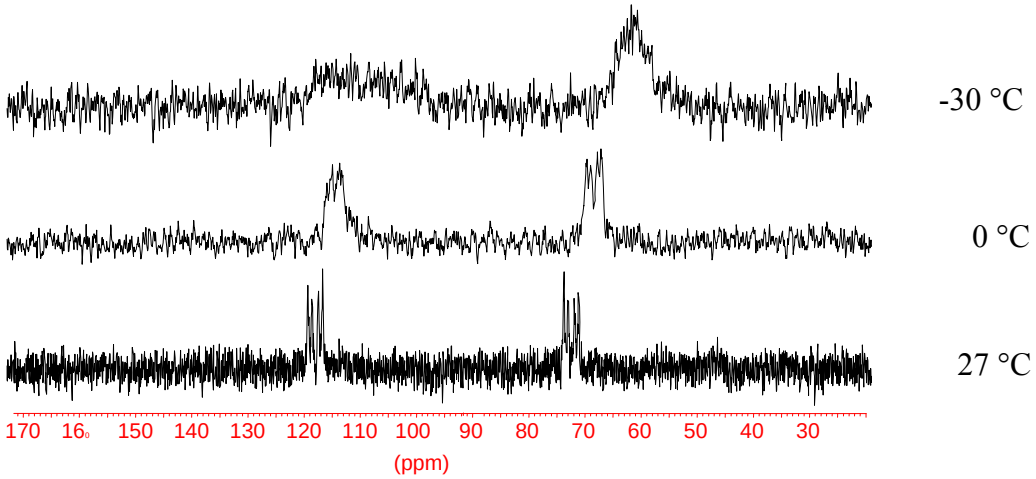

Figure 3.2.28. Variable temperature $^{31}P\{^{1}H\}$ NMR spectra of the reaction mixture of **25** in a 3:1 mixture of THF-d_8 and CH_3CN.

3.2.4.2. Reaction of [Cp'''Fe(η^5-P_4C^tBu)] with CuBr and CuI

3.2.4.2.1. Reaction of [Cp'''Fe(η^5-P_4C^tBu)] with CuBr in a ratio of 1:1

When CuBr in CH_3CN was layered onto a green solution of [Cp'''Fe(η^5-P_4C^tBu)] in CH_2Cl_2 in a 1:1 ratio, dark green needles of the complex [{Cp'''Fe(μ,η^5:η^1-P_4C^tBu)}$_2$($P_8C_4{}^tBu_4$)$_2$(Cu_3Br_3)$_2$($MeCN$)$_2$] (**26**) were formed.

This compound dissolves sparingly in MeCN and CH_2Cl_2, but does not dissolve in toluene and hexane. Therefore, no NMR investigation were possible for **26**. It is air sensitive and can be stored under an inert atmosphere at ambient conditions.

The molecular structure was determined by single-crystal X-ray diffraction and is illustrated in Figure 3.2.29.

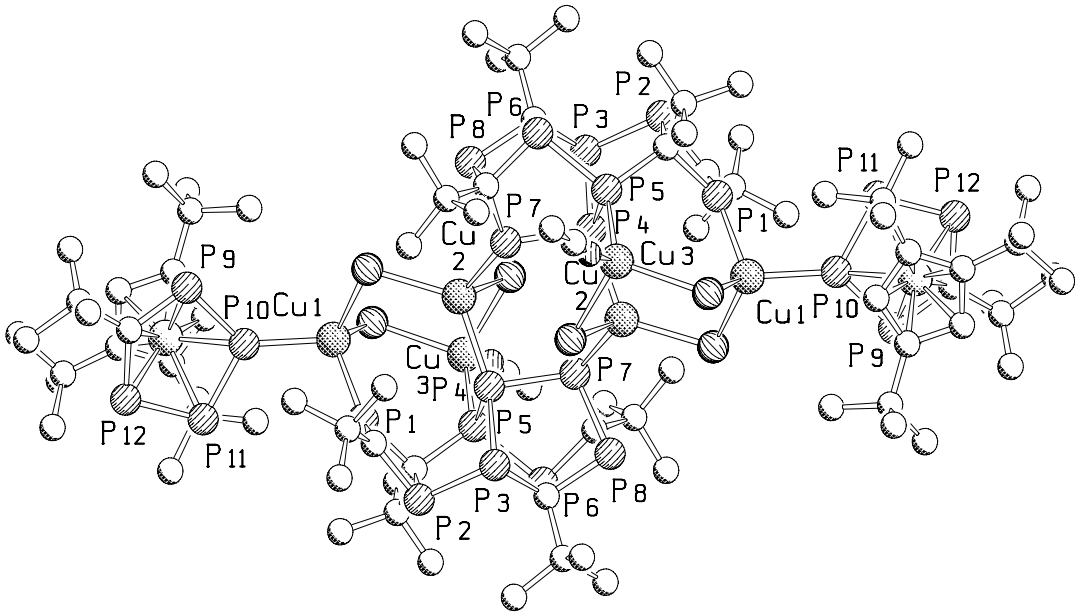

Figure 3.2.29. Molecular structure of $[\{Cp'''Fe(\mu,\eta^5{:}\eta^1\text{-}P_4C^tBu)\}_2(P_8C_4{}^tBu_4)_2(Cu_3Br_3)_2(MeCN)_2]$ (**26**) in the crystal (Hydrogen atoms are omitted for clarity). Selected bond lengths (Å) and angles (°): P2–P3 2.2429(6), P3–P4 2.2122(4), P4–P5 2.1963(6), P5–P6 2.2181(6), P7–P8 2.2007(4), P7–P4 2.2093(7), P1–C1 1.6524(3), P2–C1 1.8120(4), P1–C6 1.8594(4), P2–C6 1.9316(3), P3–C11 1.8388(4), P6–C11 1.8486(3), P7–C16 1.8697(3), P8–C11 1.9049(4), P8–C16 1.8561(3), P9–P10 2.1075(4), P10–P11 2.1089(3), P11–P12 2.0825(6), P9–C21 1.7824(4), P12–C21 1.7487(3), P1–Cu1 2.2494(4), P10–Cu1 2.2607(7), P4–Cu2 2.3150(4), P7–Cu2 2.3096(4), P5–Cu3 2.2534(3), Br3–Cu1–Br1 107.75(13), Br2–Cu2–Br1 112.42(11), Br3–Cu3–Br2 106.86(10), C1–P1–C6 88.025(16), C1–P2–P3 100.739(15), P2–P3–P4 94.405(9), P3–P4–P5 94.987(1), P4–P5–P6 94.602(12), P5–P6–C16 97.710(14), C16–P7–P8 53.511(9), C11–P8–P7 96.807(9).

The complex **26** contains four fragments, two of them are $[Cp'''Fe(\eta^5\text{-}P_4C^tBu)]$ moieties and the other two fragments are cage units composed of eight phosphorus and four carbon atoms, which are connected by two six-membered rings of $(CuBr)_3$ units. In the $(CuBr)_3$-ring, a chair-like arrangement is formed. Two of the copper atoms are tetrahedrally coordinated by

two phosphorus atoms and two bromine atoms. The third copper atom is also tetrahedrally connected to two bromine atoms, one phosphorus atom, and one CH_3CN molecule.

The cage unit consists of a cunean-like structure of P_6C_2, in which two phosphorus atoms (P3 and P5) connect to a P_2C_2 moiety. Three of the carbon atoms coordinate tetrahedrally with three phosphorus atoms and a *tert*-butyl group, whereas the fourth carbon (C1) coordinates with two phosphorus atoms and one *tert*-butyl group. The P1-C1 bond length of 1.652(1) Å indicates a double bond in comparison to the other P-C bond length (av. 1.865 Å) of the cage.

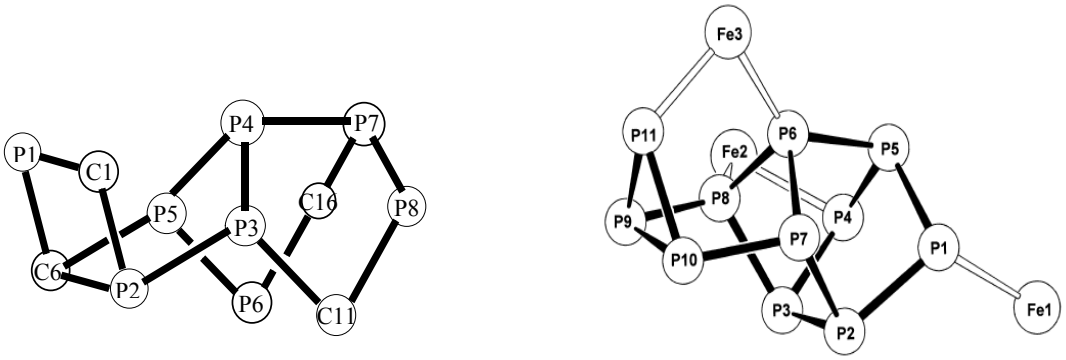

P_8C_4 cage of **26** P_{11} cage of $[\{Cp^R(OC)_4Fe_3\}P_{11}]$

Figure 3.2.30.Comparison of the cage structures of **26** and $[\{Cp^R(OC)_4Fe_3\}P_{11}]$.

The framework of the P_8C_4 cage is comparable to the P_{11} structure $[\{Cp^R(OC)_4Fe_3\}P_{11}]$ (Cp^R = 1,2,4-$C_5H_2{}^tBu_3$, $C_5{}^iPr_5$) prepared by Scherer and coworkers[14], in which the P_8 cunean is connected via the two phosphorus atoms P7 and P8 to a P_3 moiety whereas in complex **26** a C_2P_2 unit connects to the P_6C_2 cunean. This cage of P_8C_4 also reveals an interesting polycyclic structure consisting of the annelation of one three-membered, two four-membered, and four five-membered rings (Figure 3.2.30).

The P–P bond lengths of the P_8C_4 cage lie in the range of 2.1966(5) Å (P4–P5) and 2.2426(6) Å (P2–P3). The average values of the P–P bonds (2.21 Å) differ slightly from that in $[\{Cp^R(OC)_4Fe_3\}P_{11}]$ (2.22 Å), but are similar to the compounds $(Me_3EtN)_3P_{11}$[62] and $(iC_3H_7)_3P_{11}$ (2.21 Å) [63,64]. The average length of the P–Cu bond of **26** (2.281 Å) is a little longer than that in $[\{Cp'''Fe(\eta^5:\eta^1:\eta^1:\eta^1\text{-}P_4C^tBu)\}_2(\mu\text{-}CuBr)_2]_\infty$ (2.267 Å) (**27**).

The ESI-MS spectrum of **26** reveals cation peaks corresponding to the P_8C_4 cage structure $[(P_8C_4{}^tBu_4)_2Cu_2]^+$ and $[(P_8C_4{}^tBu_4)Cu]^+$. Furthermore, peaks attributable to $[\{Cp'''Fe(\eta^5\text{-}P_4C^tBu)\}Cu_3Br_2]^+$ and $[Cp'''Fe(\eta^5\text{-}P_4C^tBu)CuBr]^+$ were also detected.

3.2.4.2.2. [Cp'''Fe(η^5-$P_4{}^tBuC$)] with CuBr and CuI in a ratio of 1:2

A similar procedure to that used for the synthesis of **25** was carried out, in which acetonitrile/CH_2Cl_2 solutions of CuBr and CuI, respectively, were layered onto CH_2Cl_2 solutions of [Cp'''Fe(η^5-P_4C^tBu)] in a 2:1 ratio, thus yielding [{Cp'''Fe(η^5:η^1:η^1:η^1-P_4C^tBu)}$_2$(μ-CuBr)$_2$]$_\infty$ (**27**) and [{Cp'''Fe(η^5:η^1:η^1:η^1-P_4C^tBu)}$_2$(μ-CuI)$_2$]$_\infty$ (**28**), respectively. One equivalent of CuI in acetonitrile/CH_2Cl_2 solutions layered on CH_2Cl_2 solutions of [Cp'''Fe(η^5-P_4C^tBu)] also results in the formation of complex **28**.

The brown crystalline compounds **27** and **28**, dissolve sparingly in CH_2Cl_2 and acetonitrile, and do not dissolve in toluene and hexane. These compounds can be stored under an inert atmosphere at ambient conditions.

The molecular structures of **27** and **28** were determined by single-crystal X-ray diffraction and are illustrated in Figure 3.2.31. and Figure 3.2.32., respectively. The structures of **27** and **28** are similar to that of **25**.

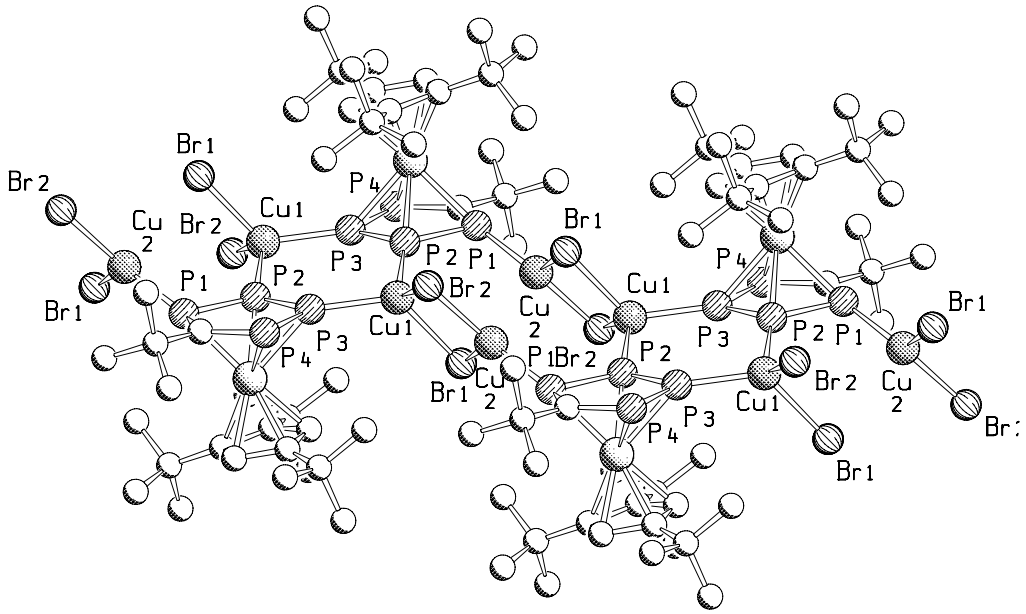

Figure 3.2.31. Section of the 1D polymeric structure of **27** in the crystal (Hydrogen atoms are omitted for clarity). Selected bond lengths (Å) and angles (°): P1–P2 2.092(2), P2–P3 2.103(2), P3–P4 2.119(2), P3–Cu1 2.2586(17), P2–Cu1 2.3296(17), P1–Cu2 2.2123(18), Cu1–Br1 2.4995(10), Cu1–Br2 2.4840(10), Cu2–Br1 2.4243(11), Cu2–Br2 2.3736(11), P2–Cu1–P3 103.25(6), P2–P3–Cu1 124.96(9), P3–P2–Cu1 127.85(8), P2–P1–Cu2 106.26(8),

Br1–Cu1–Br2 101.71(3), Br1–Cu2–Br2 107.33(4), Br1–Cu2–P1 123.29(6), P1–Cu2–Br2 126.57(6).

The difference in these three otherwise similar structures lies in the coordination geometry of the copper atoms in the $(CuX)_2$ (X = Cl (**25**), Br (**27**), I (**28**)) unit. Except for one tetrahedrally coordinated copper atom in all three complexes, the coordination geometry of the other copper atoms in **25** is trigonal, with the sum of the three angles around the copper atom being 360°. This sum in **27** is 357.2° and in complex **28** is 336.3° in which the copper atom (Cu1) coordinates tetrahedrally. The distance between this copper atom (Cu1) and the iodine atom (I2) of the other $(CuI)_2$ units in **28** is 2.848 Å whereas those distances are 3.666 Å in **25** and 3.111 Å in **27**. The distance between Cu1 and I2 indicates a chemical bond exists (The sum of van der Waals radii of copper and iodine is 3.38 Å[65]). Thus, a tendency to obtain a higher coordination number of the halogen atom was observed in the case of the iodide derivative **28**, in which a ladder-like $(CuI)_4$ substructure was formed. From the Table 3.2.6, a gradual increase in bond length of Cu–P, P–P, P–Fe, and Cu–X from **25** to **28** can be observed.

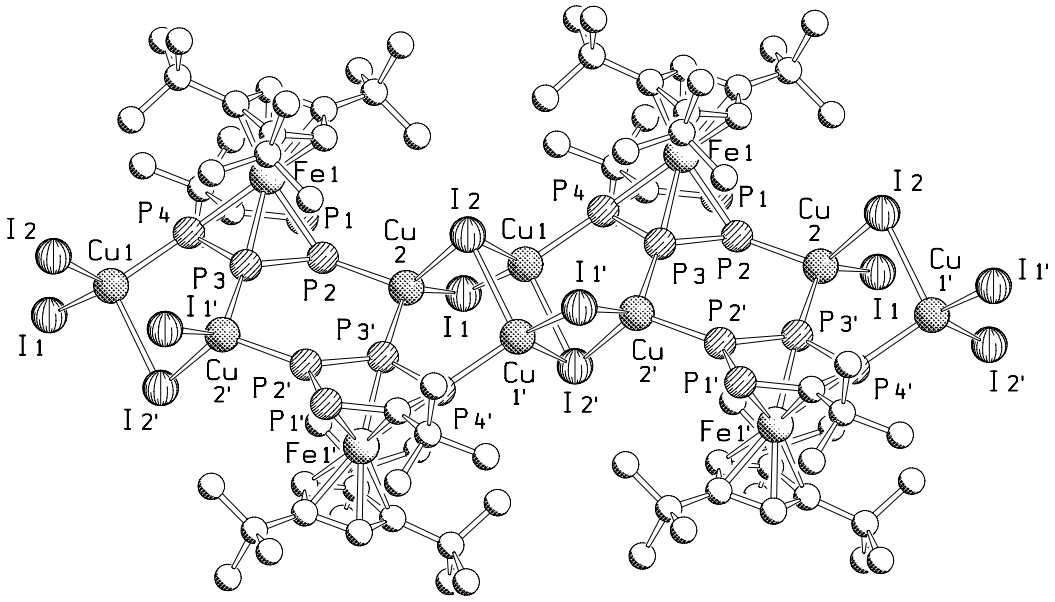

Figure 3.2.32. Section of the polymeric structure of **28** in the crystal (Hydrogen atoms are omitted for clarity). Selected bond lengths (Å) and angles (°): P1–P2 2.1224(1), P2–P3 2.1292(1), P3–P4 2.1070(1), P2–Cu2 2.2594(1), P3–Cu2 2.3384(2), P4–Cu1 2.3143(1),

Cu1–I1 2.561(2), Cu1–I2 2.626(2), Cu2–I1 2.643(2), Cu2–I2 2.681(2), P2–Cu2–P3 102.33(16), P2–P3–Cu2 125.7(2), P3–P4–Cu1 102.70(19), P3–P2–Cu2 27.7(2), I1–Cu2–I2 107.97(7), I1–Cu1–I2 101.54(8), I1–Cu1–P4 120.69(13), P4–Cu1–I2 114.04(15).

Table 3.2.6. Comparison of selected bond lengths (Å) and distances between selected atoms in [Cp'''Fe(η^5-P_4C^tBu)] **3** and its copper halide complexes.

	25	**27**	**28**	**3**
Cu(1)–P(2)	2.2350(6)	2.2586(4)	2.2594(1)	
Cu(1)–P(3)	2.2879(6)	2.3296(3)	2.3384(2)	
Cu(2)–P(4)	2.1490(5)	2.2124(4)	2.3143(1)	
P(1)–P(2)	2.1176(5)	2.1191(3)	2.1224(1)	2.119(11)
P(2)–P(3)	2.1173(6)	2.1030(3)	2.1292(1)	2.131(12)
P(3)–P(4)	2.0826(6)	2.0925(3)	2.1070(1)	2.106(14)
P–Fe(av.)	2.3735	2.3728	2.3874	2.3673
Cu–X(av.)	2.3064	2.4454	2.6275	

In the positive ESI-MS of **27** at the room temperature, peaks attributable to $[\{Cp'''Fe(P_4C^tBu)\}_2Cu]^+$ and $[Cp'''Fe(P_4C^tBu)CuBr]^+$ were detected. Furthermore fragments attributable to $[\{Cp'''Fe(P_4C^tBu)\}_2Cu]^+$ and $[Cp'''Fe(P_4C^tBu)Cu_2]^+$ were also detected in the ESI-MS spectrum of **28**. The fragments in these mass spectra are very similar to those in the spectrum of **25** and indicate that the two complexes dissolve under depolymerisation.

Table 3.2.7. Comparison of the ^{31}P NMR chemical shifts of compound [Cp'''Fe(η^5-P_4C^tBu)] (**3**) and its copper complexes.

Compound	Solvent	$\delta(P_M, P_{M'})$ ppm	$\delta(P_A, P_{A'})$ ppm
3	C_6D_6	81.6	122.8
25	C_6D_6/CH_2Cl_2/MeCN	57.7	107.1
	THF-d_8/MeCH: 3:1	73.6	119.2
27	THF-d_8/MeCH: 3:1	74.2	119.7
28	THF-d_8/MeCH: 3:1	74.3	120.2
	C_6D_6/CH_2Cl_2/MeCN	65.4	113.7

Since the complexes **25**, **27**, and **28** are only sparingly soluble in common solvents, reaction mixtures were used for NMR measurement. In the corresponding mother liquor, detection of a monomeric or oligomeric copper complex was evident from the $^{31}P\{^1H\}$ NMR spectra of **28** ($\delta(P_A, P_{A'})$ = 120.2 ppm and $\delta(P_M, P_{M'})$ = 74.43 ppm) and **27** ($\delta(P_A, P_{A'})$ = 119.7 ppm and $\delta(P_M, P_{M'})$ = 74.2 ppm). These spectra show the AA'MM'-spin system and their shifts

are almost at the same position as those of the mother liquor of **25** (Table 3.2.7). The signals corresponding to P_M and $P_{M'}$ are 15 – 25 ppm for the C_6D_6 containing solutions and about 7 ppm for THF-d_8 containing solutions upfield shifted in comparison to those of the starting material, due to the coordination of the phosphorus atoms with copper atoms. Considering the mass spectral data of **27** and **28**, there may be dimeric copper oligomers present in the reaction solution similar to that of **25** (Figure 3.2.33).

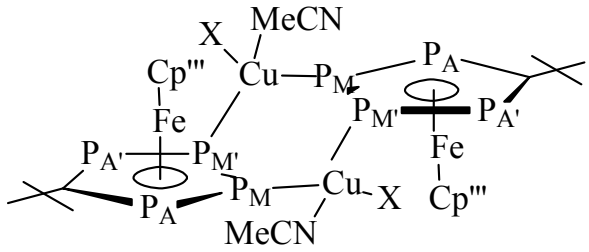

X = Br, I

Figure 3.2.33. Proposed oligomer structures in the reaction solution of [Cp'''Fe(η^5-P_4C^tBu)] and CuX (X = Br, I).

3.2.4.3. Reaction of [Cp'''Fe(η^5-P_4C^tBu)] with Ag[Al{$OC(CF_3)_3$}$_4$]

A mixture of [Cp'''Fe(η^5-P_4C^tBu)] and Ag[Al{$OC(CF_3)_3$}$_4$] in CH_2Cl_2 in a 2:1 ratio was stirred for one hour at room temperature, during which time the color of the reaction mixture turned from green to red brown. Afterwards the black powder, which resulted during the course of the stirring, was filtered and the filtrate was concentrated under reduced pressure and stored at -28 °C. Air- and light-sensitive dark red brown plates of **29** were isolated (equation 3.16).

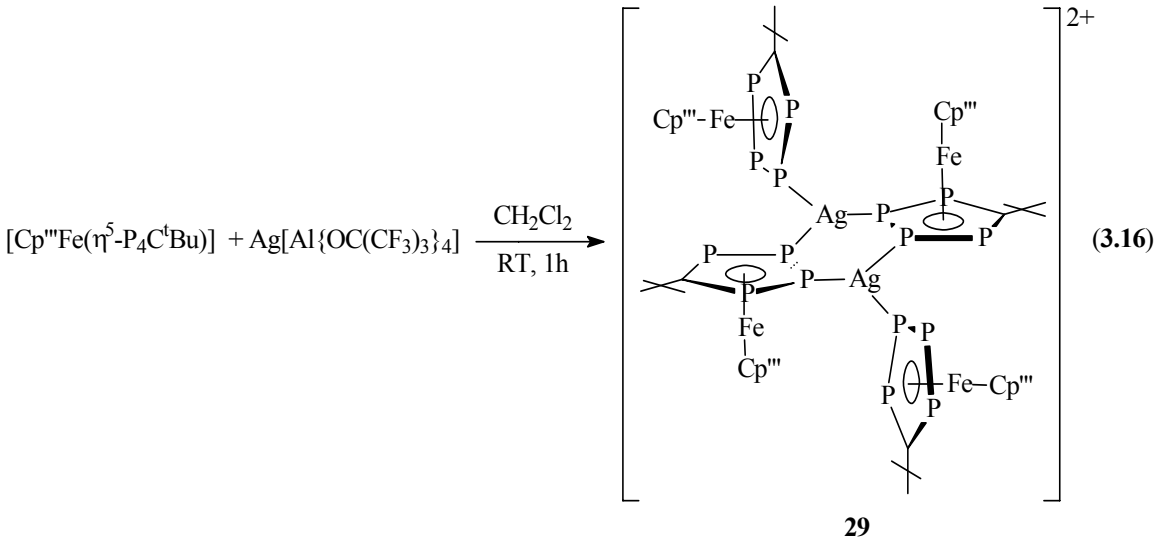

29

Compound **29** is soluble in CH_2Cl_2 and THF, but is not soluble in nonpolar solvents such as alkans. It can be stored under an inert atmosphere at low temperature (-28 °C).

The structure of complex **29** was determined by single-crystal X-ray diffraction and is illustrated in Figure 3.2.34. The dication is composed of four [Cp'''Fe(η^5-P_4C^tBu)] moieties and two silver atoms. Two silver centers are doubly bridged by two [Cp'''Fe(η^5-P_4C^tBu)] units via two adjacent phosphorus atoms of the P_4C ring, thus forming a six-membered P_4Ag_2-ring. Two further [Cp'''Fe(η^5-P_4C^tBu)] moieties, one per silver center, coordinate as terminal ligands. Similar to the P_4Cu_2-rings in the complexes **10** and **16**, the two silver atoms lie above and below the P6P7P6′P7′ plane (deviation of silver atoms from the plane = 0.520(1) Å). Each silver atom coordinates to three phosphorus atoms from three different [Cp'''Fe(η^5-P_4C^tBu)] moieties and the coordination geometry of the silver atom is slightly pyramidal since the average P–Ag–P angle is 115.73°. The bond length of P6–P7 (2.105(2) Å) is shorter than the other two P–P bond lengths (P5–P6 2.1202(2) Å, P7–P8 2.1178(2) Å) in the P_4C ring, which has a 2,3 substitution pattern because of the donation of the lone pairs of the adjacent phosphorus atoms to the silver atom. The average Ag–P bond length is 2.5068 Å.

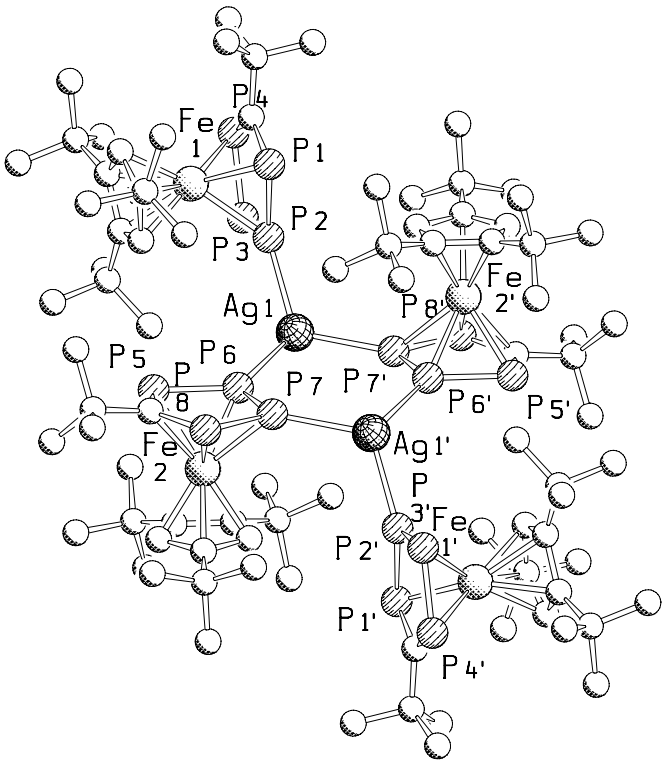

Figure 3.2.34. Structure of the dication of **29** in the crystal (Hydrogen atoms are omitted for clarity). Selected bond length (Å) and angles (°): P1–P2 2.118(2), P2–P3 2.112(2), P3–P4 2.118(2), P1–C11 1.768(6), P4–C11 1.7766(1), P2–Ag 2.4955(16), P5–P6 2.1202(2), P6–P7 2.105(2), P7–P8 2.117(2), P5–C21 1.765(6), P8–C21 1.7707(3), P6–Ag 2.5046(18), Ag–P7 2.5204(15), P(1-4)–Fe1 2.3627, P(5-8)–Fe2 2.3665, Ag–P6–P7 118.66(8), Ag–P7–P6 125.91(8), P2–Ag–P6 119.53(6), P2–Ag–P7 117.53(5), P6–Ag–P7 110.08(5).

In the negative ESI-MS spectrum of **29** at room temperature, the peak with 100% relative abundance corresponds to the anion $[Al\{OC(CF_3)_3\}_4]^-$ was detected. The positive ion ESI-MS reveals a peak attributable to $[\{Cp'''Fe(\eta^5\text{-}P_4C^tBu)\}_2Ag]^+$. The ESI-MS spectrum suggests that monocationic silver complex should exist in solution.

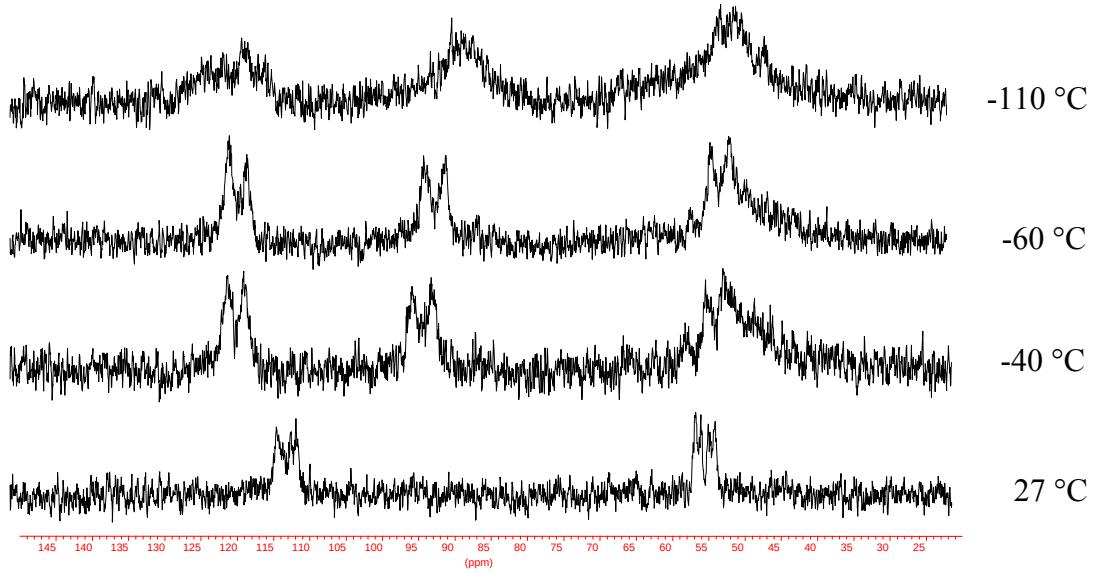

Figure 3.2.35. Variable temperature $^{31}P\{^{1}H\}$ NMR spectra of **29** in a solvent mixture of THF-d_8/CH_2Cl_2.

To study the cation equilibria in solution, variable temperature $^{31}P\{^{1}H\}$ NMR spectroscopy of **29** in a solvent mixture of THF-d_8/CH_2Cl_2 was carried out. At room temperature, only two broad signals of an AA'MM' spin system centered at δ = 112 and 54.5 ppm are observed, shifted upfield relative to the uncoordinated complex **3** (121.7 and 77.3 ppm). At -40 °C the signal at δ = 112 is split into two broad signals, centered at δ = 120 and 93 ppm and the spectrum becomes characteristic of an ADMN spin system. Upon further reduction of the temperature, the signals are shifted slightly to higher field and become broader (Figure 3.2.35). Since the spectrum at room temperature reveals broadened signals typical of an AA´MM´ spin system, a dynamic process involving fast exchange between **29a** and **29b** may be inferred, during which the coordination of the silver(I) center to the initial P_M and $P_{M'}$ atoms in the P_4C-rings is changing. At low temperatures, this exchange process becomes slower on the NMR time scale and the four phosphorus atoms in each P_4C-ring of **29a** and **29b** are rendered chemically and magnetically inequivalent. Thus, the $^{31}P\{^{1}H\}$ NMR spectrum at -60 °C is typical of an ADMN spin system (Figure 3.2.36). At -110 °C, the signals become even broader and no longer display any fine structure, which is probably indicative of the formation of the dimer.

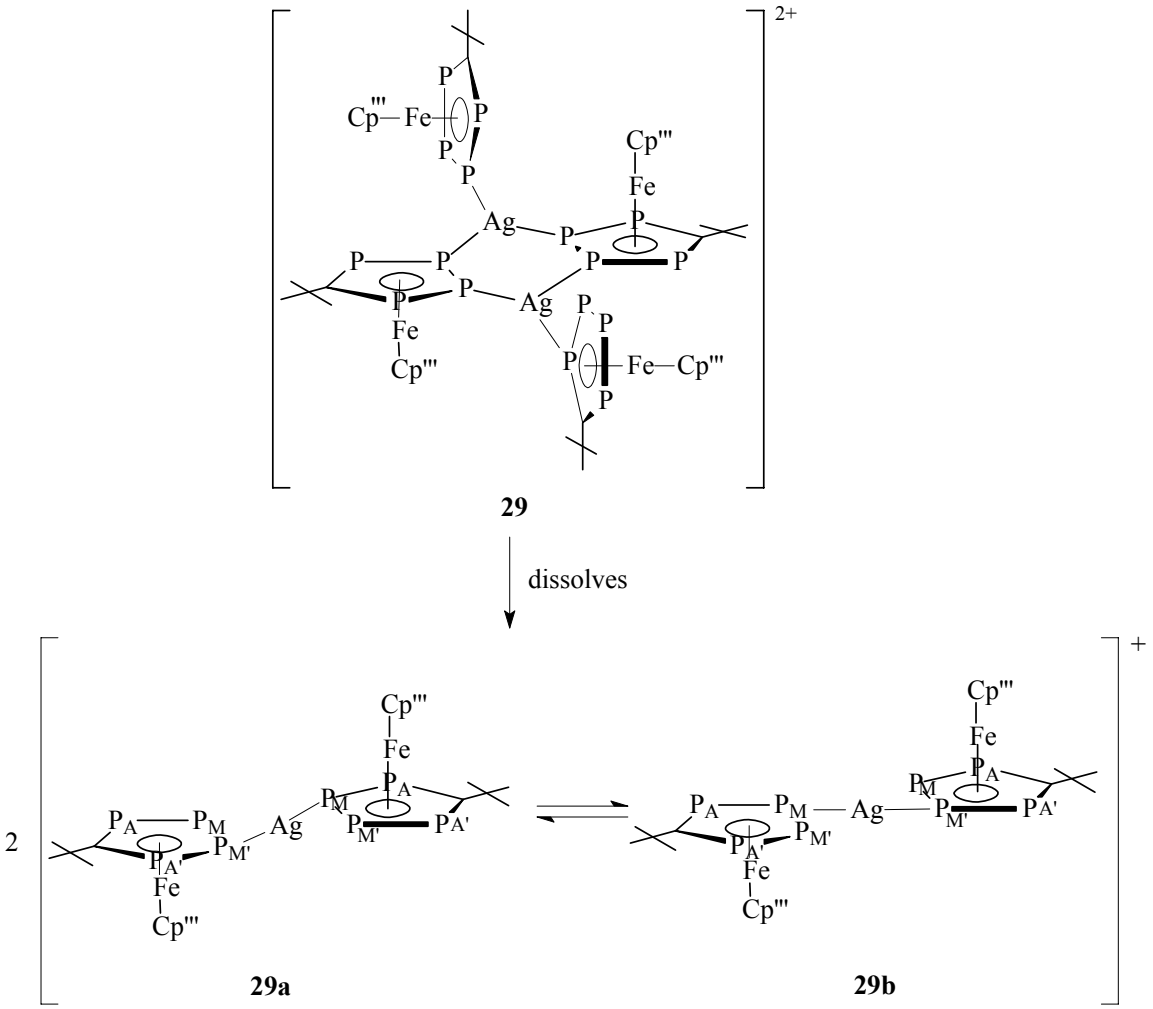

Figure 3.2.36. Proposed cation equilibria of **29** in solution.

3.2.4.4. Reaction of [Cp'''Fe(η^5-P_4C^tBu)] with AuCl[SC_4H_8]

Since the coordination of Cu(I) and Ag(I) salts with tetraphosphaferrocene presents various well-defined aggregates, the extension of the investigation to Au(I) salts is attractive. Considering the instability of [AuCl(SC_4H_8)] in solution, brief mixing of the phosphaferrocene with the gold salt was carried out.

The first attempts with [AuCl(SC_4H_8)] in MeCN layered on [Cp'''Fe(η^5-P_4C^tBu)] in CH_2Cl_2 or the two reactants mixing directly in CH_2Cl_2, in a stoichiometric ratio of 1:1 and 2:1 respectively, only resulted in the formation of black powder.

Therefore, a mixture of [AuCl(SC_4H_8)] and [Cp'''Fe(η^5-P_4C^tBu)] in CH_2Cl_2 in a 1:2 ratio was stirred for one hour at room temperature in the dark, afterwards the black powder which

resulted during the reaction was filtered and the filtrate was concentrated under vacuum and stored at -28 °C. Air- and light-sensitive dark red brown plates of complex **30** were isolated (equation 3.17).

Compound **30** dissolves in CH_2Cl_2, but not in nonpolar solvents such as hexane. It can be stored under an inert atmosphere at low temperature.

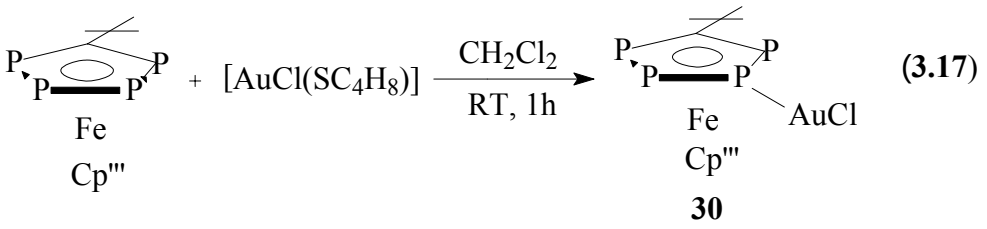

(3.17)

The molecular structure of **30** was determined by single-crystal X-ray diffraction and is illustrated in Figure 3.2.37.

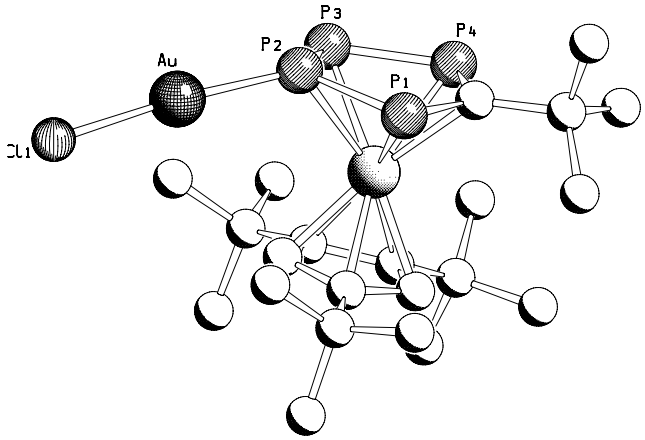

.

Figure 3.2.37. Molecular structure of **30** in the crystal (Hydrogen atoms are omitted for clarity). Selected bond lengths (Å) and angles (°): P1–P2 2.1172(2), P2–P3 2.1067(2), P3–P4 2.1138(3), P1–C1 1.7628(3), P4–C1 1.7766(1), P2–Au 2.2325(5), Au–Cl 2.2967(5), P1–Fe 2.3362(2), P2–Fe 2.3661(2), P3–Fe 2.3873(2), P4–Fe 2.3716(6), C1–Fe 2.1992(5), Au–P2–P3 125.837(6), Au–P2–P1 120.305(4), P2–Au–Cl1 175.205(7).

In compound **30,** one phosphorus atom (P2) of the P_4C-ring is bonded to a gold atom with a P–Au bond length of 2.2325(5) Å. The average distance between this phosphorus atom (P2)

and the two adjacent phosphorus atoms (P1 and P3) (2.112Å) is shorter than that in the uncoordinated tetraphosphaferrocene (2.125 Å) because of the lone pair donation of the phosphorus atom to the gold atom. Because of the shortening of this P–P bond length, the bond angle of P1–P2–P3 (108.73°(3)) is larger than that in the uncoordinated tetraphosphaferrocene (103.7°(3)).

In the ESI-MS spectrum of **30** in MeCN at room temperature a fragment attributable to $[\{Cp'''Fe(\eta^5\text{-}P_4C^tBu)\}AuClMeCN]^+$ was detected. Furthermore, a peak attributable to $[\{Cp'''Fe(\eta^5\text{-}P_4C^tBu)\}_2Au]^+$ was also found and this suggests that under certain conditions the gold atom can coordinate to more phosphorus atoms.

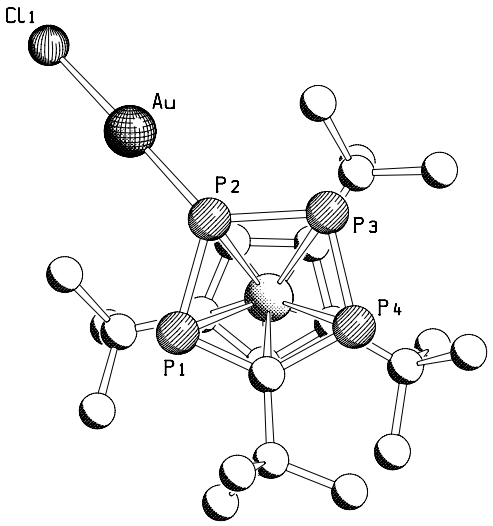

Figure 3.2.38. Top view of the complex **30**.

To study the dynamic behaviour of **30** in solution, variable temperature ^{31}P NMR spectroscopy of the compound in CH_2Cl_2/THF-d_8 (3:1) was carried out. At room temperature there are two broad signals which represent an AA'MM' similar spin system (70.2 and 108.5 ppm). These signals are about 10 ppm upfield shifted relative to the uncoordinated complex **3** (81.6 and 122.8 ppm). As the temperature is reduced, the signals are shifted gradually to higher field and become broader. At -60 °C, the downfield signal corresponding to the $P_A/P_{A'}$ atoms is split into two broad signals centered at 108.6 and 118.9 ppm and the spectrum represents an ADMN spin system. At -120 °C, these two broad signals are split further into two broad doublets centered at 111.9 and 125.8 ppm, the coupling constants ($J(P_A,P_M)$ = 421.0 Hz; $J(P_A,P_D)$ = 0.7 Hz) being somewhat smaller than those of uncoordinated **3** ($J(P_A,P_M)$ = 431.2, $J(P_A,P_{A'})$ = 54.7 Hz) according to the spectrum

simulation. The signal of the $P_M/P_{M'}$ atoms is split into two broad doublet of doublets centered at 72.4 and 78.2 ppm at -120 °C with the coupling constants ($J(P_M,P_N)$ = 465.2 Hz; $J(P_A,P_N)$ = 59.5 Hz) being larger than those of uncoordinated **3** ($J(P_M,P_{M'})$ = 425.1 and $J(P_A,P_{M'})$ = 9.4 Hz). The approximate integration ratio of these two signals is 1:1 (Figure 3.2.39).

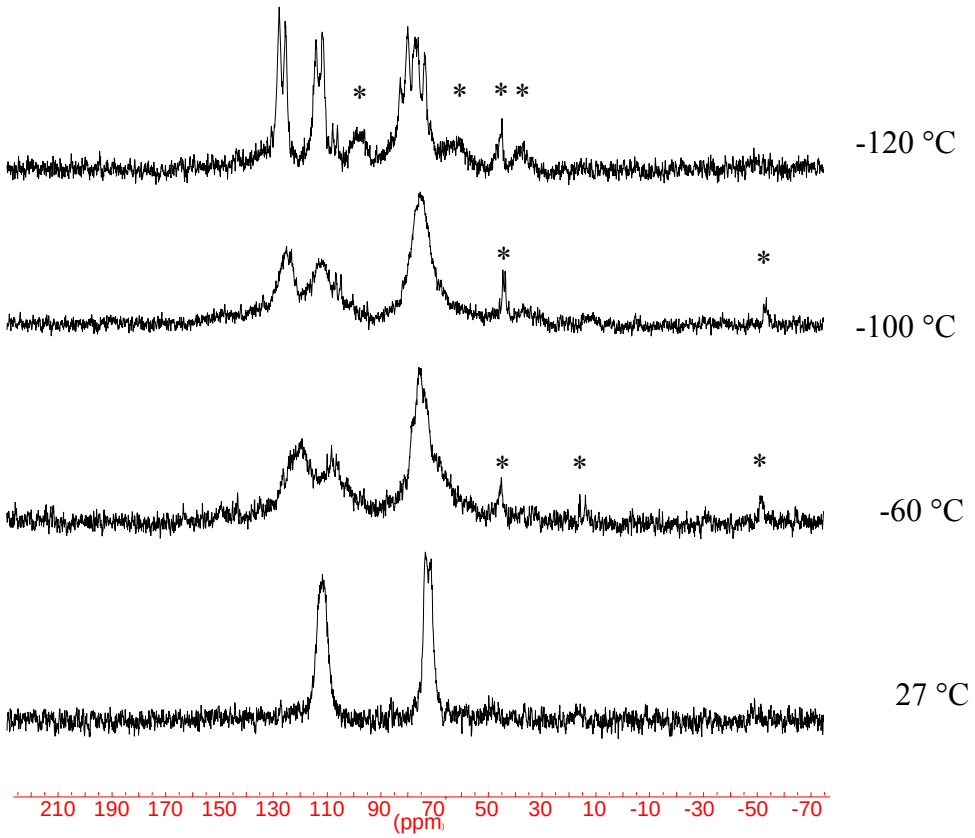

Figure 3.2.39. $^{31}P\{^1H\}$ NMR spectra of compound **30** at different temperatures (peaks marked with an asterisk are due to impurity).

A fast sigmatropic shift of the gold(I) center between the P_M and $P_{M'}$ atoms in the P_4C-ring of the **30a** to **30b** in the solution at room temperature would be expected to give the simple spectra of two broad signals, since this shift results in two sets of chemically equivalent phosphorus atoms P_A and $P_{A'}$ as well as P_M and $P_{M'}$. By "freezing" this motion in solution each of the two enantiomers **30a** and **30b** would be expected to show a doublet of doublets of doublets for the two phosphorus atoms P_M and P_N (Figure 3.2.40).

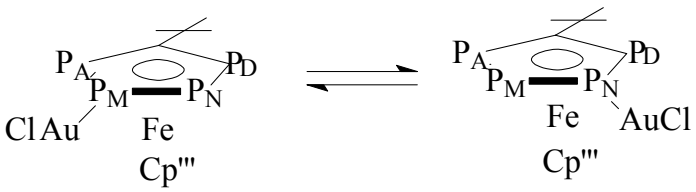

30a **30b**

Figure 3.2.40. Proposed sigmatropic shift of the Au(I) center between the P_M and P_N atoms in the P_4C-ring at low temperature in solution.

3.2.5. [Cp'''Fe(η^5-P_5)] as a ligand in coordination chemistry

The complex [Cp*Fe(η^5-P_5)] as a building block for supramolecular architectures has been exhaustively researched in our group. Reactions of this cyclo-P_5 ligand with CuX (X = Cl, Br, I) and various Ag(I) and Au(I) salts yield oligomers, 1D and 2D coordination polymers as well as remarkable fullerene-like nanoballs.[34,35] In view of the similarity of [Cp'''Fe(η^5-P_5)] with [Cp*Fe(η^5-P_5)], it was of interest to examine whether the steric factor of the bulky ^{t}Bu group on the cyclopentadiene ring can influence the reactivity and the coordination behavior of the cyclo-P_5 ligand. Reactions of [Cp'''Fe(η^5-P_5)] with CuX as well as Ag(I) and Au(I) salts were carried out and the results are discussed below.

3.2.5.1. Reaction of [Cp'''Fe(η^5-P_5)] with CuCl

Since pentaphosphaferrocene has five phosphorus atoms in the cyclo-P_5 ring, it should coordinate to more transition metal centers and lead to more complicated 1D and 2D polymers.

A CH_2Cl_2 solution of [Cp'''Fe(η^5-P_5)] (**5**) was carefully layered with a 1:1 CH_2Cl_2/THF mixture, onto which a layer of acetonitrile/CuCl solution was placed. The reactants were used in a stoichiometric ratio of 1:2. The reaction solution was allowed to diffuse at room temperature and air-sensitive dark brown crystals of [{Cp'''Fe(η^5:η^1:η^1:η^1-P_5)}(μ-$CuCl)_2$(MeCN)]$_\infty$ (**31**) were yielded. This neat solvent layer is essential in preventing the diffusion from occurring too fast, therefore avoiding the formation of amorphous material. The reaction proceeds very quickly. A color change from green to brown is observed almost immediately after the two reactants are mixed. No crystals could be obtained from the reaction between [Cp'''Fe(η^5-P_5)] and CuCl in a stoichiometric ratio of 1:1, although the NMR and mass spectra of the reaction solution are comparable to that of the 1:2 reaction solution.

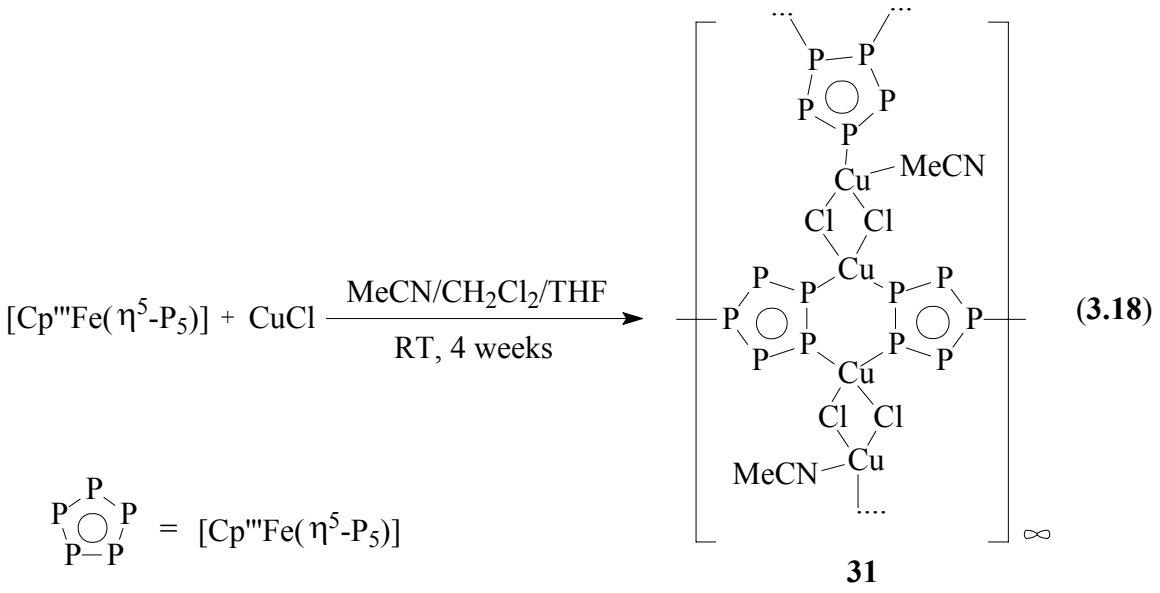

The dark brown crystals of **31** dissolve readily in CH_2Cl_2, but are not soluble in nonpolar solvents such as alkanes. They are stable under nitrogen and can be stored under an inert atmosphere at ambient conditions.

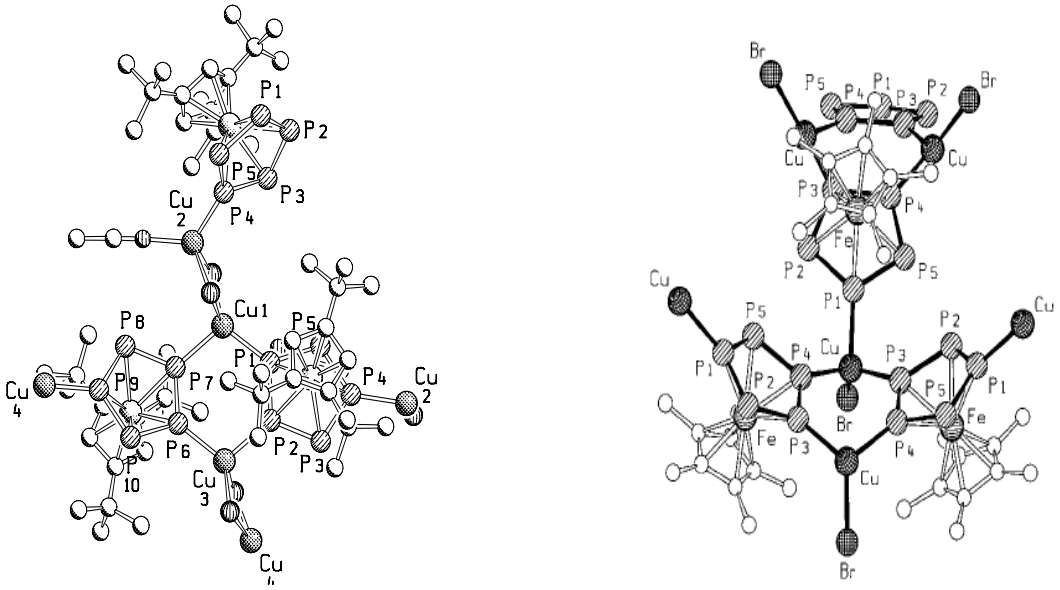

[{Cp'''Fe($\eta^5:\eta^1:\eta^1:\eta^1$-P$_5$)}(μ-CuCl)$_2$(MeCN)]$_\infty$(**31**) [{Cp*Fe($\eta^5:\eta^1:\eta^1:\eta^1$-P$_5$)}(μ-CuBr)]$_\infty$[34]

Figure 3.2.41. View of a section of the polymeric structure of **31**, demonstrating the coordination geometry around the Cu atoms and [{Cp*Fe($\eta^5:\eta^1:\eta^1:\eta^1$-P$_5$)}(μ-CuBr)]$_\infty$, respectively (Hydrogen atoms are omitted for clarity). Selected bond lengths (Å) and angles (°) of **31**: P1–P2 2.1144(2), P2–P3 2.0978(1), P3–P4 2.1089, P4–P5 2.1111(2), P5–P1

2.1093(2), P1–Cu1 2.2504(1), P2–Cu3 2.2910(2), P7–Cu1 2.3403(2), P6–Cu3 2.2393(1), P4–Cu2 2.2138(1), P9–Cu4 2.2017(1), Cu1–Cl1 2.3628(2), Cu1–Cl2 2.3268(3), Cu2–Cl1 2.3609(3), Cu2–Cl2 2.4000(2), P1–Cu1–P7 107.93(7), P2–Cu3–P6 107.05(7), Cl1–Cu1–Cl2 96.53(6), Cl1–Cu2–Cl2 94.62(6).

Complex **31** crystallizes in the monoclinic space group $P2_1/c$. As in the case in the complex $[\{Cp^*Fe(\eta^5:\eta^1:\eta^1:\eta^1\text{-}P_5)\}(\mu\text{-}CuBr)]_\infty$ synthesised in our group[34], **31** contains an $\eta^1:\eta^1:\eta^1$-coordinated P_5 ring in a 1,2,4 substitution pattern. Two adjacent phosphorus atoms (P1, P2 and P6, P7) of the cyclo-P_5 rings of two different $[Cp'''Fe(\eta^5\text{-}P_5)]$ moieties coordinate to two different metal centers (Cu1 and Cu3) to form a six-membered P_4Cu_2 ring. The two copper atoms (Cu1 and Cu3) in the P_4Cu_2 ring, which coordinate tetrahedrally to two phosphorus atoms and two chlorine atoms, are different from those in $[\{Cp^*Fe(\eta^5:\eta^1:\eta^1:\eta^1\text{-}P_5)\}(\mu\text{-}CuBr)]_\infty$, which coordinate three phosphorus atoms from three different $[Cp^*Fe(\eta^5\text{-}P_5]$ moieties. The P–Cu bond lengths in this P_4Cu_2 ring are different (Cu–P 2.2503(1), 2.3403(2) Å) and the angles around the copper atoms deviate from an ideal tetrahedral (P–Cu–P 107.93°(7), Cl–Cu–Cl 96.53°(6)). This difference may be due to the three bulky *tert*-butyl groups on the cyclopentadiene ring of **31** in comparison to the relatively less steric influence of the Cp* groups in the complex $[\{Cp^*Fe(\eta^5:\eta^1:\eta^1:\eta^1\text{-}P_5)\}(\mu\text{-}CuBr)]_\infty$.
The third phosphorus atom (P4 or P9) in **31** coordinates to the third copper atom (Cu2 or Cu4) of a $(CuCl)_2$ moiety and the coordination geometry of the copper atom is tetrahedral with a bond length of Cu–P (2.2138(1) Å), which is shorter than the other two Cu–P bond lengths in the Cu_2P_4 ring. The Cl–Cu–Cl and P–Cu–Cl bond angles are 94.62°(6) and 104.36°(5), respectively (Figure 3.2.41).

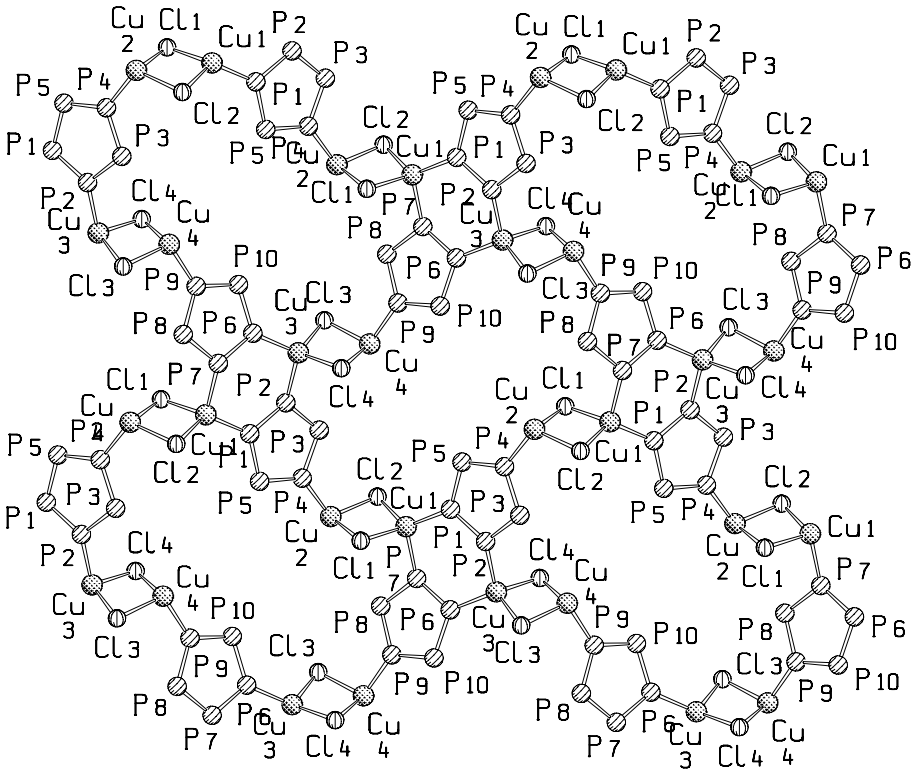

Figure 3.2.42. View of the 2D structure of complex **31** orthogonal to the a,b plane (C, H, and Fe atoms are omitted for clarity).

Complex **31** represents a 2D coordination polymer in which the layers are separated by the Cp'''Fe moieties (Figure 3.2.43). The structure of **31** consists of an alternating array of six-membered Cu_2P_4 rings and 24-membered $Cu_8Cl_4P_{12}$ rings (Figure 3.2.42) whereas in the structure of $[\{Cp^*Fe(\eta^5:\eta^1:\eta^1:\eta^1\text{-}P_5)\}(\mu\text{-}CuBr)]_\infty$ comprises an alternating array of six-membered Cu_2P_4 rings and Cu_4P_{12} rings. The P–P distances within the nearly planar cyclo-P_5 moieties of **31** (ranging from 2.098(2) to 2.114(2) Å) are comparable to that in $[\{Cp^*Fe(\eta^5:\eta^1:\eta^1:\eta^1\text{-}P_5)\}(\mu\text{-}CuBr)]_\infty$ (ranging from 2.099(2) to 2.108(2) Å) and $[\{Cp^*Fe(\eta^5:\eta^1:\eta^1:\eta^1\text{-}P_5)\}(\mu\text{-}CuI)]_\infty$ (2.114(3)–2.120(3) Å).

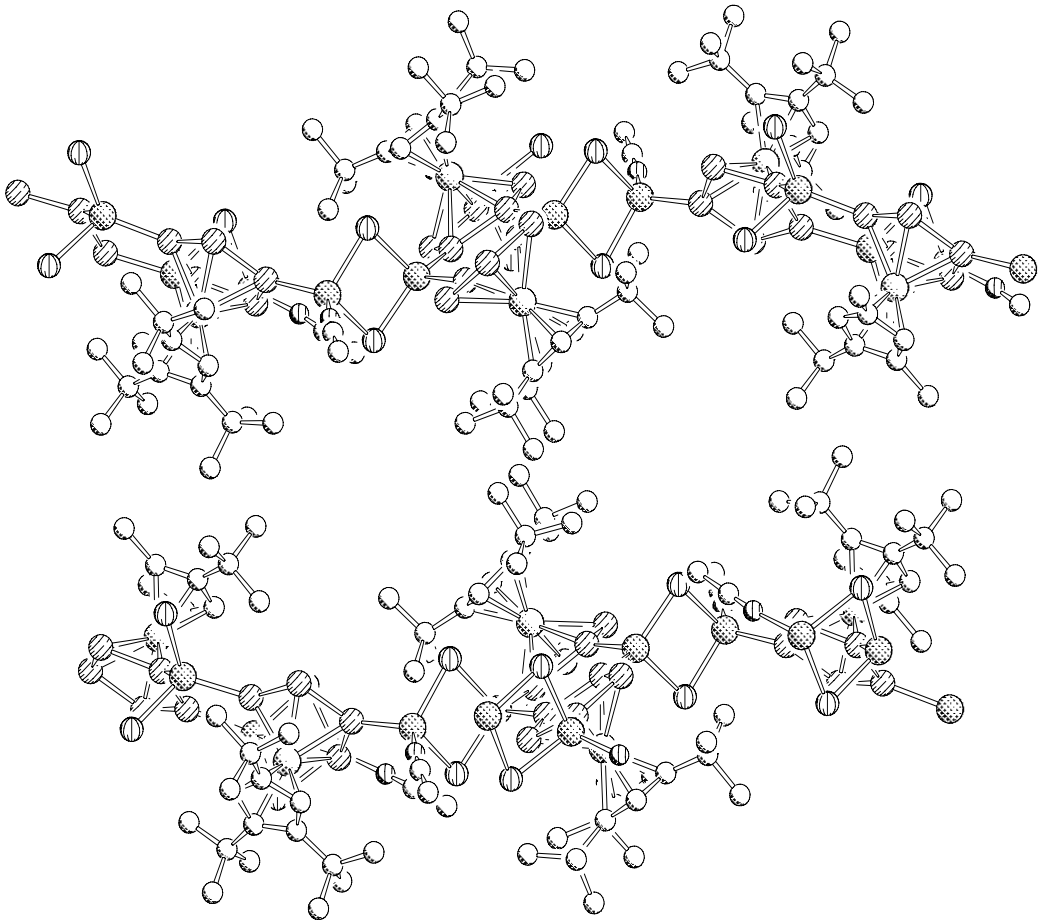

Figure 3.2.43. View of the 2D layer structure of complex **31** along the crystallographic b axis (H atoms are omitted for clarity).

In the positive ESI-MS of **31** in MeCN at room temperature, a peak corresponding to $[Cp'''Fe(\eta^5\text{-}P_5)CuCl]^+$ and $[\{Cp'''Fe(\eta^5\text{-}P_5)\}_2Cu]^+$ were detected. These mass data indicate the likely existence of monomeric and oligomeric complexes with $[Cp'''Fe(\eta^5\text{-}P_5)]$ units in solution.

The $^{31}P\{^1H\}$ NMR spectrum of **31** in THF-d_8/MeCN at room temperature shows a broad signal at δ = 163.9 ppm. Since the five phosphorus atoms of the P_5 ring in the solid state structure of compound **31** are chemically and magnetically inequivalent, there could be a dynamic process in solution at room temperature, and due to the larger solubility, complex **31** could also depolymerize in solution. Variable temperature spectra were recorded in a 3:1 mixture of THF-d_8 and CH_3CN. At -20 °C the signal is shifted to δ = 160.4 ppm. As the temperature descends, the signal becomes broader and shifts upfield. At -60 °C the signal is split into three broadend signals centered at δ = 153.0, 8.1 and 5.6 ppm. At -80 °C the

signals shift further centered at δ = 136.1, 8.6 and 5.4 ppm. These signals at high field imply the phosphorus atoms which coordinate the copper centers. The NMR data indicate **31** is depolymerized in solution to monomeric and oligomeric species, in which some interactions between the [Cp'''Fe(η^5-P_5)] moiety and CuCl is present (Figure 3.2.44).

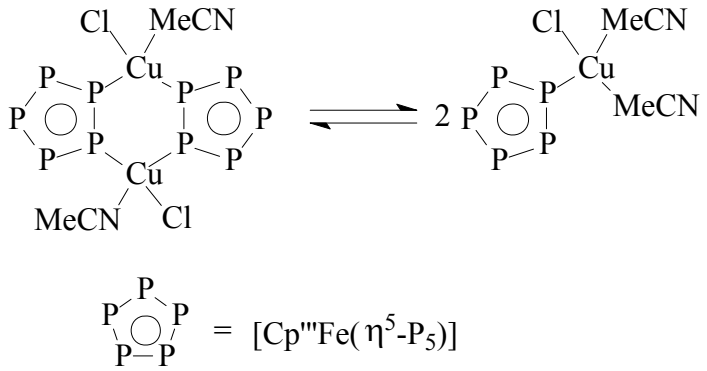

Figure 3.2.44. Proposed monomer/dimer equilibrium in solutions of **31**.

3.2.5.2. Reaction of [Cp'''Fe(η^5-P_5)] with CuBr

3.2.5.2.1. Reaction of [Cp'''Fe(η^5-P_5)] with CuBr in a ratio of 1:2

Using a synthetic method similar to that for the synthesis of **31**, air sensitive dark brown crystals of [{Cp'''Fe(η^5:η^1:η^1-P_5)}(μ-CuBr)$_2$(MeCN)]$_\infty$ (**32**) were obtained by treating [Cp'''Fe(η^5-P_5)] with CuBr in a stoichiometric ratio of 1:2 (equation 3.19). Complexes **31** and **32** are isostructural.

As with **31**, complex **32** dissolves in CH_2Cl_2, but is not soluble in nonpolar solvents such as alkans. It can be stored under an inert atmosphere at ambient conditions.

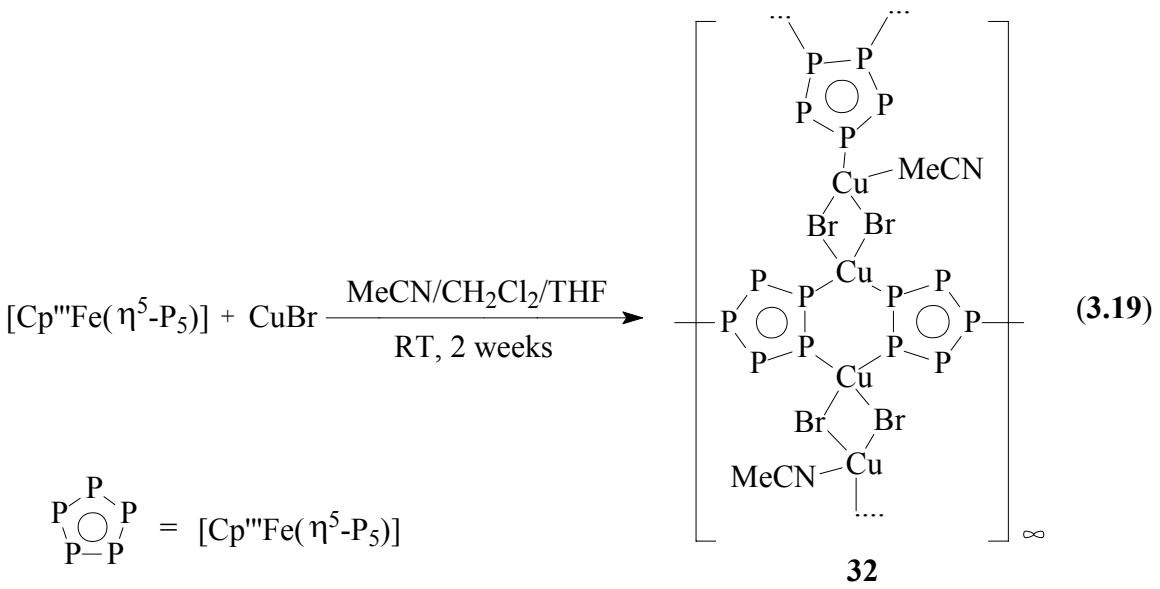

In the positive ESI-MS of **32** in MeCN at room temperature, peaks corresponding to the cations $[\{Cp'''Fe(P_5)\}_2Cu_2Br]^+$, $[\{Cp'''Fe(P_5)\}_2Cu]^+$, and $[Cp'''Fe(P_5)CuMeCN]^+$ were detected. Similar to the case of **31** the mass data indicate the likely existence of monomeric and oligomeric complexes with $[Cp'''Fe(\eta^5\text{-}P_5)]$ units in solution.

In the $^{31}P\{^1H\}$ NMR spectrum of **32** at room temperature, a broad signal at δ = 165.9 ppm was detected. Variable temperature spectra were also recorded in a 3:1 mixture of THF-d_8/CH_3CN up to -120 °C showing that with decreasing temperature the signal broadens and shifts upfield without signal splitting. This indicates that there may only be monomeric and/or oligomeric fragments in the solution. This suggestion is in agreement with the mass spectra of **32**, in which some oligomeric fragments are evident.

The molecular structure of **32** was determined by single-crystal X-ray diffraction and is illustrated in Figure 3.2.45.

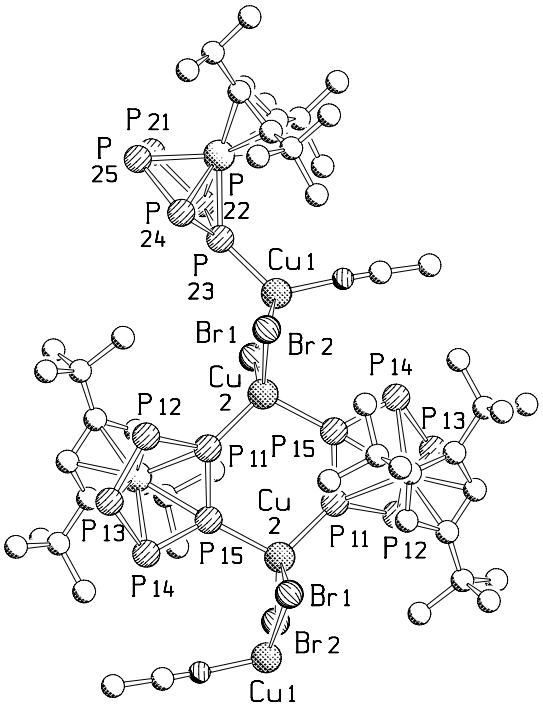

Figure 3.2.45. Section of the structure of **32** (H atoms are omitted for clarity). Selected bond lengths (Å) and angles (°): P11–P12 2.1068(2), P12–P13 2.1047, P13–P14 2.1063(2), P14–P15 2.1037, P15–P11 2.1084(2), P11–Cu2 2.2562(2), P15–Cu2 2.3073(3), P23–Cu1 2.2123, P13–Cu4 2.2146, Cu2–Br1 2.4703, Cu2–Br2 2.4442, Cu1–Br1 2.48973, Cu1–Br2 2.4870.

In parallel with the molecular structure of **31**, complex **32** contains two [Cp'''Fe(η^5-P_5)] moieties that are doubly connected by two copper atoms, thus forming an almost planar six-membered ring. The third phosphorus atom of the P_5 ring is connected to a $(CuBr)_2$ unit in a 2D structure forming an $\eta^5{:}\eta^1{:}\eta^1{:}\eta^1$ coordinated cyclo-P_5 ring in a 1,2,4-coordination mode. The copper atoms in the P_4Cu_2 ring also coordinate tetrahedrally to two phosphorus atoms and two bromine atoms with different bond lengths (Cu–P 2.2562(2), 2.3073(3) Å and Cu–Br 2.4442(3), 2.4703(3) Å) and with P–Cu–P and Br–Cu–Br angles of 109.87°(9) and 107.11°(8), respectively. The two P–Cu bond lengths of the P_4Cu_2 ring are comparable to that in complex **31** (2.2503(1), 2.3404(2) Å) and are longer than the third Cu–P bond lengths (2.2123(3) and **31** 2.2138(1) Å) (Figure 3.2.45).

3.2.5.2.2. Reaction of [Cp'''Fe(η^5-P_5)] with CuBr in a ratio of 1:1

Using the three layer technique for the synthesis of **31**, a MeCN solution of CuBr was layered onto a solvent mixture of CH_2Cl_2/MeCN, which was layered on a red CH_2Cl_2 solution of [Cp'''Fe(η^5-P_5)] (**5**) in a 1:1 stoichiometric ratio. Dark brown needles of [{Cp'''Fe(μ,η^5:η^1:η^1-P_5)}$_4$($CuBr)_3$]$_\infty$ (**33**) were obtained, which are stable under nitrogen and dissolve in CH_2Cl_2.

In the positive ESI-MS of **33** in MeCN at room temperature similar fragments to those in the mass spectrum of **32** are observed, corresponding to the cations [{Cp'''Fe(P_5)}$_2$Cu]$^+$, [{Cp'''Fe(P_5)}Cu_2BrMeCN]$^+$, and [Cp'''Fe(P_5)Cu]$^+$. These data suggest the polymer **33** depolymerizes in solution.

This suggestion was confirmed by the $^{31}P\{^1H\}$ NMR spectra. The spectrum at room temperature exhibited a broad signal at δ = 166.1 ppm. Variable temperature spectra were also recorded in a 3:1 THF-d_8/CH_3CN solution and showed that with decreasing temperature the signal broadens and shifts upfield without signal splitting (even at -130 °C). Considering the chemical shift of the starting material (δ = 165 ppm) and the broadened signal, there could be a [Cp'''Fe(η^5-P_5)] moiety interacting with CuBr units in solution.

The molecular structure of **33** was determined by single-crystal X-ray diffraction and is illustrated in Figure 3.2.46.

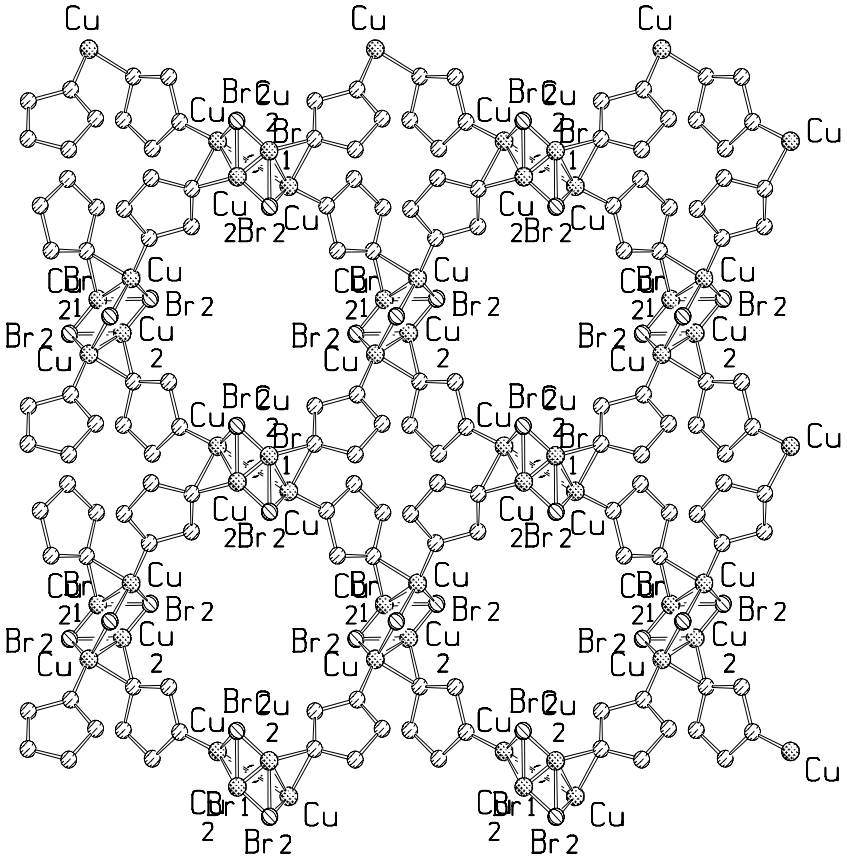

Figure 3.2.46. View of the 2D layer structure of complex **33**, orthogonal to the a,b plane (C, H and Fe atoms are omitted for clarity).

Complex **33** is a 2D polymer in which a $(CuBr)_3$ unit is connected to four [Cp'''Fe(η^5-P_5)] moieties, with the P_5 ring of the [Cp'''Fe(η^5-P_5)] moieties coordinating in a 1,3 substitution pattern to two different $(CuBr)_3$ units. Each Cu2 atom in the $(CuBr)_3$ unit is disordered over two positions with equal occupancy. The coordination geometry of the Cu2 is trigonal planar with the bond angle Br1–Cu2–Br being 127.3°(2) and Br1–Cu2–P4 being 105.9°(2), while the other two copper atoms (Cu1) coordinate in a distorted tetrahedral manner to two phosphorus atoms from two different [Cp'''Fe(η^5-P_5)] moieties and two bromine atoms (Figure 3.2.46). The Cu2–P bond length (2.393(8) Å) is between those of the other two Cu1–P bond lengths (Cu1–P1 2.230(5), Cu1–P4 2.568(5) Å). The Cu2–Br1 bond length (2.561(5) Å) is longer than the other two Cu–Br bond lengths (Cu1–Br1 2.406(4), Cu1–Br2 2.447(3) Å).

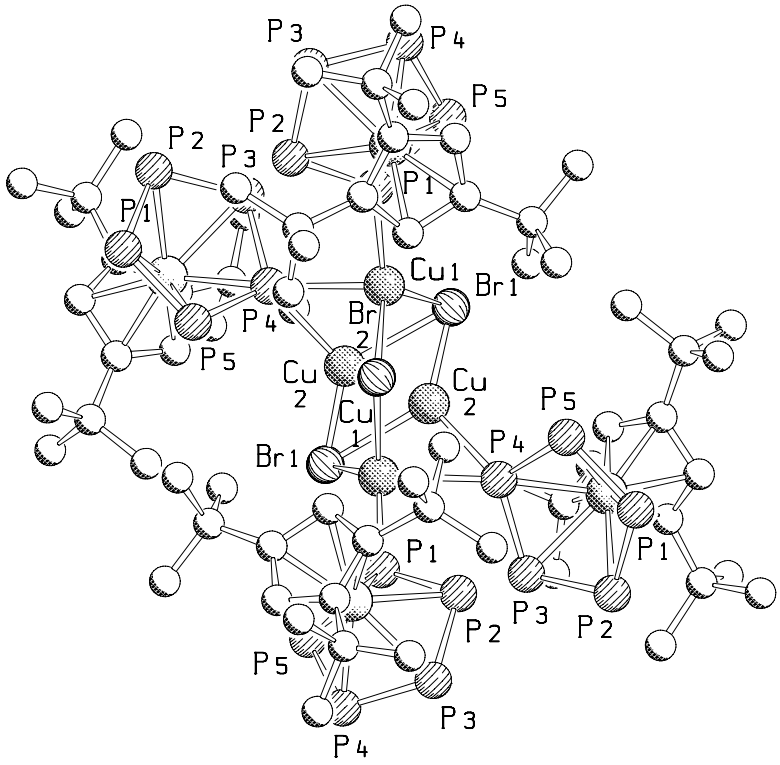

Figure 3.2.47. Section of the coordination geometry around the Cu atoms within the polymeric structure of complex **33** (H atoms are omitted for clarity, Cu2 is disordered over two positions with equal occupancy). Selected bond lengths (Å) and angles (°): P1–P2 2.102(7), P2–P3 2.111(7), P3–P4 2.120(8), P4–P5 2.105(6), P5–P1 2.109(6), Cu2–P4 2.393(8), Cu2–Br1 2.561(5), Cu1–P1 2.230(5), Cu1–P4 2.568(5), Cu1–Br1 2.406(4), Cu1–Br2 2.447(3), Br1–Cu2–Br1 127.3(2), Br1–Cu2–P4 105.9(2), P1–Cu1–P4 93.28(19), P1–Cu1–Br1 121.53(17), Br1–Cu1–Br2 112.45(13), Br2–Cu1–P4 99.01(15).

3.2.5.3. Reaction of [Cp'''Fe(η^5-P_5)] with CuI

An acetonitrile solution of CuI was carefully layered onto a CH_2Cl_2 solution of [Cp'''Fe(η^5-P_5)] in a 2:1 stoichiometric ratio at room temperature, and after the very slow diffusion was complete, the air-sensitive dark brown crystalline complex [{Cp'''Fe(μ,η^5:η^1:η^1-P_5)}$_4$$(CuI)_4]_\infty$ (**34**) was obtained.

Complex **34** dissolves sparingly in CH_2Cl_2 and MeCN, but is not soluble in hexane and toluene.

The positive ESI-MS of **34** in MeCN at room temperature reveals fragments attributable to the cations $[\{Cp'''Fe(P_5)\}_2Cu_2I]^+$, $[\{Cp'''Fe(P_5)\}_2Cu]^+$ and $[Cp'''Fe(P_5)CuMeCN]^+$.

The $^{31}P\{^1H\}$ NMR spectrum of **34** at room temperature displays a broad signal at $\delta = 163.7$ ppm. Due to the low solubility of **34** no variable temperature NMR investigations were possible. This indicates, together with the mass spectral data, that there should be oligomers in solution.

The molecular structure of **34** was determined by single-crystal X-ray diffraction and is illustrated in Figure 3.2.48.

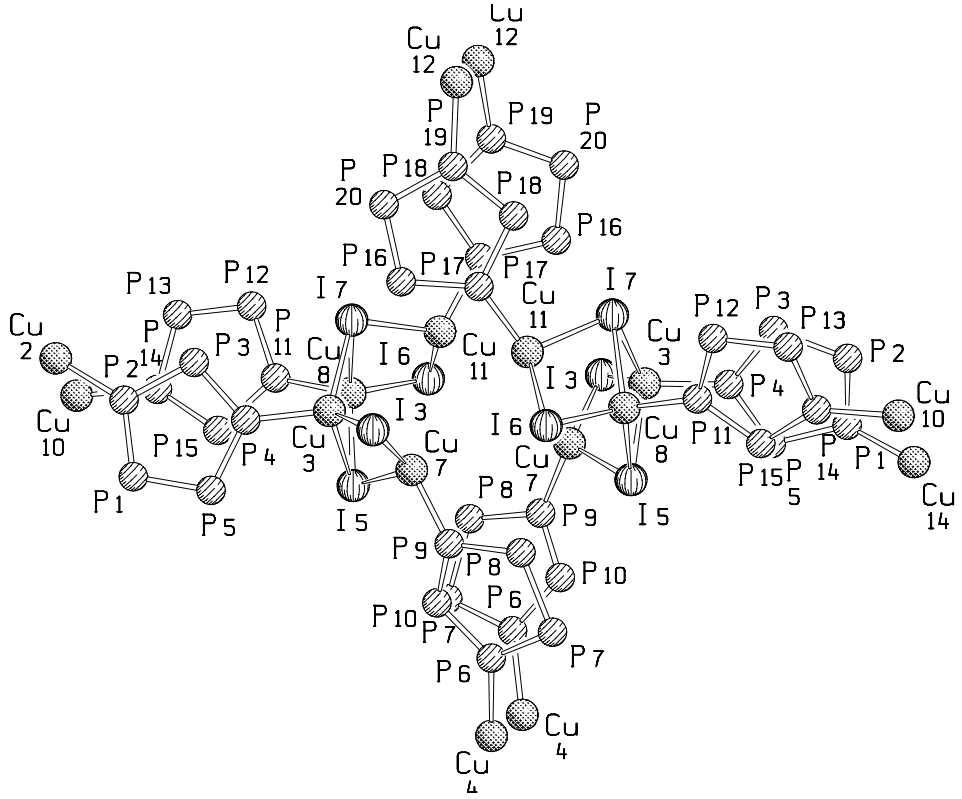

Figure 3.2.48. View of the 2D structure of complex **34** orthogonal to the a, b plane (C, H and Fe atoms are omitted for clarity). Selected bond lengths (Å) and angles (°): P1–P2 2.086(13), P2–P3 2.124(11), P3–P4 2.093(10), P4–P5 2.097(10), P5–P1 2.115(11), P2–Cu2 2.249(9), P4–Cu3 2.246(6), P11–P12 2.112(10), P12–P13 2.098(11), P13–P14 2.082(14), P14–P15 2.106(16), P15–P11 2.087(10), P11–Cu8 2.256(6), P14–Cu9 2.353(12), P19–Cu12 2.254(8), P6–Cu4 2.262(8), Cu9–I9 2.569(7), Cu9–I8 2.728(7), Cu12–I9 2.642(4), Cu12–I8 2.694(4), P14–Cu9–I9 118.3(3), I8–P9–I9 106.9(3), I8–Cu12–I9 112.72(14), I8–Cu12–P19 101.2(2).

In complex **34**, the cyclo-P_5 rings of the pentaphosphaferrocene moieties are connected to ladder-like $(CuI)_4$ units in a 1,3-substitution pattern. Two copper atoms of each $(CuI)_4$ unit, consisting of three annelated four-membered rings, coordinate tetrahedrally to three iodine atoms and one phosphorus atom while the other two copper atoms coordinate pyramidally to two iodine atoms and one phosphorus atom in the P_5 ring. Thus, a novel double layer 2D polymer is formed (Figure 3.2.49).

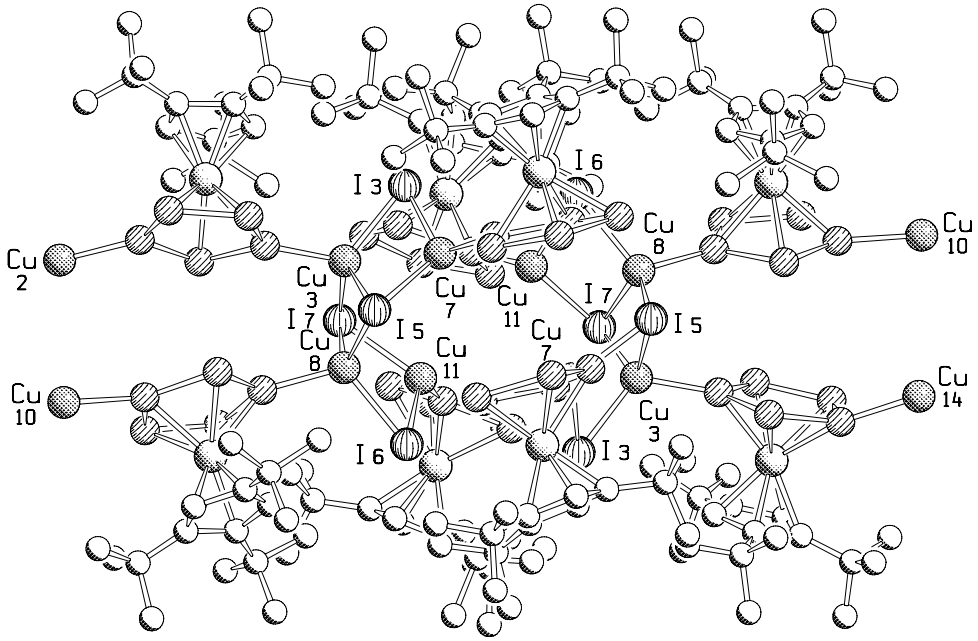

Figure 3.2.49. Double layer 2D polymeric structure of complex **34** (H atoms are omitted for clarity).

Since there are five lone pairs of electrons available on the cyclo-P_5 ring, each of them has the potential to coordinate to a metal center. Two-dimensional complexes can be formed. Because of the steric factor, successively larger cluster structures of $(CuX)_n$ are necessary to connect different [Cp'''Fe(η^5-P_5)] moieties (in **31** $(CuCl)_2$, in **33** $(CuBr)_3$, and in **34** $(CuI)_4$). The average distance between the copper and halogen atoms in the cluster increases (2.3195 Å in $(CuBr)_3$ of **33** and 2.6583Å in the cage $(CuI)_4$ of **34**). The size of the copper halides can also affect the coordination mode of P_5-ring (in **31** and **32** 1,2,4-, in **33** and **34** 1,3-substitution pattern).

3.2.5.4. Reaction of [Cp'''Fe(η^5-P_5)] with silver salts

3.2.5.4.1. Reaction of [Cp'''Fe(η^5-P_5)] with Ag[Al{$OC(CF_3)_3$}$_4$]

A mixture of [Cp'''Fe(η^5-P_5)] and Ag[Al{$OC(CF_3)_3$}$_4$] in CH_2Cl_2 was stirred at room temperature for one hour and was then layered with pentane. An air- and light-sensitive 1D polymer was obtained in the form of dark brown needles (equation 3.20).

Compound **35** is soluble in CH_2Cl_2 and THF, moderately soluble in toluene and acetonitrile, but insoluble in nonpolar solvents such as alkanes. It can be stored under an inert atmosphere at -28 °C.

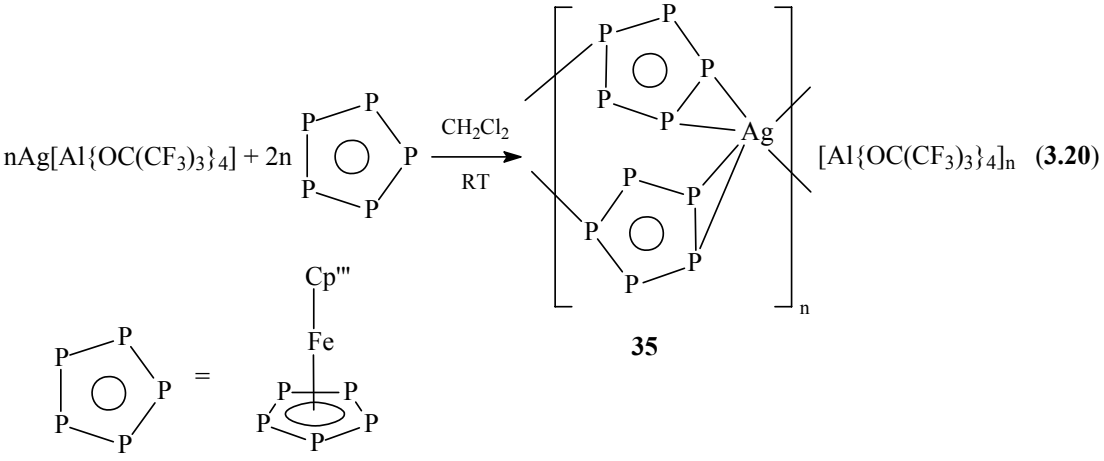

Crystals of **35** have been characterized by X-ray diffraction and a section of the polycation therein is illustrated in Figure 3.2.50.

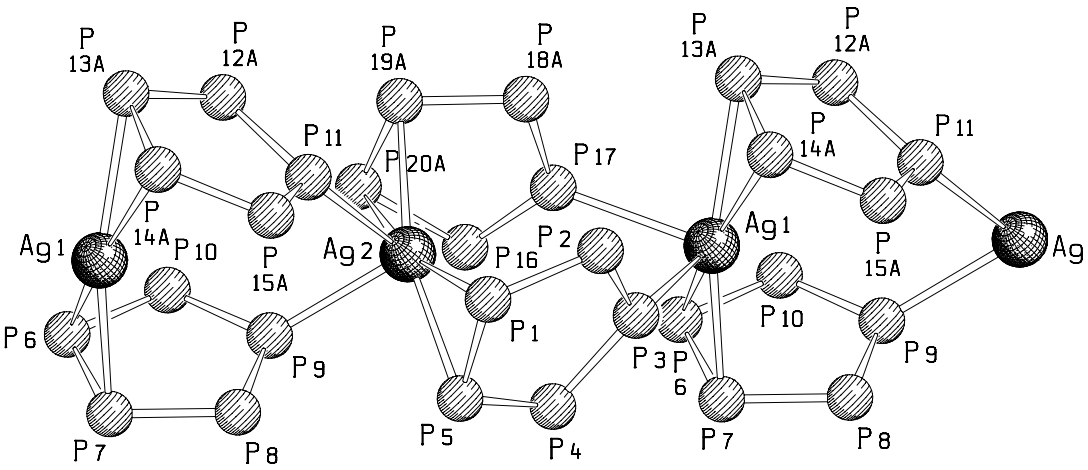

Figure 3.2.50. Portion of the cationic chain of **35**. (C, H, and Fe atoms are omitted for clarity) Selected bond lengths (Å) and angles (°): P1–P2 2.1247(9), P2–P3 2.1118(8), P3–P4 2.1053(8), P4–P5 2.1283(9), P5–P1 2.1537(9), P1–Ag2 2.7342(8), P5–Ag2 2.7337(8), P19A–Ag2 2.6525(12), P20A–Ag2 2.793(3), P9–Ag2 2.6916(7), P11–Ag2 2.8757(8), P1–Ag2–P5 46.39(2), P19A–Ag2–P20A 45.08(8), P1–Ag2–P11 80.77(2), P9–Ag2–P20A 80.94(5), P11–Ag2–P9 79.57(2).

Complex **35** crystallizes in the triclinic space group $P\bar{1}$ with two formula units in the unit cell. The core of this cation consists of a chain of Ag(I) cations that are doubly bridged at the cyclo-P_5 moieties of the [Cp'''Fe(η^5-P_5)] units in an η^2:η^1 fashion. The coordination geometry around the Ag(I) centers is tetrahedral, with six phosphorus atoms of four cyclo-P_5 moieties being coordinated through two side-on and two end-on coordination modes. A similar complex $[Ag\{Cp^*Fe(\eta^5:\eta^2:\eta^1\text{-}P_5)\}_2]_n[Al\{OC(CF_3)_3\}_4]_n$ was obtained in our group[66], which displays 1,2,3-coordination mode of the cyclo-P_5 ring and is different from the 1,2,4-coordination mode of the cyclo-P_5 ring in **35**. The polymeric core of **35** could be regarded as being built up of a chain of eight-membered Ag_2P_6 rings fused to two three-membered AgP_2 rings. The P–P bond lengths in the AgP_2 rings (2.1537(9) Å) are obviously longer than the other P–P bond lengths of the cyclo-P_5 ring (2.1248 Å (av.)), which may be due to the π-coordination mode, and are comparable to those in [Ag{Cp*Fe(η^5:η^2:η^1-

$P_5)\}_2]_n[Al\{OC(CF_3)_3\}_4]_n$ (2.156(4) Å). The two P–P edges directly adjacent to those of the AgP_2 rings are also slightly elongated (2.1247(9) and 2.1283(9) Å) in comparison to the other two P–P bond lengths (2.1053(8) and 2.1118(8) Å) and they are all longer than those in the uncoordinated starting material (2.0792 Å (av.))[14]. The average Ag–P bond length (2.7468 Å) is longer than that of **19** (2.4473 Å) and **29** (2.5068 Å), possibly due to steric hindrance. The silver center in **35** coordinates to six phosphorus atoms, in **29** to three phosphorus atoms and in **19** to two phosphorus atoms.

In the positive ESI-MS of **35** in $MeCN/CH_2Cl_2$ at room temperature, the peak with 100% relative abundance was assigned to $[\{Cp'''Fe(\eta^5\text{-}P_5)\}_2Ag]^+$ and the peak with 100% relative abundance in the negative ESI-MS corresponds to $[Al\{OC(CF_3)_3\}_4]^-$ were detected. This ESI-MS spectrum indicates, that in solution the monocation $[\{Cp'''Fe(\eta^5\text{-}P_5)\}_2Ag]^+$ probably exists. This behaviour is similar to that of $[Ag\{Cp^*Fe(\eta^5\text{:}\eta^2\text{:}\eta^1\text{-}P_5)\}_2]_n[Al\{OC(CF_3)_3\}_4]_n$.[66]

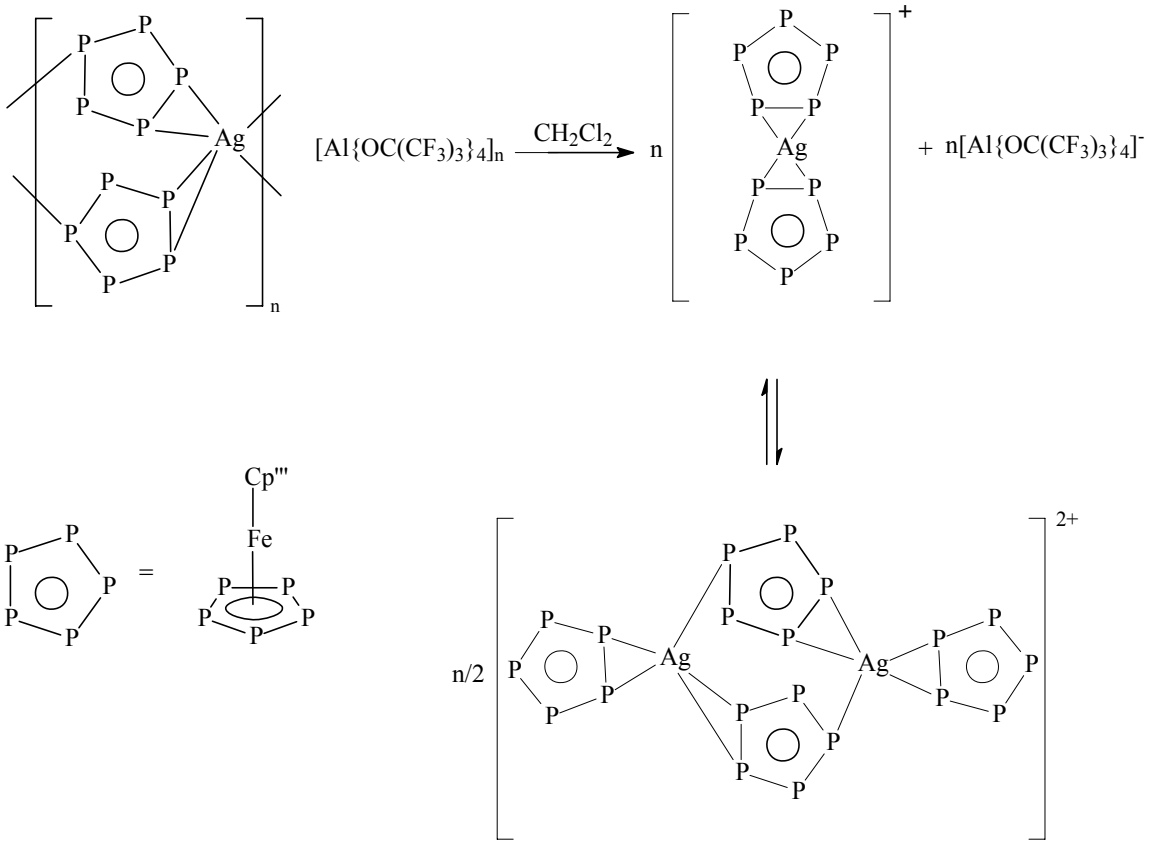

Figure 3.2.51. Proposed monomer/oligomer cation equilibria in solution.

The $^{31}P\{^{1}H\}$ NMR spectrum of **35** at room temperature shows only one signal. In the cyclo-P_5 rings of the polymer chain **35** there are three coordinated and two uncoordinated phosphorus atoms and therefore the appearance of the spectrum is attributed to dynamic behaviour in solution. In order to gain further insight into this dynamic behaviour, variable temperature $^{31}P\{^{1}H\}$ NMR spectroscopy of the compound in THF-d_8/CH_2Cl_2 was performed. At room temperature only a singlet at 162.1 ppm is observed, shifted marginally upfield relative to uncoordinated **5** (164.7 ppm). As the temperature is reduced, the signal is shifted gradually to higher field and becomes broader. At -100 °C the signal is split into two broad signals. At -110 °C the broad signals are split further (Figure 3.2.52).

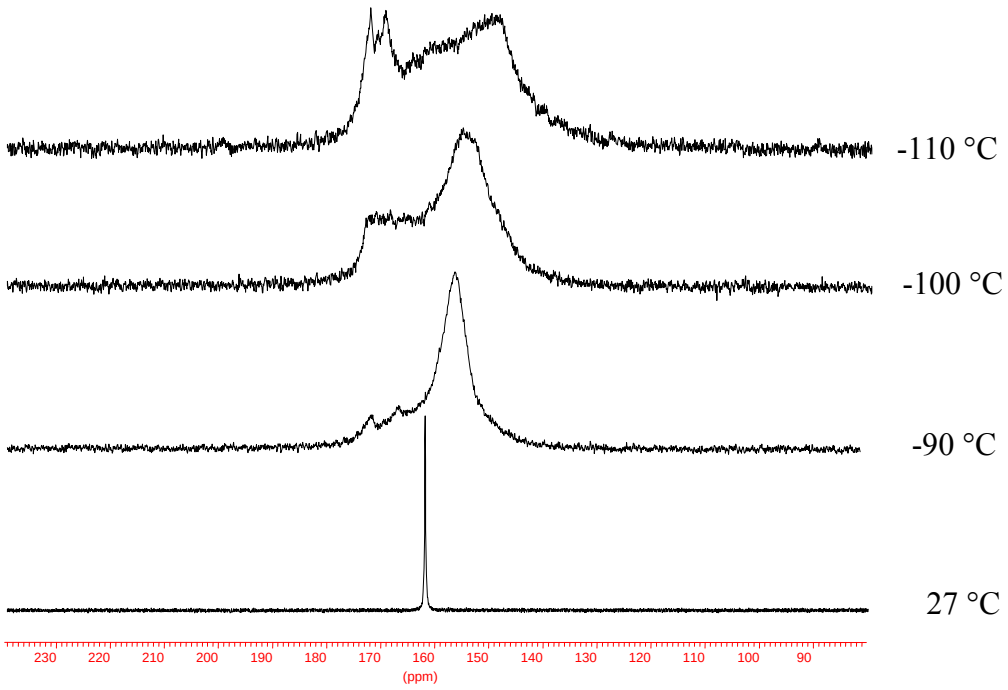

Figure 3.2.52. Variable temperature $^{31}P\{^{1}H\}$ NMR spectra of **35** in a 3:1 mixture of THF-d_8 and CH_2Cl_2 at 25 °C, -90 °C, -100 °C and -110 °C.

These variable temperature spectra, together with the data provided by the mass spectrum suggest that a monomer/oligomer equilibrium may exist in solution, similar to that of $[Ag\{Cp^*Fe(\eta^5:\eta^2:\eta^1\text{-}P_5)\}_2]_n[Al\{OC(CF_3)_3\}_4]_n$.[66] At room temperature, the cyclo-P_5 ring of a monocation probably "rotates" and thus only one signal is observed. As the temperature is reduced, the signal is split into two broad signals, which may either be attributable to the "freezing" of this P_5-ring rotation or the increase in the proportion of oligomeric species or a

combination of both. The upfield signal most likely represents the coordinated phosphorus atoms in the cyclo-P_5 rings, while the lowfield signal the uncoordinated ones (Figure 3.2.51). Unfortunately, it is not possible to perform a meaningful integration of the signals.

3.2.5.4.2. Reaction of [Cp'''Fe(η^5-P_5)] with $AgSO_3CF_3$

A mixture of $AgSO_3CF_3$ and [Cp'''Fe(η^5-P_5)] in CH_2Cl_2 was stirred in a ratio of 1:2 at room temperature and the color of the reaction mixture turned from green to greenish brown. Further concentration gave powder precipitated from the solution.

The positive ESI-MS of the reaction solution at room temperature shows a peak with 100% relative abundance corresponding to $[\{Cp'''Fe(\eta^5\text{-}P_5)\}_2Ag]^+$. In the negative ESI-MS, the peak with 100% relative abundance corresponds to $[CF_3SO_3]^-$ was found. The mass spectral data depicts a similar fragment to that observed for **35** and suggests that the reaction mixture should contain the same monocation $[\{Cp'''Fe(\eta^5\text{-}P_5)\}_2Ag]^+$.

The ^1H NMR spectrum of the reaction solution shows three signal groups: the peak at δ = 4.16 ppm represents two protons while the two singlets at δ = 1.14 and 1.26 ppm correspond to the protons of the *tert*-butyl groups in the cyclopentadiene ring.

A singlet at δ = 166.1 ppm was also observed in the $^{31}P\{^1H\}$ NMR spectrum at room temperature.

4. Experimental

4.1 General remarks

4.1.1 Methods

All manipulations, except where otherwise noted, were conducted under argon in a Braun Labmaster 130 glovebox or on a vacuum line (≤ 10–3 mbar) using standard Schlenk techniques under prepurified nitrogen or argon. All experiments were carried out exclusively under nitrogen. Solvents were degassed under vacuum and saturated with nitrogen prior to distillation. *n*-Pentane and *n*-hexane were distilled from $LiAlH_4$; diethyl ether and tetrahydrofuran from sodium/benzophenone; toluene from sodium; and methylene chloride, acetonitrile, and dimethylformamide from CaH_2. Deuterated benzene was degassed under reduced pressure, saturated with argon, distilled from sodium/benzophenone, and stored over activated 4 Å molecular sieves. All other deuterated solvents were degassed by three freeze-pump-thaw cycles, vacuum transferred from an appropriate drying agent, and stored over activated 4 Å molecular sieves. Kieselgur was routinely stored at 110 °C prior to use, then dried under vacuum and freed from traces of moisture with the aid of a heat gun. Photolysis reactions were carried out with a Hanau mercury vapor lamp (TQ 150).

4.1.2 Spectroscopy and analysis

NMR spectra were recorded on a Bruker AC250, Bruker AMX 300, Bruker Avance 300, or Bruker Avance 400. Chemical shifts are given in parts per million (ppm) and are referenced to tetramethylsilane (^{1}H NMR) or 85% phosphoric acid (^{31}P NMR) as external standards. Chemical shifts in low field relative to the standard are designated by positive signs. All coupling constants *J* are given as absolute values in Hertz (Hz).

Mass spectrometry was conducted with the mass spectrometer ThermoQuest Finnigan TSQ 7000 for ESI-MS and on a Varian MAT 711, MAT 8200, MAT 8230, or Finnigan MAT 95 for FD-MS and EI-MS.

Infrared spectra were recorded on a Bruker IFS280 FT-IR spectrometer or Varian FTS 800 spectrometer.

Elemental analyses were carried out at the microanalytical laboratories of the University of Regensburg.

All X-ray crystallographic analyses were performed either by Prof. Manfred Scheer, the X-ray crystallography department of the University of Regensburg, or Dr. Alexander V. Virovets (Russian Academy of Sciences (Siberian Division), Novosibirsk, Russia). The data were collected on either a STOE IPDS or an Oxford Diffraction Gemini Ultra CCD diffractometer. All the yield calculations refer to the corresponding P-containing starting materials.

4.2. Preparation of starting material

4.2.1 Synthesis of [Cp'''Fe(η^5-P_4C^tBu)] and [Cp'''Fe(η^5-$P_3C_2{}^tBu_2$)]

^{t}BuC≡P (0.223 g, 2.23 mmol) was added to a solution of [{Cp'''(CO)$_2$Fe}$_2$(μ,η^1:η^1-P_4)] (**1**) (1.82 g, 2.23 mmol) in toluene (150 ml) at room temperature. The reaction mixture was heated under reflux for 36 h. After the removal of all volatile materials in vacuum, the residue was dissolved in dichloromethane (10 ml) and transferred onto silica gel. The chromatographic work-up on a silica gel column (40 × 2.5 cm), eluted with hexane/dichloromethane (10:1), gave first a red fraction of **6**, then an orange-red fraction of **4**, a green fraction of **5**, and finally an olive-green fraction of **3**. Each product was recrystallized from n-hexane. A fifth band (green) contained the proposed polymeric compound mentioned in the main text. If, as in some cases, the separation was not complete after column chromatography, the separation was completed in a glovebox by thin layer chromatography (TLC) using a hexane/dichloromethane (10:1) solvent mixture.

[Cp'''Fe(η^5-P_4C^tBu)] (3): Yield: 60 mg (11%)

^{1}H NMR (C_6D_6, RT, 250 MHz): δ = 1.62 (s, 9H), 1.20 (s, 9H), 1.35 (s, 18 H), 4.22 (s, 2H) ppm.
^{31}P{^{1}H} NMR (C_6D_6, RT, 250 MHz, AA´MM´ spin system): δ(P_A) = δ($P_{A'}$) = 81.6 (m, 2P), δ (P_M) = δ($P_{M'}$) = 122.8 (m, 2P) ppm, ^1J(P_A,P_M) = -431.2 Hz, ^2J(P_A,$P_{M'}$) = 9.4 Hz, ^3J(P_A,$P_{A'}$) = -54.7 Hz, ^1J(P_M,$P_{M'}$) = -425.2 Hz (simulated values).
EI-MS (70 eV, 100 °C): m/z = 482 [Cp'''Fe(P_4C^tBu)]$^+$ (100%), 382 [Cp'''FeP_3]$^+$ (71%), 121 [$C_5H_4{}^tBu$]$^+$ (23.8%).

[Cp'''Fe(η^5-$P_3C_2{}^tBu_2$)] (4): Yield: 110 mg (20%)

^{1}H NMR (C_6D_6, RT, 250 MHz): δ = 1.25 (s, 9H), 1.24 (s, 18H), 1.36 (s, 18H), 4.58 (s, 2H) ppm.

^{31}P{^{1}H} NMR (C_6D_6, RT, 250 MHz, AB_2 spin system): δ(P_A) = 52.6 (t, 1P), δ(P_B) =42.7 (d, 2P) ppm, ^2J(P_A, P_B) = 43.9 Hz.

EI-MS (70 eV, 60 °C): m/z = 520 $[Cp'''Fe(P_3{}^tBu_2C_2)]^+$ (4%), 432 $[Cp'''FeP_2{}^tBuC_2]^+$ (71.5%), 295 $[(C_5H_3{}^tBu_2)FeP_2]^+$ (100%), 233 $[Cp''']^+$ (28%).

[Cp'''Fe(η^5-P_5)] (5): Yield: 4 mg (2%)

^{1}H NMR (C_6D_6, RT, 250 MHz): δ = 1.08 (s, 9H), 1.21 (s, 18 H), 3.9 (s, 2H) ppm.

^{31}P NMR (C_6D_6, RT, 250 MHz): δ = 165.4 ppm (s).

[(Cp'''Fe)$_2$(η^3:η^3-P_3)] (6): Yield: 5 mg (2%)

^{1}H NMR (C_6D_6, RT, 250 MHz): δ = 1.22 (s, 9H), 1.30 (s, 18 H), 4.16 (s, 2H) ppm.

^{31}P NMR (C_6D_6, RT, 250 MHz, AA´M spin system): δ(P_A), δ($P_{A'}$) = 677.8 (dd, 1P), δ(P_M) = -380.9 (t, 2P) ppm, J(P_A,P_M) = 390.2 Hz, J($P_{A'}$,P_A) = 32.6 Hz.

EI-MS (70 eV, 90 °C): m/z = 671 $[(Cp'''Fe)_2(P_3)]^+$ (5.7%), 614 $[Cp'''Cp''Fe_2P_3]^+$ (8.4%), 382 $[Cp'''Fe\ P_3]^+$ (27.8%).

Fifth fraction: ^{31}P NMR (250 MHz, C_6D_6): δ = 92 ppm, $\omega_{1/2}$ = 300 Hz.

4.2.2 Synthesis of [Cp'''Fe(η^5-P_3C_2PhH)]

PhC≡CH (0.9 g, 8.8 mmol) was added to a solution of [{Cp'''(CO)$_2$Fe}$_2$(μ,η^1:η^1-P_4)] (**1**) (1.8 g, 2.2 mmol) in toluene (200 ml) at room temperature. The reaction mixture was heated under reflux for 18 h. After removal of all volatile material in vacuum, the residue was dissolved in dichloromethane (10 ml) and transferred onto silica gel. Chromatographic work-up on a silica gel column (40 x 2.5 cm) eluting with hexane/toluene (20:1) gave the red fraction of **8**, then a green fraction of **9**. Yield: **8** 150 mg (14%), **9** 480 mg (43.6%)

[Cp'''Fe(η^5-P_3C_2PhH)] (8)

^{1}H NMR (C_6D_6, RT, 400.13 MHz): δ = 1.09 (s, 9H), 1.12 (s, 9H), 1.41 (s, 9 H), 4.00 (dd, 1H, Cp'''), 4.19 (dd, 1H, Cp'''), 6.24 (ddd, 1H, P_3C_2-ring), 7.07 (m, 3H, C_6H_5), 7.80 (m, 2H, C_6H_5) ppm.
^{31}P{^{1}H} NMR (C_6D_6, RT, 161.98 MHz, AA´M spin system): δ(P_A) = 51.7 (dd), δ($P_{A'}$) = 48.9 (dd), δ(P_M) =15.2 (dd), J(P_A,P_M) = 427.1 Hz, J(P_M,$P_{A'}$) = 399.6 Hz, ^2J(P_A,$P_{A'}$) = 4.4 Hz.
^{31}P NMR (C_6D_6, RT, 161.98 MHz, AA´M spin system): δ(P_A) = 51.7 (ddd), δ($P_{A'}$) = 48.9 (ddd), δ(P_M) =15.2 (ddd), ^2J($P_{A'}$,H_a) = 40.1, ^3J(P_M,H_a) = 10.8, ^4J(P_A,H_a) = 4.5 Hz.
EI-MS (70 eV): m/z = 484 [Cp'''Fe(P_3C_2PhH)]$^+$ (65%), 452 [Cp'''Fe(P_2C_2PhH)]$^+$ (8.2%), 377 [Cp'''Fe($P_2C_2H_2$)]$^+$ (15%).

[Cp'''Fe(η^5-$PC_4Ph_2H_2$)] (9)

^{1}H NMR (C_6D_6, RT, 400.13 MHz): δ = 1.12 (s, 9H), 1.32 (s, 9H), 1.56 (s, 9 H), 3.62 (dd, 1H, Cp'''), 3.77 (dd, 1H, Cp'''), 4.65 (d, 1H_a , PC_4-ring), 6.15 (d, 1H, PC_4-ring), 7.26 (m, 6H, C_6H_5), 7.77 (m, 4H, C_6H_5) ppm.
^{31}P NMR (C_6D_6, RT, 161.98 MHz): δ = -64.1(dd) ppm, (^2J(P,H_a) = 35.6 Hz; ^4J(P,H) = 4.9 Hz).
EI-MS (70 eV): m/z = 524 [Cp'''Fe($PC_4Ph_2H_2$)]$^+$ (28%), 493 [Cp'''Fe($C_4Ph_2H_2$)]$^+$ (100%), 421[(C_5H_3^{t}Bu^{i}Pr)Fe($PC_4Ph_2H_2$)]$^+$ (4.8%).

4.2.3 Synthesis of [Cp'''Fe(η^5-P_5)]

A mixture of white phosphorus (0.49 g, 3.95 mmol) and [{Cp'''Fe$(CO)_2$}$_2$] (0.9 g, 2.0 mmol) in decalin (200 ml) was stirred at 188 °C under reflux for 3 h. After removal of all solvent in vacuum, the residue was dissolved in dichloromethane (10 ml) and transferred onto silica gel. Chromatographic work-up on a silica gel column (20 × 2.5 cm) eluting with hexane gave a green fraction of **5**. Yield: 457 mg (40%).

^{1}H NMR (C_6D_6, RT, 400.13 MHz): δ = 3.95 (s, 2H), 1.08 (s, 9H) 1.21 (s, 18H) ppm.
^{31}P{^{1}H} NMR (C_6D_6, RT, 161.98 MHz): δ = 165.4 (s, 5P) ppm.
EI-MS (70 eV): m/z = 444 [Cp'''Fe(P_5)]$^+$ (100%), 382 [Cp'''Fe(P_3)]$^+$ (43%).

4.3 Synthesis of the complexes based on [Cp'''Fe(η^5-$P_3C_2{}^tBu_2$)]

4.3.1 Synthesis of [{Cp'''Fe(η^5:η^1:η^1-$P_3C_2{}^tBu_2$)}(μ-CuCl)]$_2$ (10)

A mixture solution of CuCl (7.5 mg, 0.075 mmol) in CH_2Cl_2/CH_3CN (5 ml/5 ml) was layered onto a solution of [Cp'''Fe(η^5-$P_3C_2{}^tBu_2$)] (40 mg, 0.075 mmol) in 10 ml of CH_2Cl_2 at room temperature. After 2 weeks, red crystals of **10** were obtained on the wall of the Schlenktube. Yield: 0.010 mmol, 12 mg (50.4%).

^{1}H NMR (CD_2Cl_2, 27 °C, 400.13 MHz): δ = 4.1 (s, 4H), 0.9 (s, 36H), 1.0 (s, 18H), 1.1 (s, 36H, P_3C_2-ring) ppm.
^{31}P{^{1}H} NMR (THF-d_8/MeCN, 27 °C, 161.98 MHz, AM_2 spin system): δ(P_A): 52.8 ppm (t), δ(P_M): 27.6 (br) ppm ($\omega_{1/2}$ = 90 Hz), J(P_A,P_M) = 44.2 Hz.
ESI-MS (MeCN, RT): m/z = 1203 [{Cp'''Fe($P_3C_2{}^tBu_2$)}$_2$$Cu_2Cl$]$^+$ (3.1%), 1103 [{Cp'''Fe($P_3C_2{}^tBu_2$)}$_2$Cu]$^+$ (21.5%), 624 [Cp'''Fe($P_3C_2{}^tBu$)CuMeCN]$^+$ (100%).
Elemental analysis: Calculated (%) for $C_{108}H_{188}Cl_4Cu_4Fe_4P_{12}$ (2477.74): C 52.35, H 7.65, found: C 48.92, H 7.82.

4.3.2. Synthesis of [{(Cp'''Fe)$_2$(μ,η^4:η^4-P_4)}{CuCl}$_2$(MeCN)]$_\infty$ (11)

CuCl (15 mg, 0.15mmol) in a CH_2Cl_2 /CH_3CN (2 ml/3 ml) solution was layered onto a solution of [Cp'''Fe(η^5-$P_3C_2{}^tBu_2$)] (39 mg, 0.075 mmol) in 5 ml CH_2Cl_2 and the solution was kept at room temperature. After four weeks, dark brown crystals were obtained on the wall of the Schlenktube. Yield: 20 mg (52.5%).

^{1}H NMR (CD_2Cl_2, 27 °C, 400.13 MHz): δ = 4.32 (s, 2H), 0.97 (s, 18H), 1.04 (s, 9H) ppm.
^{31}P{^{1}H} NMR (CD_2Cl_2/MeCN, 27 °C, 161.98 MHz): δ = 115.6 (br, 2P) ($\omega_{1/2}$ = 450 Hz), 69.1 (br, 2P) ppm ($\omega_{1/2}$ = 520 Hz).
^{31}P{^{1}H} NMR (C_6D_6/MeCN, 27 °C, 161.98 MHz): δ = 113.5 (br, 2P) ($\omega_{1/2}$ = 610 Hz), 66.5 (br, 2P) ppm ($\omega_{1/2}$ = 510 Hz).
^{31}P{^{1}H} NMR (C_6D_6/DMF, 27 °C, 161.98 MHz): δ = 78.5 (br) ppm ($\omega_{1/2}$ = 1300 Hz).
ESI-MS(MeCN, RT): m/z = 826 [{(Cp'''Fe)$_2$(P_4)}Cu_2]$^+$ (100%), 702 [(Cp'''Fe)$_2$(P_4)]$^+$ (34.8%), 536 [(Cp'''Fe)(CpFe)(P_4)]$^+$ (9.0%).

4.3.3. Synthesis of [{Cp'''Fe(μ,η^4:η^1-$P_2C_2{}^tBu_2$)}{CuBr(MeCN)}]$_2$ (13)

A solution of CuBr (3 mg, 0.019 mmol) in CH_3CN (2 ml) was layered onto a solution of [Cp'''Fe(η^5-$P_3C_2{}^tBu_2$)] (10 mg, 0.019 mmol) in 3 ml CH_2Cl_2 at room temperature. After complete diffusion of the two phases, the reaction mixture was concentrated under reduced pressure to about one half of the original volume (2.5 ml) and stored in a refrigerator at 4 °C. After 2 weeks the brown crystalline complex of **13** was obtained on the wall of the Schlenktube. Yield: 5 mg (38.8%)

ESI-MS (MeCN, RT): m/z = 1103 [{Cp'''Fe($P_2C_2{}^tBu_2$)}$_2$$Cu_2$]$^+$ (2.5%), 489 [Cp'''Fe($P_2C_2{}^tBu_2$)]$^+$ (4.2%).
ESR (RT): g = 2.026, a_1 = 10 mT, g (half field) = 5.3.

Synthesis of the proposed dimeric complex of [{Cp'''Fe(μ,η^5:η^1-$P_3C_2{}^tBu_2$)}(CuBr)]$_2$(12)

A solution of CuBr (6 mg, 0.038 mmol) and CH_3CN (2 ml) was layered onto a solution of [Cp'''Fe(η^5-$P_3C_2{}^tBu_2$)] (20 mg, 0.038 mmol) in 3 ml CH_2Cl_2 at room temperature. After complete diffusion of the two phases, the red brown reaction mixture was used for NMR and mass spectroscopic measurement.

$^{31}P\{^1H\}$ NMR (THF-d_8/MeCN, 27 °C, 161.98 MHz, AM_2 spin system): δ(P_A) = 51.6 (t), δ(P_M) = 28.4 (br) ppm, J(P_A,P_M) = 44.7 Hz.
ESI-MS (MeCN, RT): m/z = 1247 [{Cp'''Fe($P_3C_2{}^tBu_2$)}$_2$$Cu_2Br$]$^+$ (1.0%), 1103 [{Cp'''Fe($P_3C_2{}^tBu_2$)}$_2$Cu]$^+$ (1.7%), 832 [Cp'''Fe($P_3C_2{}^tBu$)Cu_3BrMeCN]$^+$ (3.1%), 624 [Cp'''Fe($P_3C_2{}^tBu$)CuMeCN]$^+$ (22%), 582 [Cp'''Fe($P_3C_2{}^tBu$)Cu]$^+$ (82%).

4.3.4. Synthesis of [{(Cp'''Fe)$_2$(μ,η^4:η^4-P_4)}(CuBr)$_2$(MeCN)]$_\infty$ (14)

A solution of CuBr (12 mg, 0.075 mmol) and 5 ml CH_3CN was layered onto a solution of [Cp'''Fe(η^5-$P_3C_2{}^tBu_2$)] (20 mg, 0.0375 mmol) in 7 ml CH_2Cl_2 at 4 °C. After 1 week, a dark

brown crystalline complex was obtained at the bottom of the Schlenktube. Yield: 16 mg (73.4%).

$^{31}P\{^{1}H\}$ NMR (CD_2Cl_2/MeCN, 27°C, 161.98 MHz): δ = 120.6 (br, 2P) ($\omega_{1/2}$ = 490 Hz), 76.2 (br, 2P) ppm ($\omega_{1/2}$ = 520 Hz).

$^{31}P\{^{1}H\}$ NMR (C_6D_6/MeCN, 27°C, 161.98 MHz): δ = 120.0 (br, 2P) ($\omega_{1/2}$ = 520 Hz), 74.8 (br, 2P) ppm ($\omega_{1/2}$ = 520 Hz).

$^{31}P\{^{1}H\}$ NMR (C_6D_6/DMF, 27 °C, 161.98 MHz): δ = 82.3 (br) ppm ($\omega_{1/2}$ = 970 Hz).

ESI-MS (MeCN, RT): m/z = 1611 $[\{(Cp'''Fe)_2(P_4)\}_2Cu_2Br]^+$ (0.22%), 1467 $[\{(Cp'''Fe)_2(P_4)\}_2Cu]^+$ (0.54%), 765 $[(Cp'''Fe)_2(P_4)Cu]^+$ (7.0%), 702 $[(Cp'''Fe)_2(P_4)]^+$ (100%).

4.3.5. Synthesis of $[\{(Cp'''Fe)_2(\mu,\eta^4{:}\eta^4\text{-}P_4)\}(CuI)_2(MeCN)]_\infty$ (15)

A solution of CuI (18.3 mg, 0.096 mmol) in CH_2Cl_2/CH_3CN (2 ml/3 ml) solvent was layered onto a solution of $[Cp'''Fe(\eta^5\text{-}P_3C_2{}^tBu_2)]$ (25 mg, 0.048 mmol) in 5 ml CH_2Cl_2 at room temperature. After one week, a dark brown crystalline complex was obtained on the wall of the Schlenktube. Yield: 15 mg (33.4%).

$^{31}P\{^{1}H\}$ NMR (CD_2Cl_2, 27 °C, 161.98 MHz): δ = 118.4 (br, 2P) ($\omega_{1/2}$ = 650 Hz), 72.9 (br, 2P) ppm ($\omega_{1/2}$ = 1300 Hz).

$^{31}P\{^{1}H\}$ NMR (C_6D_6/DMF, 27 °C, 161.98 MHz): δ = 90.2 (br) ppm ($\omega_{1/2}$ = 650 Hz).

^{1}H NMR (CD_2Cl_2, 27 °C, 400.13 MHz): δ = 4.58 (s, 2H), 1.11 (s, 18H), 1.04 (s, 9H) ppm.

ESI-MS (MeCN, RT): m/z = 953 $[(Cp'''Fe)_2(P_4)Cu_2I]^+$ (4.4%), 891 $[(Cp'''Fe)_2(P_4)CuI]^+$ (4.0%), 826 $[(Cp'''Fe)_2(P_4)Cu_2]^+$ (39.0%), 765 $[(Cp'''Fe)_2(P_4)Cu]^+$ (5.4%), 702 $[(Cp'''Fe)_2(P_4)]^+$ (100%).

4.4 Synthesis of the complexes based on $[CpFe(\eta^5\text{-}P_3C_2{}^tBu_2)]$

4.4.1 Synthesis of $[\{CpFe(\mu,\eta^5{:}\eta^1{:}\eta^1\text{-}P_3C_2{}^tBu_2)\}(CuCl)(MeCN)]_2$ (16)

A solution of CuCl (7.5 mg, 0.075 mmol) in CH_2Cl_2/CH_3CN (5 mL/5 ml) was layered onto a solution of $[CpFe(\eta^5\text{-}P_3C_2{}^tBu_2)]$ (27 mg, 0.075 mmol) in 10 ml CH_2Cl_2 at room temperature. After the reaction mixture diffused completely, the solution was concentrated and kept in

refrigerator at about 4 °C for one week. A red crystalline compound was obtained on the wall of the Schlenktube. Yield: 10 mg (10%).

^{1}H NMR (CD_2Cl_2, 27 °C, 400.13 MHz): δ = 4.79 (s, 5H), 1.33 (s, 18H) ppm.
^{31}P{^{1}H} NMR (CD_2Cl_2, 27 °C, 161.98 MHz, AM_2 spin system): $\delta(P_A)$ = 33.1(t), $\delta(P_M)$ = 15.4 (br) ppm ($\omega_{1/2}$ = 100 Hz), $J(P_A,P_M)$ = 45.7 Hz..
ESI-MS (MeCN, RT): m/z = 964 $[\{CpFe(P_3C_2{}^tBu_2)\}_2Cu_3Cl_2]^+$ (20%), 866 $[\{CpFe(P_3C_2{}^tBu_2)\}_2Cu_2Cl]^+$ (92%), 767 $[\{CpFe(P_3C_2{}^tBu)\}_2Cu]^+$ (96.4%).
Elemental analysis: Calculated (%) for $C_{68}H_{104}N_4Cl_4Cu_4Fe_4P_{12}$ (1968.56): C 41.49, H 5.32, N 2.84, found: C 36.52, H 5.0, N 2.0.

4.4.2 Reaction of [CpFe(η^5-P$_3$C$_2$^{t}Bu$_2$)] with CuBr

A solution of CuBr (17 mg, 0.11 mmol) in CH_3CN (5 ml) was layered onto a solution of $[CpFe(\eta^5\text{-}P_3C_2{}^tBu_2)]$ (20 mg, 0.056 mmol) in 5 ml CH_2Cl_2 at room temperature. After the reaction mixture diffused completely, the solution was concentrated to ca. 5 ml and kept at about 0 °C for one week. A red crystalline compound was obtained on the wall of the Schlenktube. Yield: 10 mg. The mother liquor was used for the following NMR and mass spectrospopic measurement.

^{1}H NMR (C_6D_6/MeCN, 27 °C, 400.13 MHz): δ = 4.71 (s, 5H), 1.26 (s, 18H) ppm.
^{31}P{^{1}H} NMR (C_6D_6/MeCN, 27 °C, 161.98 MHz, AM_2 spin system): $\delta(P_A)$ = 33.5 (t, 1P), $\delta(P_M)$ = 14.6 (br, 2P) ppm, $J(P_A,P_M)$ = 44.6 Hz..
^{31}P{^{1}H} NMR (CD_2Cl_2/MeCN, 27 °C, 161.98 MHz, AM_2 spin system): $\delta(P_A)$ = 25.7 (t, 1P), $\delta(P_M)$ = 2.6 (br, 2P) ppm.
ESI-MS (MeCN, RT): m/z = 456 $[\{CpFe(P_3C_2{}^tBu_2)\}CuMeCN]^+$ (28%), 599 $[\{CpFe(P_3C_2{}^tBu_2)\}Cu_2BrMeCN]^+$ (100%), 640 $[\{CpFe(P_3C_2{}^tBu_2)\}Cu_2Br_2MeCN]^+$ (78%), 767 $[\{CpFe(P_3C_2{}^tBu_2)\}_2Cu_2]^+$ (18%), 910 $[\{CpFe(P_3C_2{}^tBu_2)\}_2Cu_2Br]^+$ (17%), 951 $[\{CpFe(P_3C_2{}^tBu_2)\}_2Cu_2BrMeCN]^+$ (20%).

4.4.3 Synthesis of [{CpFe(η^5:η^1:η^1-$P_3C_2{}^tBu_2$)}$_3$(CuI)$_7$MeCN] (18)

A solution of CuI (21 mg, 0.11mmol) in CH_3CN (6 ml) was layered onto a solution of [CpFe(η^5-$P_3C_2{}^tBu_2$)] (20 mg, 0.056 mmol) in 6 ml CH_2Cl_2. After the reaction mixture diffused completely, the solution was concentrated to ca. 5 ml, layered with 5 ml of pentane, and allowed to sit for one week. A red crystalline complex was obtained on the wall of the Schlenktube. Yield: 20 mg (43.5%)

$^{31}P\{^1H\}$ NMR (CD_2Cl_2, 27 °C, 161.98 MHz, AM_2 spin system): $\delta(P_A)$ = 34.9 (br) ($\omega_{1/2}$ = 180 Hz), $\delta(P_M)$ = 8.2 (br) ppm ($\omega_{1/2}$ = 240 Hz).
^1H NMR (CD_2Cl_2, 27 °C, 400.13 MHz): δ = 3.56 (m, 5H), 1.22 (m, 9H), 0.8 (m, 9H) ppm.
EI-MS (70 eV): m/z = 2260 [{CpFe($P_3C_2{}^tBu_2$)}$_3$$Cu_7I_6$]$^+$ (22.5%), 2133 [{CpFe($P_3C_2{}^tBu_2$)}$_3$$Cu_5I_6$]$^+$ (30%), 1945 [{CpFe($P_3C_2{}^tBu_2$)}$_3$$Cu_4I_5$]$^+$ (29%).

4.4.4 Synthesis of [{CpFe(μ,η^5:η^1:η^1-$P_3{}^tBu_2C_2$)}(AgMeCN)]$_2$[Al{OC(CF_3)$_3$}$_4$]$_2$ (19)

A mixture of Ag[Al{OC(CF_3)$_3$}$_4$] (30 mg, 0.028 mmol) and [CpFe(η^5-$P_3C_2{}^tBu_2$)] (20 mg, 0.028 mmol) in 10 ml of CH_2Cl_2 and 5 ml MeCN was stirred in the dark for six hours. Afterwards the reaction mixture was filtered over diatomaceous earth and the filtrate was kept at 4 °C for one week. A red-orange needle crystalline compound was obtained on the wall of the Schlenktube.Yield: 15 mg (9%).

^1H NMR (THF-d_8, 27 °C, 400.13 MHz): δ = 3.57 (s, 5H), 1.43 (s, 18H) ppm.
$^{31}P\{^1H\}$ NMR (THF-d_8, 27 °C, 161.98 MHz, AM_2 spin system): $\delta(P_A)$ = 34.3 (t), $\delta(P_M)$ = 12.7 (d) ppm, $J(P_A,P_M)$ = 44.1 Hz.
Positive ESI-MS (MeCN, RT): m/z = 811 [{CpFe($P_3C_2{}^tBu_2$)}$_2$Ag]$^+$ (100%), 500 [CpFe($P_3C_2{}^tBu_2$)AgMeCN]$^+$ (93.5%).
Negative ESI-MS (MeCN, RT): m/z = 967 [Al{OC(CF_3)$_3$}$_4$]$^-$ (100%).

4.5. Synthesis of the complexes based on [Cp'''Fe(η^5-P_3C_2PhH)]

4.5.1. Synthesis of [{Cp'''Fe(η^5:η^1:η^1-P_3C_2PhH)}$_4$(μ-CuBr)$_4$]$_\infty$ (20)

A solution of CuBr (30 mg 0.21 mmol) in CH_3CN (8 ml) was layered onto a solution of [Cp'''Fe(η^5-P_3C_2PhH)] (50 mg, 0.10 mmol) in 8 ml CH_2Cl_2. After complete diffusion of two layers at room temperature, the mixture was concentrated under reduced pressure to about one half of the original volume (ca. 8 ml) and the concentrate was than layered with 8 ml of pentane. After one week, red plate crystals were obtained on the wall of the Schlenktube. Yield: 15 mg (38.6%)

$^{31}P\{^1H\}$ NMR (CD_2Cl_2, 27 °C, 161.98 MHz, AA´M spin system): $\delta(P_A)$ = 40.5, $\delta(P_{A'})$ = 37.8, $\delta(P_M)$ = 0.2 ppm, $J(P_A,P_M)$ = 436.4 Hz, $J(P_M,P_{A'})$ = 425.7 Hz. (reaction mixture)
ESI-MS (MeCN, RT): m/z = 1319 [{Cp'''Fe(P_3C_2PhH)}$_2$$Cu_3Br_2$]$^+$ (5.7%), 1175 [{Cp'''Fe(P_3C_2PhH)}$_2$$Cu_2Br$]$^+$ (6%), 1031 [{Cp'''Fe(P_3C_2PhH)}$_2$Cu]$^+$ (20%), 588 [{Cp'''Fe(P_3C_2PhH)}$_2$CuMeCN]$^+$ (100%).

4.5.2. Synthesis of [Cp'''Fe(μ,η^5:η^1-P_3C_2PhH)$PtCl_2PEt_3$] (21)

A solution of [Cp'''Fe(η^5-P_3C_2PhH)] (20 mg, 0.041 mmol) and [($PtCl_2PEt_3$)$_2$] (16 mg, 0.02 mmol) in 10 ml CH_2Cl_2 was stirred for one hour at room temperature. An orange-red solution was formed. After concentration under reduced pressure to about one third of the original volume, 5 ml hexane was added and brown powder was yielded. Yield: 20 mg (55.9%)

$^{31}P\{^1H\}$ NMR (CD_2Cl_2, 27 °C, 161.98 MHz): $\delta(P_a)$ = 17.4 ppm, $\delta(P_b)$ = -68.2 ppm, $\delta(P_c)$ = 77.1 ppm, $\delta(P_d)$ = 10.0 ppm, $J(P_a,P_b)$ = 420.8 Hz, $J(P_b,P_c)$ = 517.5 Hz, $J(P_c,P_d)$ = 28.0 Hz, $J(P_a,Pt)$ = 30 Hz, $J(P_b,Pt)$ = 149.0 Hz, $J(P_c,Pt)$ = 4017.5 Hz, $J(P_d,Pt)$ = 3212.9 Hz.
^{31}P NMR (CD_2Cl_2, 27 °C, 161.98 MHz): $J(P_a,H_a)$ = 6.5 Hz, $J(P_c,H_a)$ = 28.2 Hz.
ESI-MS (MeCN, RT): m/z = 750 [Cp'''Fe(P_3C_2PhH)$PtCl_2$]$^+$ (3.6%), 767 [Cp'''Fe(P_3C_2PhH)$PtPEt_2$]$^+$ (1.7%), 812 [Cp'''Fe(P_3C_2PhH)$PtCl_2PEt$]$^+$ (1.4%).

4.5.3. Synthesis of [{Cp'''Fe(μ,η^5:η^1-P_3C_2PhH)}{$W(CO)_5$}$_2$] (22)

A solution of [Cp'''Fe(η^5-P_3C_2PhH)] (20 mg, 0.041 mmol) and [$W(CO)_5$THF] (30 mg, 0.08 mmol) in 15 ml THF was stirred for one hour at room temperature. The color of the reaction solution changed from red to red orange. After removal of all solvent in vacuum, the residue was dissolved in about 2 ml dichloromethane and the solution was kept at -28 °C for one week. Orange-red crystals were obtained (10 mg, 21.5%).

$^{31}P\{^1H\}$ NMR (CD_2Cl_2, 27 °C, 161.98 MHz, AA´M spin system): $\delta(P_A)$ = 49.1 ppm, $\delta(P_M)$ = -80.9 ppm, $\delta(P_{A'})$ = 38.0 ppm
$^{31}P\{^1H\}$ NMR (THF-d_8/CH_2Cl_2 (3:1), 27 °C, 161.98 MHz, AA´M spin system): $\delta(P_A)$ = 48.5 ppm, $\delta(P_M)$ = -81.0 ppm, $\delta(P_{A'})$ = 38.1 ppm
$^{31}P\{^1H\}$ NMR (THF-d_8/CH_2Cl_2 (3:1), -40 °C, 161.98 MHz, AA´M spin system): $\delta(P_A)$ = 48.8 ppm, $\delta(P_M)$ = -85.0 ppm, $\delta(P_{A'})$ = 37.4 ppm
$^{31}P\{^1H\}$ NMR (THF-d_8/CH_2Cl_2 (3:1), -80 °C, 161.98 MHz, AA´M spin system): $\delta(P_A)$ = 48.7 ppm, $\delta(P_M)$ = -87.0 ppm, $\delta(P_{A'})$ = 37.2 ppm, $J(P_A,P_M)$ = 462.3 Hz, $J(P_M,P_{A'})$ = 466.3 Hz, $J(P_A,P_{A'})$ = 14.9 Hz, $J(P_A,^{183}W)$ = 250.6 Hz, $J(P_{A'},^{183}W)$ = 251.8 Hz.
IR(CH_2Cl_2): ν(CO) [cm^{-1}]: 2976, 1975, 1950.
EI-MS (70eV): m/z = 484 [Cp'''Fe(P_3C_2PhH)]$^+$ (100%), 667 [Cp'''Fe(P_3C_2PhH)W]$^+$ (42%), 807 [Cp'''Fe(P_3C_2PhH)$W(CO)_5$]$^+$ (66%), 1131 [{Cp'''Fe(P_3C_2PhH)}{$W(CO)_5$}$_2$]$^+$ (35%).

4.5.4. Synthesis of [{Cp'''Fe(μ,η^5:η^1-P_3C_2PhH)}{$W(CO)_5$}$_3$] (23)

A solution of [Cp'''Fe(η^5-P_3C_2PhH)] (20 mg, 0.041 mmol) and [$W(CO)_5$THF] (60 mg, 0.16 mmol) in 25 ml THF was stirred for 16 hours at room temperature. After removal of all solvents in vacuum the residue was dissolved in about 3 ml of dichloromethane and the solution was kept at -28 °C for one week. Orange-red crystals were obtained (20 mg, 33.4%).

$^{31}P\{^1H\}$ NMR (CD_2Cl_2, 27 °C, 161.98 MHz, AA´M spin system): $\delta(P_A)$ = 2.7 ppm, $\delta(P_M)$ = -54.9 ppm, $\delta(P_{A'})$ = -3.7 ppm, $J(P_A,P_M)$ = 412.4 Hz, $J(P_M,P_{A'})$ = 446.7 Hz.
IR(CH_2Cl_2): ν(CO) [cm^{-1}]: 2055, 1942, 1908.
EI-MS (70eV): m/z = 484 [Cp'''Fe(P_3C_2PhH)]$^+$ (10%), 668 [Cp'''Fe(P_3C_2PhH)W]$^+$ (54%), 807 [Cp'''Fe(P_3C_2PhH)$W(CO)_5$]$^+$ (17%), 1131 [{Cp'''Fe(P_3C_2PhH)}{$W(CO)_5$}$_2$]$^+$ (5%).

4.6 Synthesis of the complexes based on [Cp'''Fe(η^5-P_4C^tBu)]

4.6.1. Synthesis of complex [{Cp'''Fe(η^4-$P_3C^tBuP(O)^tBu$)}$_4${(μ-$Cu_2Cl)(MeCN)_2$}$_2${(μ-$CuCl)_2(MeCN)$}$_2$] (24)

A solution of CuCl (2 mg, 0.02 mmol) in a mixture of CH_2Cl_2 /CH_3CN (3 ml/3 ml) was layered onto a solution of [Cp'''Fe(η^5-P_4C^tBu)] (10 mg, 0.02 mmol) in 6 ml CH_2Cl_2. After the two layers were completely diffused, the mixture was slowly concentrated under reduced pressure to about one third of the original volume (ca. 4 ml). The concentrate was kept at room temperature for four months and a red brown crystalline complex was obtained on the wall of the Schlenktube. Yield: 12 mg (50%).

$^{31}P\{^1H\}$ NMR (CD_2Cl_2, 27 °C, 161.98 MHz): δ = 15.3 (br), 25.1 (br), 57.0 (br), 87.9 (br) ppm. (reaction solution)
^1H NMR (CD_2Cl_2, 27 °C, 400.13 MHz): δ = 5.3 (s, 2H), 1.96 (br, 36H) ppm.
ESI-MS (MeCN, RT): m/z = 659 $[Cp'''Fe(P_4O^tBu)Cu_2Cl]^+$ (2.5%), 596 $[Cp'''Fe(P_4O^tBuC)CuCl]^+$ (0.25%).

4.6.2. Synthesis of [{Cp'''Fe(η^5:η^1:η^1-P_4C^tBu)}$_2$(μ-CuCl) $_2$]$_\infty$ (25)

A solution of CuCl (7.5 mg, 0.075 mmol) in a mixture of CH_2Cl_2/CH_3CN (2 ml/3 ml) was layered onto a solution of [Cp'''Fe(η^5-P_4C^tBu)] (18 mg, 0.0375 mmol) in 5 ml CH_2Cl_2. After the two layers of solvent were completely diffused, the mixture was slowly concentrated under reduced pressure to about one third of the original volume. The concentrate was kept at room temperature for one month and a brown crystalline complex was obtained on the wall of the Schlenktube. Yield: 12 mg (55.4%).

^1H NMR (THF-d_8/CH_2Cl_2 (3:1) 27°C, 400.13 MHz): δ = 4.41 (s), 1.61 (s), 1.40 (s), 1.30 (s) ppm.
$^{31}P\{^1H\}$ NMR (THF-d_8/CH_2Cl_2 (3:1), 0 °C, 161.98 MHz, AA´MM´ spin system): δ(P_M/$P_{M'}$) = 69.7 (br), δ(P_A/$P_{A'}$) = 115.6 (br) ppm.
$^{31}P\{^1H\}$ NMR (THF-d_8/CH_2Cl_2 (3:1), 27 °C, 161.98 MHz, AA´MM´ spin system): δ(P_M/$P_{M'}$) = 73.6 (br), δ(P_A/$P_{A'}$) = 119.2 (br) ppm.

ESI-MS (MeCN, RT): m/z = 1127 [{Cp'''Fe(P_4C^tBu)}$_2Cu_2Cl$]$^+$ (11%), 1027 [{Cp'''Fe(P_4C^tBu)}$_2$Cu]$^+$ (25.5%), 586 [Cp'''Fe(P_4C^tBu)CuMeCN]$^+$ (100%).

4.6.3. Synthesis of [{Cp'''Fe(η^5-P_4C^tBu)}$_2$($P_8C_4{}^tBu_4$)$_2$(Cu_3Br_3)$_2$($MeCN$)$_2$] (26)

A solution of CuBr (3 mg, 0.021mmol) in CH_3CN (5 ml) was layered onto a solution of [CpFe(η^5-P_4C^tBu)] (10 mg, 0.021 mmol) in 5 ml CH_2Cl_2. After the 2 layers of solvent were completely diffused, the mixture was slowly evaporated and afterwards kept at 4 °C. After two months, dark green needle-like crystals were obtained on the wall of the Schlenktube. Yield: 8 mg (74.6%)
ESI-MS (MeCN, RT): m/z = 586 [($P_8C_4{}^tBu_4$)Cu]$^+$ (100%), 624 [Cp'''Fe(P_4C^tBu)CuBr]$^+$ (24%), 1171 [($P_8C_4{}^tBu_4$)$_2Cu_2$]$^+$ (22%), 1315 [{Cp'''Fe(P_4C^tBu)}$_2Cu_3Br_2$]$^+$ (6.3%).

4.6.4. Synthesis of [{Cp'''Fe(η^5:η^1:η^1-P_4C^tBu)}$_2$(μ-CuBr)$_2$]$_\infty$ (27)

A solution of CuBr (10.8 mg, 0.075 mmol) in CH_2Cl_2 /CH_3CN (2 ml/3 ml) was layered onto a solution of [CpFe(η^5-$P_4{}^tBuC$)] (18 mg, 0.0375 mmol) in 5 ml of CH_2Cl_2. After the two layers were completely diffused, the mixture was slowly concentrated under reduced pressure to about one third of the original volume. The concentrate was kept at room temperature for four weeks and brown crystals were obtained on the wall of the Schlenktube. Yield: 10 mg (30%).

^{1}H NMR (THF-d_8/CH_2Cl_2 (3:1), 27°C, 400.13 MHz): δ = 4.41 (s), 1.61 (s), 1.40 (s), 1.24 (s) ppm.
^{31}P{H} NMR (THF-d_8/CH_2Cl_2 (3:1), 27°C, 161.98 MHz, AA´MM´ spin system): δ(P_M/$P_{M'}$) = 74.2 (br), δ(P_A/$P_{A'}$) = 119.7 (br) ppm.
ESI-MS(MeCN, RT): m/z = 1315 [{Cp'''Fe(P_4C^tBu)}$_2Cu_3Br_2$]$^+$ (6.35%), 1171[{Cp'''Fe(P_4C^tBu)}$_2Cu_2Br$]$^+$ (22.0%), 624 [Cp'''Fe(P_4C^tBu)CuBr]$^+$ (23%).

4.6.5. Syntheses of [{Cp'''Fe(η^5:η^1:η^1-P_4C^tBu)}$_2$(μ-CuI)$_2$]$_\infty$ (28)

A solution of CuI (14.3 mg, 0.15 mmol) in CH_2Cl_2 /CH_3CN (2 ml/5 ml) was layered onto a solution of [Cp'''Fe(η^5-$P_4{}^tBuC$)] (18 mg, 0.0375 mmol) in 7 ml CH_2Cl_2. After three weeks, a light brown crystalline complex was obtained on the wall of the Schlenktube. Yield: 15 mg (19.8%).

^{1}H NMR (THF-d_8/CH_2Cl_2 (3:1), 27 °C, 400.13 MHz): δ = 4.41 (s, 2H), 1.61 (s, 9H of ^{t}Bu in P_4C-ring) 1.40 (s, 18H), 1.29 (s, 9H) ppm.
^{31}P{^{1}H} NMR (C_6D_6/MeCN, 27 °C, 161.98 MHz, AA´MM´ spin system): δ(P_M/$P_{M'}$) = 65.4 (br), δ(P_A/$P_{A'}$) = 113.7 (br) ppm.
^{31}P{^{1}H} NMR (THF-d_8/CH_2Cl_2 (3:1), 27 °C, 161.98 MHz, AA´MM´ spin system): δ(P_M/$P_{M'}$) = 74.3 (br), δ(P_A/$P_{A'}$) = 120.2 (br) ppm.
ESI-MS (MeCN, RT): m/z = 1155 [{Cp'''Fe($P_4{}^tBuC$)}$_2$CuI]$^+$ (1.8%), 1027 [{Cp'''Fe($P_4{}^tBuC$)}$_2$Cu]$^+$ (6.4%), 610 [Cp'''Fe($P_4{}^tBuC$)Cu_2]$^+$ (48.0%).

4.6.6. Syntheses of [Ag_2{Cp'''Fe(η^5:η^1-P_4C^tBu)}$_2${Cp'''Fe(η^5:η^1-P_4C^tBu)}$_2$] [Al{$OC(CF_3)_3$}$_4$]$_2$ (29)

A mixture of Ag[Al{$OC(CF_3)_3$}$_4$] (30 mg, 0.06 mmol) and [Cp'''Fe(η^5-P_4C^tBu)] (55 mg, 0.115 mmol) in 10 ml CH_2Cl_2 was stirred for one hour. Afterwards the black powder was filtered over diatomaceous earth and the elute was evaporated under reduced pressure to about one third of the original volume. The concentrated solution was kept at -28 °C for four weeks and red brown crystals of **29** were obtained on the wall of the Schlenktube. Yield: 10 mg (8.6%).

^{1}H NMR (THF-d_8/CH_2Cl_2 (3:1), 27 °C, 400.13 MHz): δ = 4.45 (s, 2H), 1.59 (s, 9H of ^{t}Bu in P_4C-ring) 1.38 (s, 18H), 1.29 (s, 9H) ppm.
^{31}P{^{1}H} NMR (THF-d_8/CH_2Cl_2 (3:1), 27 °C, 161.98 MHz, AA´MM´ spin system): δ(P_M/$P_{M'}$) = 54.1 (br), δ(P_A/$P_{A'}$) =111.9 (br) ppm.
^{31}P{^{1}H} NMR (THF-d_8/CH_2Cl_2 (3:1), -40 °C, 161.98 MHz, ADMN spin system): δ(P_M/P_N) = 54.6 (br), δ(P_D) = 93.3 (br), δ(P_A) = 118.9 (br) ppm.
^{31}P{^{1}H} NMR (THF-d_8/CH_2Cl_2 (3:1), -60 °C, 161.98 MHz, ADMN spin system): δ(P_M/P_N) = 50.6 (br), δ(P_D) = 91.3 (br), δ(P_A) =118.5 (br) ppm.

$^{31}P\{^{1}H\}$ NMR (THF-d_8/CH_2Cl_2 (3:1), -110 °C, 161.98 MHz, ADMN spin syste): $\delta(P_M/P_N)$ = 51.3 (br), $\delta(P_D)$ = 88.7 (br), $\delta(P_A)$ = 118.0 (br) ppm.
Positive ESI-MS (MeCN, RT): m/z = 1071 $[\{Cp'''Fe(P_4C^tBu)\}_2Ag]^+$ (22.5%), 630 $[Cp'''Fe(P_4C^tBu)AgMeCN]^+$ (55%).
Negative ESI-MS: m/z = 967 $[Al\{OC(CF_3)_3\}_4]^-$ (100%).

4.6.7. Syntheses of [CpFe(η^5:η^1-P_4C^tBu)AuCl] (30)

A mixture of [AuCl(SC_4H_8)] (18 mg, 0.058 mmol) and [CpFe(η^5-$P_4{}^tBuC$)] (28 mg, 0.058 mmol) in 15 ml CH_2Cl_2 was stirred in the dark for one hour. Afterwards the resulted black powder was filtered over diatomaceous earth and the filtrate was concentrated under reduced pressure to about one third of the original volume. The concentrated solution was kept at -28 °C for four weeks and brown plates of **30** were obtained. Yield: 5 mg (21.8 %).

^{1}H NMR (THF-d_8/CH_2Cl_2 (3:1), 27 °C, 400.13 MHz): δ = 4.42 (s, 2H), 1.60 (s, 9H of ^tBu in P_4C-ring) 1.40 (s, 18H), 1.31 (s, 9H) ppm.
$^{31}P\{^{1}H\}$ NMR (THF-d_8/CH_2Cl_2 (3:1), 27 °C, 161.97 MHz, AA'MM' spin system): $\delta(P_M/P_{M'})$ = 70.2 (br), $\delta(P_A/P_{A'})$ =108.5 (br) ppm.
$^{31}P\{^{1}H\}$ NMR (THF-d_8/CH_2Cl_2 (3:1), -60 °C, 161.97 MHz, ADMN spin system): $\delta(P_M/P_N)$ = 74.8 (br), $\delta(P_D)$ = 108.6 (br), $\delta(P_A)$ =118.9 (br) ppm.
$^{31}P\{^{1}H\}$ NMR (THF-d_8/CH_2Cl_2 (3:1), -100 °C, 161.97 MHz, ADMN spin system): $\delta(P_M/P_N)$ = 75.2 (br), $\delta(P_D)$ = 113.5 (br), $\delta(P_A)$ = 125.8 (br) ppm.
$^{31}P\{^{1}H\}$ NMR (THF-d_8/CH_2Cl_2 (3:1), -120 °C, 161.97 MHz,): $\delta(P_N)$ = 72.4 (br), $\delta(P_M)$ = 78.2 (br), $\delta(P_D)$ = 111.9 (br), $\delta(P_A)$ = 125.8 (br) ppm. $J(P_M,P_N)$ = 465.2, $J(P_D,P_N)$ = 421.0, $J(P_M,P_A)$ = 415.8, $J(P_M,P_D)$ = $J(P_A,P_N)$ = 59.5, $J(P_A,P_D)$ = 0.7 Hz. (simulated values. ADMN spin system: P_D = P1, P_N = P2, P_M = P3, P_A = P4)
ESI-MS (MeCN, RT): m/z = 1161 $[\{Cp'''Fe(P_4{}^tBuC)\}_2Au]^+$ (9.2%).

4.7. Synthesis of the complexes based on [Cp'''Fe(η^5-P_5)]

4.7.1. Synthesis of [{Cp'''Fe(η^5:η^1:η^1:η^1-P_5)}(μ-CuCl)$_2$(MeCN)]$_\infty$ (31)

A solution of CuCl (15 mg, 0.15 mmol) in acetonitrile (3 ml) was carefully layered by a solvent mixture of CH_2Cl_2 and THF (2 ml) in a ratio of 1:1, onto which a CH_2Cl_2 solution (3 ml) of [Cp'''Fe(η^5-P_5)] (34 mg, 0.075 mmol) was layered. The reaction mixture diffused at room temperature very slowly to yield air-sensitive dark brown crystals of [{Cp'''Fe(η^5:η^1:η^1:η^1-P_5)}(μ-CuCl)$_2$(MeCN)]$_\infty$ (**31**).Yield: 10 mg (24%).

^{1}H NMR (THF-d_8/MeCN, 27 °C, 400.13 MHz): δ = 4.26 (s, 2H), 1.34 (s, 18H), 1.21 (s, 9H) ppm.
^{31}P{^{1}H} NMR (THF-d_8/CH_2Cl_2 (3:1), 27 °C, 161.98 MHz): δ = 163.9 (br) ppm.
^{31}P{^{1}H} NMR (THF-d_8/CH_2Cl_2 (3:1), -20 °C, 161.98 MHz): δ = 160.4 (br) ppm.
^{31}P{^{1}H} NMR (THF-d_8/CH_2Cl_2 (3:1), -60 °C, 161.98 MHz): δ = 153.0, 8.1, 5.6 (br) ppm.
^{31}P{^{1}H} NMR (THF-d_8/CH_2Cl_2 (3:1), -80 °C, 161.98 MHz): δ = 136.1, 8.6, 5.4 (br) ppm.
ESI-MS (MeCN, RT): m/z = 951 [{Cp'''Fe(P_5)}$_2$Cu]$^+$ (1.4%), 832 [{Cp'''Fe(P_5)}{CpFe(P_5)}CuCl]$^+$ (4.5%), 544 [Cp'''Fe(P_5)CuCl]$^+$ (67%).

4.7.2. Synthesis of [{Cp'''Fe(η^5:η^1:η^1:η^1-P_5)}(μ-CuBr)$_2$(MeCN)]$_\infty$ (32)

A solution of CuBr (22 mg, 0.15 mmol) in 3 ml acetonitrile was carefully layered onto a 3 ml CH_2Cl_2 solution of [Cp'''Fe(η^5-P_5)] (34 mg, 0.075 mmol) and the reaction mixture was kept at room temperature for two weeks. Dark brown crystals were obtained. Yield: 20 mg (44.5%).

^{1}H NMR (THF-d_8/CH_2Cl_2 (3:1), 27°C, 400.13 MHz): δ = 4.18 (s, 2H), 1.34 (s, 18H), 1.22 (s, 9H) ppm.
^{31}P{^{1}H} NMR (THF-d_8/CH_2Cl_2 (3:1), 27 °C, 161.98 MHz): δ = 165.9 (br) ppm.
^{31}P{^{1}H} NMR (THF-d_8/CH_2Cl_2 (3:1), -20 °C, 161.98 MHz): δ = 164.2 (br) ppm.
^{31}P{^{1}H} NMR (THF-d_8/CH_2Cl_2 (3:1), -60 °C, 161.98 MHz): δ = 163.4 (br) ppm.
^{31}P{^{1}H} NMR (THF-d_8/CH_2Cl_2 (3:1), -100 °C, 161.98 MHz): δ = 162.6 (br) ppm.
^{31}P{^{1}H} NMR (THF-d_8/CH_2Cl_2 (3:1), -130 °C, 161.98 MHz): δ = 162.3 (br) ppm.
ESI-MS (MeCN, RT): m/z = 1095 [{Cp'''Fe(P_5)}$_2$$Cu_2$Br]$^+$ (5.2%), 951 [{Cp'''Fe(P_5)}$_2$Cu]$^+$ (19%), 548 [Cp'''Fe(P_5)CuMeCN]$^+$ (88%).

4.7.3 Synthesis of [{Cp'''Fe(η^5:η^1:η^1-P_5)}$_4$(μ-CuBr)$_3$]$_\infty$ (33)

A solution of CuBr (11 mg, 0.075 mmol) in 2 ml of acetonitrile was carefully layered by a 1 ml solvent mixture of CH_2Cl_2 and THF in a ratio of 1:1, onto which a 3 ml CH_2Cl_2 solution of [Cp'''Fe(η^5-P_5)] (34 mg, 0.075 mmol) was layered. After the reaction mixture diffused completely at room temperature, the solution was kept at 4 °C for two weeks and an air-sensitive dark brown crystalline complex was obtained. Yield: 5 mg (36.6%)

^{1}H NMR (THF-d_8/CH_2Cl_2 (3:1), 27 °C, 400.13 MHz): δ = 4.18 (s, 2H), 1.34 (s, 18H), 1.20 (s, 9H) ppm.
^{31}P{^{1}H} NMR (THF-d_8/CH_2Cl_2 (3:1), 27 °C, 161.98 MHz): δ = 166.11 (br) ppm.
^{31}P{^{1}H} NMR (THF-d_8/CH_2Cl_2 (3:1), -20 °C, 161.98 MHz): δ = 164.32 (br) ppm.
^{31}P{^{1}H} NMR (THF-d_8/CH_2Cl_2 (3:1), -60 °C, 161.98 MHz): δ = 162.17 (br) ppm.
^{31}P{^{1}H} NMR (THF-d_8/CH_2Cl_2 (3:1), -80 °C, 161.98 MHz): δ = 162.28 (br) ppm.
^{31}P{^{1}H} NMR (THF-d_8/CH_2Cl_2 (3:1), -100 °C, 161.98 MHz): δ = 162.34 (br) ppm.
^{31}P{^{1}H} NMR (THF-d_8/CH_2Cl_2 (3:1), -120 °C, 161.98 MHz): δ = 162.12 (br) ppm.
ESI-MS (MeCN, RT): m/z = 951 [{Cp'''Fe(P_5)}$_2$Cu]$^+$ (22.5%), 691 [Cp'''Fe(P_5)Cu_2BrMeCN]$^+$ (21.4%), 507 [Cp'''Fe(P_5)Cu]$^+$ (36%).

4.7.4. Synthesis of [{Cp'''Fe(η^5:η^1:η^1-P_5)}$_4$(μ-CuI)$_4$]$_\infty$ (34)

A solution of CuI (29 mg, 0.15 mmol) in a solvent mixture of acetonitrile (3 ml) and THF (1 ml) was carefully layered onto a CH_2Cl_2 (4 ml) solution of [Cp'''Fe(η^5-P_5)] (34 mg, 0.075 mmol) and the reaction mixture was kept at room temperature for two days and a dark brown crystal was obtained. Yield: 10 mg (20.6%).

^{1}H NMR (THF-d_8/MeCN, 27 °C, 400.13 MHz): δ = 4.26 (s, 2H), 1.34 (s, 18H), 1.21 (s, 9H) ppm.
^{31}P{^{1}H} NMR (THF-d_8/MeCN, 27 °C, 161.98 MHz): δ = 163.7 (br) ppm.
ESI-MS (MeCN, RT): m/z = 1141 [{Cp'''Fe(P_5)}$_2$$Cu_2$I]$^+$ (8%), 951 [{Cp'''Fe(P_5)}$_2$Cu]$^+$ (37%), 548 [Cp'''Fe(P_5)CuMeCN]$^+$ (100%).

4.7.5. Synthesis of $[Ag\{Cp'''Fe(\eta^5:\eta^2:\eta^1\text{-}P_5)\}_2]_n[Al\{OC(CF_3)_3\}_4]_n$ (35)

A mixture of $Ag[Al\{OC(CF_3)_3\}_4]$ (20 mg, 0.019 mmol) and $[Cp'''Fe(\eta^5\text{-}P_5)]$ (17 mg, 0.0375 mmol) in 3ml of CH_2Cl_2 was stirred for one hour. Afterwards the solution was layered by 3 ml of hexane and this was kept at -28°C for one week. Brown crystalline needles were obtained on the wall of the Schlenktube. Yield: 10 mg (26.6%).

^1H NMR (THF-d_8, 27 °C, 400.13 MHz): δ = 4.31 (s, 2H), 1.35 (s, 18H), 1.21 (s, 9H) ppm.
$^{31}P\{^1H\}$ NMR (THF-d_8/CH_2Cl_2 (3:1), 27 °C, 161.98 MHz): δ = 162.1 (s) ppm.
$^{31}P\{^1H\}$ NMR (THF-d_8/CH_2Cl_2 (3:1), -70 °C, 161.98 MHz): δ = 156.4 (s) ppm.
$^{31}P\{^1H\}$ NMR (THF-d_8/CH_2Cl_2 (3:1), -80 °C, 161.98 MHz): δ = 156.3 (s) ppm.
$^{31}P\{^1H\}$ NMR (THF-d_8/CH_2Cl_2 (3:1), -90 °C, 161.98 MHz): δ = 171.5 (br), 166.5 (br), 155.9 (br) ppm.
$^{31}P\{^1H\}$ NMR (THF-d_8/CH_2Cl_2 (3:1), -100 °C, 161.98 MHz): δ = 169.1 (br), 163.2 (br), 155.6 (br) ppm.
$^{31}P\{^1H\}$ NMR (THF-d_8/CH_2Cl_2 (3:1), -110 °C, 161.98 MHz): δ = 173.4 (br), 172.0 (br), 170.6 and 151.2 (br) ppm.
Positive ESI-MS (MeCN, RT): m/z = 995 $[\{Cp'''Fe(P_5)\}_2Ag]^+$(100%).
Negative ESI-MS (MeCN, RT): m/z = 967 $[Al\{OC(CF_3)_3\}_4]^-$ (100%).

4.7.6. Reaction of $[Cp'''Fe(\eta^5\text{-}P_5)]$ with $AgSO_3CF_3$

A mixture of $AgSO_3CF_3$ (10 mg, 0.0375 mmol) and $[Cp'''Fe(\eta^5\text{-}P_5)]$ (34 mg, 0.075 mmol) in 10 ml of CH_2Cl_2 was stirred in the dark for one hour. Afterwards the resulted green powder was filtered over diatomaceous earth and the greenish brown filtrate was concentrated under reduced pressure to about one half of the original volume. The concentrated solution was used for the NMR and mass spectroscopic measurements.

^1H NMR (THF-d_8/CH_2Cl_2 (3:1), 27 °C, 400.13 MHz): δ = 4.16 (s, 2H), 1.26 (s, 18H), 1.14 (s, 9H) ppm.
$^{31}P\{^1H\}$ NMR (THF-d_8/CH_2Cl_2 (3:1), 27 °C, 161.98 MHz): δ = 166.1 ppm.
Positive ESI-MS (MeCN, RT): m/z = 995 $[\{Cp'''Fe(P_5)\}_2Ag]^+$(100%).
Negative ESI-MS (MeCN, RT): m/z = 148 $[CF_3SO_3]^-$ (100%).

5. Conclusions

In the preceding work, chemical properties and coordination behaviors of different P_n-ligand complexes (see below) were studied and following aspects are engaged: i) the lone pairs of electrons on the phosphorus atoms in the P_n-ligands give a ligation propensity to transition metal centers, which lead to oligomers or polymers; ii) The ligation mode of $P_{5-n}C_n$-ring (n = 0-2) ligands toward the transition metal centers can be side-on or end-on; iii) The $P_{5-n}C_n$-ring (n = 0-2) of polyphosphaferrocenes during their reactions with transition metal salts can remain intact or fragmentise; iv) Replacement of CR fragments by phosphorus atoms in the $P_{5-n}C_n$-ring (n = 0-2) and different substituent groups on the cyclopentadiene ring additionally coordinated to the iron atom can influence the results of the coordination; and v) different copper halide clusters can be formed in these coordination reactions.

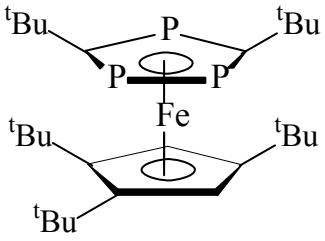

4

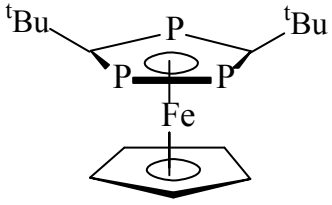

7

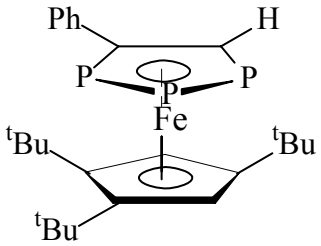

8

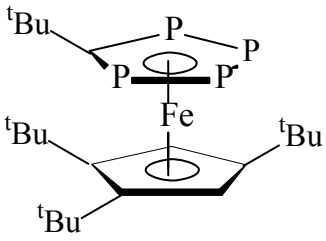

3

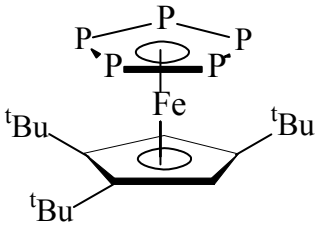

5

5.1 Triphosphaferrocene [Cp'''Fe(η^5-$P_3C_2{}^tBu_2$)] (4) as a ligand

Reactions of the triphosphaferrocene [Cp'''Fe(η^5-$P_3C_2{}^tBu_2$)] (**4**) with CuX (X = Cl, Br) in a ratio of 1:1 lead to the formation of dimeric copper complexes (reaction **a** in Scheme 5.1). In

these reactions, the two adjacent phosphorus atoms in the cyclo-P_3C_2 ring ligate the copper centers and the P–P bond lengths are shortened in comparison to that in the uncoordinated ligand because of the coordination of these two phosphorus atoms to the copper centers through the phosphorus lone pairs.

When the reaction condition of the triphosphaferrocene with CuBr in a ratio of 1:1 changes, another dimeric copper complex was obtained (reaction **b** in Scheme 5.1). In this reaction, the P_3C_2-ring is fragmentized and a new four-membered P_2C_2-ring of a 1,2-diphosphete is formed. The ESR study shows that the complex is paramagnetic and there are 17 electrons in each Fe valence orbital. These unpaired electrons of two iron atoms are probably delocalized over the whole area consisting of two P_2C_2-rings and the six-membered P_4Cu_2 ring.

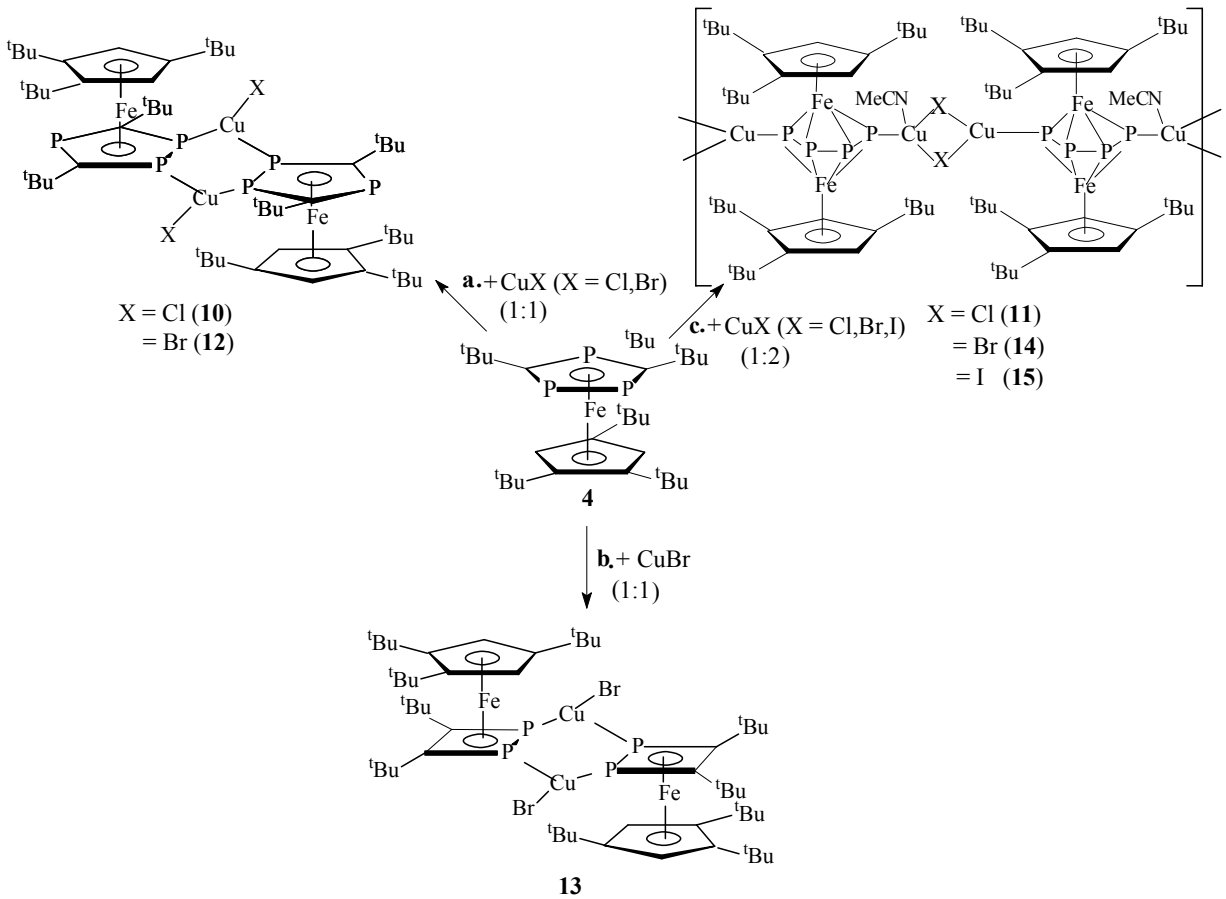

Scheme 5.1. Products based on [Cp'''Fe(η^5-$P_3C_2{}^tBu_2$)] (**4**).

In the reaction of **4** with two equivalents of CuX (X = Cl, Br and I), the P_3C_2-ring is also fragmented and rearranged to form a novel tetraphosphabutadiene ligand in a triple-decker

unit of [{(Cp'''Fe)$_2$(η^4-P$_4$)}] (reaction **c** in Scheme 5.1). The two phosphorus atoms at the end of the tetraphosphabutadiene ligand in the [{(Cp'''Fe)$_2$(η^4-P$_4$)}] unit can coordinate to the metal center to form the 1D polymers **11**, **14** and **15**. The ESI-MS spectra of the complexes **11**, **14** and **15** suggest that the triple-decker units are quite stable.

In all these reactions of the triphosphaferrocene complex **4** with transition metal salts, only the two adjacent phosphorus atoms in the cyclo-P$_3$C$_2$ ring coordinate to the metal centers. The ^{31}P NMR spectra of the reaction mixture of [Cp'''Fe(η^5-P$_3$C$_2$^{t}Bu$_2$)] and CuX (X = Cl, Br and I) in a ratio of 1:2 show that unaltered [Cp'''Fe(η^5-P$_3$C$_2$^{t}Bu$_2$)] interacts by the two adjacent phosphorus atoms with CuX units. The reason for the "inactive" third phosphorus atom may be the steric hindrance of the two bulky *tert*-butyl groups on the P$_3$C$_2$-ring. Furthermore, the unusual fragmentation reaction of the P$_3$C$_2$-ring of **4** in reaction **c** with an excess of CuX (X = Cl, Br and I) to form novel polymers containing the tetraphosphabutadiene ligand is probably a result of the steric strain imposed by the ^{t}Bu groups of the Cp'''- and the P$_3$C$_2$-rings.

5.2. The Triphosphaferrocene [CpFe(η^5-P$_3$C$_2$^{t}Bu$_2$)] (7) as a Ligand

The reaction of [CpFe(η^5-P$_3$C$_2$^{t}Bu$_2$)] (**7**) with CuCl in a stoichiometric ratio of 1:1 leads to a dimeric copper complex **16**, in which two [CpFe(η^5-P$_3$C$_2$^{t}Bu$_2$)] moieties bridge the copper centers through their two adjacent phosphorus atoms in the P$_3$C$_2$-rings (reaction **a** in Scheme 5.2). With two equivalents of CuCl, the same product (**16**) was yielded. In contrast to the Cp''' derivate **10**, the coordination environment of the copper atoms in **16** is tetrahedral due to the coordination of an additional MeCN ligand. Obviously, due to the bulky Cp''' substituent in **10** the copper atom can only adopt a trigonal planar coordination mode.

A dimeric complex similar to **16** was also obtained by treating [CpFe(η^5-P$_3$C$_2$^{t}Bu$_2$)] with Ag[Al{OC(CF$_3$)$_3$}$_4$] (reaction **b** in Scheme 5.2). In this dimeric silver complex **19**, the two silver atoms are triply coordinated to two phosphorus atoms of two different P$_3$C$_2$ rings and one nitrogen atom of an acetonitrile molecule.

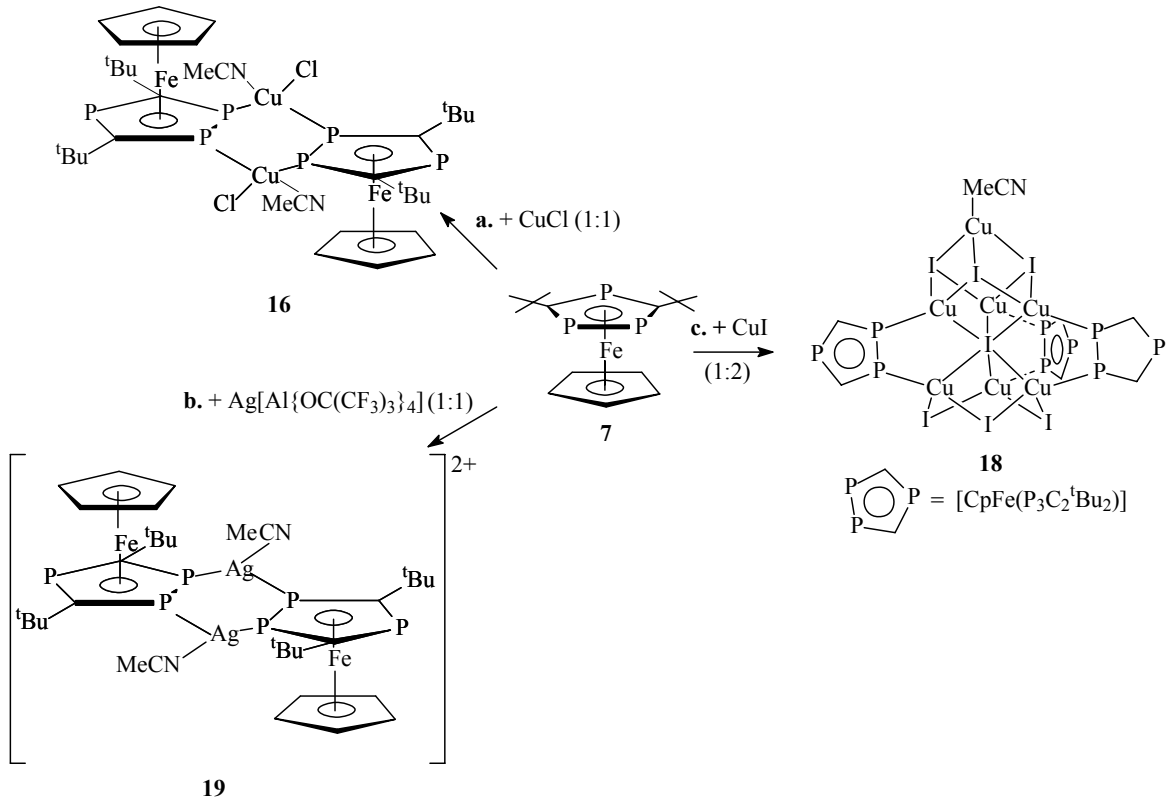

Scheme 5.2. Products based on [CpFe(η^5-$P_3C_2{}^tBu_2$)] (**7**).

The reaction of [CpFe(η^5-$P_3C_2{}^tBu_2$)] with CuI in a 1:2 ratio leads to an oligomeric complex (**18**) (reaction **c** in Scheme 5.2). In **18** the $(CuI)_7$ unit, which consists of a distorted $(CuI)_4$ cubic and a chair-like six-membered $(CuI)_3$ ring, is surrounded by three [CpFe(η^5-$P_3C_2{}^tBu_2$)] moieties.

In all three cases (**16**, **18** and **19**), two adjacent phosphorus atoms in the P_3C_2-ring coordinate to the metal centers simultaneously and the P–P bond lengths in **18** and **19** are shortened in comparison to that in the starting material **7** as a result of the coordination of the lone pairs of the phosphorus atoms to the metal centers. In contrast, the P–P bond length in **16** remains unchanged in comparison to the uncoordinated [CpFe(η^5-$P_3C_2{}^tBu_2$)] (**7**) complex.

5.3. The Triphosphaferrocene [Cp'''Fe(η^5-P_3C_2PhH)] (8) as a Ligand

The reaction of [Cp'''Fe(η^5-P_3C_2PhH)] (**8**) with CuBr leads to complex **20**. This complex is made up of a polymer chain, in which $(CuBr)_4$ units were doubly bridged by two [Cp'''Fe(η^5-P_3C_2PhH)] moieties, which coordinates in a 1,3-coordination mode of the P_3C_2-ring (reaction **a** in Scheme 5.3). Unlike the cubic shaped $(CuI)_4$ unit in complex **18**, the $(CuBr)_4$ unit in **20**

consists of three annelated four-membered $(CuBr)_2$ ring. As a polymer, the solubility of **20** is low. The NMR and mass spectra suggest that **20** dissolves under depolymerization to oligomeric species.

The reaction of **8** and $[\{PtCl_2(PR_3)\}_2]$ in a stoichiometric ratio of 2:1 leads to a adduct product (**21**) (reaction **b** in Scheme 5.3). The ^{31}P NMR spectrum shows that the P_c atom in the P_3C_2-ring coordinates the platinum atom. Complex **21** represents a sterically demanding cis-platinum complex and is nonfluxional in solution. When one or more equivalents of $[\{PtCl_2(PR_3)\}_2]$ react with compound **8**, no further adduct products were obtained except for the decomposition of the starting material **8**. Since **21** could not be crystallographically characterised, no precise information on the topology of the Pt center coordinated to the P_3C_2-ring of **8** is available. Thus, it remains uncertain why only one Pt centre can coordinate. However, assuming a nearly coplanar arrangement of the square planar Pt complex and the P_3C_2-ring, steric crowding might be responsible for hindering further substitution.

In contrast reactions of **8** with tungstenpentacarbonyl units reveal multiple coordination behaviour of the P_3C_2-ring of **8**. When **8** is treated with one or two equivalents of tungsten pentacarbonyl, complex **22** was yielded (reaction **c** in Scheme 5.3). In the **22**, the two adjacent P_M and $P_{A'}$ atoms coordinate to the tungsten centers in the solid state. The bond length of P_M–$P_{A'}$ is longer than that of P_M–P_A and reveals the steric interaction of both $W(CO)_5$ units. Unlike the platinum complex **21**, the tungsten derivative **22** shows dynamic behavior in solution according to the variable temperature ^{31}P NMR spectra. Interestingly, the spectra at low temperatures reveal that the P_A and $P_{A'}$ atoms coordinate to the tungsten centers, which is in contrast to the solid state structure.

When three equivalents of tungstenpentacarbonyl reacted with $[Cp'''Fe(\eta^5\text{-}P_3C_2PhH)]$, complex **23** was obtained (reaction **d** in Scheme 5.3). In this complex, all three phosphorus atoms in the phospholyl-ring coordinate to three tungsten centers. Due to the coordination of all phosphorus atoms to the tungsten pentacarbonyl moieties the P-P bonds are lengthend. In comparison to the Pt(II) complex, tungsten seems to coordinate more readily to P_n-ligands.

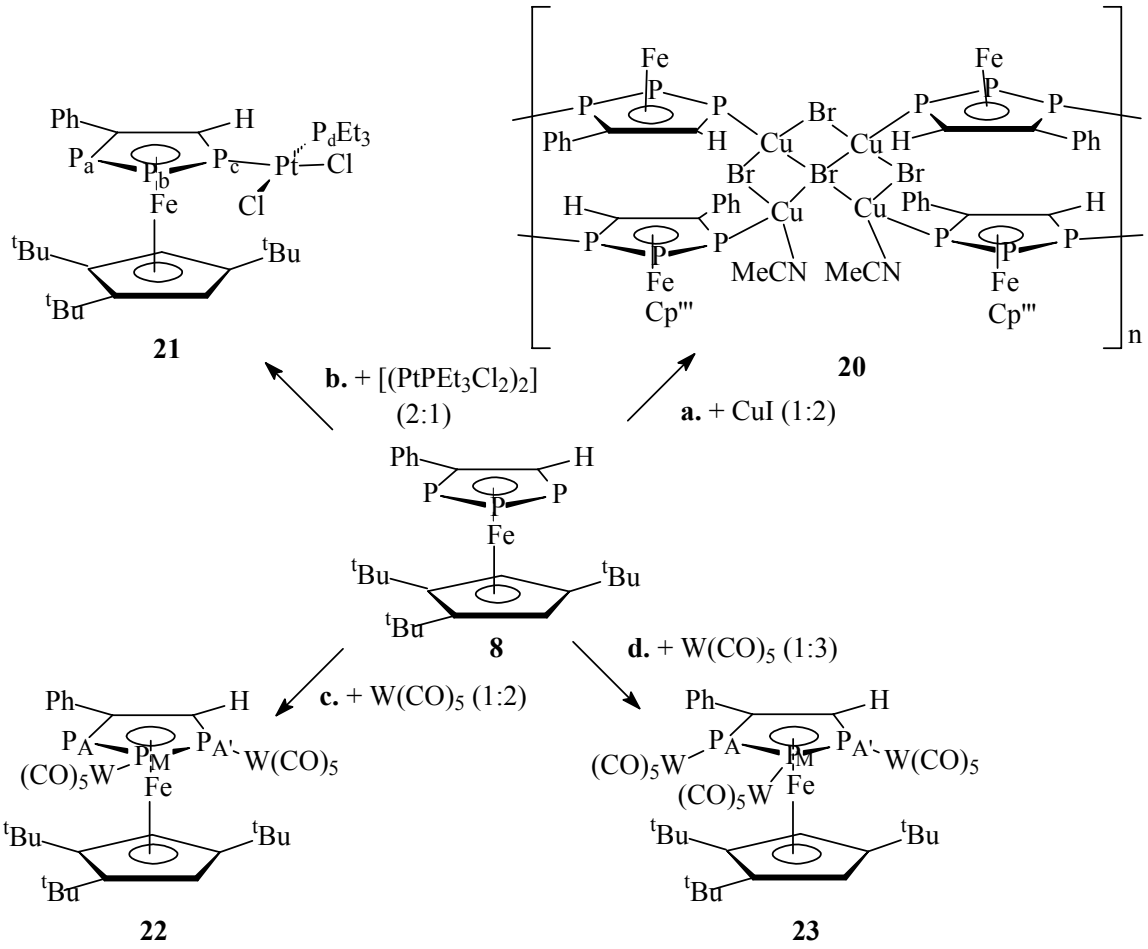

Scheme 5.3. Products based on [Cp'''Fe(η^5-P_3C_2PhH)].

In comparison to the 1,2,4-triphosphaferrocenes, in which only the two adjacent phosphorus atoms in the P_3C_2-ring can coordinate to metal centers, all three phosphorus atoms in [Cp'''Fe(η^5-P_3C_2PhH)] can ligate to metal centers and the coordination modes are more various (1-, 1,2-, 1,3- and 1,2,3-coordination mode).

5.4.Tetraphosphaferrocene [Cp'''Fe(η^5-P_4C^tBu)] (3) as a ligand

The reaction of [Cp'''Fe(η^5-P_4C^tBu)] (**3**) with CuCl in a ratio of 1:1 leads to the formation of complex **24**, which contains four [Cp'''Fe(η^5-P_4C^tBu)] moieties. In this complex, three phosphorus atoms in the P_4C-ring ligate to copper atoms (reaction **a** in scheme 5.4). The reaction of **3** with CuBr in the ratio of 1:1 can also lead to oligomer **26**. In complex **26**, the

P_4C-ring was fragmented and rearranged into a P_8C_4 unit, which consists of a cunean-like structure of a P_6C_2 moiety which is connected by a four-membered P_2C_2-ring.

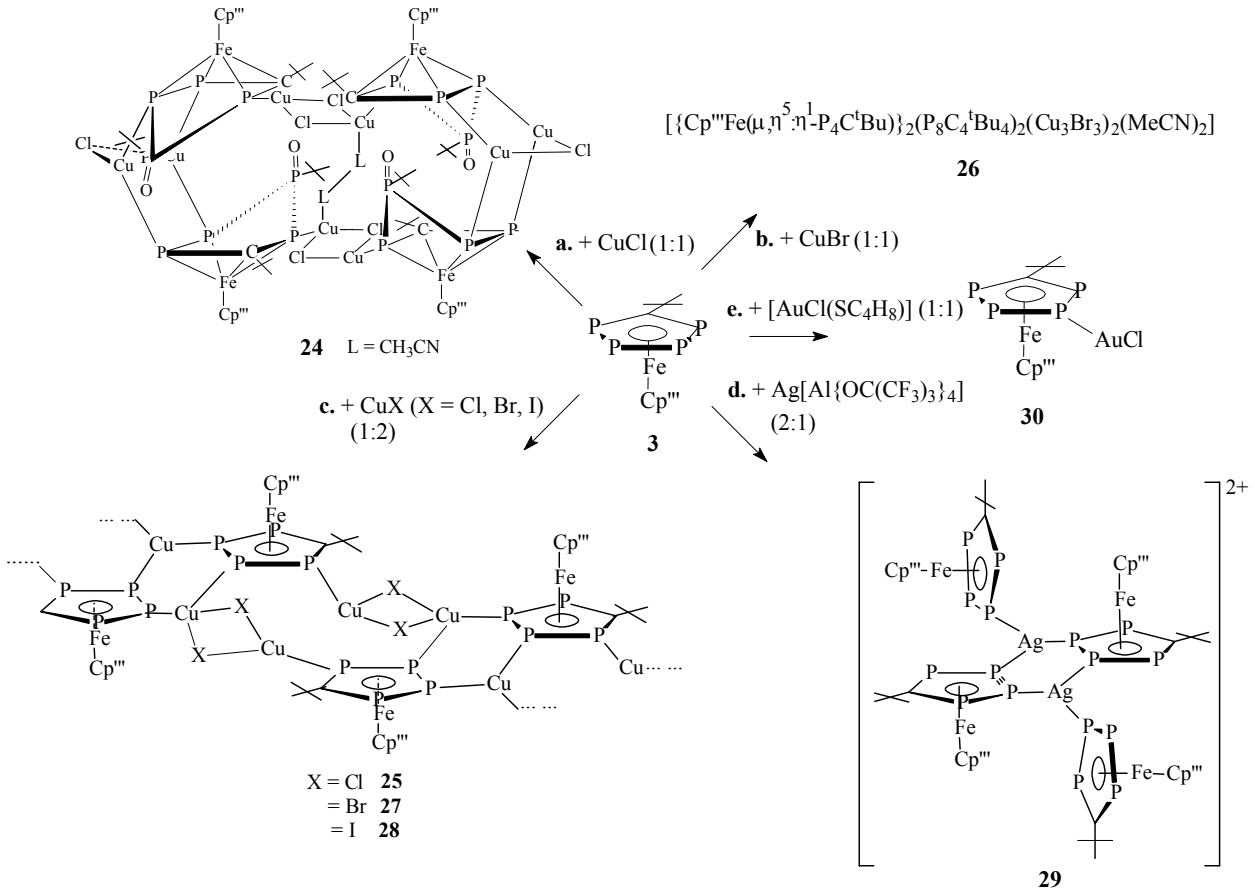

Scheme 5.4. Products based on [Cp'''Fe(η^5-P_4C^tBu)] (**3**).

The reactions of compound **3** and CuX (X = Cl, Br and I) in a stoichiometric ratio of 1:2 result in the formation of the polymers **25**, **27** and **28** (reaction **c** in scheme 5.4). In these polymers, two adjacent phosphorus atoms in the P_4C-ring of [Cp'''Fe(η^5-P_4C^tBu)] coordinate to two copper centers to form a six-membered ring. The [Cp'''Fe(η^5-P_4C^tBu)] moieties are linked by coordination to $(CuX)_2$ moieties via the third neighboring phosphorus atoms, thus forming a double chain structure. The coordination geometry of one copper atom in the $(CuX)_2$ unit is tetrahedral while that of the other copper atom ranges from trigonal (**25**) to tetrahedral (**28**) depending on the size of the halide.

The reaction of **3** with $Ag[Al\{OC(CF_3)_3\}_4]$ leads to the formation of a dicationic complex, which contains four [Cp'''Fe(η^5-P_4C^tBu)] moieties (reaction **d** in scheme 5.4). In comparison with the dimeric silver complex **19**, each silver atom of **29** coordinates to three phosphorus

atoms from three different phosphaferrocenes. Since the lone pair of electrons of the two adjacent phosphorus atoms in the two P_4C-rings donate to the silver atoms, the P–P bond lengths are shortened in comparison to that in the uncoordinated ligand **3**. This is similar to the case of the two adjacent phosphorus atoms in the P_3C_2-ring of 1,2,4-triphosphaferrocene ligating to two copper atoms. Complex **29** dissolves in CH_2Cl_2 and THF. In the solution of **29**, the $[Ag_2\{Cp'''Fe(\eta^5:\eta^1:\eta^1\text{-}P_4C^tBu)\}_2\{Cp'''Fe(\eta^5:\eta^1\text{-}P_4C^tBu)\}_2]^{2+}$ dication is depolymerised to the $[Ag\{Cp'''Fe(\eta^5:\eta^1:\eta^1\text{-}P_4C^tBu)\}_2]^+$ monocation. This monocation fragment was also found in the mass spectrum. The variable temperature $^{31}P\{^1H\}$ NMR spectra of solutions of **29** reveal dynamic behavior of the monocation. At room temperature fast exchange between **29a** and **29b** results in an AA´MM´ spin system. At low temperature, this motion is slowed down and the NMR spectra are typical of an ADMN spin system representing the four chemically and magnetically inequivalent phosphorus atoms in the P_4C-rings (Figure 3.2.34 and 3.2.35).
Compound $[Cp'''Fe(\eta^5\text{-}P_4C^tBu)]$ reacts with $[AuCl(SC_4H_8)]$ leading to an adduct product (**30**), in which one phosphorus atom on the P_4C-ring coordinates to the gold atom (reaction **e** in scheme 5.4). Dynamic behavior of **30** was also observed in solution. At room temperature, the ^{31}P NMR spectrum shows an AA´MM´ spin system. At low temperature, the ^{31}P NMR spectrum shows an ADMN spin system, which represents four chemically inequivalent phosphorus atoms and reveals a windscreen wiper behaviour of the AuCl moiety.
In comparison with the triphosphaferrocenes **4** and **7**, the introduction of a fourth phosphorus atom in **3** leads to additional coordination modes (1-, 2,3-, 1,2,3- and 1,2,4-) of the P_4C-ring.

5.5. Pentaphosphaferrocene $[Cp'''Fe(\eta^5\text{-}P_5)]$ (5) as a ligand

If all positions of the five-membered phospholyl ring are occupied by phosphorus atoms, coordination to metal centers involving even the entire P_5 ring can be expected. Indeed, 2D polymers **31** and **32** were obtained by treating $[Cp'''Fe(\eta^5\text{-}P_5)]$ with CuX (X = Cl, Br) in a stoichiometric ratio of 1:2 (reaction **a** in Scheme 5.5). In these complexes, three phosphorus atoms in the P_5-ring coordinate to three copper centers in a 1,2,4-coordination mode to form 2D polymers.
The reaction of $[Cp'''Fe(\eta^5\text{-}P_5)]$ with CuBr in a stoichiometric ratio of 1:1 leads to $[\{Cp'''Fe(\mu,\eta^5:\eta^1:\eta^1\text{-}P_5)\}_4(CuBr)_3]_\infty$ (**33**) (reaction **b** in Scheme 5.5). In complex **33**, a $(CuBr)_3$

unit connects four [Cp'''Fe(η^5-P_5)] moieties in a 1,3-coordination mode of the cyclo-P_5 ring to form a 2D polymer.

As the size of the halide increases, the number of the atoms in CuX cluster grows too. When [Cp'''Fe(η^5-P_5)] is treated with CuI in a 1:2 stoichiometric ratio, two $(CuI)_4$ units connect eight [Cp'''Fe(η^5-P_5)] moieties in a 1,3-coordination mode of the cyclo-P_5 ring to form an even a double-layer 2D polymer complex (**34**) (reaction c in scheme 5.5).

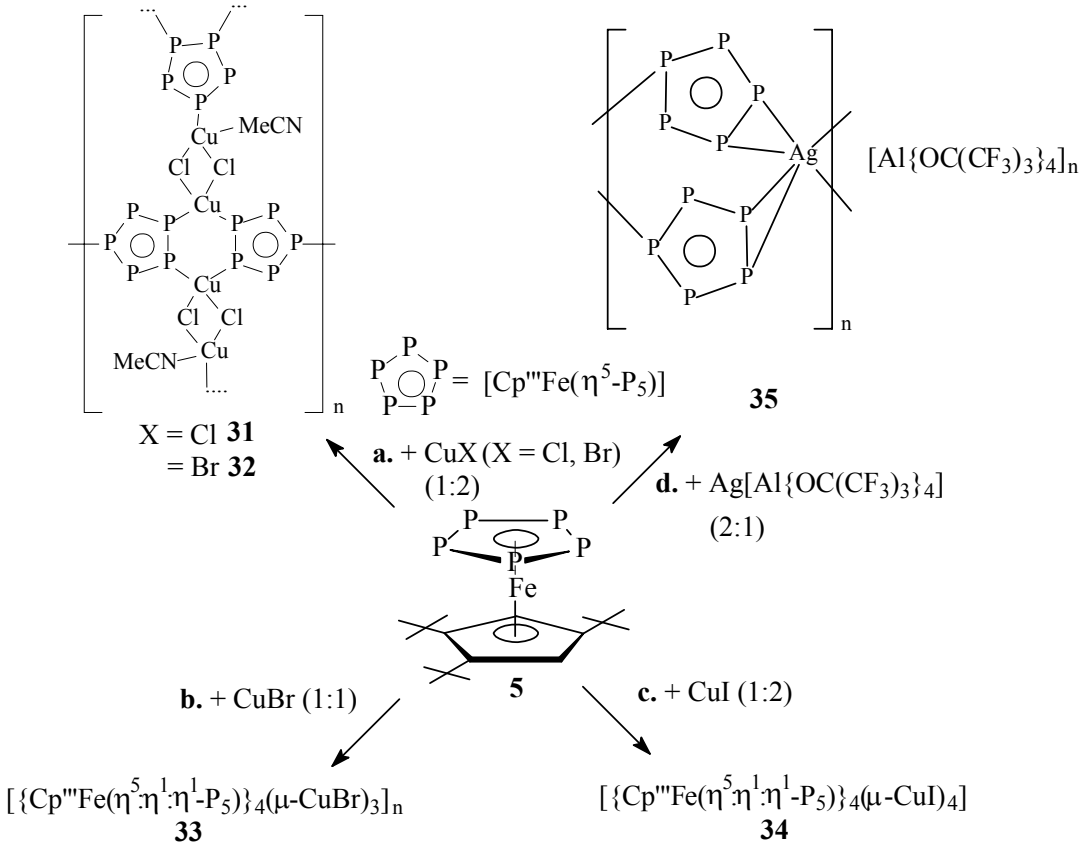

Scheme 5.5. Products based on [Cp'''Fe(η^5-P_5)] (**5**).

The polymers **31-34** dissolve in CH_2Cl_2 under depolymerisation. This is confirmed by the $^{31}P\{^1H\}$ NMR of these complexes.

The reaction of [Cp'''Fe(η^5-P_5)] with Ag[Al{$OC(CF_3)_3$}$_4$] leads to the polymer **35** (reaction **d** in Scheme 5.5). In the cationic chain of **35**, silver atoms are doubly bridged by [Cp'''Fe(η^5-P_5)] moieties and each silver coordinates six phosphorus atoms with two end-on and two side-on modes. In comparison to the Cp*-substituted derivate [Ag{Cp*Fe(η^5:η^2:η^1-P_5)}$_2$]$_n$[Al{$OC(CF_3)_3$}$_4$]$_n$ synthesised in our group, in which a 1,2,3-coordination mode of the cyclo-P_5 ring was observed, the 1,2,4-coordination mode in **35** demonstrates the steric

influence of the bulky Cp''' group in **35**. The $^{31}P\{^{1}H\}$ NMR spectra suggest that complex **35** dissolves in CH_2Cl_2/THF under depolymerization. This suggestion is confirmed by the ESI-MS mass spectrum, since the fragment of a $[\{Cp'''Fe(\eta^5\text{-}P_5)\}_2Ag]^+$ monocation with 100% relative abundance was detected. The ^{31}P NMR spectra at different temperatures also reveal dynamic behavior of **35** in solution.

6. Notes and References

[1] E. Urnezius, W.W. Brennessel, C. J. Cramer, J. E. Ellis, P. v. R. Schleyer, *Science* **2002**, 295, 832 – 834.

[2] J. Frunzke, M. Lein,G. Frenking, *Organometallics* **2002**, 21, 3351 – 3359.

[3] F. Mathey in *Phosphorus-Carbon Heterocyclic Chemistry*: The Rise of a New Domain (Ed.: F. Mathey), Pergamon, Oxford, **2001**, pp. 767; *Homogeneous Catalysis with Organometallic Compounds*, Vol. 1 and 2 (Eds.: B. Cornils, W. A. Herrmann), VCH, Weinheim, **1996**;

[4] K. B. Dillon, F. Mathey, J. F. Nixon in Phosphorus: *The Carbon Copy*, Wiley, New York, **1998**;

[5] F.Mathey, *Angew. Chem*. **2003**, 115, 1616 – 1643; *Angew. Chem*. *Int. Ed*. **2003**, 42, 1578 – 1604.

[6] F. Mathey, *Tetrahedron Lett*. **1976**, 4155 – 4158.

[7] O. J. Scherer, T. Brück, *Angew. Chem*. **1987**, 99, 59; *Angew. Chem*. *Int. Ed. Engl*. **1987**, 26, 59.

[8] F. Mathey, *Coord. Chem. Rev*. **1994**, 137, 1 – 52.

[9] N. Maigrot, N. Avarvari, C. Charrier, F. Mathey, *Angew. Chem*. **1995**, 107, 623 – 625; *Angew. Chem*. *Int. Ed. Engl*. **1995**, 34, 590 – 592.

[10] C. Müller, R. Bartsch, A. Fischer, P. G. Jones, R. Schmutzler, *J. Organomet. Chem*. **1996**, 512, 141 – 148;

[11] R. Bartsch, P. B. Hitchcock, J. F. Nixon, *J. Organomet. Chem*. **1988**, 340, C37 – C39;

[12] R. Bartsch, P. B. Hichcock, J. F. Nixon, *J. Chem. Soc.Chem. Commun*. **1987**, 1146 – 1148;

[13] C. Müller, R. Bartsch, A. Fischer, P. G. Jones, *J. Organomet. Chem.* **1993**, 453, C16 – C18.

[14] O. J. Scherer, T. Hilt, G. Wolmershäuser, *Angew. Chem*. **2000**, 112, 1484 – 1485; *Angew. Chem. Int. Ed*. **2000**, 39, 1425 – 1427.

[15] P. Lemoine, M. Gross, P. Braunstein, F. Mathey, B. Deschamps, J. H. Nelson, *Organometallics* **1984**, 3, 1303 – 1307.

[16] R. Bartsch, S. Datsenko, N. V. Ignatiev, C. Müller, J. F. Nixon and C. J. Pickett, *J. Organomet. Chem*. **1997**, 529, 375 – 378.

[17] C. Muller, R. Bartsch, A. Fischer, P.G. Jones, *Polyhedron* **1993**, 11, 1383 – 1390.

[18] J. F. Nixon, *Coord. Chem. Rev*. **1995**, 145, 201 – 258.

[19] M. Detzel, G. Friedrich, O.J. Scherer, G. Wolmershauser, *Angew.Chem. Int. Ed. Engl.* **1995**, 34, 1321 – 1323.

[20] C. S. J. Callaghan*, D. Phil. Thesis,* University of Sussex, **1997**.

[21] O. J. Scherer, H. Sitzmann, G. Wolmershäuser, *J. Organomet. Chem.* **1984**, *268*, C9 – C12.

[22] C. A. Ghilardi, S. Midollini, A. Orlandini, L. Sacconi, *Inorg. Chem.* **1980**, *19*, 301 – 306.

[23] C. Bianchini, C. Mealli, A. Meli, L. Sacconi, *Inorg. Chem. Acta* **1979**, *37*, L543 – L544.

[24] J. Bai, E. Leiner, M. Scheer, *Angew. Chem.* **2002**, 114, 820 – 823.

[25] O. J. Scherer, T. Brück, G. Wolmershäuser, *Chem. Ber*. **1989**, 122, 2049 – 2054.

[26] B. Rink, O. J. Scherer, G. Wolmershäuser, *Chem. Ber*. **1995**, 128, 71–74.

[27] O. J. Scherer, *Acc. Chem. Res*. **1999**, 32, 751 – 762.

[28] O. J. Scherer, T. Mohr, G. Wolmershäuser, *J. Organomet. Chem*. **1997**, 529, 379 – 385.

[29] C. Hoffmann, O. J. Scherer, G.Wolmershäuser, *J. Organomet. Chem*. **1998**, 559, 219 – 222.

[30] B. Koch, O. J. Scherer, G.Wolmershäuser, *Z. Anorg. Allg. Chem*. **2000**, 626, 1797 – 1802.

[31] M. Detzel , T. Mohr, O. J. Scherer, G. Wolmershäuser, *Angew. Chem*. **1994**, 106, 1142 – 1144; *Angew. Chem. Int. Ed. Engl*. **1994**, 33,1110 – 1112.

[32] G. Friedrich, *D.Phil.Thesis*, Universität Kaiserslautern, **1995**; M. Detzel, *D. Phil. Thesis*, Universität Kaiserslautern, **1995**.

[33] O. J. Scherer, S. Weigel, G. Wolmershäuser, *Chem. Eur. J*. **1998**, 4, 1910 – 1916.

[34] J. Bai, A. V. Virovets, M. Scheer, *Angew. Chem.* **2002**, *114*, 1808 – 1811; *Angew. Chem. Int. Ed.*, **2002**, *41*, 1737 – 1740.

[35] J. Bai, A. V. Virovets, M. Scheer, *Science* **2003**, *300*, 781 – 783.

[36] Sizes reported refer to interatomic distances without regard to van-der-Waals radii.

[37] A. Hirsch, B. Nuber, *Acc. Chem. Res.* **1999**, *32*, 795 – 804.

[38] C. Möschel, M. Jansen, *Z. Anorg. Allg. Chem.* **1999**, *625*, 175 – 177.

[39] O. J. Scherer, T. Hilt, G. Wolmershäuser, *Organometallics* **1998**, *17*, 4110 – 4112.

[40] S. Deng, *Diplom thesis*, Karlsruhe **2002**.

[41] M. Scheer, K. Schuster, U. Becker, *Phosphorus Sulfur and Silicon* **1996**, 109–110, 114 – 141.

[42] M. Scheer, U. Becker, *Chem. Ber*. **1996**, *129*, 1307 – 1310.

[43] M. Scheer, U. Becker, J. Magull, *Polyhedron* **1998**, *17*, 1983 – 1989.

[44] C. Eichhorn, *PhD thesis*, Kaiserslautern, **2003**.

[45] O. J. Scherer, *Acc. Chem. Res*. **1999**, *32*, 751 – 762.

[46] K. H.Whitmire, *Adv. Organomet. Chem*. **1998**, *42*, 1 – 145.

[47] A. Barth, G. Huttner, M. Fritz, L. Zsolnai, *Angew. Chem*. **1990**, *102*, 956 – 958; *Angew. Chem. Int. Ed. Engl*. **1990**, 29, 929 – 931.

[48] The crystallographic data of **3** and **4** can be referenced in my *Diplom thesis*, **2002**.

[49] M. Scheer, K. Schuster, U. Becker, A. Krug, H. Hartung, *J. Organomet. Chem*. **1993**, *460*, 105 – 110.

[50] M. Lein, J. Frunzke, G. Frenking, *Inorg. Chem*. **2003**, *42*, 2504 –2511.

[51] R. F. W. Bader, *Chem. Rev*. **1991**, *91*, 893 – 928.

[52] F. Mathey, A. Mitschler, P. Weiss, *J. Am. Chem*. Soc. **1977**, *99*, 3537–3538.

[53] F. Mathey, *New. J. Chem*. **1987**, *11*, 585 – 589.

[54] C. S. J. Callaghan, P. B. Hitchcock, J. F. Nixon, *J. Organomet. Chem*. **1999**, *584*, 87 – 93.

[55] V. A. Milluykov, O. G. Sinyashin, P. Loennecke, E. Hey-Hawkins, *Mendeleev Commun*. **2003**, 212-213.

[56] F. W. Heinemann, S. Kummer, U. Seiss-Brandl, U. Zenneck, *Organometallics* **1999,** *18,* 2021-2029.

[57] M. T. Garland, J. F. Halet, J-Y. Saillard, *Inorg. Chem.* **2001***,40*, 3342 – 3350.

[58] Y. Moreno, E. Spodine, A. Vega, J-Y. Saillard, *Inorg. Chim. Acta* **2003**, *350*, 651 – 655.

[59] A. Vega, J-Y. Saillard, *Inorganic Chemistry*, **2004**, Vol. 43, 4012 – 4018.

[60] A. Schindler, M. Scheer, unpublished results.

[61] Holleman Wiberg, *Lehrbuch der anorganische Chemie*, page 761, 101 auflage, de Gruyter, Berlin **1995**

[62] N. Korber, J. Danniels, H. G. von Schnering, *Angew. Chem*. **1996**, *108*, 1188-1190; *Angew. Chem. Int. Ed. Engl*. **1996**, 35, 1107-1110.

[63] M. Baudler, H. Jochow, J. Germershausen, *Z. Anorg. Allg. Chem*. **1987**, *553*, 15-23;

[64] K.-F. Tebbe, *Z. Anorg. Allg. Chem*. **1989**, *572*, 115-125.

[65] http://www.webelements.com.

[66] M. Scheer, L. J. Gregorisdes, A. V. Virovets, W. Kunz, R. Neueder, I. Krossing, *Angew. Chem. Int. Ed*. **2006**, *45*, 5689-5693.

7. Appendix

7.1. Directory of abbreviations

1D, 2D, 3D	One-, two-, three-dimensional
Ar	Aryl group
^{t}Bu	*tert*-Butyl, -C(CH$_3$)$_3$
Cp	Cyclopentadienyl, η^5-C$_5$H$_5$
Cp'	*tert*-Butylcyclopentadienyl, η^5-^{t}BuC$_5$H$_4$
Cp''	1,3-Di-*tert*-butylcyclopentadienyl, η^5-1,3-^{t}Bu$_2$C$_5$H$_3$
Cp'''	1,2,4-Tri-*tert*-butylcyclopentadienyl, η^5-1,2,4-^{t}Bu$_3$C$_5$H$_2$
Cp*	Pentamethylcyclopentadienyl, η^5-C$_5$(CH$_3$)$_5$
Cp^x	Any cyclopentadienyl ligand, as specified in text
δ	Chemical shift
$\omega_{1/2}$	Half-width
DME	1,2-Dimethoxyethane, MeOCH$_2$CH$_2$OMe
DMF	Dimethylformamide, (CH$_3$)$_2$NCHO
EI-MS	Electron-ionization mass spectrometry
ESI-MS	Electrospray ionization mass spectrometry
Et	Ethyl, -CH$_2$CH$_3$
Hz	Hertz
IR	Infrared
J	Coupling constant
L	Ligand
M	Metal atom
Me	Methyl, -CH$_3$
NMR	Nuclear magnetic resonance
Ph	Phenyl, -C$_6$H$_5$
^{i}Pr	*iso*-Propyl, -CH(CH$_3$)$_2$
ppm	Parts per million
X	Halogen/halide or pseudohalide
THF	Tetrahydrofuran, C$_4$H$_8$O

br	broad
s	singlet
d	doublet
t	triplet
q	quartet
sept	septet
m	multiplet

Combinations of multiplicity symbols are also used, such as “dd” for “doublet of doublets”

7.2. Directory of compounds

1	$[\{Cp'''(CO)_2Fe\}_2(\mu,\eta^1{:}\eta^1\text{-}P_4)]$
2	$^tBuC{\equiv}P$
3	$[Cp'''Fe(\eta^5\text{-}P_4C^tBu)]$
4	$[Cp'''Fe(\eta^5\text{-}P_3C_2{}^tBu_2)]$
5	$[Cp'''Fe(\eta^5\text{-}P_5)]$
6	$[(Cp'''Fe)_2(\eta^3{:}\eta^3\text{-}P_3)]$
7	$[CpFe(\eta^5\text{-}P_3C_2{}^tBu_2)]$
8	$[Cp'''Fe(\eta^5\text{-}P_3C_2PhH)]$
9	$[Cp'''Fe(\eta^5\text{-}PC_4Ph_2H_2)]$
10	$[\{Cp'''Fe(\eta^5{:}\eta^1{:}\eta^1\text{-}P_3C_2{}^tBu_2)\}(\mu\text{-}CuCl)]_2$
11	$[\{(Cp'''Fe)_2(\eta^4{:}\eta^4\text{-}P_4)\}\{\mu\text{-}CuCl\}_2(MeCN)]_\infty$
12	$[\{Cp'''Fe(\eta^5{:}\eta^1{:}\eta^1\text{-}P_3C_2{}^tBu_2)\}(\mu\text{-}CuBr)]_2$
13	$[\{Cp'''Fe(\eta^4{:}\eta^1{:}\eta^1\text{-}P_2C_2{}^tBu_2)\}\{\mu\text{-}CuBr(MeCN)\}]_2$
14	$[\{(Cp'''Fe)_2(\eta^4{:}\eta^4\text{-}P_4)\}(\mu\text{-}CuBr)_2(MeCN)]_\infty$
15	$[\{(Cp'''Fe)_2(\eta^4{:}\eta^4\text{-}P_4)\}(\mu\text{-}CuI)_2(MeCN)]_\infty$
16	$[\{CpFe(\eta^5{:}\eta^1{:}\eta^1\text{-}P_3C_2{}^tBu_2)\}(\mu\text{-}CuCl)(MeCN)]_2$
17	$[\{CpFe(\eta^5{:}\eta^1{:}\eta^1\text{-}P_3C_2{}^tBu_2)\}(\mu\text{-}CuCl)(MeCN)]_2$
18	$[\{CpFe(\eta^5{:}\eta^1{:}\eta^1\text{-}P_3{}^tBu_2C_2)\}_3(CuI)_7MeCN]$
19	$[\{CpFe(\eta^5{:}\eta^1{:}\eta^1\text{-}P_3{}^tBu_2C_2)\}(\mu\text{-}AgMeCN)]_2[Al\{OC(CF_3)_3\}_4]_2$
20	$[\{Cp'''Fe(\eta^5{:}\eta^1{:}\eta^1\text{-}P_3C_2PhH)\}_4(\mu\text{-}CuBr)_4]_\infty$

21	$[Cp'''Fe(\mu,\eta^5:\eta^1\text{-}P_3C_2PhH)PtCl_2PEt_3]$
22	$[\{Cp'''Fe(\mu,\eta^5:\eta^1:\eta^1\text{-}P_3C_2PhH)\}\{W(CO)_5\}_2]$
23	$[\{Cp'''Fe(\mu,\eta^5:\eta^1:\eta^1\text{-}P_3C_2PhH)\}\{W(CO)_5\}_3]$
24	$[\{Cp'''Fe(\eta^4\text{-}P_3C^tBuP(O)^tBu)\}_4\{(\mu\text{-}Cu_2Cl)(MeCN)_2\}_2$ $\{(\mu\text{-}CuCl)_2(MeCN)\}_2]$
25	$[\{Cp'''Fe(\eta^5:\eta^1:\eta^1:\eta^1\text{-}P_4C^tBu)\}_2(\mu\text{-}CuCl)_2]_\infty$
26	$[\{Cp'''Fe(\eta^5\text{-}P_4C^tBu)\}_2(P_8C_4{}^tBu_4)_2(Cu_3Br_3)_2(MeCN)_2]$
27	$[\{Cp'''Fe(\eta^5:\eta^1:\eta^1:\eta^1\text{-}P_4C^tBu)\}_2(\mu\text{-}CuBr)_2]_\infty$
28	$[\{Cp'''Fe(\eta^5:\eta^1:\eta^1:\eta^1\text{-}P_4C^tBu)\}_2(\mu\text{-}CuI)_2]_\infty$
29	$[Ag_2\{Cp'''Fe(\eta^5:\eta^1:\eta^1\text{-}P_4C^tBu)\}_2\{Cp'''Fe(\eta^5:\eta^1\text{-}P_4C^tBu)\}_2]$ $[Al\{OC(CF_3)_3\}_4]_2$
30	$[CpFe(\eta^5:\eta^1\text{-}P_4C^tBu)AuCl(SC_4H_8)]$
31	$[\{Cp'''Fe(\eta^5:\eta^1:\eta^1:\eta^1\text{-}P_5)\}(\mu\text{-}CuCl)(MeCN)]_\infty$
32	$[\{Cp'''Fe(\eta^5:\eta^1:\eta^1:\eta^1\text{-}P_5)\}(\mu\text{-}CuBr)]_\infty$
33	$[\{Cp'''Fe(\eta^5:\eta^1:\eta^1\text{-}P_5)\}_4(\mu\text{-}CuBr)_3]_\infty$
34	$[\{Cp'''Fe(\eta^5:\eta^1:\eta^1\text{-}P_5)\}_4(\mu\text{-}CuI)_4]_\infty$
35	$[Ag\{Cp'''Fe(\eta^5\ \eta^2:\eta^1\text{-}P_5)\}_2]_n[Al\{OC(CF_3)_3\}_4]_n$

7.3. Crystallographic Data for the Reported Structures

7.3.1. [{Cp'''Fe(η^5:η^1-$P_3{}^tBu_2C_2$)}(μ-CuCl)]$_2$ (10)

Crystal data and structure refinement for **10**.

Empirical formula	$C_{27}H_{47}ClCuFeP_3$
Formula weight	619.40
Crystal size	0.15 × 0.08 × 0.02 mm
Crystal description	plate
Crystal colour	dark red
Crystal system	Monoclinic
Space group	$P2_1/n$
Unit cell dimensions	a = 12.531(3) Å, α = 90°
	b = 15.849(3) Å, β = 90.00(3)°
	c = 14.912(3) Å, γ = 90°
Volume	2961.6(10) Å^3
Z, Calculated density	4, 1.389 Mg/m^3
Absorption coefficient	1.475 mm^{-1}
F(000)	1304
Measurement device type	STOE-IPDS diffractometer
Measurement method	rotation
Temperature	203(2) K
Wavelength	0.71073 Å
θ range for data collection	2.57 to 27.47°
Index ranges	-15 ≤ h ≤ 11, -18 ≤ k ≤ 17, -19 ≤ l ≤ 17
Reflections collected / unique	9210 / 4667 [R(int) = 0.0706]
Reflections greater I>2\s(I)	3484
Refinement method	Full-matrix least-squares on F^2
Data / restraints / parameters	4667 / 0 / 313
Goodness-of-fit on F^2	1.045
Final R indices [I>2sigma(I)]	R_1 = 0.0507, wR_2 = 0.1211
R indices (all data)	R_1 = 0.0768, wR_2 = 0.1373
Largest diff. peak and hole	0.593 and -0.671 e Å^{-3}

7.3.2. [{(Cp'''Fe)$_2$(η^4:η^1:η^1-P$_4$)}{ μ-CuCl(MeCN)}$_2$]$_\infty$(11)

Crystal data and structure refinement for **11**· CH_2Cl_2.

Empirical formula	$C_{37}H_{63}Cl_4Cu_2Fe_2NP_4$
Formula weight	1097.24
Crystal size	0.25 × 0.10 × 0.08 mm
Crystal description	rod
Crystal colour	brown to black
Crystal system	Orthorhombic
Space group	*Pbcn*
Unit cell dimensions	a = 24.7495(17) Å, α = 90°
	b = 16.9685(11) Å, β = 90°
	c = 23.9773(15) Å, γ = 90°
Volume	10069.6(11) Å^3
Z, Calculated density	8, 1.448 Mg/m^3
Absorption coefficient	1.870 mm^{-1}
F(000)	4512
Measurement device type	STOE-IPDS diffractometer
Measurement method	rotation
Temperature	173(1) K
Wavelength	0.71073 Å
Monochromator	graphite
θ range for data collection	1.89 to 25.28°
Index ranges	-29 ≤ h ≤ 29, -20 ≤ k ≤ 20, -28 ≤ l ≤ 28
Reflections collected / unique	70439 / 9107 [R(int) = 0.0892]
Reflections greater I>2\s(I)	5233
Absorption correction	Numerical
Max. and min. transmission	0.9226 and 0.7260
Refinement method	Full-matrix least-squares on F^2
Data / restraints / parameters	9107 / 0 / 424
Goodness-of-fit on F^2	0.830
Final R indices [I>2sigma(I)]	R_1 = 0.0438, wR_2 = 0.0991
R indices (all data)	R_1 = 0.0844, wR_2 = 0.1079
Largest diff. peak and hole	0.596 and -0.262 e. Å^{-3}

7.3.3. [{Cp'''Fe(η^4:η^1:η^1-$P_2{}^tBu_2C_2$)}{μ-CuBr(MeCN)}]$_2$ (13)

Crystal Data and Details of the Structure Determination for **13**·$2CH_2Cl_2$

Empirical formula	$C_{56}H_{98}Br_2Cu_2Fe_2P_4Cl_2$,
Formula weight	1435.62
Crystal size	0.22 × 0.14 × 0.04 mm
Crystal description	plate
Crystal colour	dark brown
Crystal system	Triclinic
Space group	$P\bar{1}$
Unit cell dimensions	a = 1.072(3) Å, α= 84.271(19)°
	b = 11.461(2) Å, β = 75.60(2)°
	c = 14.659(4) Å, γ = 63.03(2)°
Volume	1605.6(8) Å^3
Z, Calculated density	1, 1.485 Mg/m^3
Absorption coefficient	8.477 mm^{-1}
F(000)	742
Measurement device type	Oxford Diffraction Gemini Ultra
Measurement method	omega-scan
Temperature	150 K
Wavelength	1.54178 Å
θ range for data collection	4.3 to 51.7°
Index ranges	-11 ≤ h ≤ 10, -10 ≤ k ≤ 11, -14 ≤ l ≤ 14
Reflections collected / unique	8218 / 3413 [R(int) = 0.099]
Reflections greater I>2\s(I)	1688
Refinement method	Full-matrix least-squares on F^2
Data / restraints / parameters	3413/168/331
Goodness-of-fit on F^2	1.032
Final R indices [I>2sigma(I)]	R_1 = 0.1010, wR_2 = 0.2594
R indices (all data)	R_1 = 0.1834, wR_2 = 0.3174
Largest diff. peak and hole	-2.27 and 1.84 e Å^{-3}

7.3.4. [{(Cp'''Fe)$_2$(η^4:η^4-P$_4$)}(μ-CuBr)$_2$(MeCN)]$_\infty$ (14)

Crystal data and structure refinement for **14**·CH_2Cl_2

Empirical formula	$C_{37}H_{63}Br_2Cu_2Fe_2NP_4Cl_2$
Formula weight	1115.26
Crystal size	0.400 × 0.020 × 0.010 mm
Crystal description	needle
Crystal colour	dark green
Crystal system	Orthorhombic
Space group	$P2_12_12_1$
Unit cell dimensions	a = 10.1451(3) Å, α = 90°
	b = 13.4635(4) Å, β = 90°
	c = 33.2088(16) Å, γ = 90°
Volume	4535.9(3) Å^3
Z, Calculated density	4, 1.633 Mg/m^3
Absorption coefficient	10.766 mm^{-1}
F(000)	2264
Measurement device type	Oxford Diffraction Gemini Ultra
Measurement method	omega-scan
Temperature	150 K
Wavelength	1.54184 Å
θ range for data collection	2.66 to 62.94°
Index ranges	-11 ≤ h ≤ 9, -15 ≤ k ≤ 15, -35 ≤ l ≤ 38
Reflections collected / unique	15442 / 6822 [R(int) = 0.0575]
Reflections greater I>2\s(I)	5218
Absorption correction	Semi-empirical from equivalents
Max. and min. transmission	1.61961 and 0.49105
Refinement method	Full-matrix least-squares on F^2
Data / restraints / parameters	6822 / 0 / 271
Goodness-of-fit on F^2	1.115
Final R indices [I>2sigma(I)]	R_1 = 0.0962, wR_2 = 0.2259
R indices (all data)	R_1 = 0.1200, wR_2 = 0.2373
Absolute structure parameter	0.493(17)
Largest diff. peak and hole	1.603 and -1.353 e.A^{-3}

7.3.5 $[\{(Cp'''Fe)_2(\eta^4:\eta^4\text{-}P_4)\}(\mu\text{-}CuI)_2(MeCN)]_\infty$ (15)

Crystal data and structure refinement for **15**

Empirical formula	$C_{37}H_{63}Cl_2Cu_2Fe_2I_2NP_4$
Formula weight	1209.24
Crystal size	0.24 × 0.17 × 0.10 mm
Crystal description	block
Crystal colour	brown
Crystal system	Orthorhombic
Space group	$P2_12_12_1$
Unit cell dimensions	a = 10.2433(6) Å, α = 90°
	b = 13.3511(8) Å, β = 90°
	c = 33.422(2) Å, γ = 90°
Volume	4570.7(5) $Å^3$
Z, Calculated density	4, 1.757 Mg/m^3
Absorption coefficient	3.175 mm^{-1}
F(000)	2408
Measurement device type	Bruker SMART Apex
Measurement method	CCD area detector
Temperature	100(2) K
Wavelength	0.71073 Å
θ range for data collection	1.64 to 28.00°
Index ranges	$-12 \le h \le 13$, $-17 \le k \le 12$, $-40 \le l \le 42$
Reflections collected / unique	20115 / 10078 [R(int) = 0.0370]
Reflections greater I>2\s(I)	7915
Absorption correction	Semi-empirical from equivalents
Max. and min. transmission	0.773 and 0.462
Refinement method	Full-matrix least-squares on F^2
Data / restraints / parameters	10078 / 17 / 515
Goodness-of-fit on F^2	0.990
Final R indices [I>2sigma(I)]	R_1 = 0.0376, wR_2 = 0.0710
R indices (all data)	R_1 = 0.0535, wR_2 = 0.0735
Absolute structure parameter	0.469(17)
Largest diff. peak and hole	1.167 and -0.916 $e.A^{-3}$

7.3.6. [{CpFe(η^5:η^1:η^1-$P_3C_2{}^tBu_2$)}(μ-CuCl)(MeCN)]$_2$ (16)

Crystal data and structure refinement for **16**.

Empirical formula	$C_{34}H_{52}Cl_2Cu_2Fe_2N_2P_6$
Formula weight	984.28
Crystal size	0.25 × 0.24 × 0.18 mm
Crystal description	plate
Crystal colour	red
Crystal system	Monoclinic
Space group	$P2_1/n$
Unit cell dimensions	a = 11.5601(11) Å, α = 90°
	b = 7.3514(6) Å, β = 97.286(15)°
	c = 24.991(4) Å, γ = 90°
Volume	2106.7(4) Å^3
Z, Calculated density	2, 1.552 Mg/m^3
Absorption coefficient	2.052 mm^{-1}
F(000)	1008
Measurement device type	Oxford Diffraction Gemini Ultra
Measurement method	omega-scan
Temperature	200(2) K
Wavelength	0.71073 Å
θ range for data collection	3.22 to 25.80°
Index ranges	-14 ≤ h ≤ 14, -8 ≤ k ≤ 8, -30 ≤ l ≤ 26
Reflections collected / unique	9475/3719 [R(int) = 0.0637]
Reflections greater I>2\s(I)	2613
Absorption correction	No Abs.
Refinement method	Full-matrix least-squares on F^2
Data / restraints / parameters	3707 / 0 / 217
Goodness-of-fit on F^2	0.999
Final R indices [I>2sigma(I)]	R_1 = 0.0656, wR_2 = 0.1653
R indices (all data)	R_1 = 0.0942, wR_2 = 0.1791
Largest diff. peak and hole	1.032 and -1.001 e.Å^{-3}

7.3.7. [{CpFe(η^5:η^1:η^1-$P_3C_2{}^tBu_2$)}$_3$(μ-CuI)$_7$(MeCN)] (18)

Crystal data and structure refinement for **18**

Empirical formula	$C_{92}H_{168}Cu_{14}Fe_6I_{14}NP_{18}$
Formula weight	4846.99
Crystal size	0.13 × 0.11 × 0.07 mm
Crystal description	block
Crystal colour	red
Crystal system	orthorhombic
Space group	*Cmcm*
Unit cell dimensions	a = 15.592(3) Å, α = 90°
	b = 26.504(3) Å, β = 90°
	c = 21.542(3) Å, γ = 90°
Volume	8902.2 (2) $Å^3$
Z, Calculated density	2, 1.808 g/cm^3
Absorption coefficient	26.348 mm^{-1}
F(000)	4602
Measurement device type	Oxford Diffraction Gemini Ultra
Measurement method	omega-scan
Temperature	105 K
Wavelength	1.5418 Å
θ range for data collection	3.29 to 65.01°
Index ranges	-18 ≤ h ≤ 17, -30 ≤ k ≤ 30, -25 ≤ l ≤ 23
Reflections collected / unique	37709/4030 [R(int) = 0.0482]
Reflections greater I>2\s(I)	3226
Absorption correction	multi-scan
Max. and min. transmission	1.668 and 0.529
Refinement method	Full-matrix least-squares on F^2
Data / restraints / parameters	4030/7/234
Goodness-of-fit on F^2	0.997
Final R indices [I>2sigma(I)]	R_1 = 0.0499, wR_2 = 0.1916
R indices (all data)	R_1 = 0.0582, wR_2 = 0.1966
Largest diff. peak and hole	3.594 and -1.565 $e.Å^{-3}$

7.3.8. [{CpFe(η^5:η^1:η^1-$P_3C_2{}^tBu_2$)}(μ-AgMeCN)]$_2$[Al{OC(CF_3)$_3$}$_4$]$_2$ (19)

Crystal data and structure refinement for **19**·2CH_2Cl_2

Empirical formula	$C_{62}H_{56}Ag_2Fe_2P_6N_2Cl_4O_8Al_2F_{72}$
Formula weight	3142
Crystal size	0.08 × 0.06 × 0.05 mm
Crystal description	prism
Crystal colour	orange
Crystal system	monoclinic
Space group	$P2_1/c$
Unit cell dimensions	a=10.7479(9) Å, α = 90°
	b=31.3800(49) Å, β=97.78(1)°
	c=15.6278(29) Å, γ = 90°
Volume	5222.23(14) Å^3
Z, Calculated density	2, 2.054 g/cm^3
Absorption coefficient	8.893 mm^{-1}
F(000)	3160
Measurement device type	Oxford Diffraction Gemini Ultra
Measurement method	omega-scan
Temperature	293 K
Wavelength	1.54184 Å
θ range for data collection	2.82 to 51.36°
Index ranges	-10 ≤ h ≤ 10, -31 ≤ k ≤ 31, -15 ≤ l ≤ 14
Reflections collected / unique	18263 / 5575 [R(int) = 0.0558]
Reflections greater I>2\s(I)	2954
Absorption correction	semi-empirical from equivalents
Max. and min. transmission	1.17191 and 0.74373
Refinement method	Full-matrix least-squares on F^2
Data / restraints / parameters	5575 / 0 / 416
Goodness-of-fit on F^2	1.308
Final R indices [I>2sigma(I)]	R_1 = 0.1456, wR_2 = 0.3788
R indices (all data)	R_1 = 0.2069, wR_2 = 0.4004
Largest diff. peak and hole	1.465 and -1.096 e.Å^{-3}

7.3.9. $[Cp'''Fe(\eta^5\text{-}P_3C_2PhH)_4(CuBr)_4]_\infty$ (20)

Crystal data and structure refinement for **20**·$2CH_3CN$.

Empirical formula	$C_{54}H_{76}Br_4Cu_4Fe_2N_2P_6$
Formula weight	1760.18
Crystal size	0.060 × 0.060 × 0.020 mm
Crystal description	plate like
Crystal colour	orange
Crystal system	Triclinic
Space group	$P\bar{1}$
Unit cell dimensions	a = 15.1002(10) Å, α = 110.545(7)°
	b = 15.5709(11) Å, β = 94.432(6)°
	c = 16.3950(12)Å, γ = 104.171(6)°
Volume	3442.8(5) $Å^3$
Z, Calculated density	2, 1.690 Mg/m^3
Absorption coefficient	10.019 mm^{-1}
F(000)	1750
Measurement device type	Oxford Diffraction Gemini Ultra
Measurement method	omega-scan
Temperature	123 K
Wavelength	1.54184 Å
θ range for data collection	3.07 to 62.95°
Index ranges	$-17 \le h \le 17$, $-17 \le k \le 17$, $-18 \le l \le 18$
Reflections collected / unique	25040 / 10799 [R(int) = 0.0395]
Reflections greater I>2\s(I)	8079
Absorption correction	Semi-empirical from equivalents
Max. and min. transmission	1.07613 and 0.89630
Refinement method	Full-matrix least-squares on F^2
Data / restraints / parameters	10799 / 0 / 734
Goodness-of-fit on F^2	1.079
Final R indices [I>2sigma(I)]	R_1 = 0.0411, wR_2 = 0.0846
R indices (all data)	R_1 = 0.0619, wR_2 = 0.0894
Largest diff. peak and hole	1.208 and -0.577 $e.A^{-3}$

7.3.10. [Cp'''Fe(η^5-P_3C_2PhH){$W(CO)_5$}$_2$] (22)

Crystal data and structure refinement for **22**.

Empirical formula	$C_{35}H_{35}FeO_{10}P_3W_2$
Formula weight	1132.07
Crystal size	0.03 × 0.06 × 0.14 mm
Crystal description	thin plate
Crystal colour	red
Crystal system	Monoclinic
Space group	C2/c
Unit cell dimensions	a = 32.8307(5) Å, α = 90°
	b = 11.56806(18) Å, β = 107.9860(17)°
	c = 21.5150(3) Å, γ = 90°
Volume	7771.8 (2) $Å^3$
Z, Calculated density	8, 1.935 Mg/m^3
Absorption coefficient	15.281 mm^{-1}
F(000)	4352
Measurement device type	Oxford Diffraction Gemini Ultra
Measurement method	Omega-scan
Temperature	123 K
Wavelength	1.54184 Å
θ range for data collection	2.8 and 51.5°
Index ranges	-33 ≤ h ≤ 27, -11 ≤ k ≤ 10, -21 ≤ l ≤ 21
Reflections collected / unique	11470 / 4150 [R(int) = 0.032]
Reflections greater I>2\s(I)	3534
Absorption correction	multi-scan
Max. and min. transmission	0.37878 and 1.0000
Refinement method	Full-matrix least-squares on F^2
Data / restraints / parameters	4150 / 0 / 466
Goodness-of-fit on F^2	1.066
Final R indices [I>2sigma(I)]	R_1 = 0.0325, wR_2 = 0.0693
R indices (all data)	R_1 = 0.0431, wR_2 = 0.0743
Largest diff. peak and hole	-0.92 and 1.02 e.A^{-3}

7.3.11. [Cp'''Fe(η^5-P_3C_2PhH){$W(CO)_5$}$_3$] (23)

Crystal data and structure refinement for **23**·CH_2Cl_2.

Empirical formula	$C_{41}H_{37}FeO_{15}P_3W_3Cl_2$
Formula weight	1540.89
Crystal size	0.200 × 0.170 × 0.130 mm
Crystal description	prism
Crystal colour	puple
Crystal system	Triclinic
Space group	$P\bar{1}$
Unit cell dimensions	a = 11.4506(6) Å, α = 78.287(4)°
	b = 12.8637(7)Å, β = 78.727(4)°
	c = 18.9303(9) Å, γ = 65.317(5)°
Volume	2461.6(2) $Å^3$
Z, Calculated density	2, 2.079 Mg/m^3
Absorption coefficient	17.411 mm^{-1}
F(000)	1460
Measurement device type	Oxford Diffraction Gemini Ultra
Measurement method	omega-scan
Temperature	123 K
Wavelength	1.54184 Å
θ range for data collection	2.40 to 62.17°
Index ranges	$-13 \le h \le 13$, $-14 \le k \le 14$, $-20 \le l \le 21$
Reflections collected / unique	23456 / 7607 [R(int) = 0.0219]
Reflections greater I>2\s(I)	7083
Absorption correction	Semi-empirical from equivalents
Max. and min. transmission	1.00000 and 0.61563
Refinement method	Full-matrix least-squares on F^2
Data / restraints / parameters	7607 / 0 / 595
Goodness-of-fit on F^2	1.034
Final R indices [I>2sigma(I)]	R_1 = 0.0343, wR_2 = 0.0848
R indices (all data)	R_1 = 0.0370, wR_2 = 0.0868
Largest diff. peak and hole	2.298 and -2.830 $e.A^{-3}$

7.3.12. [{Cp'''Fe(η^4-$P_3C^tBuP(O)^tBu$)}$_4${(μ-Cu_2Cl)(MeCN)$_2$}$_2${(μ-$CuCl)_2$ (MeCN)}$_2$] (24)

Crystal Data and Details of the Structure Determination for **24**

Empirical formula	$C_{114}Cl_6Cu_8Fe_4N_6O_4P_{16}$
Formula weight	3077.32
Crystal size	0.28 × 0.04 × 0.03 mm
Crystal description	needle
Crystal colour	dark green
Crystal system	Orthorhombic
Space group	$P2_12_12_1$
Unit cell dimensions	a = 23.016(5) Å, α = 90°
	b = 23.738(5) Å, β = 90°
	c = 15.658(3) Å, γ = 90°
Volume	8555(3) $Å^3$
Z, Calculated density	2, 1.212 Mg/m^3
Absorption coefficient	1.622 mm^{-1}
F(000)	2992
Measurement device type	Oxford Diffraction Gemini Ultra
Measurement method	omega-scan
Temperature	150 K
Wavelength	0.71073 Å
θ range for data collection	1.56 to 26.78°
Index ranges	$-29 \le h \le 24$, $-28 \le k \le 28$, $-19 \le l \le 19$
Reflections collected / unique	72242 / 16745 [R(int) = 0.0842]
Reflections greater I>2\s(I)	13085
Refinement method	Full-matrix least-squares on F^2
Data / restraints / parameters	16745 / 0 / 757
Goodness-of-fit on F^2	1.037
Final R indices [I>2sigma(I)]	R_1 = 0.0917, wR_2 = 0.2553
R indices (all data)	R_1 = 0.1111, wR_2 = 0.2767
Largest diff. peak and hole	2.540 and -1.382 $e.A^{-3}$
Flack parameter	0.43

7.3.13. [{Cp'''Fe(η^5:η^1:η^1:η^1-P_4C^tBu)}$_2$(μ-CuCl)$_2$]$_\infty$ (25)

Crystal Data and Details of the Structure Determination for **25**·CH_2Cl_2

Empirical formula	$C_{23}H_{40}Cl_4Cu_2FeP_4$
Formula weight	764.17
Crystal size	0.02 × 0.04 ×0.10
Crystal description	plate
Crystal colour	brown
Crystal system	Triclinic
Space group	$P\bar{1}$
Unit cell dimensions	a = 10.049(2) Å, α = 81.37(3)°
	b = 12.045(2)Å, β = 87.98(3)°
	c = 14.813(3) Å, γ = 87.13(3)°
Volume	1769.7 $Å^3$
Z, Calculated density	2, 1.434 Mg/m^3
Absorption coefficient	3.445 mm^{-1}
F(000)	778
Measurement device type	STOE-IPDS diffractometer
Measurement method	rotation
Temperature	203 K
Wavelength	0.71073 Å
θ range for data collection	1.7 to 22.4°
Index ranges	$-9 \le h \le 10$, $-12 \le k \le 12$, $-15 \le l \le 13$
Reflections collected / unique	7796 / 4292 [R(int) = 0.152]
Reflections greater I>2\s(I)	2057
Absorption correction	none
Data / restraints / parameters	4292 / 0 / 314
Goodness-of-fit on F^2	1.065
Final R indices [I>2sigma(I)]	R_1 = 0.1221, wR_2 = 0.3132
R indices (all data)	R_1 = 0.2180, wR_2 = 0.3775
Largest diff. peak and hole	1.23 and -1.03 $e.A^{-3}$

7.3.14. [{Cp'''Fe(η^5-P_4C^tBu)}$_2$($P_8C_4{}^tBu_4$)$_2$(Cu_3Br_3)$_2$($MeCN$)$_2$] (26)

Crystal Data and Details of the Structure Determination for **26**·4C_2H_3N

Empirical formula	$C_{96}H_{166}Br_6Cu_6Fe_2N_6P_{24}$
Formula weight	3120.04
Crystal size	0.26 × 0.04 × 0.03 mm
Crystal description	needle
Crystal colour	green
Crystal system	Monoclinic
Space group	$P2_1/c$
Unit cell dimensions	a = 16.531(3) Å, α = 90°
	b = 14.727(6) Å, β = 104.73(3)°
	c = 28.715(6) Å, γ = 120°
Volume	6761(3) Å^3
Z, Calculated density	2, 1.533 Mg/m^3
Absorption coefficient	3.231mm^{-1}
F(000)	3160
Measurement device type	STOE-IPDS diffractometer
Measurement method	rotation
Temperature	203 K
Wavelength	0.71073 Å
θ range for data collection	1.9 to 24.0°
Index ranges	-18 ≤ h ≤ 15, -16 ≤ h ≤ 16, -32 ≤ h ≤ 26
Reflections collected / unique	18900/9865 [R(int) = 0.208]
Reflections greater I>2\s(I)	3757
Refinement method	Full-matrix least-squares on F^2
Data / restraints / parameters	9865 / 0 / 643
Goodness-of-fit on F^2	0.958
Final R indices [I>2sigma(I)]	R_1 = 0.0878, wR_2 = 0.1439
R indices (all data)	R_1 = 0.2379, wR_2 = 0.1998
Largest diff. peak and hole	-0.82 and 0.74 e/Å^3

7.3.15. [{Cp'''Fe(η^5:η^1:η^1:η^1-P_4C^tBu)}$_2$(μ-CuBr)$_2$]$_\infty$ (27)

Table 1. Crystal data and structure refinement for **27**.

Empirical formula	$C_{22}H_{38}Br_2Cu_2FeP_4$
Formula weight	769.15
Crystal size	0.24 × 0.18 × 0.17 mm
Crystal description	needle
Crystal colour	yellow to brown
Crystal system	Trigonal
Space group	$R\bar{3}$
Unit cell dimensions	a = 41.272(3) Å, α = 90°
	b = 41.272(3) Å, β = 90°
	c = 10.012(7) Å, γ = 120°
Volume	14770(18) Å^3
Z, Calculated density	18, 1.556 Mg/m^3
Absorption coefficient	4.359 mm^{-1}
F(000)	6912
Measurement device type	STOE-IPDS diffractometer
Measurement method	rotation
Temperature	123(1) K
Wavelength	0.71073 Å
θ range for data collection	1.97 to 25.86°
Index ranges	-50 ≤ h ≤ 50, -50 ≤ k ≤ 50, -12 ≤ l ≤ 12
Reflections collected / unique	36362 / 6337 [R(int) = 0.0807]
Reflections greater I>2\s(I)	3616
Absorption correction	Analytical
Max. and min. transmission	0.5227 and 0.4431
Refinement method	Full-matrix least-squares on F^2
Data / restraints / parameters	6337 / 0 / 280
Goodness-of-fit on F^2	0.786
Final R indices [I>2sigma(I)]	R_1 = 0.0368, wR_2 = 0.0746
R indices (all data)	R_1 = 0.0767, wR_2 = 0.0811
Largest diff. peak and hole	0.595 and -0.523 e.Å^{-3}

7.3.16. $[\{Cp'''Fe(\eta^5:\eta^1:\eta^1:\eta^1\text{-}P_4C^tBu)\}_2(\mu\text{-}CuI)_2]_\infty$ (28)

Crystal data and structure refinement for **28**

Empirical formula	$C_{22}H_{38}Cu_2FeI_2P_4$
Formula weight	863.15
Crystal size	0.536 × 0.016 × 0.014 mm
Crystal description	needle
Crystal colour	light yellow
Crystal system	Trigonal
Space group	$R\bar{3}$
Unit cell dimensions	a = 42.269(3) Å, α = 90°
	b = 42.269(3) Å, β = 90°
	c = 10.0582(8) Å, γ = 120°
Volume	15563(2) $Å^3$
Z, Calculated density	18, 1.658 Mg/m^3
Absorption coefficient	3.612 mm^{-1}
F(000)	7560
Measurement device type	STOE-IPDS diffractometer
Measurement method	rotation
Temperature	123(1) K
Wavelength	0.71073 Å
θ range for data collection	2.10 to 20.00°
Index ranges	$-38 \le h \le 40$, $-40 \le k \le 40$, $-9 \le l \le 9$
Reflections collected / unique	18614 / 3235 [R(int) = 0.1615]
Reflections greater I>2\s(I)	1558
Absorption correction	Numerical
Max. and min. transmission	0.9583 and 0.8021
Refinement method	Full-matrix least-squares on F^2
Data / restraints / parameters	3235 / 0 / 275
Goodness-of-fit on F^2	0.576
Final R indices [I>2sigma(I)]	R_1 = 0.0378, wR_2 = 0.0654
R indices (all data)	R_1 = 0.0944, wR_2 = 0.0747
Largest diff. peak and hole	0.535 and -0.490 e.$Å^{-3}$

7.3.17. $[Ag_2\{Cp'''Fe(\eta^5:\eta^1:\eta^1\text{-}P_4C^tBu)\}_2\{Cp'''Fe(\eta^5:\eta^1\text{-}P_4C^tBu)\}_2]\ [Al\{OC(CF_3)_3\}_4]_2$ (29)

Crystal data and structure refinement for **29**.

Empirical formula	$C_{138}H_{192}Ag_2Al_2F_{72}Fe_4O_{10}P_{16}$
Formula weight	4367.54
Crystal size	0.018 × 0.096 × 0.061 mm
Crystal description	plate
Crystal colour	brown
Crystal system	Triclinic
Space group	$P\bar{1}$
Unit cell dimensions	a = 15.274(2) Å, α = 104.909(9)°
	b = 17.1586(17) Å, β = 107.086(11)°
	c = 18.7961(19) Å, γ = 95.886(10)°
Volume	4464.7(9) $Å^3$
Z, Calculated density	1, 1.624 Mg/m^3
Absorption coefficient	6.862 mm^{-1}
F(000)	2212
Measurement device type	Oxford Diffraction Gemini Ultra
Measurement method	omega-scan
Temperature	103(2) K
Wavelength	1.54178 Å
θ range for data collection	2.58 to 51.18°
Index ranges	$-14 \le h \le 15$, $-16 \le k \le 17$, $-18 \le l \le 18$
Reflections collected / unique	24732 / 9506 [R(int) = 0.0396]
Reflections greater I>2\s(I)	6331
Absorption correction	multi-scan
Max. and min. transmission	1.2263 and 0.7748
Refinement method	Full-matrix least-squares on F^2
Data / restraints / parameters	9506 / 1 / 1125
Goodness-of-fit on F^2	0.992
Final R indices [I>2sigma(I)]	R_1 = 0.0402, wR_2 = 0.0976
R indices (all data)	R_1 = 0.0706, wR_2 = 0.1114
Largest diff. peak and hole	0.694 and -0.704 $e.Å^{-3}$

7.3.18. [{Cp'''Fe(η^5:η^1-P_4C^tBu)}(μ-AuCl)][(SC_4H_8)](30)

Crystal Data and Details of the Structure Determination for **30**

Empirical formula	$C_{22}H_{38}AuClFeP_4$, CH_2Cl_2
Formula weight	799.60
Crystal size	0.08 × 0.15 × 0.20 mm
Crystal description	block
Crystal colour	dark brown
Crystal system	Orthorhombic
Space group	$P2_12_12_1$
Unit cell dimensions	a = 9.6911(11) Å, α = 90°
	b = 17.063(5) Å, β = 90°
	c = 18.1151(16) Å, γ = 90°
Volume	2995.5(10) $Å^3$
Z, Calculated density	4, 1.773 Mg/m^3
Absorption coefficient	17.524 mm^{-1}
F(000)	1576
Measurement device type	Oxford Diffraction Gemini Ultra
Measurement method	omega-scan
Temperature	123 K
Wavelength	1.54184 Å
θ range for data collection	3.45 to 64.91°
Index ranges	$-11 \leq h \leq 8$, $-19 \leq k \leq 19$, $-21 \leq l \leq 20$
Reflections collected / unique	17654 / 4892 [R(int) = 0.1009]
Reflections greater I>2\s(I)	4442
Absorption correction	multi-scan
Max. and min. transmission	1.40508 and 0.38663
Refinement method	Full-matrix least-squares on F^2
Data / restraints / parameters	4892 / 0 / 166
Goodness-of-fit on F^2	1.062
Final R indices [I>2sigma(I)]	R_1 = 0.0626, wR_2 = 0.1539
R indices (all data)	R_1 = 0.0704, wR_2 = 0.1655
Largest diff. peak and hole	3.01 and -4.05 e.$Å^{-3}$

7.3.19. [{Cp'''Fe(η^5:η^1:η^1:η^1-P_5)}(μ-$CuCl)_2$(MeCN)]$_\infty$ (31)

Crystal data and structure refinement for **31**·$2C_6H_4Cl_2$

Empirical formula	$C_{31}H_{40}Cl_6Cu_2FeNP_5$
Formula weight	977.14
Crystal size	0.130 × 0.100 × 0.070 mm
Crystal description	platelike
Crystal colour	brown
Crystal system	Monoclinic
Space group	$P2_1/c$
Unit cell dimensions	a = 16.4942(10) Å, α = 90°
	b = 16.6306(10) Å, β = 106.2320(10)°
	c = 15.2677(10) Å, γ= 90°
Volume	4021.11(5) $Å^3$
Z, Calculated density	4, 1.614 Mg/m^3
Absorption coefficient	9.825 mm^{-1}
F(000)	1976
Measurement device type	Oxford Diffraction Gemini Ultra
Measurement method	omega-scan
Temperature	123 K
Wavelength	1.54184 Å
θ range for data collection	2.79 to 62.22°
Index ranges	-18 ≤ h ≤ 18, -18 ≤ k ≤ 18, -17 ≤ l ≤ 17
Reflections collected / unique	43051 / 6294 [R(int) = 0.0291]
Reflections greater I>2\s(I)	5349
Absorption correction	multi-scan
Max. and min. transmission	0.41268 and 1.00000
Refinement method	Full-matrix least-squares on F^2
Data / restraints / parameters	6294 / 0 / 425
Goodness-of-fit on F^2	1.039
Final R indices [I>2sigma(I)]	R_1 = 0.0266, wR_2 = 0.0677
R indices (all data)	R_1 = 0.0323, wR_2 = 0.0707
Largest diff. peak and hole	0.717 and -0.282 $e.A^{-3}$

7.3.20. [{Cp'''Fe(η^5:η^1:η^1:η^1-P_5)}(μ-CuBr)$_2$(MeCN)]$_\infty$ (32)

Crystal Data and Details of the Structure Determination for **32**·2$C_6H_4Cl_2$

Empirical formula	$C_{31}H_{40}Br_2Cu_2FeNP_5Cl_4$
Formula weight	1066.04
Crystal size	0.16 × 0.10 × 0.06 mm
Crystal description	plate
Crystal colour	brown
Crystal system	Monoclinic
Space group	*P 2$_1$/c*
Unit cell dimensions	a = 16.76410(10) Å, α = 90°
	b = 16.4557(2) Å, β = 106.3860(10)°
	c = 15.53930(10) Å, γ = 90°
Volume	4112.63(7) Å^3
Z, Calculated density	4, 1.722 Mg/m^3
Absorption coefficient	10.688 mm^{-1}
F(000)	2120
Measurement device type	Oxford Diffraction Gemini Ultra
Measurement method	omega-scan
Temperature	123 K
Wavelength	1.54184 Å
θ range for data collection	2.75 to 62.17°
Index ranges	-19 ≤ h ≤ 18, -17 ≤ k ≤ 18, -17 ≤ l ≤ 17
Reflections collected / unique	29378 / 6383 [R(int) = 0.0421]
Reflections greater I>2\s(I)	5160
Absorption correction	Semi-empirical from equivalents
Max. and min. transmission	1.00000 and 0.56969
Refinement method	Full-matrix least-squares on F^2
Data / restraints / parameters	6383 / 0 / 425
Goodness-of-fit on F^2	1.064
Final R indices [I>2sigma(I)]	R_1 = 0.0403, wR_2 = 0.1006
R indices (all data)	R_1 = 0.0530, wR_2 = 0.1140
Largest diff. peak and hole	1.041 and -0.615 e/Å^3

7.3.21. [{Cp'''Fe(η^5:η^1:η^1-P_5)}$_2$(μ-CuBr)$_3$]$_\infty$ (33)

Crystal Data and Details of the Structure Determination for **33**

Empirical formula	$C_{34}H_{58}Br_3Cu_3Fe_2P_{10}$
Formula weight	1318.55
Crystal size	0.22 × 0.14 × 0.04 mm
Crystal description	plate
Crystal colour	brown
Crystal system	Tetragonal
Space group	$I\bar{4}$
Unit cell dimensions	a = 13.7650(19) Å, α = 90°
	b = 13.7650(19) Å, β = 90°
	c = 25.552(5) Å, γ = 90°
Volume	4841.5(13) Å^3
Z, Calculated density	4, 1.809 Mg/m^3
Absorption coefficient	12.369 mm^{-1}
F(000)	2624
Measurement device type	Oxford Diffraction Gemini Ultra
Measurement method	omega-scan
Temperature	123 K
Wavelength	1.5418 Å
θ range for data collection	3.5 to 51.1°
Index ranges	-12 ≤ h ≤ 13, -12 ≤ k ≤ 10, -24 ≤ h ≤ 25
Reflections collected / unique	4466 / 2294, [R(int) = 0.057]
Reflections greater I>2\s(I)	2152
Refinement method	Full-matrix least-squares on F^2
Data / restraints / parameters	2294 / 0 / 249
Goodness-of-fit on F^2	1.089
Final R indices [I>2sigma(I)]	R_1 = 0.0636, wR_2 = 0.1717
R indices (all data)	R_1 = 0.0681, wR_2 = 0.1759
Largest diff. peak and hole	-0.59 and 0.65 e/Å^3

7.3.22. [{Cp'''Fe(η^5:η^1:η^1-P_5)}$_4$(μ-CuI)$_4$]$_\infty$ (34)

Crystal data and structure refinement for **34**.

Empirical formula	$C_{68}H_{116}Cu_9Fe_4I_9P_{20}$
Formula weight	3562.46
Crystal size	0.510 × 0.390 × 0.040 mm
Crystal description	plate
Crystal colour	brown
Crystal system	Monoclinic
Space group	*C2/c*
Unit cell dimensions	a = 25.7748(7) Å, α = 90°
	b = 25.7261(5) Å, β = 95.795(2)°
	c = 34.0933(6) Å, γ = 90°
Volume	22491.2(9) Å^3
Z, Calculated density	8, 2.104 Mg/m^3
Absorption coefficient	28.166 mm^{-1}
F(000)	13616
Measurement device type	Oxford Diffraction Gemini Ultra
Measurement method	omega-scan
Temperature	150(1) K
Wavelength	1.5418 Å
Monochromator	graphite
θ range for data collection	2.43 to 51.06°
Index ranges	-25 ≤ h ≤ 25, -25 ≤ k ≤ 24, -34 ≤ l ≤ 34
Reflections collected / unique	28722 / 11581 [R(int) = 0.0763]
Reflections greater I>2\s(I)	7814
Absorption correction	Semi-empirical from equivalents
Max. and min. transmission	1.62451 and -0.00319
Refinement method	Full-matrix least-squares on F^2
Data / restraints / parameters	11581 / 0 / 731
Goodness-of-fit on F^2	1.046
Final R indices [I>2sigma(I)]	R_1 = 0.0916, wR_2 = 0.2624
R indices (all data)	R_1 = 0.1309, wR_2 = 0.2898
Largest diff. peak and hole	2.710 and -2.175 e.Å^{-3}

7.3.23 $[Ag\{Cp'''Fe(\eta^5:\eta^2:\eta^1\text{-}P_5)\}_2]_n[Al\{OC(CF_3)_3\}_4]_n$ (35)

Crystal data and structure refinement for **35**.

Empirical formula	$C_{100}H_{116}Ag_2Fe_4P_{20}Al_2F_{72}O_8$
Formula weight	3926.13
Crystal size	0.408 × 0.049 × 0.018 mm
Crystal description	flat rod
Crystal colour	brown to red
Crystal system	Triclinic
Space group	$P\bar{1}$
Unit cell dimensions	a = 11.0690(11) Å, α = 89.562(11)°
	b = 21.991(3) Å, β= 85.907(11)°
	c = 30.807(5) Å, γ = 80.095(9)°
Volume	7368.3(17) $Å^3$
Z, Calculated density	2, 1.770 Mg/m^3
Absorption coefficient	8.625 mm^{-1}
F(000)	3904
Measurement device type	Oxford Diffraction Gemini Ultra
Measurement method	omega-scan
Temperature	150(1) K
Wavelength	1.5418 Å
θ range for data collection	2.49 to 62.89°
Index ranges	$-12 \leq h \leq 12$, $-24 \leq k \leq 25$, $-35 \leq l \leq 35$
Reflections collected / unique	106402 / 23426 [R(int) = 0.0491]
Reflections greater I>2\s(I)	15914
Absorption correction	Semi-empirical from equivalents
Max. and min. transmission	1.17131 and 0.58772
Refinement method	Full-matrix-block least-squares on F^2
Data / restraints / parameters	23426 / 0 / 1932
Goodness-of-fit on F^2	1.082
Final R indices [I>2sigma(I)]	R_1 = 0.0549, wR_2 = 0.1450
R indices (all data)	R_1 = 0.0809, wR_2 = 0.1556
Largest diff. peak and hole	3.058 and -2.686 e.$Å^{-3}$

8. Acknowledgments

I would like to express my gratitude to the following people:

Prof. Dr. Manfred Scheer for intellectual and professional guidance, for the opportunity to work in his research group and on such an exciting project, for allowing me a large degree of independence and creative freedom to explore a wide range of synthetic aspirations.

Karin Kilgert and Anette Baust for administrative assistance.

Dr. Manfred Zabel, Ms. Sabine Stemfhuber, Dr. Alexander Virovets and Eugenia Peresypkina for their patience in measuring and solving the "tiny" crystals I delivered.

The NMR departments of the universities of Karlsruhe (Dr. Eberhard Matern, Ms. Helga Berberich, Ms. Sibylle Schneider) and Regensburg (Dr. Thomas Burgemeister, Mr. Fritz Kastner, Ms. Annette Schramm, Ms. Georgine Stühler) for their competent support and patient help in elaboration of the spectra.

The MS departments of the universities of Karlsruhe (Mr. Dieter Müller) and Regensburg (Dr. K. K. Mayer, Mr. Josef Kiermaier, Mr. Wolfgang Söllner) for their skill and cooperation.

Prof. Dr. Elmar Lang and Prof. Dr. Rainer Winter for the measurements and discussions of the ESR spectrum.

Dr. Marek Sierka, Humboldt-Universität zu Berlin, for DFT calculations.

Prof. Dr. John F. Nixon for supplying some very interesting starting materials.

Special thanks to Brian Wegley and Laurence Gregoriades for improving my dissertation.

Prof. Dr. Qianfeng Zhang for many chemical suggestions and advices; Dr. Shuzhong Zhan and Dr. Baoli Fei for the tips in growing crystals.

Gábor Balázs and Taike Duan for solving and discussion some structures of the crystals.

Dr. Joachim Wachter for the advices for the IR spectra explanation.

Members of the Scheer group: Barbara Treitinger, Elisabeth "Lizzy" Ederer for helping to the cyclovoltametry measurement, Naziha Muschiol, Manfred "Musch" Muschiol, Walter Meier, Thomas "Schotti" Schottenhammer for the concerning my daughter, Andreas "Andi" Lange for his computer administration work, Alexander "Alex" Ebner, Ariane "Ari" Adolf, Dr.Ulf Vogel for simulate and explanation the NMR spectra, Karl-Christian "Kalle" for the helping in computer works, Christian Kunz, Roger Merkle for organising stuff, Christian Eisenhut, Miriam Eberl, Cornelia "Conny" Dreher, Hannes Krauss, Andrea Schindler, Michael Bodensteiner, Michael Pronold, Fabian Dielmann, Stefan Almstätter, Patrick Schwarz.

Former members of the Scheer group: Daniel Himmel for supervising me "cooking" the Cp'''H, Dr. Sergej Konchenko, Dr. Rajiv Trivedi, Dr. Junfeng Bai, Johann, Nikolai, Anton.

Brian Johnson for the great deal of interesting and happily discussions during daily trips to the Mensa.

Gábor Balázs for disclosure the snaps brews and Brian Wegley, for the spirited daily conversations and his powerful music.

Thomas Roßmeier for interesting discussions about chemistry and others……

My grandfather, Anping Deng, for his anticipations on me; my parents, Yulan Tao and Zhiliang Deng, for their endless loving concerns and unconditional support; My uncle, Zhiquan Deng, for the versatile intellectual advices and personal inspiration.

My cousins Xiaohua, Xiaomei and her husband Jingsong for their concerns and encouragements.

My wife, Jing, for her patience, understanding and long-distance support.